JOURNAL OF GEOPHYSICAL RESEARCH

The continuation of

TERRESTRIAL MAGNETISM AND ATMOSPHERIC ELECTRICITY
(1896-1948)

An International Quarterly

VOLUME 61 March, 1956 NUMBER 1

CONTENTS

COSMIC RADIO-FREQUENCY RADIATION NEAR ONE MEGACYCLE, *Grote Reber and G. R. Ellis* 1

ON DERIVING GEOMAGNETIC DIPOLE-FIELD COORDINATES FROM COSMIC-RAY OBSERVATIONS, *J. A. Simpson, F. Jory, and M. Pyka* 11

THE ANNUAL VARIATIONS OF THE ATMOSPHERICS—EXISTENCE AND EXPLANATION OF A SECOND MAXIMUM IN WINTER, IF ONLY STRONG IMPULSES ARE COUNTED, *Reinhold Reiter* 23

IONIZATION OF RADIOACTIVE PARTICLES IN THE FREE AIR, - - - - - - *S. M. Greenfield* 27

STANFORD-SEATTLE WHISTLER OBSERVATIONS, *J. H. Crary, R. A. Helliwell, and R. F. Chase* 35

ATMOSPHERIC TEMPERATURES AND WINDS BETWEEN 30 AND 80 KM, *W. G. Stroud, W. Nordberg, and J. R. Walsh* 45

NOTE ON THE ADJUSTMENT OF ISOMAGNETIC CHARTS TO MUTUAL CONSISTENCY, *A. J. Zmuda* 57

RELATIONSHIPS BETWEEN AURORA AND SPORADIC-*E* ECHOES AT BARROW, ALASKA, *R. W. Knecht* 59

(Contents concluded on outside back cover)

Published at

THE WILLIAM BYRD PRESS, INC.

P. O. BOX 2-W, SHERWOOD AVE. AND DURHAM ST.

RICHMOND 5, VIRGINIA

Address all correspondence to

JOURNAL OF GEOPHYSICAL RESEARCH

5241 BROAD BRANCH ROAD, NORTHWEST

WASHINGTON 15, D.C., U.S.A.

SIX DOLLARS A YEAR SINGLE NUMBERS, TWO DOLLARS

JOURNAL OF GEOPHYSICAL RESEARCH

The continuation of

Terrestrial Magnetism and Atmospheric Electricity
(1896-1948)

An International Quarterly

Founded 1896 by L. A. BAUER *Continued 1928-1948 by* J. A. FLEMING

Fields of Interest

Terrestrial Magnetism
Atmospheric Electricity
The Ionosphere
Solar and Terrestrial Relationships
Aurora, Night Sky, and Zodiacal Light
The Ozone Layer
Meteorology of Highest Atmospheric Levels
The Constitution and Physical States of the Upper Atmosphere
Special Investigations of the Earth's Crust and Interior, including experimental seismic waves, physics of the deep ocean and ocean bottom, physics in geology
And similar topics

This Journal serves the interests of investigators concerned with terrestrial magnetism and electricity, the upper atmosphere, the earth's crust and interior by presenting papers of new analysis and interpretation or new experimental or observational approach, and contributions to international collaboration. It is not in a position to print, primarily for archive purposes, extensive tables of data from observatories or surveys, the significance of which has not been analyzed.

Forward *manuscripts* to one of the Associate Editors, or to the editorial office of the Journal at 5241 Broad Branch Road, Northwest, Washington 15, D. C., U. S. A. It is preferred that manuscripts be submitted in English, but communications in French, German, Italian, or Spanish are also acceptable. A brief abstract, preferably in English, must accompany each manuscript. A *publication charge* of $8 per page will be billed by the Editor to the institution which sponsors the work of any author; private individuals are not assessed page charges. Manuscripts from outside the United States are invited, and should not be withheld or delayed because of currency restrictions or other special difficulties relating to page charges. Costs of publication are roughly twice the total income from page charges and subscriptions, and are met by subsidies from the Carnegie Institution of Washington and international and private sources.

Back issues and *reprints* are handled by the Editorial Office, 5241 Broad Branch Road, N.W. Washington 15, D.C., U.S.A.

Subscriptions are handled by the Editorial Office, 5241 Broad Branch Road, N.W., Washington 15, D.C., U.S.A.

Second-class mail privileges authorized at Richmond, Virginia

Journal of

GEOPHYSICAL RESEARCH

The continuation of

Terrestrial Magnetism and Atmospheric Electricity

VOLUME 61 MARCH, 1956 No. 1

COSMIC RADIO-FREQUENCY RADIATION NEAR ONE MEGACYCLE

BY GROTE REBER* AND G. R. ELLIS†

**Research Corporation, New York, N. Y.; and †Commonwealth Observatory Ionospheric Prediction Service, Hobart, Tasmania, Australia*

(Received November 22, 1955)

ABSTRACT

Observations of cosmic radio-frequency radiation on frequencies of 2130 kc/sec, 1435 kc/sec, 900 kc/sec, and 520 kc/sec have been made, using a method of recording which effectively reduces interference from atmospherics. At these frequencies, the intensity of the radiation is approximately 10^{-19} watt per square metre per cycle per second** per steradian. The ionospheric effects associated with observations near the critical frequency are discussed.

INTRODUCTION

The lowest frequency on which cosmic radio-frequency radiation had previously been studied was 9.15 Mc/sec (Higgins and Shain, 1954). Their observations were made in circumstances where ionospheric effects were small, and they suggested that at lower frequencies high radiation intensities could be expected. The ionosphere can be a controlling factor in any measurements at these frequencies, but by observing at a place of high magnetic latitude and near a sunspot-minimum the frequency range available for studying the radiation can be extended several octaves lower. In addition to providing information about the intensity of the radiation in a previously unexplored frequency region, such measurements, if made in the vicinity of the critical frequency, can supply new data concerning the propagation of radio waves through the ionosphere.

**The authors suggest the name "jansky" for this unit.

It is the purpose of this paper to describe the results of observations whi have been made at Hobart, Tasmania, on frequencies of 2130 kc/sec, 1435 kc/se 900 kc/sec, and 520 kc/sec.

2. EXPERIMENTAL

At 2130 kc/sec and 520 kc/sec, specially-built battery-operated receive with a band-width of 6 kc/sec were used. At 1435 kc/sec and 900 kc/sec, th receivers were standard communication types (R.A.F. R1155) with a ban width of 4.2 kc/sec. The antennas at 2130 kc/sec and 520 kc/sec were cage-dipole 374 feet long, consisting of six parallel wires arranged in a cage, 6 feet in diamet and 70 feet above the ground. Each was connected to its receiver with a resona 600-ohm line, 300 feet long. The 1435 kc/sec and 900 kc/sec receivers were operate with single half-wave dipoles, 60 feet above the ground. Figure 1 shows the com puted acceptance pattern for the 2130 kc/sec antenna.

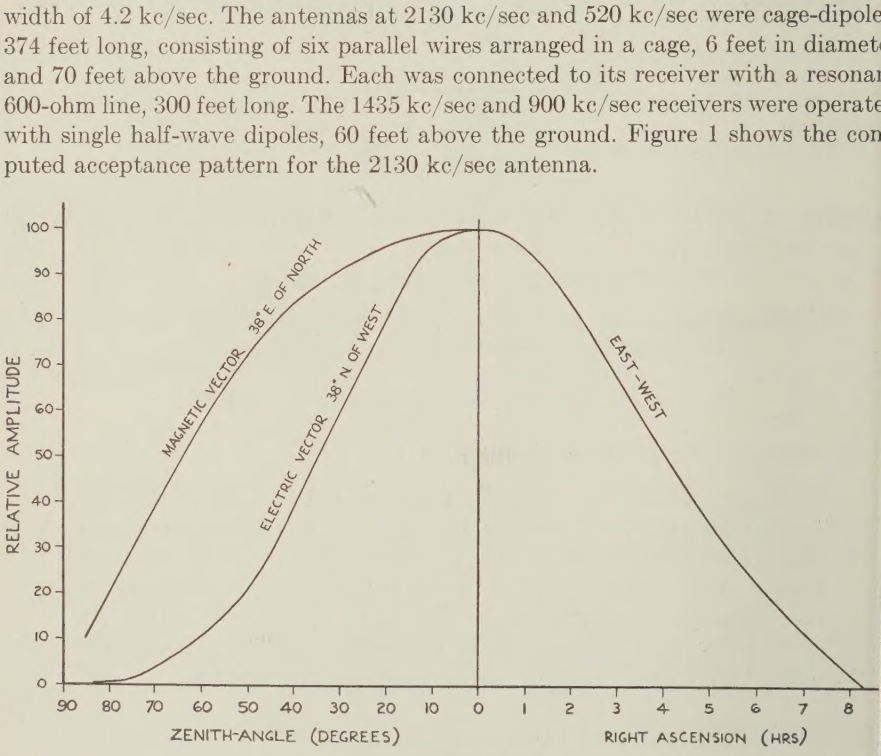

FIG. 1—Antenna acceptance pattern at 2130 kc/sec in three representative vertical planes

The most novel feature of the experimental arrangements was the method recording. In the past, pen recorders with a time-constant of about one seco have been used. These have been quite satisfactory at frequencies above abo 20 Mc/sec, where the interference from atmospherics is small. Near 1 Mc/s however, the atmospheric interference is normally sufficiently intense at night make this system useless. Even a fast pen recorder with a time-constant of 0. second was found cumbersome and unreliable in these circumstances, althou some of the early records at 2130 kc/sec were obtained with it. However, using fast photographic recording with a cathode-ray indicator, it was fou possible to produce satisfactory records at night at Hobart on all frequenci

With a time-constant of about 10^{-2} second, the average level of the continuous background radiation was recorded during the short quiet periods between atmospherics. The records were made on 35-mm film, moving at the rate of one and a half inches per hour. Time-marks were made on the records by switching the receivers to dummy antennas every 10 minutes. It was found that the amplitude of the radiation had a characteristic slow variation, which could be recognised even in the presence of weak interference from transmitting stations, although it was not difficult at Hobart to find frequencies which were normally free from such interference.

A later development, following a suggestion by Dr. J. L. Pawsey, was the use of a minimum-reading circuit, which, in a way analogous to a peak-reading voltmeter, reads the minimum average value of the receiver voltage reached between atmospherics. This enabled a pen recorder to be used instead of a photographic recorder. A minimum-reading time-constant of one minute, combined with an averaging time-constant of 10^{-2} second, was found to produce satisfactory pen recordings. The majority of the records were obtained with the photographic system, although some of the later ones were made with the minimum-reading pen recorder.

THE OBSERVATIONS

(*a*) 2130 *kc/sec*—Observations were made at 2130 kc/sec during the period from March to October, 1955. On almost every night, strong continuous radiation was observed for periods which ranged from approximately one hour to 12 hours. The variation in the amplitude of the radiation with change in critical frequency and occurrence of sporadic *E* made it clear that the radiation was of extraterrestrial origin. Photographs of sample records are shown in Figure 2. In circumstances where the critical frequency varied between about 1.6 Mc/sec and 2.13 Mc/sec, there was a strong correlation between the critical frequency and the amplitude of the radiation. Figure 3 shows a clear example of this situation. When the critical frequency became lower than about 1.6 Mc/sec, the amplitude increased to a limiting value, which was not affected by further variations of critical frequency. This is illustrated by Figure 4, which was obtained during the decline in intensity between 20^h and 00^h R.A.

By plotting only those readings when the critical frequency was below 1.6 Mc/sec, the variation in intensity with sidereal time shown in Figure 5 was obtained. By correcting this for the receiver antenna pattern (Bracewell, 1955), the shape of the curve remained substantially the same, but the ratio of maximum to minimum intensity became 1.8:1.

(*b*) 1435 *kc/sec*—At this frequency, observations were made from April to September and, during this period, records showing the cosmic radiation were obtained on 31 nights. These records reproduced in general form the results at 2130 kc/sec. Typical examples are shown in Figure 2. Figure 6 shows a simple case on this frequency of the effect of sporadic *E* on the amplitude, together with the slow increase in level due to the decrease in *F*2 critical frequency.

On five nights between June and September, the amplitude of the radiation appeared to reach a limiting maximum value, with critical frequencies in the

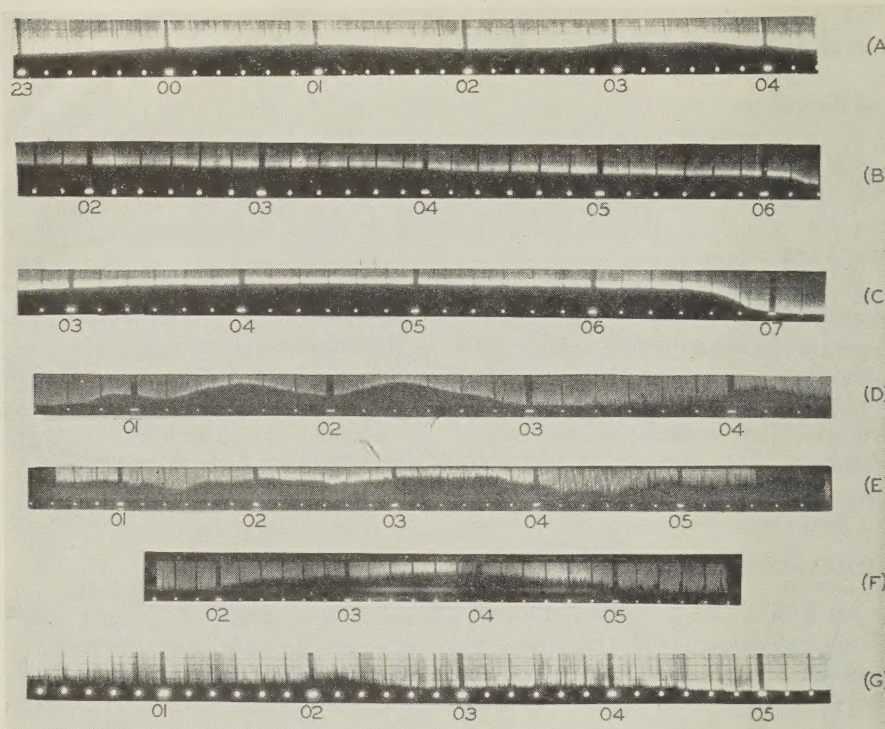

FIG. 2—(*a*) Actual record at 2130 kc/sec described in Figure 3; (*b*) actual record at 2130 kc/s described in Figure 4; (*c*) 2130 kc/sec record showing the dawn cut-off; (*d*) and (*e*) samples records at 1435 kc/sec; (*f*) and (*g*) samples of records at 900 kc/sec and 520 kc/sec, respective

vicinity of 1 Mc/sec. Figure 7 shows the variation of intensity with sidereal tim obtained from these five records. The level was slightly higher at 17^h R.A. tha at 06^h, and the ratio of maximum to minimum less than at 2130 kc/sec.

(*c*) 900 *kc/sec*—Observations were made on this frequency from June October, and six records showed the slow rise and fall of the base-level characte istic of ionosphere-controlled cosmic radiation. A sample record is shown in Figu 2. Since the ionosphere recorder used did not operate below 1 Mc/sec, no corr lation with critical frequency could be made, although on four of the six occasio the critical frequency appeared to be below 1 Mc/sec. The observations at 14 kc/sec and 900 kc/sec were all made between 0100 and 0500 hours local time avoid interference from broadcast stations.

(*d*) 520 *kc/sec*—Approximately 80 nights of observations were secured fr late May to early September. Only three produced records which could reasonab be interpreted as evidence of cosmic radiation. On one of these nights, the 9(kc/sec equipment was not operating. On the remaining two nights, the radiati was observed also at 900 kc/sec. Although observations were made at lo frequencies at various times, 520 kc/sec was the lowest frequency on which th

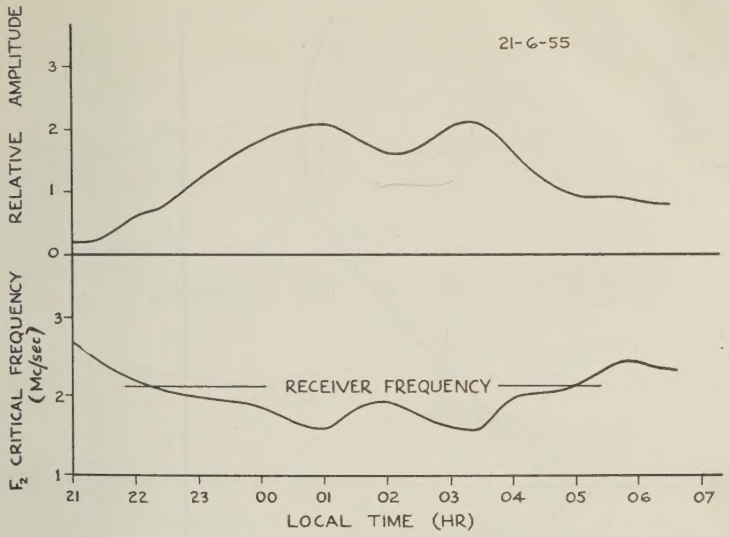

FIG. 3—Record at 2130 kc/sec, showing the variation in amplitude with changes in critical frequency near the operating frequency

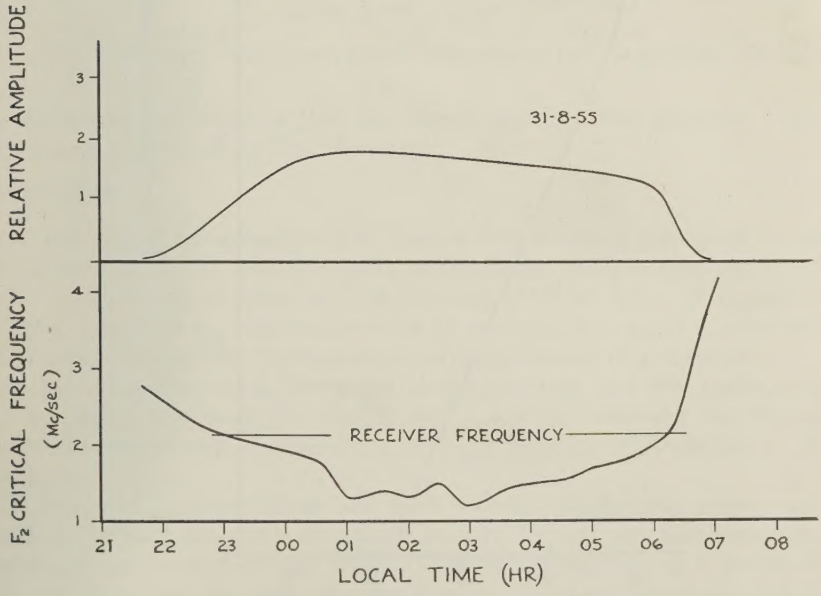

FIG. 4—Record at 2130 kc/sec, showing the limiting maximum amplitude observed when the critical frequency was less than about 1.6 Mc/sec

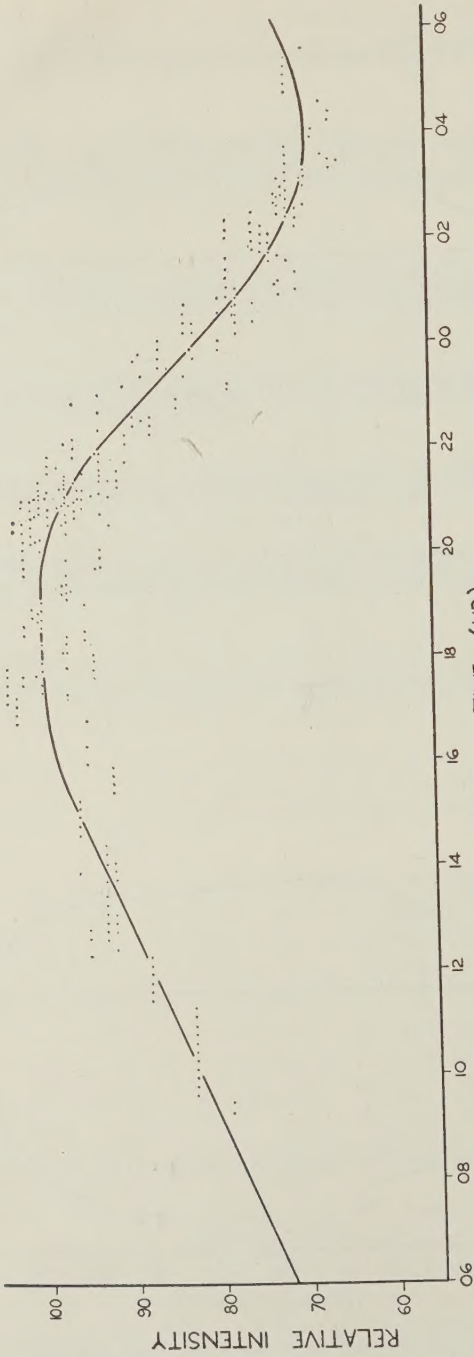

FIG. 5—Variation of intensity with sidereal time at 2130 kc/sec

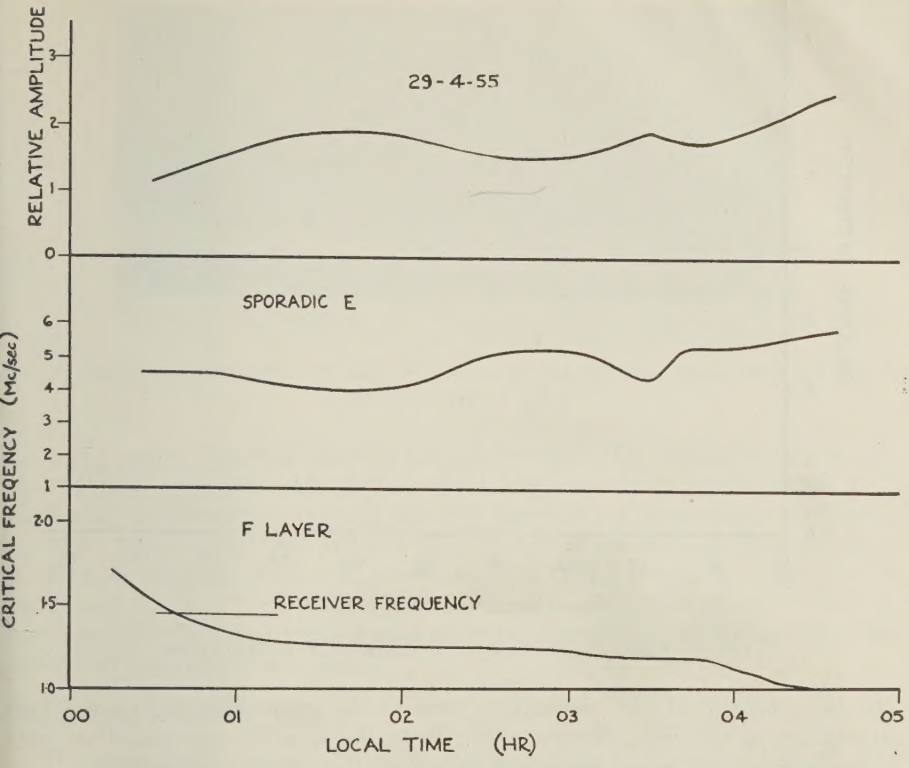

FIG. 6—Record at 1435 kc/sec, showing the combined effect of changing f_oF2

was any reason for believing that the cosmic radiation was detected. Figure 2 shows one of the records at this frequency.

4. DISCUSSION

(*a*) *Intensity of the radiation*—The maximum intensity of the cosmic radiation arriving from the zenith when the plane of the galaxy was overhead was found to be 10^{-19} watt per square metre per cycle per second $[W.M^{-2}(c/s)^{-1}]$* per steradian at 2130 kc/sec, with an estimated error of 50 per cent. This result is corrected for both modes of ionospheric propagation and for all planes of polarisation.

At the other frequencies, the wider antenna pattern and the inadequacy of the ionospheric data made the results more uncertain, although the intensities were of the same order of magnitude, with perhaps lower intensities at lower frequencies.

(*b*) *Ionospheric effects*—There are three ways in which radio waves may be propagated through the entire ionosphere, namely, the ordinary and extraordinary quasi-transverse modes, and the oblique longitudinal ordinary or *Z* mode (Ellis, 1955). Of these, only the first was important in the observations recorded here.

*The authors suggest the name "jansky" for this unit.

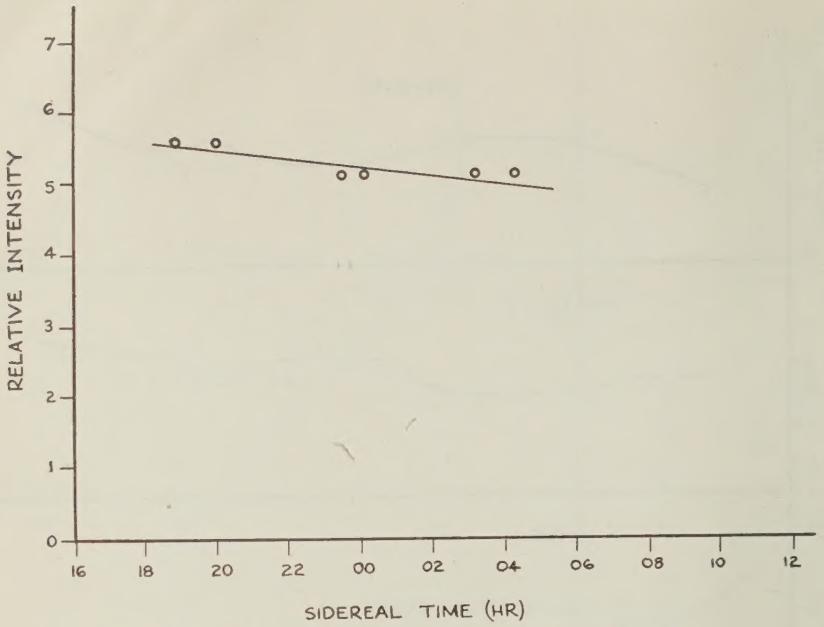

FIG. 7—Variation of intensity with sidereal time at 1435 kc/sec

The frequencies used were sufficiently close to the gyrofrequency to cause high attenuation of the extraordinary mode, while the Z mode can contribute only second-order effects in the absence of strong point-sources of radiation.

The ordinary mode provides a nearly elliptical hole in the ionosphere, normally centered on the zenith, which shrinks in size as the critical frequency rises towards the observing frequency. It may be shown (Ellis, 1956) that the opening and closing of this hole provides an adequate explanation of the variation in the amplitude of the radiation when the critical frequency is varying in the vicinity of the observing frequency. It is not necessary to assume high absorption in the F region. The theory also shows that the residual amplitude observable when the critical frequency is greater than the operating frequency is normally explainable by the asymmetry with respect to the zenith of the ordinary-wave hole. This occurs whenever there is a strong horizontal gradient of electron-density and causes the trapping of some of the radiation beneath the ionosphere. An interesting illustration is shown in Figure 8. Here the residual amplitude continues to fall after dawn, until approximately an hour after the F-region critical frequency has risen above the observing frequency the propagation of the trapped radiation is suddenly inhibited by the increase in the E-region critical frequency. This produces a downward step in the record.

The radiation may also be observable below the nominal critical frequency during disturbed ionospheric conditions, which often produce on the $P'f$ records additional cusps near the main $F2$ trace. In a typical sequence, an extra trace showing lower critical frequency and greater virtual height detaches itself from

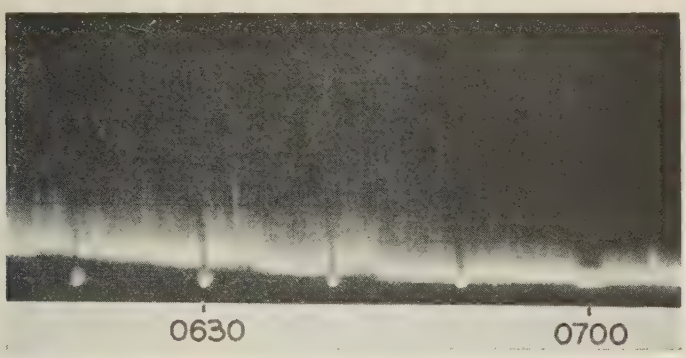

FIG. 8—Record at 2130 kc/sec, showing the sudden decrease in the residual amplitude caused by the increase of f_0E

the main trace. Figure 9 shows a typical example. The radiation is normally observable at frequencies above the critical frequency shown by the extra trace, which may be interpreted as being due to a region of low electron-density passing overhead. It is possible that all the records at 520 kc/sec were due to phenomena of this sort, although they could not be detected at this frequency because of the inadequacy of the $P'f$ recorder. When the condition known as spread F occurred, it was always found that the radiation could be observed at frequencies above the minimum frequency of the spread.

5. FURTHER POSSIBILITIES

The present rise in solar activity means rapidly increasing values of f_0F2 during the next few years. As a result, the opportunities for studying low-frequency

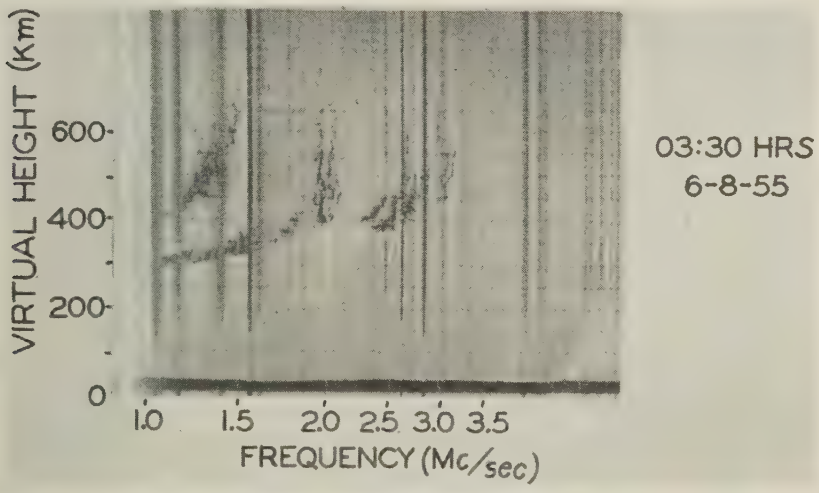

FIG. 9—$P'f$ record, showing a typical example of an additional low-frequency trace due to a region of low electron-density

radio astronomy will become increasingly rare until after the next sunspot-maximum. However, the cosmological implications of measurements below 10 Mc/sec are sufficiently important to warrant measurements on such frequencies that remain available. Observations should be made using antennas with as small an acceptance pattern as possible. Not only is the angular resolution increased, but the size of the hole required in the ionosphere is then small, and it is possible to make measurements of intensity much closer to the critical frequency. Investigations of discrete sources could profitably be undertaken in this frequency region, using interferometer techniques. Also, the use of the Z-propagation hole on the strong sources in the northern hemisphere may prove practicable. In this case, an effective angular resolution of about 1° could be achieved.

To study the radiation at the lowest possible frequencies, it will probably be necessary to wait until the approach of the next sunspot-minimum. In addition, observations should be conducted at places where f_0F2 is low and stays low for several hours during the night. A preliminary investigation indicates that the most favourable places lie between 50° and 60° magnetic latitude and near the agonic line. An effective ionospheric recorder with a low-frequency limit of half or less the lowest observing frequency is an essential part of any medium-wave radio-astronomy investigation.

ACKNOWLEDGMENTS

This investigation has been carried out under the sponsorship of the Research Corporation and of the Commonwealth Observatory Ionospheric Prediction Service at the Ionospheric Station, Hobart. Thanks are due to the University of Tasmania for the provision of technical facilities.

References

Higgins, C. S., and C. A. Shain (1954); Aust. J. Phys., **7**, 460-470.
Bracewell, R. N. (1955); Aust. J. Phys., **8**, 200-205.
Ellis, G. R. (1955); J. Atmos. Terr. Phys., in press.
Ellis, G. R. (1956); to be published.

ON DERIVING GEOMAGNETIC DIPOLE-FIELD COORDINATES FROM COSMIC-RAY OBSERVATIONS*

BY J. A. SIMPSON, F. JORY, AND M. PYKA

Institute for Nuclear Studies,
The University of Chicago,
Chicago 37, Illinois

(Original manuscript received June 30, 1955; revised November 2, 1955)

ABSTRACT

The earth's external magnetic field, extending far beyond the ionosphere, is at present inaccessible to direct observation. However, the measurement of the nucleonic component longitude and latitude effects in the region of the geomagnetic equator now offers the possibility for determining the coordinates of an equivalent geomagnetic dipole which represents this external field without encountering the problems that have heretofore beset the use of meson intensity observations for this purpose. The method of measurement and the theory relating the cosmic-ray intensity changes to the geomagnetic coordinates are outlined for deriving the two angles which determine the orientation of the dipole and the three coordinates giving the position of the magnetic center with respect to the center of the earth.

I. INTRODUCTION

The present description of the earth's external magnetic field is derived from world-wide surface measurements of vector field intensity. Since the charged particles in the cosmic radiation begin to interact with the earth's external field at considerable distances from the earth, the question arises as to whether the description of the magnetic field required to account for the distribution of cosmic-ray particles is the same as the field described by the classical surface magnetic measurements.

The theory for the motion of charged particles moving in the main external field of the earth has been explored extensively. Since at large distances the local anomalies in the magnetic field become negligible, the interesting possibility arises that, without resorting to surface magnetic measurements, the orientation and magnetic center coordinates for the equivalent dipole moment of the earth's magnetic field may be measured. Thus, the incoming charged particles may be looked upon as "probes" in the magnetic field around the earth. These measurements will also be of interest in interpreting auroral and ionospheric observations.

The application of cosmic rays to the description of the earth's field has been occasionally discussed over many years. However, since it is apparent that con-

*Assisted in part by the Office of Scientific Research and the Geophysics Research Directorate, Air Force Cambridge Research Center, Air Research and Development Command, U. S. Air Force.

tinuous cosmic-ray observations are required for a world-wide description of the field, the investigator is limited to measuring deep within the atmosphere the secondary components produced by the primary cosmic radiation. Earlier considerations of this problem, based upon the measurement of meson intensity (the "hard" component), were not fruitful; for example, the dependence of meson intensity on latitude is very small over the geomagnetic latitude range 0° to ±20°. We wish to point out in the present paper that within the last few years the nucleonic component has been investigated and found to possess a larger dependence on latitude than any other known secondary particle component in the cosmic radiations (see Fig. 1). In addition, this component does not display an atmos-

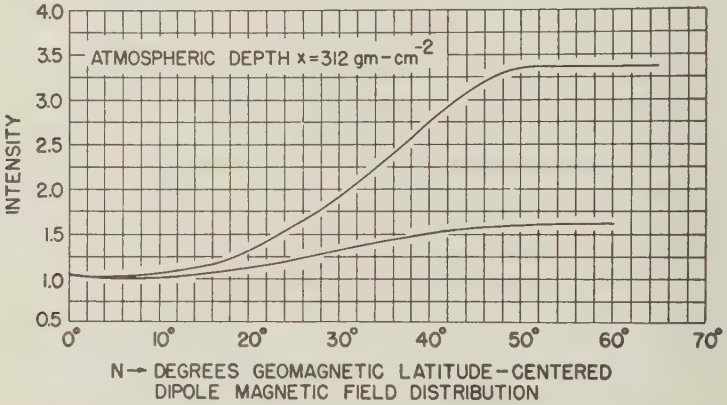

FIG. 1—The upper curve shows the dependence of the neutron intensity (nucleonic component) on geomagnetic latitude in 1948; the lower curve gives the largest latitude effect which can be obtained under similar conditions for the charged particle component. For the case of the neutron measurements, it should be noted that the minimum intensity does not appear to coincide with the location of the geomagnetic equator derived from geomagnetic coordinates based upon magnetic field intensity observations.

pheric temperature effect. Accordingly, we propose to explore the possibility of using this component to obtain a description of the geomagnetic equator and the location of the magnetic center of the earth for the field distribution at appreciable distances from the earth.

Specifically, we shall attempt to outline how *measurements* may be undertaken to determine:

(*a*) The plane of the geomagnetic equator for the off-centered dipole moment of the earth's main field,
(*b*) The eccentricity of the equivalent dipole.

II. RELATIONSHIP BETWEEN MAGNETIC FIELDS AND COSMIC-RAY INTENSITY

The permanent field of the earth is described by the gradient of a magnetic potential. The potential is generally expanded in spherical harmonics with coefficients determined from the world-wide surface measurements [see 1 of "Refer-

ences" at end of paper]. The first three coefficients represent a dipole; the next ive coefficients represent quadrupole terms. It can be shown that these eight oefficients of the expansion are equivalent to a single dipole displaced from the enter of the earth, plus two remaining quadrupole terms.

At considerable distances from the surface of the earth, the main field is epresented by the eccentric dipole alone, and it is this field which accounts for he main geomagnetic effects on charged cosmic-ray particles [2]. The off-center ipole constitutes an axially symmetric field system and, therefore, the Störmer quations will describe the motion. Even though this is a good approximation, it nay be possible that very near the surface of the earth the particles experience the ffects of the two residual quadrupole contributions. Although in this paper we shall rimarily be concerned with the eccentric dipole field model, we shall also discuss he possibility of detecting the effect of these residual quadrupole terms.

Irrespective of the cosmic-ray component being measured, the geomagnetic ield produces two principal effects upon the total observed intensity: first, it is ninimum at the geomagnetic equator and increases as the observer moves toward ither pole. This is the well-known latitude effect.

Second, there is a longitude effect on cosmic-ray intensity which is most pro- ounced at the geomagnetic equator. The distance between the center of the eoid and its magnetic center is approximately 400 km, and the minimum energies vhich particles may have to reach the atmosphere is a function of their distance

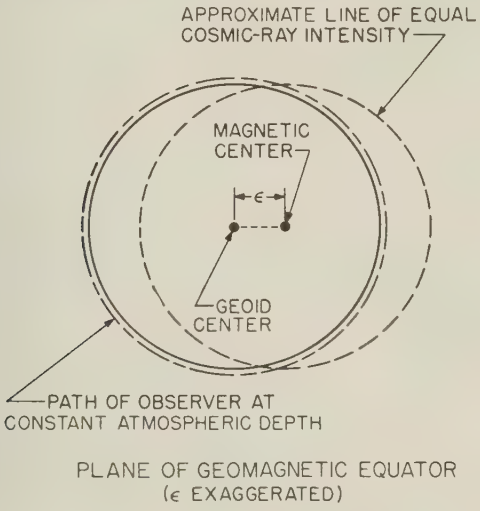

Fig. 2

rom this magnetic center (Fig. 2). Consequently, as an observer moves around ne equator of the earth within the atmosphere, the cosmic-ray intensity varies ith the longitude of observation.

Conversely, if we know the position of minimum cosmic-ray intensity for all ongitudes, we may (*a*) define the plane of the geomagnetic equator for charged

particles, or the degree to which the magnetic equator lies in a plane, and (*b*) obtain a measure for the eccentricity of the magnetic dipole. This corresponds to measuring the three coordinates of the magnetic center of the earth and the direction angles of the eccentric magnetic dipole. In the following discussion, we shall consider the quantitative determination of these five parameters from the measurement of cosmic-ray intensity near the surface of the earth.

Since the magnetic field interacts with incoming primary particles and we are measuring the secondary particles produced by these primaries, our first task is to relate observed secondary cosmic-ray intensity to the primaries, and the trajectories of these primary particles to the parameters of the external geomagnetic field.

The primary cosmic radiation is composed of approximately 85 per cent protons, 14 per cent alpha particles, and 1 per cent heavier nuclei, all stripped of their outer electrons. These charged particles experience deflections in a magnetic field which depend upon their charge and momentum. Particles undergo the same deflection in a magnetic field, provided the quantity pc/Ze is the same for all of the particles, where p is particle momentum, Ze the charge, and c velocity of light. This quantity is called the magnetic rigidity N, measured in units of 10^9 volts, that is, Bv. By expressing the motion of particles in the geomagnetic field in terms of N, we describe the behavior of particles over the entire charge spectrum.

We noted earlier that the primary radiation produces not only the secondary meson component, but also the nucleonic component, which is strongly dependent on magnetic latitude [3]. For the measurements of nucleonic intensity deep within the atmosphere of the earth, we are concerned with the primary radiation producing the secondary nucleonic component which reaches the detector at large atmospheric depths.

Although the primary radiation at great distances from the earth is remarkably isotropic, it has been shown that the nucleonic component intensity at large atmospheric depth arises principally from primary radiation approaching the atmosphere at, or near, the vertical.

More precisely, we observe the counting rate of nucleonic component particles within a detector at atmospheric depth x gm/cm^2, arising from the integral cosmic-ray intensity of all particles arriving near or from the vertical. We call R_v the counting rate for primaries arriving from the vertical. If we define the differential primary particle intensity

$$j_Z = \frac{C_Z}{\left[\frac{pc}{Ze}\right]^n} = \frac{C_Z}{N^n}$$

(n lies in the range $2 < n < 2.7$) for particles of charge Ze, we may then write an expression for the observed counting rate [4],

$$R_v(\varphi, \lambda, x, t) = \sum_Z \int_{N_c(\varphi,\lambda)}^{\infty} S(N, x) j_Z(N, t)\, dN \quad \ldots\ldots\ldots\ldots (1)$$

where S is defined as the average specific yield function of secondary nucleonic component particles per incoming primary particle of charge $Z = 1$ or 2, since we neglect the effect of all heavier nuclei. We see that R depends on magnetic

ongitude φ, magnetic latitude λ, atmospheric depth x, and the time of the measurement t. The integration is carried over the primary spectrum from the highest particle rigidities down to the minimum rigidity which a particle may possess and yet reach the atmosphere near the vertical. This critical cut-off rigidity is defined as $N_c(\varphi, \lambda)$. N_c is a function of geomagnetic field parameters, and it is through this functional relationship that we obtain our information on the symmetry properties of the geomagnetic field of the earth using nucleonic component detectors.

To determine N_c, we have noted that the motion of charged particles, with momentum p and charge Ze, in the field of a magnetic dipole is described by the equations of motion derived by Störmer. An integral of the motion is given by

$$R \cos\lambda \cos\omega + \frac{\cos^2\lambda}{R} = \text{const.} = \beta \quad \ldots\ldots\ldots\ldots\ldots\ldots (2)$$

where R is the radius vector from the dipole expressed in units of $r\sqrt{rM}$, with M = magnetic moment of the dipole and r = radius of the earth; λ is the latitude of particle arrival with respect to the dipole axis (the geomagnetic latitude); ω is the angle between the particle velocity vector and a vector pointing west from the meridian plane. For a vertically incident particle, $\cos\omega = 0$. β is a constant of the motion, that is, the impact parameter.

For the special case in which we wish to obtain $N_c(\lambda, \varphi)$, we set $\cos\omega = 0$, and $\beta = 2$ will define the minimum rigidity a particle may have for vertical arrival at λ, φ.

If the magnetic center coincided with the center of the geoid, then $N_c \approx 15$ Bv at $\lambda = 0$, independent of φ. However, since the magnetic center is off the geoid center by an amount ϵ, we obtain, using equation 2 for N_c at $\lambda = 0°$,

$$N_c(\varphi, 0) = 15(1 + \delta^2 - 2\delta\cos\varphi)^{-1} \quad \ldots\ldots\ldots\ldots\ldots\ldots (3)$$

where $\delta = \epsilon/r$.

Before integrating equation (1), we must determine the dependence of S and on magnetic rigidity. For a constant atmospheric depth x, S has been shown to be approximately constant from 4 to 14 Bv for protons, and 10 to 14 Bv rigidity for $Z = 2$ particles [5]. It further appears probable that it is essentially constant for $N > 10$ Bv. Since we are concerned with relative intensities as a function of φ, we assign $S = 1$.

For the primary differential spectrum $j_Z = C_Z/N^n$, measurements over the past few years indicate that n changes from about 2.3 at rigidities the order of 10 Bv to $n \approx 2.6$ for very high rigidities. To take into account this change of exponent with particle rigidity without averaging the value of the exponent, we shall split the integration into two parts, assigning the exponent m for $N_c < 30$ Bv $= N'$ and n for $N_c > N'$. The value $N' = 30$ is not critical. Then, for $\lambda = 0°$,

$$R_c(\varphi, 0, x, t) = \sum_Z \int_{N_c(\varphi,\lambda)}^{N'} j_{Z,m}(N, t)\, dN + \sum_Z \int_{N'}^{\infty} j_{Z,n}(N, t)\, dN \ldots\ldots (4)$$

III. THE DIPOLE ECCENTRICITY AND EQUATORIAL PLANE

We now wish to determine the fractional change in counting rate for maximum intensity R_{max} to minimum intensity R_{min} at $\lambda = 0°$ as the detector is carried from

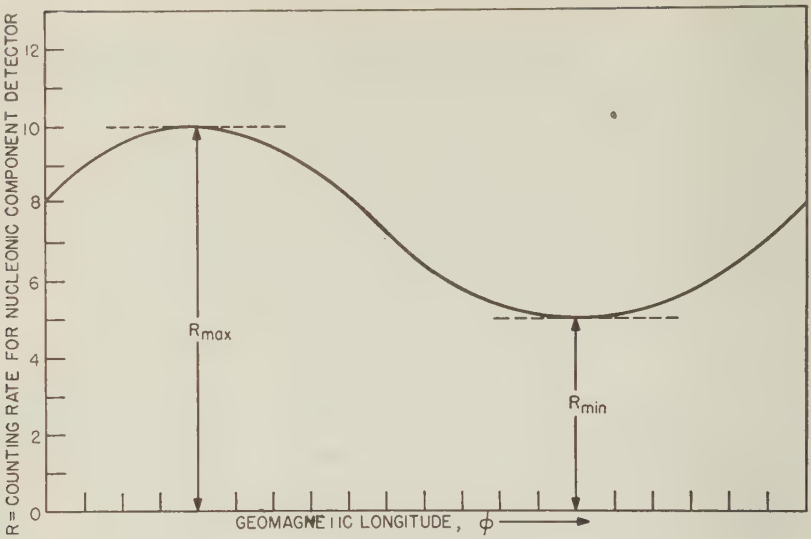

FIG. 3

$\varphi = 0$ to 2π, as shown in Figure 3. We shall define this change as the peak to peak fractional change of intensity A,

$$A = 2\left\{\frac{R_v(\max) - R_v(\min)}{R_v(\max) + R_v(\min)}\right\} \text{ at time } t = \text{const}; \lambda = 0^\circ$$

Therefore, in very good approximation for $Z = 1$,

$$A = \frac{[(1+\delta)^{2m-2} - (1-\delta)^{2m-2}]}{\left[\frac{(1+\delta)^{2m-2}}{2} + \frac{(1-\delta)^{2m-2}}{2} - \left(\frac{15}{N'}\right)^{m-1}\right] + \frac{m-1}{n-1}\left[\frac{(15)^{m-1}}{(N')^{n-1}}\right]} \quad \ldots\ldots(5)$$

A is determined from the nucleonic component measurements. To indicate the magnitude of the effect, we have found that $\delta = 0.0629$ for the 1945 magnetic survey [1]; hence, $A = 0.45$ for $m = 2.35$, $n = 2.60$, $N' = 30$ Bv. Clearly the precision with which δ may be determined depends upon our knowledge of the primary spectrum. Although the above values of m and n fit closely the spectrum studies in recent years, there remains some evidence that m and n may be as large as 2.5 and 2.7, respectively; for this case, $A = 0.46$.

To obtain the experimental points from which A, and hence δ, may be determined, we must know the location of the geomagnetic equator for incoming cosmic-ray particles at several longitudes. This may be determined directly by searching for the minimum value of $R(\lambda)$ along a constant longitude φ (Fig. 1) and corresponds to the equatorial minimum intensity for the latitude curve of the nucleonic component.

If, as we have assumed earlier, we are seeking coordinates for an eccentric dipole magnetic field, then three intensity minima for widely different values of longitude φ will determine a plane for the equivalent cosmic-ray equator. This

will define the axis of the dipole. Obviously, additional points will not only increase the precision in A and axis coordinates, but will also increase the precision in determining the radial direction in the equatorial plane passing through the geoid and magnetic centers; approximately eight additional points would be desirable.

On the other hand, the curve for the longitude effect at the geomagnetic equator (Fig. 3) is not a true sinusoidal curve for two reasons:

(1) From equations (3) and (4), we note that $R_{\min}(\varphi)$ will, in general, contain higher order harmonics [5*a*], and,

(2) The two residual quadrupole terms may introduce a period π. (Vallarta [6] has considered this latter aspect of the problem using the charged-particle component data available prior to 1937 and has shown that the experimental errors at that time concealed any evidence for these residual quadrupole terms.)

If there is an appreciable contribution from (1) to the curve, it may be difficult to separate these two effects unless we know the correct phase for the contribution in second order from the residual quadrupole terms.

In the above discussion, we assumed that the two residual quadrupole terms formed a sectorial quadrupole. If, on the other hand, these terms can be represented by vectors parallel to the eccentric dipole vector, they constitute a zonal quadrupole. This latter solution produces asymmetries of cosmic-ray intensity and hence asymmetries in the latitude effects in the north-south hemispheres [6*a*]. Consequently, rather than use the steep slope portion of the nucleonic component latitude curve for determining eccentricity and location of the magnetic dipole, we have restricted ourselves to the equatorial region, where these north-south asymmetries, if they exist, are negligible.

IV. THE MAGNITUDE OF PERTURBING EFFECTS

Position errors in the identification of intensity minima and other distortions of the experimental latitude curves arise from atmospheric and geomagnetic effects [7]. In this section, we consider the influence of these perturbing effects upon the intensity measurements.

The atmospheric bulge-effect—The gravitational forces acting upon the atmosphere tend to produce an equatorial bulge in the atmosphere. Since the nucleonic component intensity is corrected by a barometric pressure coefficient $\alpha = -0.96$ per cent/mm Hg, it is clear that pressure recording instruments which do not take into account the effect of changing gravitational forces (for example, the mercury barometer) may introduce a small error in the nucleonic component intensity. However, since for a $\pm 30°$ range of latitudes about the geographic equator the maximum error is less than one per cent, this effect will not perturb the location of the intensity minimum of the latitude curves.

The magnetic vs geographic zenith—With the magnetic and geoid centers separated by approximately 400 km, the radial directions for the two centers differ by a varying amount as an observer travels from $\varphi = 0$ to 2π along $\lambda = 0°$. Since the observed intensity of cosmic radiation depends on the angle of observation

with respect to the magnetic zenith, the question arises as to the magnitude of this effect near the geomagnetic equator. In the vicinity of $\lambda = 0°$, the maximum angular difference between the two respective "vertical" directions at the top of the atmosphere is the order of 3°. By measuring nucleonic component intensity, this effect becomes exceedingly small and will not interfere with the determination of the amplitude and phase of the longitude effect.

The effect of local magnetic anomalies—Any magnetic material which produces large-scale distortions of the magnetic field are defined as local magnetic anomalies. There have been several discussions of the effect of anomalies upon cosmic-ray intensity [8]. The effect of the largest known anomaly has been evaluated in Appendix I to show that its influence upon the total cosmic-ray intensity is negligible for the kind of measurements reported in this paper.

The effect of ionospheric currents—The contributions to the external magnetic field which arises from circulating currents within the ionosphere are very small when compared with the effect of the eccentricity of the dipole, and are shown in Appendix II to be unimportant under normal conditions for deflecting cosmic-ray particles.

V. THE PROPOSED MEASUREMENTS

Apparatus and techniques have already been developed for measuring the nucleonic component intensity; the apparatus consists of a geometrical arrangement of lead and neutron moderator—usually paraffin—and electronic apparatus for the measurement of local neutron production arising from the nucleonic component [3,4]. For apparatus already designed, typical equatorial counting rates range from $\sim$ 200 counts per minute at sea-level, with a laboratory-size geometry, to $\sim$ 4,000 counts per minute at 20,000 feet pressure altitude with a smaller geometry for aircraft. In this section, we wish to consider the choice of instrument carrier, surface vessel or aircraft, with respect to the problem of minimizing experimental errors.

Since the absorption mean free path for the nucleonic component in the lower half of the atmosphere is nearly independent of latitude in the range $\lambda \approx \pm 20°$, the fractional change of counting rate with λ (that is, the latitude effect) will be essentially independent of the choice of atmospheric depth for these measurements.

There are other factors, however, which influence the choice:

(*a*) *Total number of counts per degree latitude*—A surface vessel traveling at low speed readily attains a high total count per degree. However, since a latitude interval of $\sim$ 25-30° centered about the geomagnetic equator is to be covered, rather extensive atmospheric pressure corrections may be required over the 4 to 5 day interval, reducing the precision of the observations. On the other hand, aircraft are flown along a course of constant pressure-altitude within close tolerances, and even if the total number of counts per degree is less by a factor of 2 to 3—because of the high aircraft speed—the latitude curve may be determined with greater precision than with a surface vessel.

(*b*) *Corrections for variations of primary intensity with time*—World-wide

recurring intensity variations of ~1-2 per cent amplitude are observed in equatorial latitudes, along with larger, infrequent changes of intensity. The continuous neutron intensity observations at Huancayo, Peru, near the geomagnetic equator and ~ 11,000 feet altitude, are convenient for normalizing the world-wide equatorial measurements [4]. Smaller errors are introduced by these corrections if the total time required to measure the ~ 30° latitude range is short, as in the case of aircraft measurements.

Assuming that the eccentric dipole-field model will be satisfactory for the description of the external field interacting with cosmic-ray particles, some estimates of the over-all errors may be made. With a dipole off-center by ~400 km, the error in this distance would be approximately ±25 km. For the coordinates defining the axial direction, the errors may be ~ 3 per cent.

Appendix I

THE EFFECT OF LOCAL MAGNETIC ANOMALIES

The effect of localized magnetic surface anomalies [9] upon the trajectories of cosmic-ray particles moving in the magnetic dipole field of the earth can be evaluated from the following considerations, which take into account the *maximum* perturbation.

The largest reported magnetic anomaly in the world is that of Kursk, Russia [10], which produces a maximum vertical intensity of ≈ 2 gauss at the surface of the earth. We assume that this anomaly is represented by a small dipole placed in the geomagnetic equatorial plane and at the surface of the earth (see Fig. 4). The value for the magnetic moment is obtained by defining its depth below the

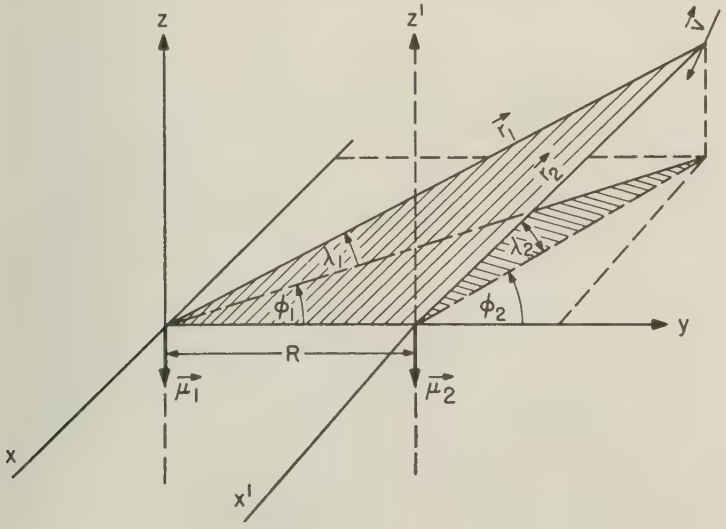

FIG. 4

earth's surface. The relativistic Lagrangian for a particle of charge Ze moving in the combined fields of the earth's centered dipole ($\vec{\mu}_1$) and this local anomaly dipole ($\vec{\mu}_2$) can be shown to be

$$L = -m_0c^2\sqrt{1-\beta^2} + \frac{Ze}{c}(\vec{A}_1 + \vec{A}_2)\cdot\vec{V}_1 \quad \ldots\ldots(6)$$

where $\vec{A}$ is the magnetic vector potential, $\vec{V}_1$ is the velocity of the particle, and where subscript "1" refers to quantities expressed in r_1 , λ_1 , φ_1 coordinate system, and subscript "2" refers to quantities expressed in the r_2 , λ_2 , φ_2 coordinate system. In addition,

$$\vec{V}_1 = \dot{r}_1\hat{e}_{r_1} + r_1\dot{\lambda}_1\hat{e}_{\lambda_1} + r_1\cos\lambda_1\dot{\varphi}_1\hat{e}_{\phi_1} \quad \ldots\ldots(7)$$

$$\left.\begin{aligned}\vec{A}_1 &= -\vec{\mu}_1 \times \vec{\nabla}_1\frac{1}{r_1} = \frac{\mu_1\cos\lambda_1}{r_1^2}\hat{e}_{\phi_1}\\ \vec{A}_2 &= -\vec{\mu}_2 \times \vec{\nabla}_2\frac{1}{r_2} = \frac{\mu_2\cos\lambda_2}{r_2^2}\hat{e}_{\phi_2}\end{aligned}\right\} \quad \ldots\ldots(8)$$

By transforming the Lagrangian to the r_1 , λ_1 , φ_1 system, we obtain (now, omitting subscripts)

$$\left.\begin{aligned}L &= -m_0c^2\sqrt{1-\beta^2} + \frac{Ze}{c}\left\{\frac{\mu_1\cos^2\lambda}{r}\dot{\varphi}\right\}\\ &+ \frac{Ze}{c}(R\mu_2)\left\{\frac{r\sin\lambda\sin\varphi\dot{\lambda} - r\cos\varphi\cos\lambda\dot{\varphi} - \dot{r}\sin\varphi\cos\lambda + \dfrac{r^2\cos^2\lambda\dot{\varphi}}{R}}{(r^2 + R^2 - 2rR\cos\lambda\cos\varphi)^{3/2}}\right\}\\ &\text{For } r > R\end{aligned}\right\} \quad \ldots\ldots(9)$$

where R = distance of dipole from earth center $\approx R_e$ (earth radius). The first two terms on the right (in eq. 9) determine the motion of a particle moving solely in the earth's dipole field, whereas the third term is the perturbation introduced by the local anomaly. The Lagrangian is no longer cyclic in the azimuth angle φ, and there is no Störmer integral of the motion. The differential equations of the motion require for their solution the methods of numerical integration. We shall proceed, however, to use approximations which will give the order of magnitude of the effect.

We begin by considering the "sphere of influence" of the local anomaly (see Fig. 5), by treating the analysis of a particle of charge $Ze(Z = 1)$ and magnetic rigidity N moving solely in the dipole field μ_2 ; thus, this region is one in which the earth's general field is assumed to be negligible. The maximum estimated depth Δ of 1,000 meters for the Kursk anomaly is used to obtain the magnitude of the magnetic moment $|\mu_2| = 2 \times 10^{15}$ ergs/gauss. The dipole lies in the negative z' direction. Vertical "equatorial" cut-off for protons in this field becomes $N_v(\Delta, 0, 0) = 15.0 \times 10^{-3}$ Bv/c. This value is smaller, by a factor of 10^3, than the cut-off at the same point in the earth's dipole field alone.

This perturbation is even less effective in influencing the trajectories of cosmic-ray particles, since (*a*) no magnetic anomalies of this large a magnitude have been found within ±30° of the geomagnetic equator, and (*b*) the above approximations were based upon the most unfavorable assumptions regarding the local magnetic

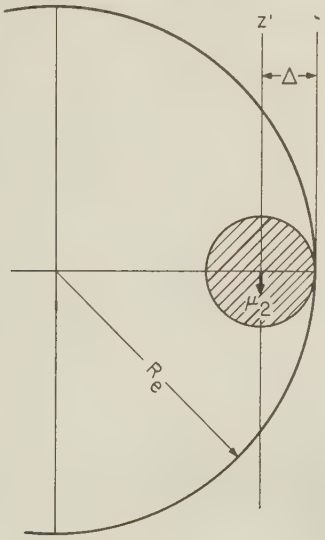

FIG. 5

field—undoubtedly the local anomaly is more closely represented by a quadrupole and higher order terms.

We conclude that local magnetic anomalies may be neglected for the purposes of the studies discussed in this paper.

Appendix II

THE EFFECT OF IONOSPHERIC CURRENT SYSTEMS

In order to minimize the influence of the sun upon the analysis of the geomagnetic field, variations in the earth's field are considered for only exceptionally quiet days of solar activity. These quiet-day, solar daily variations are then said to compose the S_q [1] component of the magnetic field disturbance.

Spherical harmonic analysis of the X, Y, and Z components of the S_q variation from many stations leads to the determination of an overhead horizontal, electric-current system in the upper atmosphere (ionosphere), plus a contribution from a secondary current system flowing within the earth [11]. The X component of the variation (ΔX) is the largest in magnitude; and, as Wasserfall shows in data taken from the Second International Polar Year (1932-33), may become as large as $0\gamma(\gamma = 10^{-5}$ gauss) at highest latitudes in the northern hemisphere. Within ±30° of the geographic equator, however, the variations are smaller in magnitude—not exceeding 40 γ. The contribution to the S_q variation from ionospheric currents is ≈ 0.6.

Although ΔX is measured near the surface of the earth, the success of the model of the infinite, plane, uniform current sheet, used by Chapman and Bartels in predicting current magnitudes, suggests that we may reasonably assume that the field between the earth and the current sheet is essentially constant—this being a property of such a current system model. Consequently, since the value of the earth's dipole field at a distance of 200 km above the earth is

$$\vec{H} = 0.285\ (\cos\lambda\hat{e}_\lambda - 2\sin\lambda\hat{e}_r)\ \text{gauss} \qquad (\lambda = \text{geomagnetic latitude})$$

the variation of the main external field at this height above the earth (approximately the region of the ionosphere) is then within 0 to 0.2 per cent over the range $0 \leqq \lambda \leqq \pi/2$. This periodic variation in the earth's main field can be neglected in so far as its effect upon cut-off energies for incoming particles is concerned.

At very large distances from the earth, the nature of the current systems becomes such that they contribute mostly to the quadrupole and higher order terms in the geomagnetic field. Comparison of the equivalent quadrupole terms of the main earth field and that arising from the current systems shows that the main quadrupole field is at least 2.5×10^2 times larger, which is in agreement with previous considerations [12].

References

[1] E. H. Vestine, *et al.*, Carnegie Institution of Washington, Pub. Nos. 578 and 580 (1947); S. Chapman and J. Bartels, Geomagnetism, Oxford, Clarendon Press (1940).
[2] M. S. Vallarta, Phys. Rev., **47**, 647 (1935); Phys. Rev., **74**, 1837 (1948); E. G. Dymond, Nature, **170**, 1078 (1952).
[3] J. Simpson, Phys. Rev., **83**, 1175 (1951).
[4] J. Simpson, W. Fonger, and S. B. Treiman, **90**, 934 (1953).
[5] S. B. Treiman, Phys. Rev., **86**, 917 (1952).
[5a] This was pointed out to us by Peter Meyer.
[6] M. S. Vallarta, Nature, **139**, 24 (1937).
[6a] F. S. Jory, Ph.D. thesis, University of Chicago (1955); unpublished.
[7] G. Lemaitre, Nature, **140**, 23 (1937).
[8] E. M. Bruins, Physica, **4**, 659 (1937).
[9] S. Chapman and J. Bartels, Geomagnetism, Oxford, Clarendon Press (1940); Vol. I, p. 137. The term "local anomaly" as used in this paper is defined as in the reference, "Deposits of iron ore or other magnetic minerals generally distort or 'disturb' the otherwise even trend of the isomagnetic lines, partly by the field of their own permanent magnetization, and partly by the additional magnetism induced in them by the general field of the earth."
[10] S. Chapman and J. Bartels, Geomagnetism, Oxford, Clarendon Press (1940); p. 150.
[11] S. Chapman and J. Bartels, Geomagnetism, Oxford, Clarendon Press (1940); also K. F. Wasserfall, J. Geophys. Res., **58**, 1 (1953).
[12] J. W. Firor, W. H. Fonger, and J. A. Simpson, Phys. Rev., **94**, 1031 (1954).

THE ANNUAL VARIATIONS OF THE ATMOSPHERICS—EXISTENCE AND EXPLANATION OF A SECOND MAXIMUM IN WINTER, IF ONLY STRONG IMPULSES ARE COUNTED

By Reinhold Reiter

Physikalisch-Bioklimatische Forschungsstelle München, Farchant bei Garmisch, Germany

(Received August 30, 1955)

ABSTRACT

During a period of five years, impulses of atmospherics have been recorded on the following frequency ranges: Range I, about 10 to 50 kc; range II, about 4 to 12 kc. Only such impulses are counted and recorded the amplitudes of which exceed the relatively high threshold value of the amplifier.

Considering the monthly means of the impulse sum per hour, we note that each of these five years shows two maxima. The first maximum, appearing during the summer months (May to August), can be explained easily by the frequency of thunderstorms occurring in central Europe in summer. The second one, however, which appears in winter, is strange.

An exact analysis of the large-scale weather processes results in the following: In the fall, the thunderstorm frequency in central Europe and in the Mediterranean regions is lowered because of large anticyclones (Azores high). During the winter months, violent invasions of polar air-masses into the Mediterranean basin take place. Thus, moist labile gradients are formed over the relatively warm sea-water, which give rise to renewed thunderstorms. These large-scale changes of air-masses are the reason for the observed winter maximum.

During a period of five years, at the Physikalisch-Bioklimatische Forschungsstelle München (Physical-Bioclimatic Research Institute, Munich), readings of atmospherics were recorded continuously. These readings have been evaluated for meteorological and biometeorological purposes. In order to obtain best results with regard to these problems, methods were applied which differed considerably from those generally used for the measurement of the atmospherics, that is to say, from the recording of the *world-wide* thunderstorm atmospherics. By these methods, only those impulses were counted whose amplitudes exceeded a given, relatively high threshold value. This value was of such a dimension that only those impulses were recorded which were emitted by electric discharges occurring in the atmosphere immediately surrounding the station within a distance of about 500 km and, according to the intensity of the individual discharge, up to 2,000

km. For this purpose, two low-frequency amplifiers were established, whose maximum sensitivities moved within the following ranges:

Frequency range I—about 10 to 50 kc
Frequency range II—about 4 to 12 kc

Reception was obtained by means of simple T-aerials of approximately 20-meter length, located 8 meters above the ground-level. According to their purpose, the receiving sets can be rendered so insensitive as to guarantee the omission of artificial disturbances caused by electric apparatus, railways, overhead lines, etc. [for more complete description of the procedure, see 1 of "References" at end of paper] For both frequency ranges, we compared the hourly and diurnal variations of the measured values with the meteorological processes over central Europe. In doing so, we could observe [2] that it was primarily those meteorological processes which caused the temporal variations of the atmospherics. Variations of the ionospheric conditions of transmission for the electric waves applied are of almost no efficacy in our case.

Thanks to the continuous observations covering a period of five years, it is now possible to make accurate statements with regard to the annual variations of the atmospherics thus recorded. The monthly means for both frequency ranges show that two maxima are reached in the course of the year. The higher one appears *in the early summer*, and the other maximum is to be seen *in the middle of the winter*. Figure 1 demonstrates this fact graphically:

Ordinate: Logarithm of the mean impulse sum per hour of the frequency ranges I and II for the respective calendar month

Abscissa: Calendar months of the successive years 1949–1954

A renewed rise of the impulse sum can be seen regularly in December and January. While the summer maximum can easily be explained by the frequency of thunderstorms taking place over central Europe, other explanations have to be found for the winter maximum. The winter thunderstorms over the European continent, which are relatively rare and of short duration, are not sufficient to account for such a maximum.

In our opinion, the winter maximum is due to the invasion of cold air into the western basin of the Mediterranean during winter. The shift of the subtropical high-pressure belt of the northern hemisphere (that is to say, in our case, of the Azores high) towards the north in summer and autum results in a stabilization of the general weather situation over large areas in southern and central Europe during the autumn. This situation is characterized by the formation of large anticyclones. The effect is that a considerable quantity of heat may still be conveyed to the water-masses of the Mediterranean, or at least a too early cooling will be prevented. As is known, the large-scale circulation over the European continent will be transformed between the end of December and the middle of January due to a series of invasions of arctic or polar air-masses, which deeply penetrate also into the Mediterranean basin. This process involves the formation of moist labile gradients over the relatively warm surface of the water, thus creating

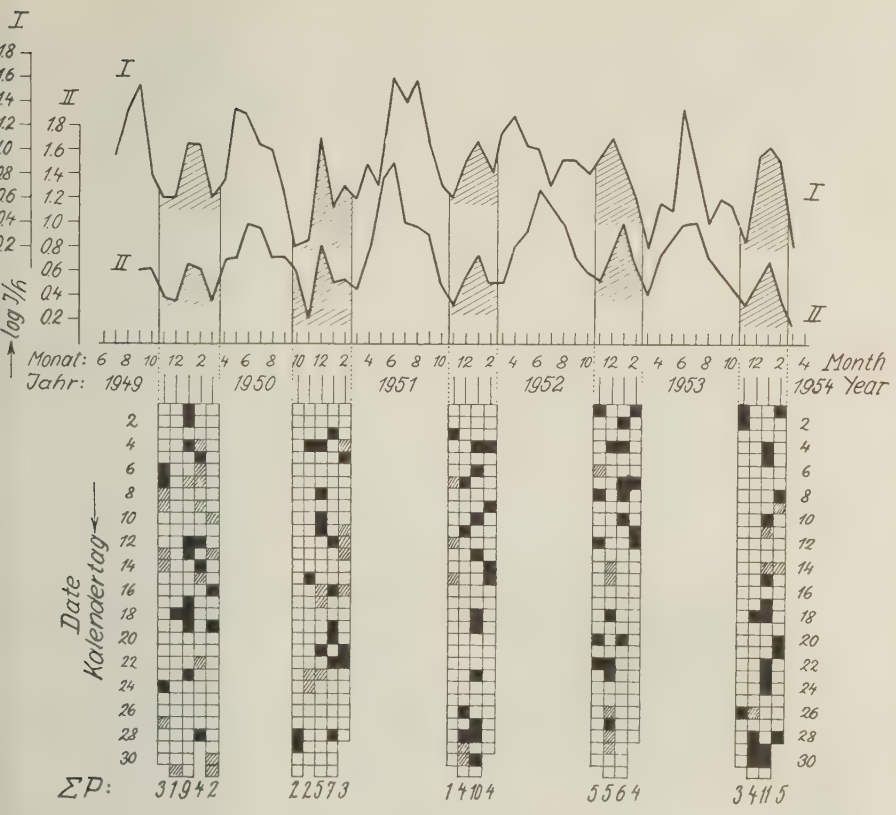

Fig. 1

avorable conditions for violent thunderstorms, especially during the night. These conditions continue until, in the course of some weeks, the water near the urface of the Mediterranean has cooled sufficiently. These thunderstorms over he Mediterranean Sea are an obvious explanation for the winter maximum of the tmospherics recorded in our Institute. In order to prove this statement, we lotted in Figure 1 the invasions of polar air into the western Mediterranean uring the winter months. For the instances of such an invasion, we blackened he square of the day concerned in the monthly column. In doing so, we only ounted the invasion of "fresh" polar air-masses, irrespective of their origin. If he polar air was warmed during a longer way before it invaded the Mediterranean, he square was only hatched. The sum of the invasions of fresh polar air per month s indicated at the bottom of each column. Now, if we compare the frequency of hese invasions of cold air in the individual months with the respective variations f the atmospherics, we can observe a good agreement.

A graph summarizing these considerations (see Fig. 2) will exhibit the following: Ve have entered the monthly means (that is to say, the logarithm impulses per our) obtained from the five years of measurements. The two curves are very

smooth and show distinctly the second maximum. The summer maximum is reached in June (where thunderstorms are the most frequent!), and the winter maximum in January. Furthermore, we have plotted (dashed line) the monthly mean value of the daily frequencies of an invasion of polar air into the western

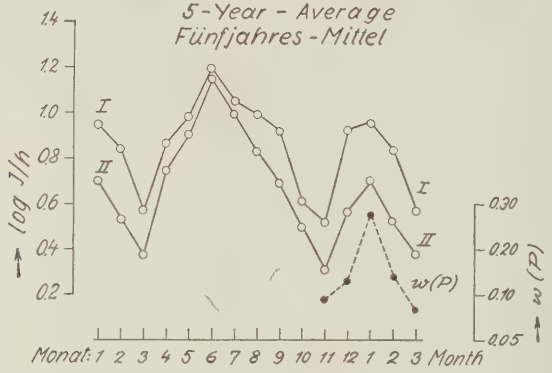

FIG. 2

Mediterranean basin [$w(p)$] for the winter months. From the variations of these means, which run parallel to the variations of the atmospherics, we conclude that the explanation given above for the winter maximum is well-founded.*

A comparison between the monthly means of the frequency ranges I and II shows the following: There is almost no difference between the values of the ordinates I and II as regards the summer maximum, whereas a considerable one is observed for the winter maximum. In the case of the summer maximum, we are mainly concerned with the reception of impulses emitted from sources of the immediate surroundings, whereas in the case of the winter maximum reception is obtained from sources which are at least 600 to 800 km distant. We may probably presume from the above-mentioned difference in the ordinates that over a large distance the low-frequency impulses (frequency range II) arrive with less field intensity than those of the frequency range I.

The example we have considered may demonstrate how useful those recordings of the atmospherics are—if appropriate methods are applied—also for the study of such tropospheric processes which extend over *large areas*.

These results can still be considerably improved by means of a direction-finder, which we have also applied over a certain period.

References

[1] R. Reiter, Arch. Met. Geophys. Biokl., B, 4, 327 (1953).
[2] R. Reiter, Meteorol. Rundschau, 5, 138 (1952).

*It is evident that the temporal coincidence of the maxima of two different functions does not mean that these are bound to be of the same origin. But as the atmospherics measured are caused, in *both* frequency ranges, by thunderstorms, the temporal coincidences of maxima of the two frequency ranges are directly to be understood. It may be mentioned that, also studying the individual days (invasions of cold air), we see that in the statistical mean the atmospherics are increased during these days or in their immediate temporal surroundings.

IONIZATION OF RADIOACTIVE PARTICLES IN THE FREE AIR*

By S. M. GREENFIELD

The RAND Corporation, Santa Monica, California

(Received October 10, 1955)

ABSTRACT

In order to evaluate the possible role of radioactive particles from an atomic cloud as condensation nuclei, an analysis has been made to determine their degree of ionization. Individual radioactive particles become ionized due to β emission, and an estimate of the half-life of these ions has been made for various times in the life history of an atomic cloud. It is concluded that while there is a transient charge on these particles, its half-life is small compared to the disintegration rate, with the result that for all practical purposes radioactive particles in the free air are not necessarily preferred condensation nuclei.

NTRODUCTION

The dust particles in the atmosphere play a specific role in the formation of ur day-to-day weather. Aside from their effect on atmospheric visibility, it is felt nat under the right conditions these aerosols could act as condensation nuclei or the formation of liquid or solid water particles. It has further been suggested nat a particle may be considerably more effective as a condensation nucleus if is ionized.

In the last few years, relatively large quantities of minute radioactive particles ave been released into the atmosphere by the detonation of atomic bombs. Since adioactive decay is accompanied by β emission (electron emission), these particles n their resulting ionized form could conceivably be effective in "seeding" a suitable tmosphere.

It is not the purpose of this paper to examine the argument as to the role of ondensation nuclei in the formation of weather, but rather to attempt to answer ne more detailed question: Do individual particles in a radioactive cloud become onized, and, if so, do they remain charged for any length of time?

HE CHARGE ON A RADIOACTIVE PARTICLE

To determine the possible charge that might appear on a radioactive particle, ne has to make several assumptions about the physical picture. However, since re are interested in the greatest possible ionization of a particle, we will attempt o make assumptions that will in every case maximize this possibility. With this n mind, the following assumptions are made:

*This work was supported by the U. S. Atomic Energy Commission.

1. We will consider an air burst of an atomic bomb of nominal yield an assume that the mass of solid material in the cloud is equal to 1000 kg
2. We will assume that the density of these particles is about 2.7 gm/cm
3. For the first run-through of the problem, we will assume that the clou is made up entirely of particles 0.1 micron in diameter. In this case each 0.1-micron particle will weigh 1.4×10^{-15} gm and the cloud wi contain $10^6/(1.4 \times 10^{-15})$ particles, or 7.1×10^{20} particles.
4. Also, for the first run-through, we will examine the charge on the particl when the cloud is five minutes old and already stabilized. We wil assume that at 5 minutes this atomic cloud is composed of a toroic which contains essentially all the radioactive material, immersed i a cloud formed of condensed water vapor. We will further assume tha this toroid occupies approximately one-half of the total cloud volume It can be said, then, that the bomb debris is contained in a volum of 20 km^3 (20×10^{15} cc) and that the particle density is 3.55×10 particles per cubic centimeter. Because approximately two β particle are given off for every γ photon ray [see 1 of "References" at end o paper], we can express the total activity on a single particle (in dis integrations per second) as a function of time as follows:

$$A_T = 3(F)(A_\gamma)_1(D)t^{-1.2} \quad (1$$

where $(A_\gamma)_1$ is the total γ emission of the fission products at on minute in megacuries, D is the number of disintegrations per secon (dps) per megacurie, F is the fraction of the total active cloud con tained in one particle, and t is the time in minutes. From the atomi weapons handbook [1], we obtain the fact that at one minute th total γ emission from fission products from an atomic bomb of nomina yield is of the order of 8.2×10^5 megacuries. Since each particl contains $(1.4 \times 10^{-15})/10^6$ of the total mass and one megacurie o activity is equivalent to 3.7×10^{16} dps, we can say that the tota activity per particle at one minute is

$$A_1 = (1.4)(3.7)(8.2)(3)(1) \cong 130 \text{ dps/particle}$$

At five minutes, then, the activity per particle is

$$A_5 = \frac{130}{6.9} = 18.9 \text{ dps/particle}$$

and at five minutes we have (18.9) 3.55×10^4 dps in each cubi centimeter, or 6.7×10^5 dps/cc.

We will further assume that

5. The emission of a γ-ray photon does not contribute to charging th particle. This assumption can be shown to be reasonable, even thoug a fission-product γ ray having an energy of 0.7 Mev is in the regio of the Compton effect. For example, if the particle is composed o aluminum oxide, the absorption coefficient of 0.7-Mev γ-ray photon

is < 0.2 cm^{-1}. Putting this in the standard absorption equation, $I = I_0 e^{-\mu x}$, where I is the intensity of a beam of photons after penetrating a distance x (in cm) through a material whose absorption coefficient is μ, will indicate the probable reduction of the beam intensity due to the Compton effect. Since the average path length of a γ-ray photon through a particle is approximately the radius of the particle, we see that for a 0.1μ aluminum-oxide particle the average intensity is

$$\bar{I} = I_0 e^{-<2\times10^{-6}} \cong I_0(1 - < 2 \times 10^{-6})$$

or a reduction in the beam of less than two parts in a million. This reduction would certainly result in a negligible amount of electron emission.

Having set down the above assumptions and some of the more quantitatively available parameters, one can complete the outline of the problem by stating the physical picture of what happens when radioactive particles emit electrons in the atmosphere. When an electron is emitted from a particle, two basic things occur: first, the particle becomes positively ionized; second, the electron produces a succession of ion-pairs along its path as it travels through the atmosphere. The exact number of ion-pairs produced per centimeter of travel depends essentially on the atmospheric density. Since the electron gives up approximately 33 electron volts for every ion-pair formed, it will have a very definite range in the atmosphere.

We have the situation of a particle being ionized and at the same time a relatively large number of atmospheric ions being formed in close proximity to it. These atmospheric ions can recombine or can drift off and attach themselves to charged or uncharged particles, any of these events having a finite probability of occurring. With atmospheric and particle ions constantly being produced and destroyed, the question of whether or not a particle builds up a charge is simply the question of whether ionization takes place on the particle faster than neutralizing atmospheric ions can attach themselves to it. To answer this question, let us postulate the condition of ion balance, that is, the condition when the rate of production of atmospheric ions and charged and uncharged particles is equal to their rate of destruction. This can be stated mathematically, as follows:

$$\frac{dN_-}{dt} = q_- + q_p - \alpha_1 N_- N_+ - \alpha_2 N_- N_p^+ - \alpha_3 N_- N_p = 0 \quad \ldots\ldots(2)$$

$$\frac{dN_+}{dt} = q_+ - \alpha_1 N_+ N_- - \alpha_4 N_+ N_p - \alpha_5 N_+ N_p^- = 0 \quad \ldots\ldots(3)$$

$$\frac{dN_p^+}{dt} = q_p \frac{N_p}{N_{pT}} - \alpha_2 N_- N_p^+ + \alpha_4 N_+ N_p = 0 \quad \ldots\ldots(4)$$

$$\frac{dN_p^-}{dt} = \alpha_3 N_- N_p - \alpha_5 N_p^- N_+ - q_p \frac{N_p^-}{N_{pT}} = 0 \quad \ldots\ldots(5)$$

$$\frac{dN_p}{dt} = \alpha_2 N_- N_p^+ + \alpha_5 N_+ N_p^- - \alpha_1 N_+ N_p - \alpha_3 N_- N_p + q_p \left[\frac{N_p^- - N_p}{N_{pT}}\right] = 0 \quad \ldots\ldots(6)$$

where

q_+ and q_- are the number of atmospheric ions formed per cc per second
N_- is the number of negative ions per cc
N_+ is the number of positive ions per cc
N_p^+ is the number of positively charged particles per cc
N_p^- is the number of negatively charged particles per cc
N_p is the number of neutral particles per cc
N_{pT} is the total number of particles per cc
q_p is the number of dps/cc due to β decay
α_1 is the recombination coefficient for positive and negative ions
$\alpha_2 = \alpha_5$ is the recombination coefficient for negative and positive ions and charged particles
$\alpha_3 = \alpha_4$ is the attachment coefficient for positive or negative ions and neutral particles

Values can be assigned to several of these parameters, as follows:

$N_{pT} = 3.55 \times 10^4/\text{cm}^3$ (from assumption 5 of this section)
$q_p = \frac{2}{3}(6.7) \times 10^5$ dps/cc $= 4.5 \times 10^5$ dps/cc
$\alpha_1 = 1.6 \times 10^{-6}$ cm^3/sec [2]
α_3 and $\alpha_4 = 10^{-6}$ cm^3/sec [3]

Values of α_2 and α_5 can be obtained from the following equation of J. J. Thompson:

$$\alpha = \frac{\pi\sigma 2Ae^2}{\sqrt{3RT}}\left(\frac{1}{M_p}+\frac{1}{M_i}\right)^{1/2} \quad \ldots\ldots\ldots\ldots\ldots\ldots\ldots\ldots (7)$$

where

σ is the radius of capture $\cong$ radius of particle (10^{-5}cm)
A is Avogadro's number $= 6.03 \times 10^{23}$
e is the charge of the electron $= 4.8 \times 10^{-10}$ esu
R is the universal gas constant $= 83.15 \times 10^6$ ergs/deg
T is the temperature (say at 20,000 feet) $\approx 250°$K
M_p is the molecular weight of particle
M_i is the molecular weight of the ion (28 to 32)—we will assume 30

Since $M_p \gg M_i$, we can neglect $1/M_p$; therefore, $\alpha_2 = \alpha_5 = 6 \times 10^{-6}$. The values of q_+ and q_- are essentially equal to the number of ion-pairs formed per cubic centimeter. From the atomic weapons handbook [1], we find that β rays have an average energy of 0.5 Mev and therefore a range of about 100 cm in air (the effective range of these rays is actually much less due to collisions). These β rays will produce an average of 150 ion-pairs per centimeter of travel. At five minutes, since only two-thirds of the disintegrations are β rays and therefore effective in producing ion-pairs, we can say that $\frac{2}{3}$ (6.7×10^5) (1.5×10^4) ion-pairs/cc/second are formed, or 6.7×10^9 ions/cc/second. That this is a reasonable figure can be seen if one takes a volume whose dimensions are large relative to the effective range of the β particle. In this case, on the average, as many paths will extend out of this

volume as will enter it, and if one then computes the number of ion-pairs/cc/second that are formed, it will be found to agree with the figure as given.

It should be noted that in the assumption of equilibrium conditions (ion balance) and in the use of J. J. Thompson's equation, it is indirectly assumed that both the atmospheric ions and the particles are no more than singly charged. It is normally assumed that atmospheric ions are also singly charged. If, in the solution of these equations, it turns out that $N_p^+ < N_{pT}$, then the complete assumption is valid. If, however, $N_p^+ > N_{pT}$, it is evident that the particles are multiply charged and this analysis is no longer valid.

SOLVING THE EQUATIONS

Unfortunately, these equations cannot be solved directly. A solution was found, however, under the assumption that the negative atmospheric ion density was equal to the positive ion density. If we accept the necessary condition of conservation of charge, we can examine the validity of this assumption. This condition is expressed in the following relationship:

$$0 = N_+ - N_- + N_p^+ - N_p^- \quad \ldots\ldots\ldots\ldots\ldots\ldots (8)$$

Using this equation and the values obtained for N_p^- and N_p^+ in the solution of the ion-balance equations, it is possible to show that $N_+ = N_-$ to within one part in 10,000. Therefore, we will accept the value for N_p, N_p^+, and N_p^- as obtained. These values were $N_p = 2.18 \times 10^4$ particles/cc, $N_p^+ = 0.732 \times 10^4$ particles/cc, and $N_p^- = 0.638 \times 10^4$ particles/cc. Stated in percentages, 61.5 per cent of the particles contained *no charge*, 20.6 per cent contained a single positive charge, and 17.9 per cent contained a single negative charge. Under the assumption of equality, $N_+ = N_- = 6.5 \times 10^7$ ions/cc. Furthermore, the half-life of the singly-charged positive particle is given by

$$\lambda = \frac{1}{\alpha_2 N_-} = \frac{1}{390} \text{ sec} \quad \ldots\ldots\ldots\ldots\ldots\ldots (9)$$

as compared to the time between disintegrations of 1/12.6 second. In other words, a few particles will be singly charged, but the half-life of these charges is less than 1/20 of the time between disintegrations. This indicates a very short lifetime, with practically no probability of becoming more than singly charged. We may say, then, that although these particles might conceivably contain a small intermittent positive or negative charge, effectively their net charge is zero.

Dr. R. E. Holzer, of the Institute of Geophysics at the University of California at Los Angeles, in consultation with RAND, has concurred with the above analysis, and has indicated how it might easily be extended (in a semi-quantitative way) to include particles whose diameters are greater or less than 0.1μ. From Eqs. (2) to (6), we can arrive at the following relationship:

$$N_p^- \propto \frac{\alpha_3}{\alpha_2} N_p$$

As we go to larger and larger particles, the recombination and attachment coefficients α_2 and α_3 approach each other in magnitude. This is mainly because in

the limit the size of the charge center becomes very small relative to the actual size of the particle; hence, the capture cross-section becomes more dependent on the geometrical size of the particle rather than on the energy due to the charge. In this case, the actual size of the particle assumes the major role in determining its capture cross-section. Since the geometric sizes of a charged and an uncharged particle are essentially equal, in the limit their capture cross-sections must also be equal. As $N_p^+ \approx N_p^-$, we can say further, for very large particles, that as the limiting condition is approached, $N_p^+ = N_p^- = N_p = \frac{1}{3} N_p$. This, however, still provides us with only a fraction of the particles singly charged with any one sign at a given time, and with a relatively short half-life.

In a similar manner, we may consider particles smaller than 0.1μ. As we decrease the diameter of the charged particles, their recombination coefficients approach the limit of $\alpha_1 = 1.6 \times 10^{-6}$, the recombination coefficient of molecular ions. However, α_3, being determined only by geometric considerations, can continue to decrease below this limit. This means that the ratio α_3/α_2 will continue to decrease, so that the ratio of charged to neutral particles decreases. Although the total number of charged particles increases, the relative number of charged to uncharged particles decreases, and the conclusions of the primary analysis continue to be valid.

NUMERICAL CALCULATIONS

Let us examine the results of varying the parameters in the above equations and analysis.

A. We will examine the cloud at $H + 4$ hours rather than at $H + 5$ minutes, and we will assume that the particle concentration remains the same at $3.55 \times 10^4/\text{cm}^3$. In this case, the number of atmospheric ions of any one sign is decreased to $6.3 \times 10^6/\text{cm}^3$. The percentage of neutral particles increases to 74.6 per cent, and the percentages of positively charged and negatively charged particles are, respectively, 12.8 and 12.6 per cent.

B. For the second case, we will consider time $H + 36$ hours and assume that the concentration of particles has decreased by a factor of 10^3 (particle concentration now $35.5/\text{cm}^3$). In this case, the number of atmospheric ions of any one sign has dropped to 5.36×10^4, whereas the percentages remain essentially the same; for example, the percentage of neutral particles has dropped to 69.4 per cent.

The above simple calculation serves to show the relative insensitivity of the percentages of charged and uncharged particles to changes in concentration and ion density, and bears out the previous contention that these percentages should be determined almost completely by the relative values of attachment and recombination coefficients.

CONCLUSIONS

It appears reasonable to state that for all practical purposes there is no net charge on radioactive particles in the free air due to β emission. This does not mean

t a particle does not have a charge at any time, but rather that the half-life of s charge is small compared to the disintegration rate. This is shown by Eq. (9), ording to which it is conceivable that after many hours (or days) of decay a rticle that is singly charged by β emission could retain its charge for several onds. For example, in Case B of the preceding paragraph, after 36 hours the arge on a particle has a half-life of the order of 3 seconds, whereas the time ween disintegrations is of the order of 80 seconds. This is contrasted with the f-life of the order of 0.003 second for the charge on a particle which has undergone ly 5 minutes of decay, at which time the time between disintegrations is of the der of 0.08 second.

Apparently, so far as the effect of radioactivity-induced ionization is concerned, omic debris cannot claim a priority position as condensation nuclei, but must ke their place in the long line of other small particles normally present in our nosphere.

One final point of clarification: According to our assumption that the attachnt and recombination coefficients of large and small ions are equal regardless sign, one would expect $N_p^+ = N_p^-$. As was indicated above, this is not exactly ue. The value of N_p^+ is slightly higher than N_p^- in all cases. It is felt that this all discrepancy is mainly due to the prejudicing in favor of N_p^+ that occurs in β ission. This is shown explicitly when Eqs. (4) and (5) are solved simultaneously. should be noted, however, that this slight discrepancy in no way changes the ginal premise, in that the total number of charged particles is still considerably aller than the number of neutral particles.

References

[1] The effects of atomic weapons (prepared for and in cooperation with the U. S. Department of Defense and the U. S. Atomic Energy Commission), Los Alamos Scientific Laboratory, Los Alamos, New Mexico (August, 1950).

[2] Terrestrial magnetism and electricity (edited by J. A. Fleming), *Physics of the Earth—VIII*, auspices of National Research Council, 2nd ed., pub. by Dover Publications, Inc., New York (1949); chap. 4 by O. H. Gish, p. 178.

[3] Compendium of meteorology (edited by Thomas F. Malone), American Meteorological Society, pub. by Waverly Press, Inc., Baltimore (1951); p. 123.

STANFORD-SEATTLE WHISTLER OBSERVATIONS

BY J. H. CRARY,‡ R. A. HELLIWELL,‡ AND R. F. CHASE†

‡*Radio Propagation Laboratory, Stanford University, Stanford, California*
†*Boeing Airplane Company, Seattle, Washington*

(Received November 1, 1955)

ABSTRACT

Simultaneous observations of times of occurrence of whistlers were made at Seattle, Washington, and Stanford, California, two hours every week from October 1951 to October 1952. Times were measured to an accuracy of about ±1 second. The objective was to determine the percentage of whistlers received at either station which were coincident at both.

A total of 318 whistlers was received at Stanford and 283 at Seattle during simultaneous observations. The occurrence rate of whistlers (during a two-hour period) varied from 0 to roughly 55 per hour at Stanford and from 0 to 70 per hour at Seattle. The correlation between the occurrence rates was poor.

The number of true coincidences was found by subtracting the number of chance coincidences from the number of total coincidences. A method for computing the number of chance coincidences from a knowledge of the time intervals between whistlers at the one station was derived. The analysis showed that approximately 22 per cent were observed simultaneously at both stations.

This result is examined in relation to possible theories of whistler origin and propagation, and is shown to support the Storey-Eckersley theory.

Introduction

It is the purpose of this paper to describe a two-station study of "whistlers." he results are interpreted as supporting the Eckersley-Storey theory of origin. ollowing Storey [see 1 of "References" at end of paper], the term whistler as ed herein includes the type of audio-frequency atmospheric frequently described the term "swish." The phenomenon is quite distinct from the related "tweek," "chink" (sometimes called "short whistler") which results from repeated re-ections between earth and ionosphere of the pulse from a distant lightning scharge.

Whistlers may be observed on long telephone lines or with the aid of a sensitive udio-amplifier connected to a long wire or loop antenna. They resemble a rough histling tone, with varying degrees of "musical" quality, descending in frequency om several kilocycles to a few hundred cycles in an interval of about one second. ney are frequently found to follow ordinary atmospherics with a delay of one to

three seconds. Sometimes they occur in trains of echoes or multiples, separated by one to three seconds, and with an attenuation of about 10 db from one echo to the next.

An explanation of the frequency variation of whistlers was proposed many years ago by Eckersley [2], following a suggestion by Barkhausen [3]. Eckersley pointed out that energy at very low frequencies can travel through the ionosphere in the extraordinary longitudinal mode because of the effect of the earth's magnetic field. The magneto-ionic equations require that the group velocity be proportional to the square root of the frequency f of the wave energy. This relation was verified by the experimental results, which showed that $f^{1/2}$ varies linearly with elapsed time.

Recently, Storey [1] obtained new experimental data, with which he confirmed and extended Eckersley's theory. He showed that a static magnetic field in the presence of sufficient ionization exerts a guiding effect on energy traveling at frequencies well below the gyromagnetic frequency. He postulated that the energy from a lightning discharge which enters the ionosphere is guided by the earth's field far out into space and back to earth in the opposite hemisphere. There it is reflected and the process is repeated. This theory accounts both for the atmospherics which sometimes precede whistlers, and for the multiples sometimes observed. Whistlers not preceded by atmospherics are explained as being generated by lightning in the opposite hemisphere. An important point in the theory is the requirement of appreciable ionization over a path extending several earth radii out into space.

A consequence of the theory is that whistlers should not be present at the magnetic equator. Extensive listening tests at Achimota, Gold Coast, West Africa, failed to detect a single whistler [4], thus giving further support to the theory.

Whistlers may also serve as a tool for study of the outer ionosphere, which is virtually inaccessible by other means. This possibility arises from the fact that the Eckersley-Storey theory of origin, which is based on the extraordinary longitudinal mode of propagation, requires a transmission path extending far beyond the limits of the known ionosphere. It may even be practical to use man-made signals for this purpose, and thus provide direct control of the location and nature of the transmitted signal. Progress in this field is particularly timely now, because of the great potential value of whistlers in the forthcoming International Geophysical Year (1957-58).

Observations and Results

Whistlers were observed at Seattle, Washington, and at Stanford, California (separated by 1130 km), for the purpose of determining the degree of correlation between the occurrences of whistlers at the two locations. It was expected that the results would determine to what extent whistlers are localized geographically. The negative results of an earlier coincidence test* between the east and west

*Simultaneous observations were made during 1940 and 1941 by R. F. Chase at Seattle and E. T. Burton of the Bell Telephone Laboratories at New York. These tests were made on a once-a-week basis, each listening period varying from two to four hours. There were 29 whistlers observed at Seattle, and 80 whistlers at New York. No coincidences were obtained.

oasts of the United States indicated that whistlers could not be detected simultaneously over such distances. However, Storey's theory indicates that a strong whistler should be detectable over an area with a radius of several hundred kilometers. Therefore, if Storey's theory is correct in this respect, an appreciable coincidence rate should be observed between Stanford and Seattle.

The antenna used at Stanford was a 12-turn loop in the form of a square, 13 eet on a side. This fed a conventional preamplifier of approximately 80-db gain. Filters were used to attenuate frequencies below one kilocycle and above 20 kc. The output of the preamplifier was connected to a commercial tape-recorder and nd audio-monitoring amplifier with loud-speaker.

The equipment used at Seattle was constructed and operated by R. F. Chase. t was similar to the Stanford equipment in most respects, but the loop was smaller. Head-phones were used for monitoring.

Observations were made simultaneously, except for occasional equipment ailures, between the hours of 1900 and 2300 PST for a period of two hours one ay per week from October 1951 to October 1952. There were 318 whistlers bserved at Stanford and 283 at Seattle during periods of simultaneous obserations. The time of occurrence of each whistler was recorded to the nearest half-econd, using a watch or clock with a sweep second-hand. Timepieces were checked gainst WWV time-signals at regular intervals. The systematic watch-error was easured and removed from the data. The whistlers observed at Stanford were ecorded on magnetic tape, and for the stronger ones the frequency variation with me was determined with a spectrum analyzer. About 20 whistlers were analyzed n this manner, and in each case the curve of $f^{-1/2}$ *versus* time was linear, showing hat they are the same type of whistling atmospheric studied by Eckersley and torey. It is believed that at both locations the sensitivity of detection was appreciably limited by a combination of internal set-noise and power-line interference, s well as by the usual impulsive atmospherics. More whistlers might have been btained had receiving conditions been better.

The hourly rates of occurrence for each observing period at both Seattle and tanford are plotted in Figure 1. Days on which no observations were made are ndicated by the symbol "NR." It is seen that the occurrence of whistlers varies idely from week to week, as has been noted by Storey [1]. On May 12, 1952, for xample, the rate was 55.4 per hour at Stanford, but on many days no whistlers ere heard during the two-hour listening period. It is difficult to establish the etailed seasonal variation of whistler occurrence from these data; however, the ata show a tendency for whistler activity to be a maximum during springtime. here was a tendency for periods of activity to coincide at the two stations. There ere also days, such as 18 August, on which the rate was high at one station and low r zero at the other.

To determine the number of apparent coincidences, the time of occurrence f each whistler at Stanford was subtracted from that of the nearest Seattle histler and the number of such pairs was plotted as a function of the time differnce of the pair for all values less than 50 seconds. Ninety-seven such differences ere obtained. The results are shown in Figure 2. Seven cases lie between the lotted interval and about 750 seconds. The data include both true coincidences nd chance coincidences.

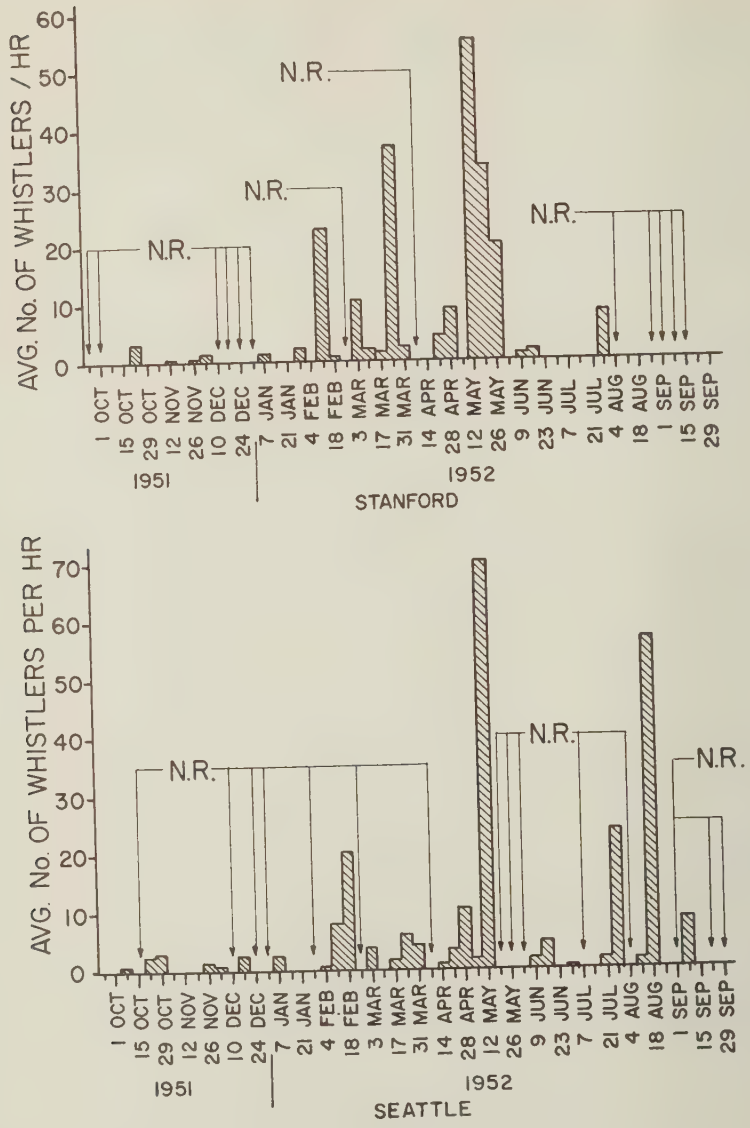

FIG. 1—Average hourly rate of occurrence of whistlers at Seattle and Stanford; observatio were made once each week for approximately two hours between 1900 and 2300 PST from Octob 1951 to October 1952

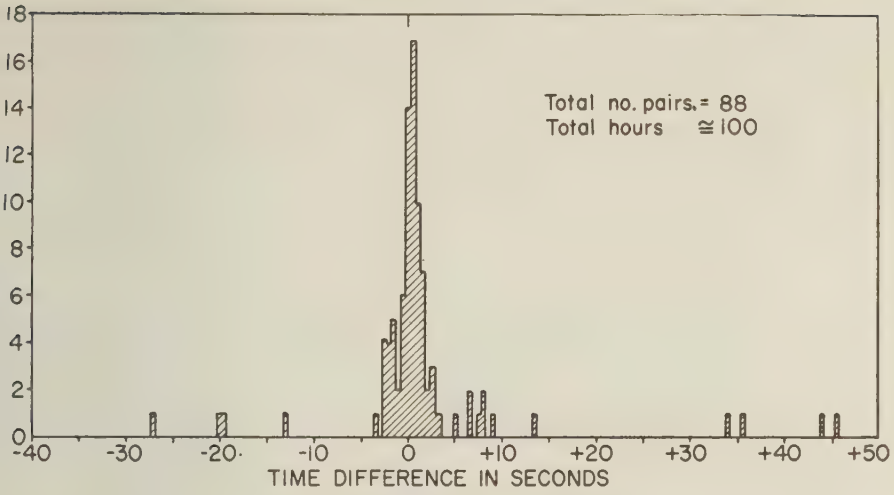

IG. 2—Total number of coincidences of whistlers at Stanford and Seattle *vs* difference in times of occurrence

A true coincidence is defined as the occurrence of the same whistler at both ocations. In general, the times recorded at Stanford and Seattle for a single histler differed because of errors introduced by factors such as the reaction time the listener, ability to read the clock, calibration of the clock, and local noise-vel. Appearing among the true coincidences are what might be called chance incidences, which result when different whistlers are observed at the two loca-ons. It is assumed that the times of occurrence of different whistlers are unrelated. he problem is to estimate the total number of chance coincidences and subtract is from the number of apparent coincidences. This difference is then the total umber of true coincidences.

The number of chance coincidences may be estimated by considering the atistics of the times of occurrence of whistlers at one location. Consider that a histler occurs at the reference station, Stanford. What is the probability that a ifferent whistler will occur at Seattle within a given time-interval centered on the me of occurrence of the Stanford whistler? Since it is assumed that the two histlers in question are unrelated, this is the same as the probability of the ccurrence of a whistler at Seattle within the same time-interval centered on any rbitrary point in time. This probability may be determined as follows: The time xis is divided into N equal intervals of 0.5 second (corresponding to the timing recision). From the center of each such interval at time t_k , the interval m to the earest whistler is determined to the nearest 0.5 second and the number of occur-nces of each value of m determined as a function of m. When there are two histlers at equal intervals, the convention of taking the later whistler was llowed. Thus, for every time t_k , there will be one and only one value for m. The robability of a chance occurrence within a given interval j is then measured by e number of occurrences x_m within this interval, divided by the number of

occurrences in all intervals, which is equal to N. The probability $p(j)$ may then be written as

$$p(j) = \left.\begin{aligned} &\frac{\sum_{-j/2}^{j/2} x_m}{\sum_{-\infty}^{\infty} x_m} \\ &= \frac{1}{N} \sum_{-j/2}^{j/2} x_m \end{aligned}\right\} \quad \ldots\ldots\ldots\ldots\ldots\ldots\ldots\ldots (1)$$

The use of the interval symmetrical about zero simplifies the determination of the number of coincidences. Now, let n_j be the total number of apparent coincidences within the interval $-j/2$ to $j/2$. The expected number of chance coincidences is then $n_j p(j)$. The number of true coincidences is the difference between the total and the chance coincidences, or

$$n_j - \frac{n_j}{N} \sum_{-j/2}^{j/2} x_m \quad \ldots\ldots\ldots\ldots\ldots\ldots\ldots\ldots (2)$$

This curve should rise from zero and approach a horizontal asymptote, at which no further true coincidences are added.

Using the time differences between Seattle whistlers, a simple method of computation was devised. Consider a series of whistlers occurring at arbitrary times t_i at Seattle, as in Figure 3. There is a time difference T_i to the next whistler.

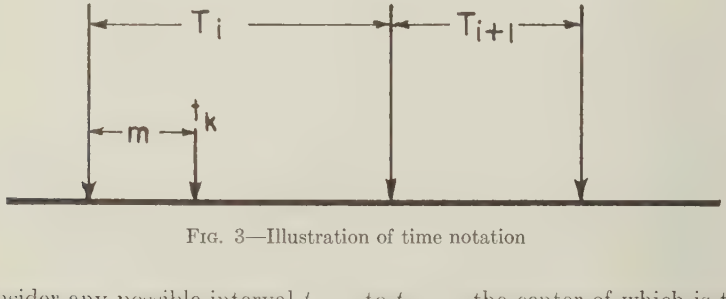

FIG. 3—Illustration of time notation

Now consider any possible interval $t_{k-1/2}$ to $t_{k+1/2}$, the center of which is time t_k. For any value of t_k, there will be a time interval m to the nearest whistler at time t_i. If all the possible t_k's are considered, all positive and negative values of m will occur between 0 and $T_i/2$. For example, at time $t_k = t_i$, $m = 0$. As t_k increases, $m = t_i - t_k$ when $t_k < \{t_i + [(t_{i+1} - t_i)/2]\}$. For $\{t_i + [(t_{i+1} - t_i)/2]\} < t_k < \{t_{i+1} + [(t_{i+2} - t_{i+1})/2]\}$, then $m = t_{i+1} - t_k$. Or, all positive and negative values of m from 0 to $T_i/2$ are encountered. When t_k lies half-way between t_i and t_{i+1}, the convention of taking the positive sign for m is followed.

The computation was carried out as follows. For each whistler at Seattle which was one of a pair with a Stanford whistler, the time difference to the next

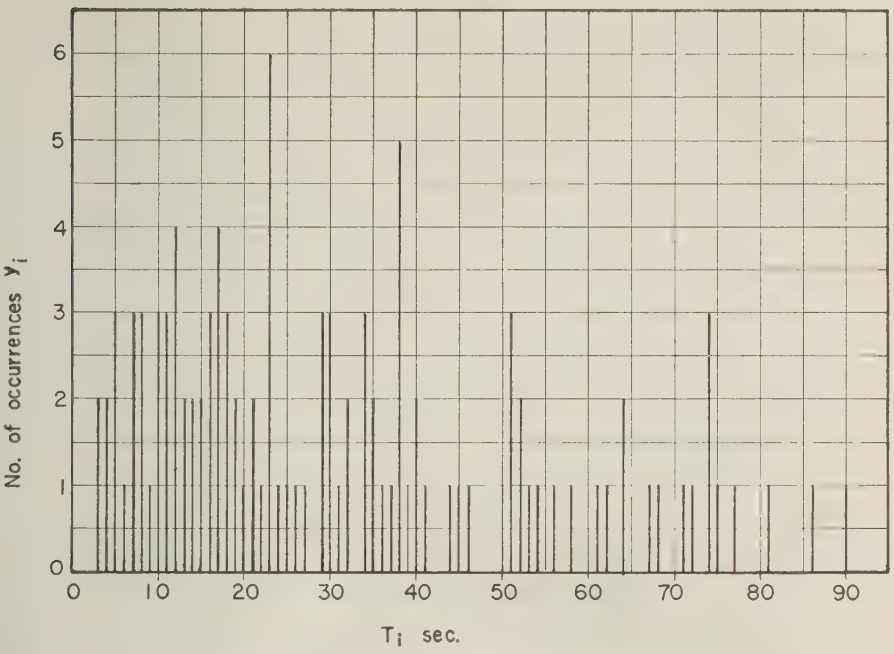

FIG. 4—Frequency of occurrence of interval between Seattle whistlers

whistler in each direction was computed. The results were tabulated as number of occurrences y_i for each time difference T_i , shown in Figure 4.

The total number of cases x_m for any positive m is clearly equal to the total number of recorded time-differences equal to or greater than $2m$ and for negative m the total number greater than $|\ 2m\ |$. This difference results from the convention of taking the positive sign when t_k lies midway between two whistlers. Each time this occurs, a case is added to the positive half of the curve but not the negative. Thus, we can write

$$x_m = \sum_{i=2m}^{+\infty} y_i \ , \qquad m \geqq 0 \ \ldots\ldots\ldots\ldots\ldots\ldots\ldots\ldots (3)$$

or

$$x_m = \sum_{i=2m+1}^{+\infty} y_i \ , \qquad m < 0 \ \ldots\ldots\ldots\ldots\ldots\ldots\ldots\ldots (4)$$

The probability $p(j)$ may then be computed from (1), and is shown in Figure 5.

The values of n_i , $n_i p(j)$ and $n_i - n_i p(j)$ are shown as a function of j in Figure 6. Although the curve should theoretically approach a horizontal asymptote, it actually reaches a broad maximum at $j = 19$ and then falls off slowly. The reasons for this behavior are not quite clear, although the following factors are to be considered. One possibility is inadequate number of data. Another is the possibility that the probability of occurrence of a whistler at one location depends on the

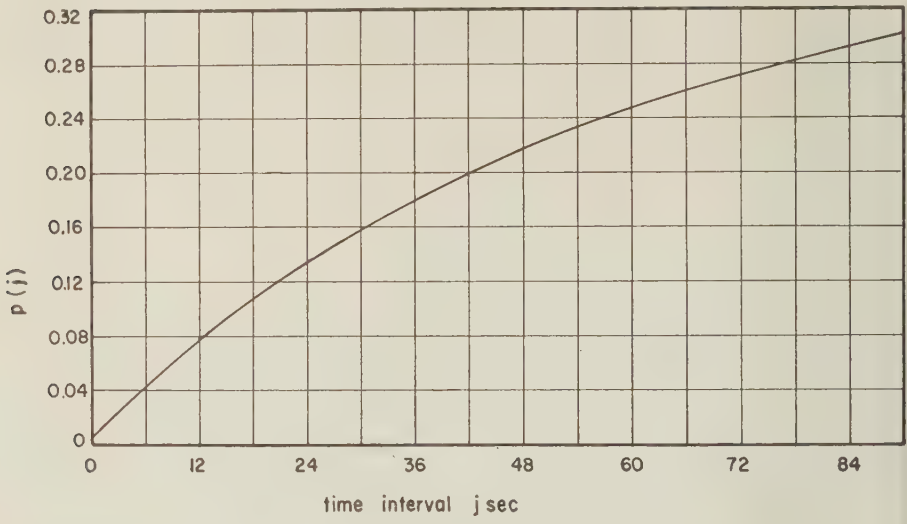

FIG. 5—Probability of the occurrence of a whistler at Seattle within a given time-interval

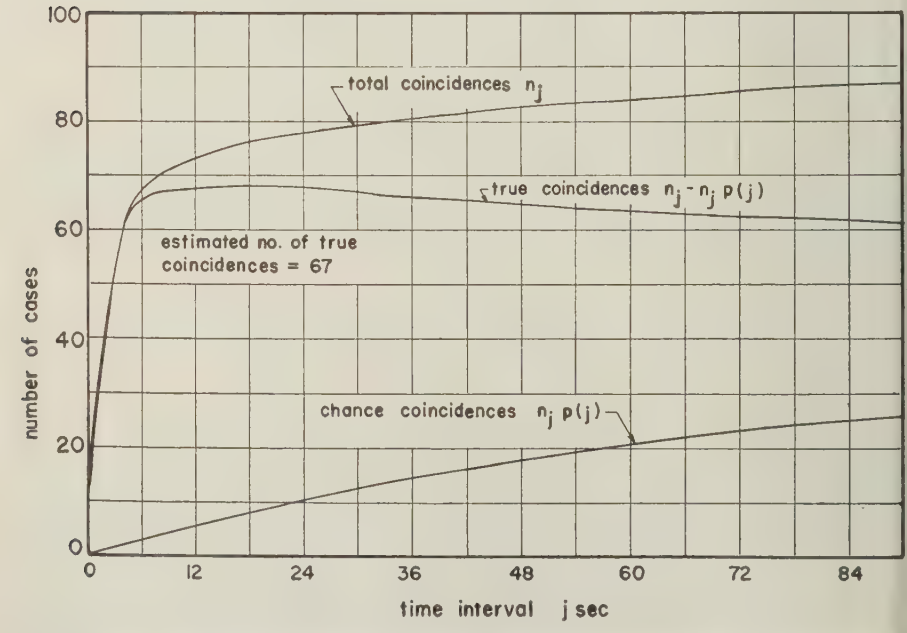

FIG. 6—Total number of coincidences n_j, number of chance coincidences $n_j p(j)$, and number of true coincidences $n_j - n_j p(j)$ within a given time-interval

occurrence of a different whistler at the other station. No attempt was made to evaluate this factor, if it exists. A more likely cause is a bias resulting from diversion of the observer's attention while recording data. Thus, there is a tendency for the observer to concentrate on the timing and recording of data for a period of about one to 15 seconds following a whistler, and so possibly to overlook a whistler in this short interval; this seems highly probable when a strong whistler is followed by a weak one. Any increase in the number of cases in this short interval would tend to raise the $p(j)$ curve and thus flatten the $n_i - n_i p(j)$ curve. On this basis, the asymptotic value of the curve, which is the number of true coincidences, was estimated to be 67.

The total number of whistlers observed was 283 at Seattle and 318 at Stanford. The estimated true coincidence rates are then

$$\left.\begin{aligned} \text{Stanford:}\quad & \frac{67}{318} = 21.1 \text{ per cent} \\ \text{Seattle:}\quad & \frac{67}{283} = 23.7 \text{ per cent} \end{aligned}\right\} \text{Average } 22.4 \text{ per cent}$$

The difference in the total number of whistlers at the two locations is probably due to a combination of differences in local noise-conditions and geographical distribution of the lightning discharges that produced the whistlers. There was no correlation between coincidence rate and occurrence rate of whistlers.

Discussion

The results of this experiment show that a whistler is neither highly localized nor world-wide in geographical extent. Thus, in this experiment, in which the stations were separated by 1130 km, approximately 22 per cent of the observed whistlers were coincident at the two locations. This result bears on the question of the source and path of the whistler.* In addition, it should be useful for the planning of new experiments.

Consider now the question of a possible extra-terrestrial source of whistlers, such as the sun. In this case, one would expect the geographical coverage to be similar to that of phenomena which affect large areas of the earth's surface. For example, an SID will produce effects which can be observed over the entire sunlit half of the earth. Such a mechanism suggests that the phenomenon should be detectable over an appreciable part of the earth's surface. However, the facts that only 22 per cent of the whistlers were simultaneous during the Stanford-Seattle tests and none during the Seattle-New York tests argue against an extra-terrestrial source. Furthermore, such a theory would be difficult to reconcile with the observational data which show that many whistlers are preceded by strong impulses from lightning discharges.

On the other hand, the coincidence data provide strong support for Storey's theory, which predicts a concentration of whistler energy within an area having

*No question is raised regarding the mode of propagation. As has been pointed out, the measured law of frequency variation of sample whistlers is in good agreement with Eckersley's theory of the dispersion.

a radius of the order of 1,000 km. However, we cannot regard this evidence as conclusive proof of Storey's theory. Neither Storey's experimental results nor those of the Stanford-Seattle experiments tell us that whistlers actually appear at the surface of the earth in the hemisphere opposite to that in which they are observed, as required in the theory. We cannot be sure, for example, that whistlers are not reflected from clouds of ionization located at considerable distances beyond the earth's atmosphere. Such a model would be consistent with most of the experimental data and would be free from the requirement that appreciable ionization be present along the entire path of the whistler. Although we leave the nature of the path in doubt, it should be pointed out that there is as yet no alternative to Storey's theory which does not conflict in some way with the observational data.

An important test of Storey's theory would be to correlate whistlers at one end of a magnetic field line with impulsive atmospherics occurring in the vicinity of the opposite end. Under good observing conditions, it should be possible to observe the whistler at both ends of the path. The theory requires that one of the two coincident whistlers be preceded by an observable atmospheric and that its dispersion be twice that of the other. These are readily determined properties. The Stanford-Seattle results show that, if many observations are made at opposite ends of a field line, a reasonable coincidence rate can be expected, even when one station is as far as 1,000 km from the correct location. This test is of special importance now, because of the potential value of whistlers in the forthcoming International Geophysical Year (1957-58). If the Eckersley-Storey explanation of whistlers can be established beyond any doubt, a new tool will have become available for a world-wide coordinated program of exploration of the outer ionosphere.

Acknowledgment

The experimental portion of this work was partially supported by the National Bureau of Standards under contract CST-10751. The later analysis work was supported by the Air Force Cambridge Research Center under Contract AF19(604)-795. The authors appreciate the suggestions of L. A. Manning in connection with the probability analysis.

References

[1] L. R. O. Storey, An investigation of whistling atmospherics, Phil. Trans. R. Soc., A, **246**, 113-141 (1953).
[2] T. L. Eckersley, Musical atmospherics, Nature, **135**, 104 (1935).
[3] H. Barkhausen, Whistling tones from the earth, Proc. Inst. Radio Eng., **18**, 1155 (1930).
[4] J. R. Koster and L. R. O. Storey, An attempt to observe whistling atmospherics near the magnetic equator, Nature, **175**, 36-37 (1955).

ATMOSPHERIC TEMPERATURES AND WINDS BETWEEN 30 AND 80 KM

By W. G. Stroud, W. Nordberg, and J. R. Walsh

Signal Corps Engineering Laboratories,
Fort Monmouth, New Jersey

(Received October 31, 1955)

ABSTRACT

The method and analysis of the rocket-grenade experiment are briefly described. The 59 values of temperatures and of wind speeds and directions between 30 and 80 km obtained during 12 Aerobee rocket firings are summarized. The mean temperature distribution has a maximum of about 270°K at 50 km, with a lapse rate of about 2.5°/km above the peak. The winds are strong and from the west during the winter months (October through February); less strong and from the east during the summer months (April through August); and are comparatively weak and predominantly from the north during the fall (September). The maximum wind speed measured was a value of 104 m/sec at 55 km during a winter firing.

The average probable error for the temperature data is ±5°C; the average errors in wind speed and direction are ±10 m/sec and ±18°, respectively.

1. INTRODUCTION

During the period of July 1950 to September 1953, a series of 12 successful ocket-grenade experiments using the Aerobee rocket was carried out at White ands Proving Ground, New Mexico (32° north). The purpose of the experiment as to measure the temperatures and wind velocities in the region of the atmos- here between 30 and 80 km. At least one firing was made each month of the ear, except in January and March, when unfavorable surface conditions made rings too difficult.

A detailed description of the rocket instrumentation, the exposition of the ethod of analysis, and the results of the first six firings have been published ee 1, 2, and 3 of "References" at end of paper]. In this paper, brief descriptions the experimental method and of the reduction of the data are given. The temper- ure and wind results of all 12 firings are summarized, and an analysis of the results presented. No attempt was made to create a model atmosphere from these ngle-latitude data.

2. METHOD

xperimental

Temperatures and winds are determined by measuring the velocities of sound nd the deflections of the sound waves from seven or nine grenades successively

ejected and exploded from an Aerobee rocket along the nearly-vertical upward leg of its trajectory. Figure 1 illustrates the field conditions during the firing. This arrangement yields the basic data required; that is, the times of the explosions, the positions of the explosions in space, and the times and angles of arrival of the sound waves at the sound-ranging array.

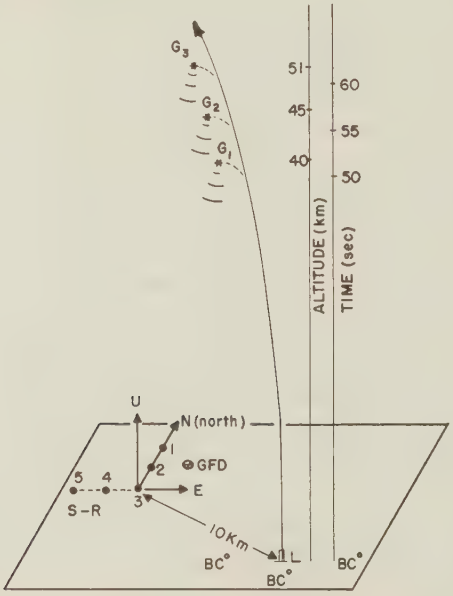

Fig. 1—Illustration of the rocket-grenade experiment

The grenades explode at G_1, G_2, etc., after ejection from the Aerobee launched from L. The ground-flash detector (GFD) records the times of the flashes. Three ballistic cameras (BC) are used to locate the explosions in space by photographing them against the star-field. The rectangular sound-ranging array, consisting of five microphones, 1, 2, 3, 4, 5, detects the times and angles of arrival of the sound waves from G_1, G_2, etc. The basic coordinate system (E, N, U), a right-handed Cartesian system, has its origin at the corner microphone, 3.

Mathematical

From these basic data, the average temperatures and the average wind speeds and directions in the layers between adjacent grenades may be determined. A complete description of the method of analysis has been published [2, 3], but a brief recapitulation of the basic ideas may be worth while, especially since a simplification in the method of computing the travel times in the layers (τ_L) has been found. In this review, only the two-dimensional case in an isothermal lower atmosphere will be considered in order to simplify the discussion.

In a gaseous medium, the acoustic speed c and the absolute temperature T are related through the well-known equation

$$C = KT^{1/2} \quad \ldots\ldots\ldots\ldots\ldots\ldots\ldots\ldots\ldots\ldots (1)$$

where K is a function of the molecular weight and the ratio of specific heats and is assumed to be constant up to at least 80 km.

In the idealized case, where the grenades lie *along* the vertical axis u and there no wind, the temperature in the layer between two adjacent grenades follows rectly from equation (1). However, the problem is severely complicated by the mbination of the facts that (*a*) the grenades are rather arbitrarily distributed ith respect to the vertical axis, and (*b*) there are winds present, which means at the velocity of propagation measured is a function of both the elastic properties the medium (the temperature) and the motion of the medium (the winds).

The effect of a uniform horizontal wind on the propagation of the sound wave

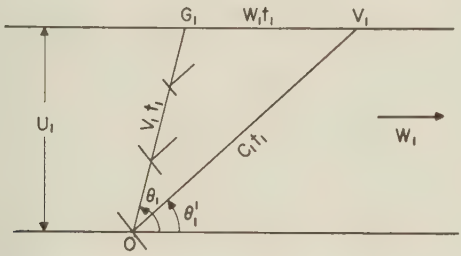

FIG. 2—Illustration of the effect of a uniform wind on the propagation of a sound wave

om a grenade is illustrated in Figure 2. The G_1 is the grenade explosion; O the igin of the sound-ranging array. The measured elevation angle of arrival of the ave normal is θ_1' . Extrapolating the wave normal at O upwards, we intersect e level of the grenade explosion at V_1 , which is defined as the "virtual" source the sound wave. Thus, G_1V_1 is equal to w_1t_1 , where w_1 is the average wind eed and t_1 is the time required for the sound wave to travel from G_1 to O. This nd can be readily calculated, since θ_1 , θ_1' , and t_1 are known. In the same way, e average wind up to each grenade can be determined. The average wind velocity, $_L$, in the layer between adjacent grenades can be obtained by the vector addition the winds up to each grenade, provided the time τ_L the sound wave spends in e layer is known. However, τ_L is not exactly known, since we are not dealing ith the idealized case initially discussed. The fact that the propagation is nearly rtical permits the calculation of a good approximate τ_L . The τ_L is computed om the equation

$$\tau_L = t_2 - \gamma t_1 \quad \ldots\ldots\ldots\ldots\ldots\ldots\ldots\ldots\ldots\ldots (2)$$

here t_2 and t_1 are the travel times from the upper and lower grenades to ground, spectively, and γ is the ratio sine θ_1'/sine θ_2' , the θ's being the acoustical elevation gles of arrival, as shown in Figure 2. The γ corrects the measured time of travel for the differences in spatial coordinates between the two grenade explosions d for the different effects of the winds below each of the explosions. With τ_L , e wind in the layer can be calculated for use in the calculation of the temperature.

Referring to Figure 2, it is apparent that the distance $OV_1 = c_1t_1$, where c_1 the acoustic speed. Then,

$$c_1 = \frac{u_1}{t_1} \csc \theta_L \quad \ldots\ldots\ldots\ldots\ldots\ldots\ldots\ldots\ldots\ldots (3)$$

TABLE 1—*Summary of results*

Date of firing	Altitude	Temp.	Probable error	Wind speed	Probable error	Wind dir.	Probable error	Layer thickness
	km	°*K*	°*K*	*m/sec*	*m/sec*	°	°	*km*
14 Jul.	35.4	260.7	1.4	19	3	79	9	6.6
1950	41.6	251.4	1.4	33	4	102	7	5.9
0137	47.3	267.5	1.5	46	5	72	6	5.3
MST	56.0	249.7	3.8	63	2	75	2	12.1
16 Oct.	50.0	264.7	3.0	46	7	272	9	8.5
1950	57.8	261.1	3.6	58	9	277	9	7.1
2100	64.4	233.5	4.0	42	11	256	16	6.1
MST	70.1	224.4	4.8	35	14	234	24	5.2
	75.4	225.5	5.0	47	14	217	18	5.6
	80.3	211.5	7.2	53	20	260	22	4.2
11 Dec.	35.9	234.9	1.4	44	3	269	4	6.5
1950	41.8	261.5	1.6	64	4	270	4	5.4
2106	48.1	266.0	1.4	83	4	265	2	7.2
MST	54.7	251.5	1.7	104	5	272	3	5.9
	60.1	249.0	2.1	83	7	273	5	4.8
	64.5	244.7	2.3	68	8	284	7	4.1
12 Dec.	33.3	231.5	4.5	43	1	263	2	12.7
1950	43.5	266.5	1.1	74	3	267	2	7.8
0210	53.1	261.0	5.9	87	2	286	2	11.3
MST	61.2	211.6	1.4	92	6	204	4	4.9
8 Jun.	29.6	234.6	3.0	12	6	59	29	6.7
1951	38.7	253.0	1.4	23	5	96	11	11.5
2311	46.9	264.2	2.3	15	13	55	53	4.9
MST	51.5	260.4	1.7	61	16	113	16	4.3
	55.4	265.6	4.6	89	21	66	14	3.6
	58.7	258.9	7.2	73	22	158	18	3.0
	61.9	252.2	1.3	30	23	109	46	3.5
1 Nov.	33.7	229.0	2.1	13	6	258	27	7.4
1951	40.5	253.4	2.3	71	8	262	7	6.2
0246	46.3	265.0	2.7	66	11	268	10	5.4
MST	53.3	263.4	1.7	87	8	274	6	8.5
	60.5	241.8	5.8	64	13	255	12	5.9
24 Sep.	42.1	266.5	3.2	23	6	317	133	6.3
1952	48.2	270.0	3.6	14	8	259	33	5.8
2050	54.0	274.1	4.0	35	10	314	16	5.6
MST	59.6	254.3	3.8	18	10	328	32	5.6
	67.3	222.1	1.8	23	6	357	15	9.8
	76.5	204.3	2.8	17	8	201	26	8.6

TABLE 1—*Summary of results*—Concluded

Date of firing	Altitude	Temp.	Probable error	Wind speed	Probable error	Wind dir.	Probable error	Layer thickness
	km	°*K*	°*K*	*m/sec*	*m/sec*	°	°	*km*
22 Oct.	47.3	255.6	3.1	33	7	228	13	6.1
1952	53.3	278.2	3.7	77	10	277	7	6.0
2045	59.0	263.9	4.2	63	11	278	10	5.3
MST	66.6	223.4	1.8	15	6	178	13	9.8
17 Feb.	48.3	262.6	1.4	48	4	290	5	12.1
1953	59.3	246.2	1.8	64	5	283	5	9.9
2350	69.0	235.3	1.8	54	7	219	7	9.4
MST	77.8	214.5	1.8	41	8	335	12	8.2
24 Apr.	47.1	257.3	0.4	30	2	93	4	7.9
1953	54.7	262.5	0.4	7	2	61	20	7.3
0319	61.8	244.6	0.4	28	3	145	6	6.7
MST	68.1	222.6	0.4	43	3	95	5	5.9
31 Aug.	49.9	283.7	2.2	48	6	340	7	8.5
1953	58.1	239.9	1.9	57	7	193	7	7.8
2205	65.7	236.0	1.9	22	9	340	22	7.3
MST	72.7	240.6	4.4	44	5	327	7	6.7
4 Sep.	58.5	259.0	1.6	7	5	46	38	7.7
1953	65.8	224.5	1.4	8	6	353	41	7.0
2236	72.5	207.1	2.1	30	10	51	20	6.4
MST	78.7	203.4	3.0	25	16	344	36	5.8

This basic relation may be applied to the layers between two grenades, so that

$$C_L = \frac{H}{\tau_L} \csc \theta_L \quad \text{.....(3a)}$$

where H is the layer thickness, τ_L the time the sound wave spends in the layer, and θ_L the elevation angle of the wave normal in the layers. The θ_L may be determined by applying Snell's law to the wave; that is,

$$\frac{C_0}{\cos \theta_0} + W_0 = \frac{C_L}{\cos \theta_L} + W_L \quad \text{.....(4)}$$

The subscript 0 defines the ground values of the parameters; the L, the values in the layer. At the ground, W_0 is zero, since firings are made only when the surface wind is calm; C_0 and θ_0 are measured parameters. Solving equations (3*a*) and (4) simultaneously yields an approximate C_L if the approximate values of τ_L and W_L are used. With these values of C_L and W_L , a better approximation to τ_L could be found; then, by iteration, W_L and C_L recomputed. However, the approximate values were sufficiently accurate, since the iteration yielded temperatures

usually differing by about 1°C and never by more than 3°C. By contrast, the previous procedures [2, 3] used rougher initial values of τ_L and required the iteration process.

Errors

The exact treatment of the systematic errors in the experiment has proved lengthy and difficult. However, it has been carried out to the point where we are convinced that the equations for maximum errors previously described [2, 3] from a simple model actually represent the facts. The errors given in Table 1 were calculated from the equations of the earlier papers and in most cases represent the maximum probable errors in all quantities.

3. RESULTS

The results of the 12 firings are summarized in Table 1. The temperatures *vs* altitudes are plotted in Figure 3; wind speeds and directions in Figure 5.

Temperatures

In Figure 4, the solid line is a mean curve obtained from all 59 values. The outstanding features of the temperature data are as follows:

(*a*) The maximum temperature is about 270°K at 50 km.

(*b*) The average lapse-rate between 55 and 80 km is low, being only 2.5°K/km.

(*c*) There is no seasonal effect at any altitude at this latitude.

(*d*) The temperature distributions differ considerably from firing to firing; example, the temperatures at maximum range from 256°K to 283°K.

(*e*) Unusual temperature structures appear, as on 11 October 1950 and on 31 August 1953, and there is a difference of 32°K at 60 km between the two December 1950 firings, which were five hours apart.

(*f*) Although all firings were made at night, a small diurnal temperature variation at all altitudes is suggested by the fact that there is a difference between the mean temperatures measured just after sunset and those measured at least six hours later.

Comparison of temperatures with other temperature data

As Figure 3 shows, the mean temperature curve in the region of the maximum (50 km) is 15° lower than the most recent standard atmosphere [4], which represents a compromise of all recent experimental results, including the rocket-grenade data. The differences in the results obtained by the various techniques led to a program wherein measurements were made by the different methods within one 24-hour period. These "T"-day results for 22 October 1952 are shown in Figure 4, where the grenade results of that date are compared with the results of the anomalous propagation, searchlight, and rocket-borne "aerodynamic" methods of the Air Force Cambridge Research Center [4, 5]. The results of the rocket-grenade experiment are all considerably lower than the other T-day data. Although there is a 12-hour difference between the times of the two sets of measurements, there is no evidence from the searchlight and anomalous propagation measurements made later in the day that actual temperature fluctuations could account for the differences between the rocket grenade and other measurements. From this, it

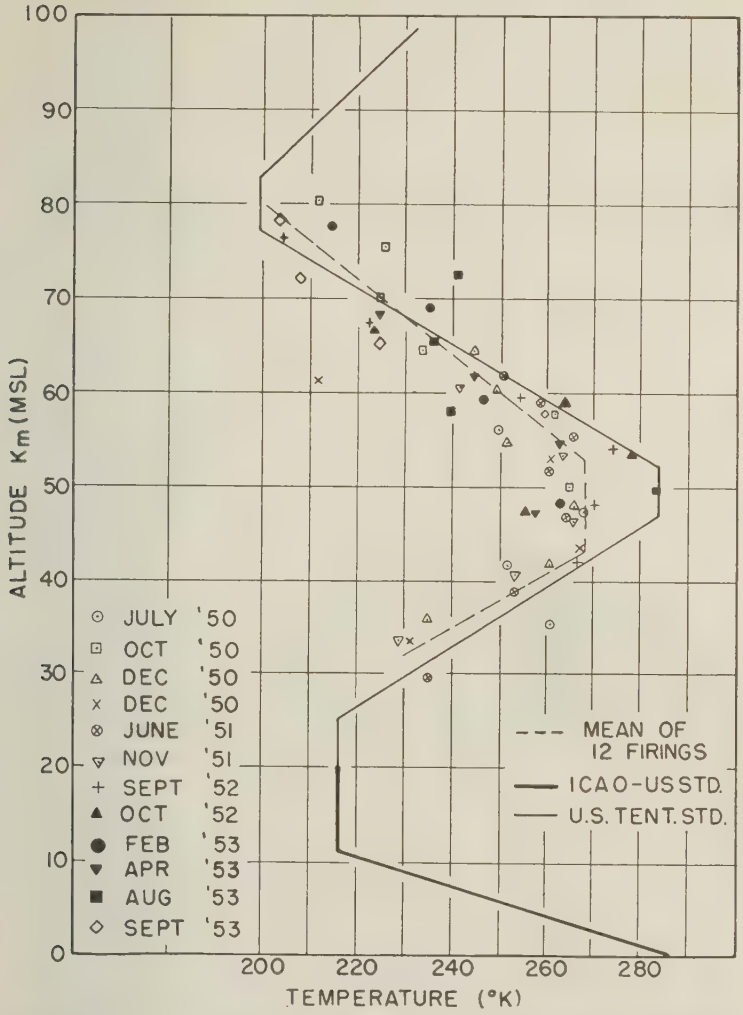

IG. 3—Temperatures in upper atmosphere measured by the rocket-grenade experiment (the ashed curve is the mean curve through the data, while the solid curve is the most recent standard atmosphere [4])

eems that the observed temperature differences are actually due to the methods f making the measurements. We were able to find no reason for suspecting that he rocket-grenade results are less accurate than the probable error indicated; hat is, ±5°K.

During the 1 November 1951 and the 11 and 12 December 1950 firings, the ignal Corps flew a number of special balloons, obtaining temperature and wind ata in the 30- to 35-km region overlapping the grenade data.* These results are ompared in Table 2.

*We are indebted to Messrs. A. Arnold and W. C. Conover for conducting these balloon flights.

TABLE 2—*Comparison of grenade and balloon temperatures*

Date	Temperature (°K)	
	Rocket	Balloon
11–12 December 1950	235 (36 km)	239 (36 km)
1 November 1951	229 (34 km)	234 (34 km)

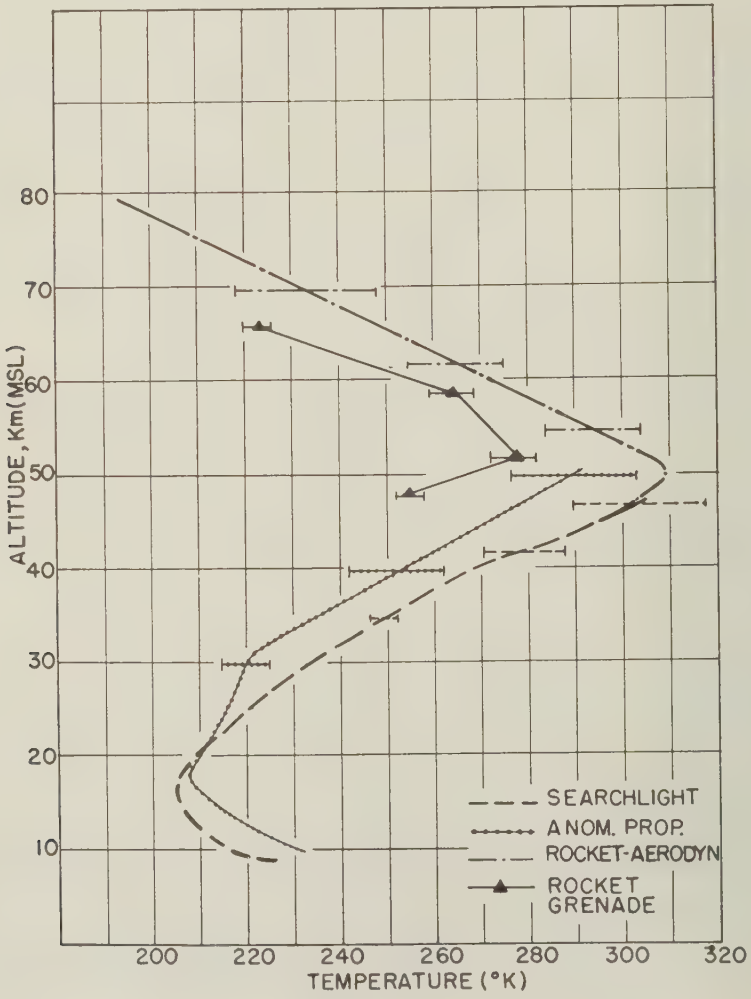

FIG. 4—Comparison of "T"-day results (probable errors at various levels are indicated by the horizontal lines)

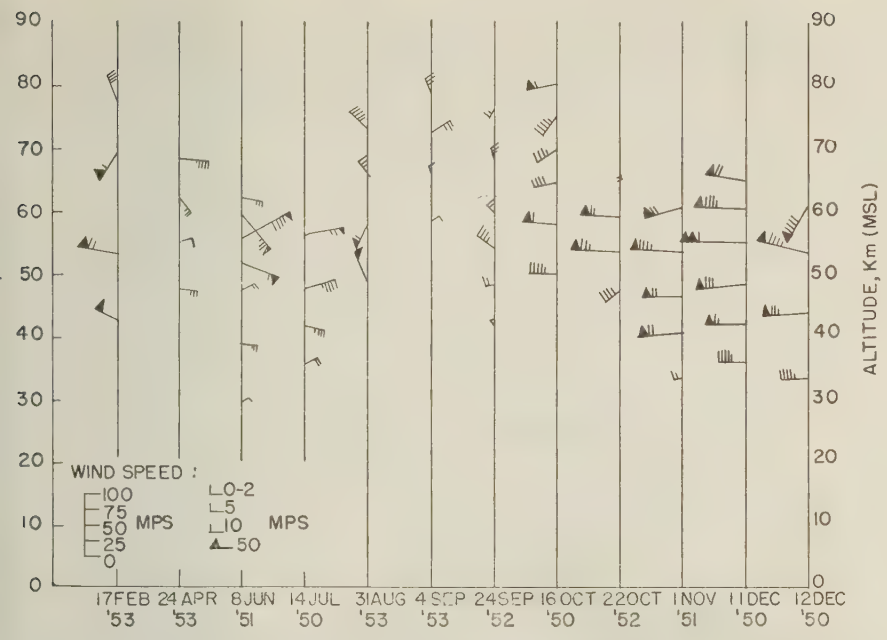

FIG. 5—Winds in the upper atmosphere measured by the rocket-grenade experiment
The wind speed is demonstrated by both the number of flags and by the length of the flagpole, pointed out in the Figure. If the end carrying the flags points upwards, the wind is from the north; if it points to the left, the wind is from the west.

Winds

The outstanding features of the wind results (Fig. 5) are

(*a*) The clear-cut seasonal effects, as follows:

(1) The winds are strong and from the west during the winter months (October through February).

(2) Winds are less strong and predominantly from the east during the summer months (April through August).

(3) Winds are weak, and from the north during the transition month of September. No March firing was made.

(*b*) In all seasons, maximum wind speeds occur between 50- and 60-km altitude. The highest wind speed measured was 104 m/sec (200 mph); the lowest, less than 5 m/sec (10 mph).

Comparison with other wind results

There are not much wind data for the region 40 to 80 km other than those from the rocket-grenade experiment. The few fortuitous noctilucent cloud observations [7, 8] at 80 km give values comparable to ours. However, in the lower regions, the grenade data overlap some of the balloon and anomalous propagation measurements. Here the agreement is good, two cases giving particularly valuable

checks. The 22 October 1952 (T-day) results from the grenade and the anomalous propagation studies match, as shown in Table 3.

TABLE 3—*Comparison of grenade winds with others*

Date	Winds	
	Grenade	Balloons
12 December 1950 (at 35 km)	43 mps, 263°	56 mps, 255°
1 November 1951 (at 34 km)	13 mps, 258°	14 mps, 258°
	Grenade	Anomalous propagation
22 October 1952 (at 47 km)	33 mps, 228°	44 mps, 266°
(at 53 km)	77 mps, 277°	74 mps, 266°

Also compared with the grenade result is the result of the balloon flights, described previously.

Relations between temperatures and winds

An outstanding feature of the temperature-wind relations is illustrated in Table 4, where the wind directions and temperatures for two unusual firings are compared. These firings were unusual in that very large temperature deviations from the normal were observed. As Table 4 shows, in those layers in which the temperatures were abnormally low, the wind directions there had far stronger southerly components than those of the adjacent layers. By contrast, in those layers in which the temperatures were higher than normal, the wind directions had far stronger northerly components.

TABLE 4—*Relation between temperature and wind direction*

Date	Altitude	Wind direction	Deviation from mean temperature
	km		°K
(1950) 12 Dec.			
	33.3	W(263)	− 2
	43.5	W(267)	− 2
	53.1	W(268)	− 2
	61.2	SW(204)	−36
(1953) 31 Aug.			
	49.9	NW(340)	+16
	58.1	SW(193)	−15
	65.7	NW(340)	+ 1
	72.7	NW(327)	+22

Further examination of all the data indicates it is generally true that when the nd veers to the north the temperature is higher. This relation is more pronounced the winter months than it is in the summer.

We looked further for possible origins of this observed connection between mperatures and wind directions. A thorough check of the method of analysis owed that the temperature and wind deviations in question cannot be accounted r by internal inconsistencies in the method. However, if in some cases the basic ysical assumptions (constant molecular weight, horizontal homogeneity, and e absence of strong vertical motions) are not met, the method will fail. There is e possibility that the molecular weight M will change, especially above 65 n [9]. This change in M will always be such that the computed temperature will too high. The fact that the unusually high temperatures are observed below km as frequently as above, and the fact that the wind directions cannot be ected by a change in M, indicate that a variable molecular weight is not re-onsible.

Horizontal inhomogeneity of the medium can influence the calculated results. owever, for physical reasons, such inhomogeneities will be limited to a very thin er near the ground and will, therefore, have only a very small effect on the nds. The temperature results will be practically unaffected.

The observed relation between temperature and wind-direction deviations uld be accounted for by strong vertical motions. We calculated the magnitudes the vertical currents required to produce the wind-direction deviations observed able 4) and found impossibly high values. For example, the 64°-shift in wind rection for the top points of the December 12 firings would require a vertical ward velocity of about 1,400 mps! The temperature changes and horizontal nd velocities that would have to be associated with such a vertical velocity e physically impossible. Therefore, we have concluded that vertical currents e not responsible for the observed temperature and wind-direction relationships.

CONCLUSIONS

Although the data from the 12 firings give us a fairly complete picture of the mperature and wind structures in the region 30 to 80 km at a specific latitude 2° north), we feel that the lack of similar data at other, especially higher, latitudes ecludes any reasonable attempt to create a model of the general circulation in e atmosphere. In addition to the lack of data, there seems to be the possibility at 32° north is more or less a nodal point in the seasonal variations at high itudes, because of the fact that there is no observed seasonal variation in the mperature, but there is a strong seasonal variation in the wind.

An attempt was made to relate the unusual temperature-wind distributions served with geophysical and solar phenomena. We could find no observed solar ents related in time to the appearance of the unusual temperatures. This and the ct that the temperatures and winds are closely related suggest that temperature omalies are associated with far-reaching dynamic processes in the atmosphere ther than by *direct* radiation processes. In addition, it was noted that ionospheric turbances which can be ascribed to dynamic processes were observed during e time of the unusually high temperatures (31 August 1953).

ACKNOWLEDGMENTS

It is a pleasure to acknowledge the assistance and the contributions of th many individuals and agencies that have made this work possible. In additio to those mentioned in the initial papers [1,2,3], we would like to thank Mr. A Babbitt and Mrs. Edith Schlussler for carrying out the computations.

References

[1] W. G. Stroud, E. A. Terhune, J. H. Venner, J. R. Walsh, and S. Weiland, Instrumentatio of the rocket-grenade experiment for measuring atmospheric temperatures and winds Rev. Sci. Instr., **26**, 427 (1955).

[2] M. Ference, Jr., W. G. Stroud, J. R. Walsh, and A. G. Weisner, The measurement o atmospheric temperatures in the region 30 to 80 km by means of the rocket-grenad experiment, in publication, J. Met., **13**, Feb., 1956.

[3] A. G. Weisner, The measurement of winds in the region 30 to 80 km by means of th rocket-grenade experiment, in publication, J. Met., **13**, Feb., 1956.

[4] R. A. Minzner, Three proposals for U. S. high-altitude standard atmosphere, presente at 2nd meeting of the working group on Extension to the Standard Atmosphere, Wash ington, D. C., 18 April 1955.

[5] W. B. Kennedy, L. Brogan, N. J. Sible, and R. A. Brown, Scientific Report No. 2, Cor tract AF 19(122)-252, Denver Research Institute, University of Denver, Denve Colorado.

[6] Minutes, Meeting on Standard Atmosphere, Boston, 2 November 1953, N. Sissenwine Geophysics Research Center, AFCRC.

[7] J. Paton, Auroras and luminous night clouds, Nature, **168**, 487 (1951).

[8] P. A. Sheppard, The exploration of the upper atmosphere, Sci. Prog., **37**, 488 (1949).

[9] K. F. Chackett, F. A. Pancth, P. Reasbeck, and B. S. Wiborg, Variations in the chemica composition of stratosphere air, Nature, **168**, 358 (1951).

NOTE ON THE ADJUSTMENT OF ISOMAGNETIC CHARTS TO MUTUAL CONSISTENCY*

BY A. J. ZMUDA

Applied Physics Laboratory, The Johns Hopkins University, Silver Spring, Maryland

(Received November 3, 1955)

ABSTRACT

Precise aeromagnetic measurements of total magnetic intensity permit the construction of isomagnetic charts which are mutually consistent in the horizontal and vertical components of the geomagnetic fields. Equations incorporating this new result are provided.

In magnetic surveys, measurements are usually made at discrete points and, drawing the isomagnetic charts, there is a problem of estimating the magnetic ues at intermediate positions and of correcting, particularly in airborne surveys, e measured data. Methods of testing and adjusting for mutual consistency of the and Y components (the northern and eastern horizontal components, respectively, the total intensity F) were discussed by Chapman [see 1 of "References" at end paper] and Vestine [2]. The present discussion treats a method of adjusting arts of the downward component Z using corrected values of X and Y coupled h measurements of F. This note is directed primarily to the adjustment of data tained in aerial surveys, but applies, in principle, to the results of ground and surveys.

With magnetometers such as the NOL VAM-2A [3], F is measured continuously ring the flight. Also, since the values are practically independent of errors in e pendulous reference, the F data are more accurately known than the angular ta (which are averaged over intervals of 100 sec) that are used in computing the ues of the other magnetic elements. Therefore, it is reasonable to assume that e measured values of F do not need adjusting. These F values may then be plied to the adjustment of the Z chart in the following manner.

First, isomagnetic charts for X and Y can be tested [1, 2], and then adjusted, determining the extent to which the values of these components satisfy the uation

$$\frac{1}{a \sin \theta}\left[\frac{\partial X}{\partial \phi} + \frac{\partial}{\partial \theta}(Y \sin \theta)\right] = 0 \qquad (1)$$

ich is the expression for the vertical component of curl $\vec{F} = 0$. In equation (1), nd ϕ represent the circular measure of colatitude and east longitude, respectively,

*This work was supported by the Department of the Navy, Bureau of Ordnance, under ntract NOrd 7386.

and a is the radius of the spherical surface over which are made the measurements

After the X and Y charts are adjusted in accordance with (1), values of Z may be computed with the aid of measured F values from the well-known relationship

$$F = [X^2 + Y^2 + Z^2]^{1/2} \quad \ldots\ldots (2$$

The surface gradients of the elements, obtained by differentiation of (2), are related by

$$F \frac{\partial F}{\partial \theta} = X \frac{\partial X}{\partial \theta} + Y \frac{\partial Y}{\partial \theta} + Z \frac{\partial Z}{\partial \theta} \quad \ldots\ldots (3$$

and

$$F \frac{\partial F}{\partial \phi} = X \frac{\partial X}{\partial \phi} + Y \frac{\partial Y}{\partial \phi} + Z \frac{\partial Z}{\partial \phi} \quad \ldots\ldots (4$$

Charts of Z obtained through the application of equations (2), (3), and (4) are consistent with adjusted X and Y data and measured F values.

When adjusted charts of X and Y are available at two closely spaced levels the surface gradients of Z may be obtained from

$$\frac{\partial Z}{\partial \phi} = -\sin \theta \left[a \frac{\partial Y}{\partial r} + Y \right] \quad \ldots\ldots (5$$

and

$$\frac{\partial Z}{\partial \theta} = a \frac{\partial X}{\partial r} + X \quad \ldots\ldots (6$$

which are the equations for the θ and ϕ components, respectively, of curl $\vec{F} = 0$

References

[1] S. Chapman, Terr. Mag., 47, 1-13 (1942).
[2] E. H. Vestine, L. Laporte, I. Lange, C. Cooper, and W. Hendrix, Washington, D. C. Carnegie Inst. Pub. 578 (1947).
[3] E. O. Schonstedt and H. R. Irons, Trans. Amer. Geophys. Union, 36, 25-41 (1955).

RELATIONSHIPS BETWEEN AURORA AND SPORADIC-*E* ECHOES AT BARROW, ALASKA

By R. W. Knecht

National Bureau of Standards, Boulder, Colorado

(Received October 15, 1955)

ABSTRACT

During March 1951, a series of visual auroral observations were made simultaneously with ionospheric soundings at Barrow, Alaska (71° north, 156° west). Aurorae were visible during 82 per cent of the 379 observations, made at least every 15 minutes during the dark hours of 10 successive clear nights. Three nights are described in detail. Statistical results include (1) a strong tendency for sporadic-*E* (*Es*) echoes at frequencies $\geq$ 7 Mc to be recorded when aurora was near the zenith; (2) a direct relationship between brightness of (inactive) aurora and the top frequency of *Es* echoes; (3) evidence for the correspondence of (oblique) *Es* echo ranges with estimated slant ranges of visible auroral forms. The observations lend support to the view that ionization in the immediate vicinity of visible auroral forms gives rise to ionospheric-type reflections at high frequencies.

1. INTRODUCTION

Studies of the association of aurora and the ionosphere were made as early as 933 by Appleton, Naismith, and Builder [see 1 of "References" at end of paper], ranz and Stoffregen [2], and others. They found that moderate geomagnetic orms, usually with aurora present, were accompanied by an increase in *E*-region nization, and that during strong magnetic storms, often with *intense* aurora sible, complete absorption of radio echoes was observed. Chapman [3] and arang [4] have done a considerable amount of work on the variation of ionospheric arameters during auroral and magnetic activity. More recently, Lovell, Clegg, nd Ellyett [5] and Aspinall and Hawkins [6] have attributed echoes on 46 and ? Mc to reflections from the aurora. Investigators at Cornell [7], Ottawa [8], and askatoon [9] have made similar observations on other frequencies, generally in e same range. Heppner, Byrne, and Belon [10] have associated absorption and s ionization with different types of auroral forms in a study that is closely related this paper.

2. OBSERVATIONS

The systematic ionospheric soundings at Barrow, Alaska (71° north, 156° est, geomagnetic latitude 68° north) were supplemented on ten clear nights by

visual observations of the aurora. Beginning March 7-8, 1951, after several months of predominantly cloudy weather, regular auroral observations (at least every 15 minutes throughout the night) were continued through March 16-17, when a brightening moon and poorer sky conditions ended the series. No auxiliary optical equipment or aids were available. For the 379 observations, the following data were logged for the major auroral forms seen:

(*a*) Maximum elevation (and range of elevation when significant)
(*b*) Arbitrary brightness index ($\frac{1}{4}$ = very faint; $\frac{1}{2}$ = faint; 1 = moderate; 2 = moderately bright; 3 = bright; 4 = intense)
(*c*) Arbitrary activity index
(*d*) Type of form—drapery, etc. (not used in results reported here)

The degree of activity was estimated from motions within the form, as well as apparent movement of the form itself. Any deviation from the characteristic

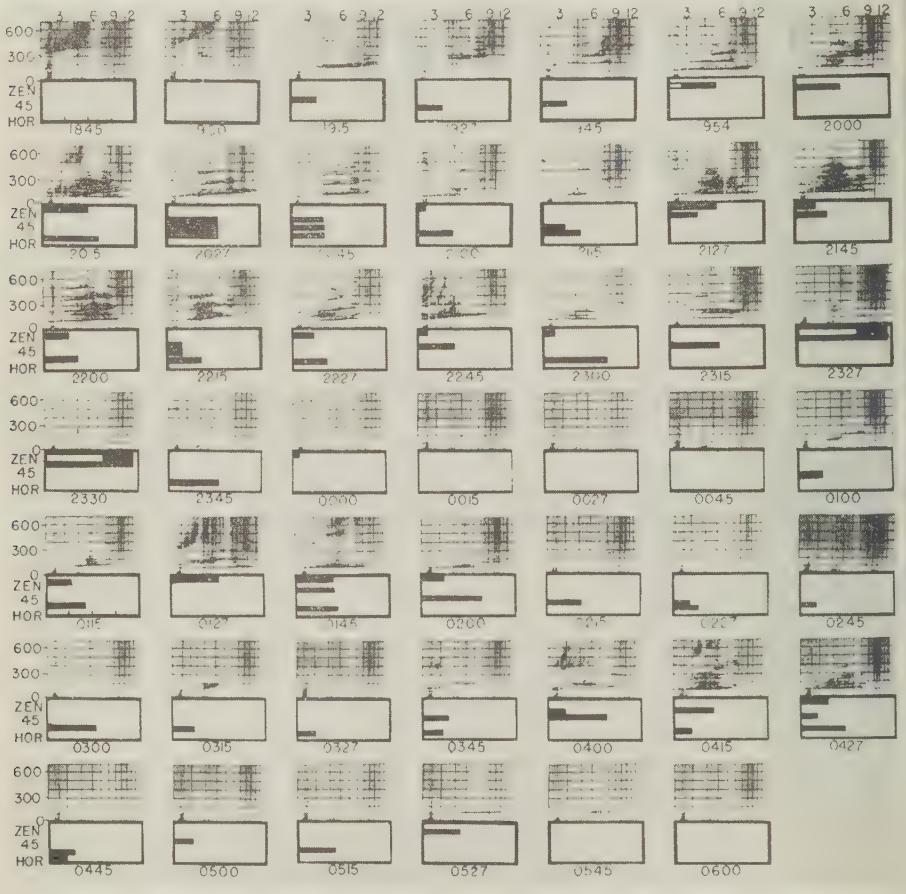

Fig. 1—Ionospheric and auroral observations at Barrow, Alaska, March 7–8, 1951

yellow-green color was also taken as a sign of activity. During times of great activity, the observations necessarily do not describe all of the many and varied forms present, but rather only the several brightest and most extensive forms closest to the zenith.

The ionospheric soundings were obtained with a National Bureau of Standards automatic ionosphere recorder, Model *C*-2. The probing frequency range of the equipment was 1 to 25 Mc, scanned in 15 seconds. The pulse repetition rate was 60 per second, the pulse length 50 microseconds, and the peak pulse power about 15 kw. The upper limit of virtual height recorded was 1,000 km.

3. DESCRIPTION OF THREE NIGHTS' OBSERVATIONS

The complete series of observations on three of the ten nights are shown in Figures, 1, 2, and 3. The ionogram is reproduced in the upper part of each diagram, limited to ranges (0 to 700 km and 2 to 14 Mc) which include all important echoes. Each important auroral form is represented in the lower part by a horizontal bar; its length indicates brightness, increasing from the left margin, and its thickness and vertical position correspond to elevation above the horizon. When a form was

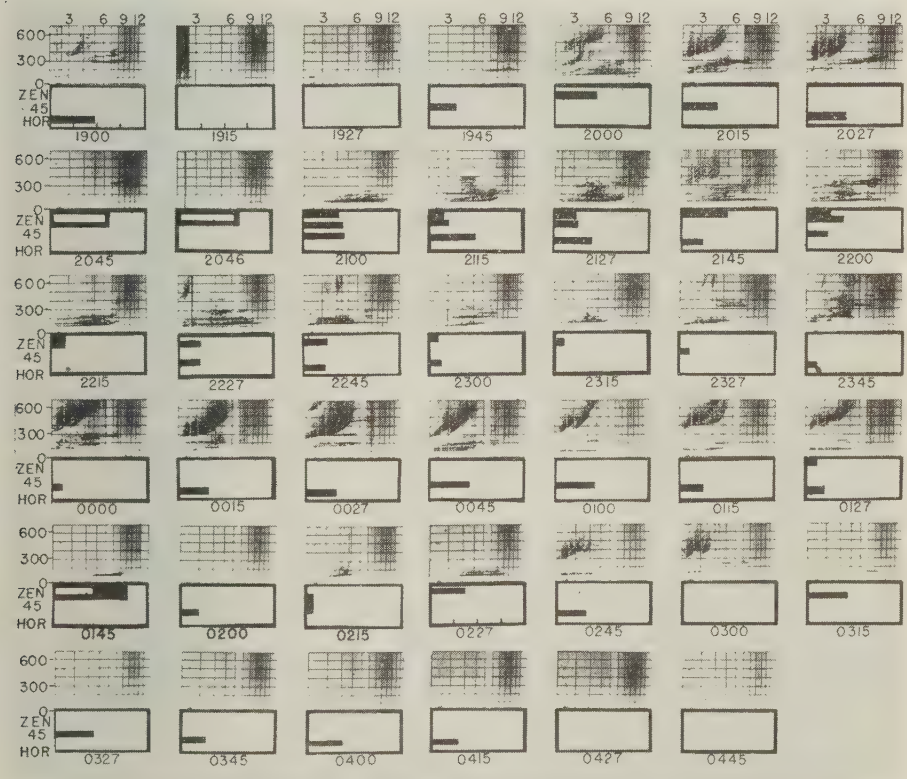

FIG. 2—Ionospheric and auroral observations at Barrow, Alaska, March 9–10, 1951

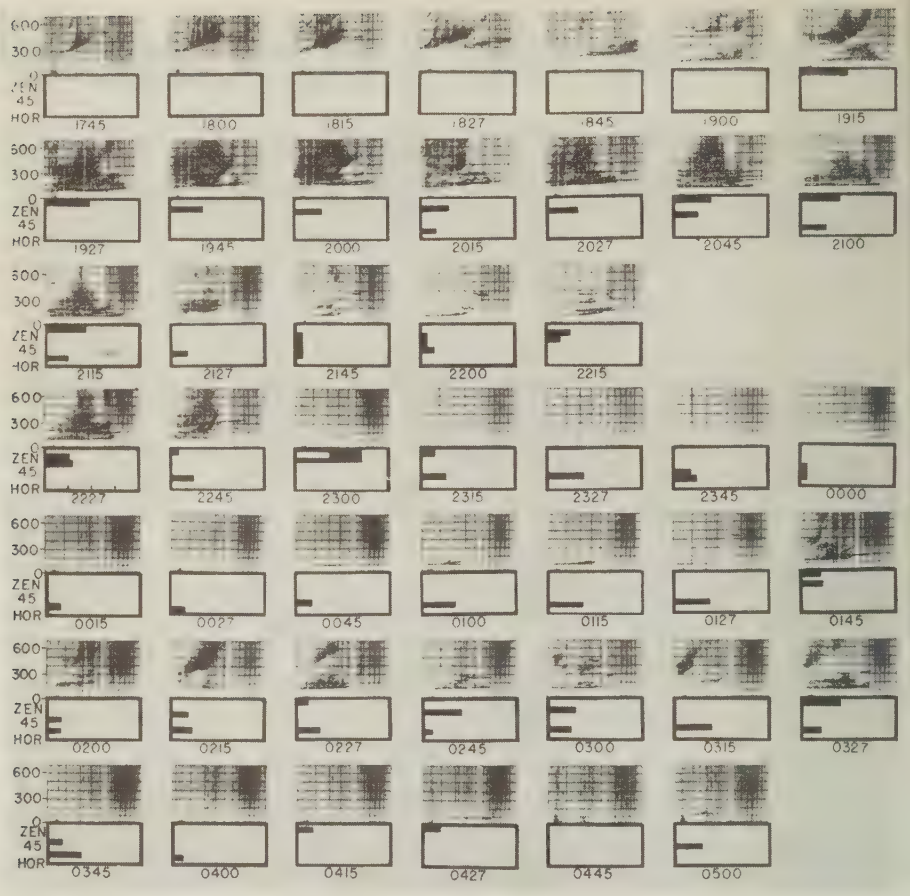

Fig. 3—Ionospheric and auroral observations at Barrow, Alaska, March 11–12, 1951

active, a white bar is superimposed, the length giving a rough indication of the degree of the activity. The times of the observations are 150° west meridian time.

March 7-8, 1951 (*Fig.* 1): The sequence from 1927 to 2015 shows an auroral form moving overhead from an elevation of about 35°. The soundings show the range of the main *Es* echoes changing progressively from 260 to 100 km as the aurora is moving overhead. Other observations showing fairly bright aurora in or near the zenith were taken at 2127, 2145, 2200, 2327, and 2330. The first three of these show strong *Es* at a range 100 to 120 km. Intense and very active aurora was present during the 2327 and 2330 soundings, which showed an increase in ionospheric absorption. Complete absorption was observed on the 2345 sounding, and the condition continued for an hour, although the auroral activity had ended. The magnetogram taken at the nearby United States Coast and Geodetic Survey's Barrow Magnetic Observatory on March 7-8 (Fig. 4) shows a sharp increase in magnetic activity simultaneous with the onset of the auroral activity at about 2327.

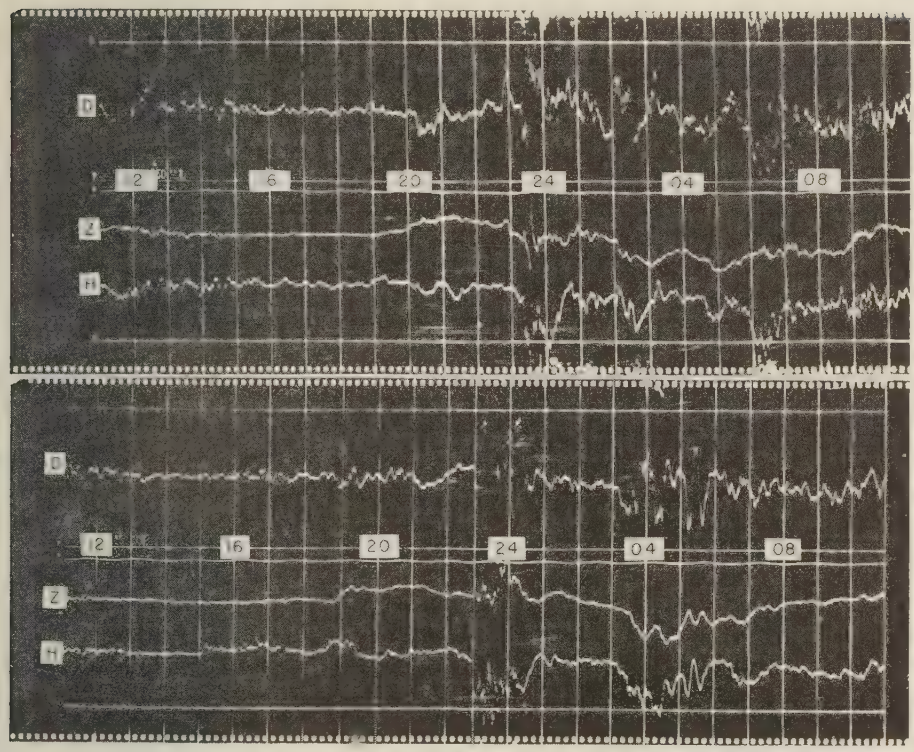

FIG. 4—Magnetograms taken at the magnetic observatory, Barrow, Alaska, March 7–8, 1951 (upper) and March 11–12, 1951 (lower)

Overhead auroral forms were again observed at 0127, 0145, 0200, and 0427. The corresponding soundings all show *Es* echoes of greater than 7 Mc and ranges of about 100 km. With the exception of the 0115, 0400, 0415, and 0527 soundings, when aurora was near the zenith, none of the remaining ionograms showed *Es* of this type.

March 9-10, 1951 (*Fig.* 2): At 1900, there was a moderately bright auroral form low in the sky (about 20° elevation). The sounding shows a strong echo at 280 km, probably an oblique. The soundings at 2000, 2015, and 2027 show the changes in the range of the echoes, which are consistent with the movement of aurora away from the zenith. Auroral activity at 2045 and 2046 was again accompanied by increased absorption. From 2100 to 2245, aurora of moderate brightness was overhead and the soundings show fairly strong *Es* echoes at ranges of about 100 km. These soundings are in marked contrast to those taken at times without overhead aurora, later in the night, when *Es* echoes are generally at less than 6 Mc. There are further examples of overhead aurora, inactive at 0227 and active at 0145.

March 11-12, 1951 (*Fig.* 3): The first visual observation of the evening was made at 1915 and, although it was still twilight, a moderately bright form was seen

overhead. The strong (12 Mc) *Es* recorded at the same time can be traced back to an echo at 500 km on the 1745 sounding. This long range is consistent with the increased heights associated with sunlit aurora, such as reported by Störmer to be at heights of between 200 and 400 km. *Es* ranges vary as if they correspond to slant ranges of fixed height aurora in the series of soundings made at 1945 to 2027 when moderately bright aurora was about 20° from the zenith, at 2045 to 2115 when the same form had moved overhead, and at 2127 to 2200 when only faint aurora was visible.

Activity in the aurora was noted at the 2300 observation. Again ionospheric absorption began at the same time, but continued for $1\frac{1}{2}$ hours after the auroral activity ceased. The magnetogram for March 11-12 (Fig. 4) shows increased magnetic activity beginning exactly (coincidentally) at 2300. The only other occurrence of fairly bright aurora in the zenith during the rest of the night was at 0327. The strongest *Es* echoes were also recorded at this time.

4. STATISTICAL ANALYSIS

The illustrations suggest relationships between characteristics of aurora and *Es* which can be further tested on the entire ten-night series of observations. The first step is to look at the distribution of fEs and $h'Es$ (Fig. 5) for the soundings

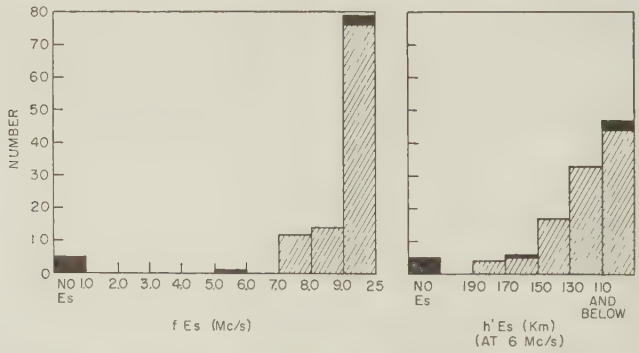

Fig. 5—Distributions of top reflected frequency and virtual height of *Es* when aurora (brightness ≥ 1) is within 30° of the zenith (nine cases of great auroral activity in black)

corresponding to the 111 observations of fairly bright (≥ 1) aurora within 30° of the zenith. On 105 of these soundings, the maximum reflected frequency of *Es* was 7 Mc or more. The five cases of "no *Es*" occurred during times of great auroral activity when absorption was high. In 96 soundings, the range of the *Es* echoes (measured at 6 Mc) was 150 km or less. These have been taken as the limits for a type of *Es* strongly associated in time with fairly bright aurora near the zenith, abbreviated *AEs* in the remainder of the paper. It is found that *AEs*, thus defined, occurred on only 8 of 137 ionograms on the ten nights when the auroral elevation was below 60°, and 24 per cent of the 124 times when auroral brightness was < 1. Further, *AEs* occurred on none of the 69 soundings when the auroral observations were negative. This experience appears to be representative, since *AEs* shows on

only 10 per cent of the 123 ionograms on the three other nights (Jan. 8-9, 9-10, and 19-20, 1951) considered free of aurora on the basis of spot observations.

Figure 6 gives the details of the elevation-brightness-*AEs* relationship for the 310 observations available for this purpose in the ten-night series. The elevation

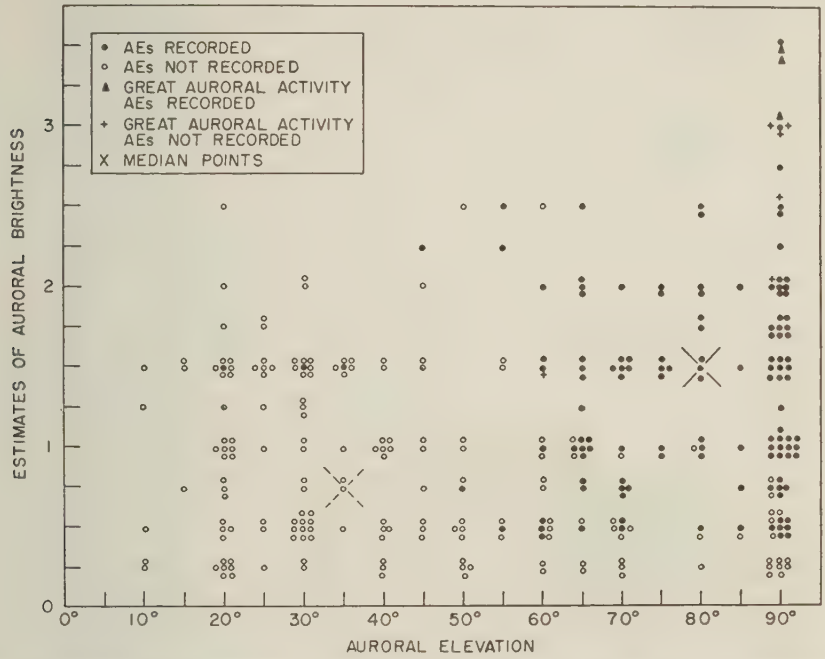

FIG. 6—Brightness and elevation of the aurora during the 310 positive visual observations, Barrow, Alaska, March 7–17, 1951

plotted is that of the principal auroral form, that is, that nearest the zenith, except for six cases when the one nearest the zenith was faint ($< \frac{1}{2}$) and a lower form was bright ($\geq 1\frac{1}{2}$). Different symbols indicate whether or not *AEs* appeared on the simultaneous ionogram and also the nine cases of great auroral activity. From the indicated median points, it would seem that the visual observations associated with *AEs* form a different population than the unassociated observations. Application of the chi-square test indicates that the probability of drawing two groups of data from the same population with discrepancies as great or greater than these is less than one per cent.

The range of *Es* echoes is plotted against the elevation of the principal auroral form in Figure 7. The *Es* echoes included were those with $f > 5.5$ Mc and $h' < 300$ km. If more than one *Es* echo was present at a time, the echo with the largest *fEs* was selected. Range was measured arbitrarily at 6 Mc, or at *fEs* if $fEs < 6$ Mc. There are 209 cases of *Es* which meet these criteria out of a possible 310 when aurora was observed visually. The 101 other cases of *Es* include 77 when the elevation of the aurora was 30° or less or faint ($\leq \frac{1}{2}$), five during periods of great

auroral activity, and only one with bright, inactive, zenith aurora, and this during a polar blackout following great auroral activity. Figure 7 indicates a clear tendency for larger *Es* ranges to correspond with lower auroral elevations. The full curves represent the slant distances to auroral forms, assuming heights of 90 and 130

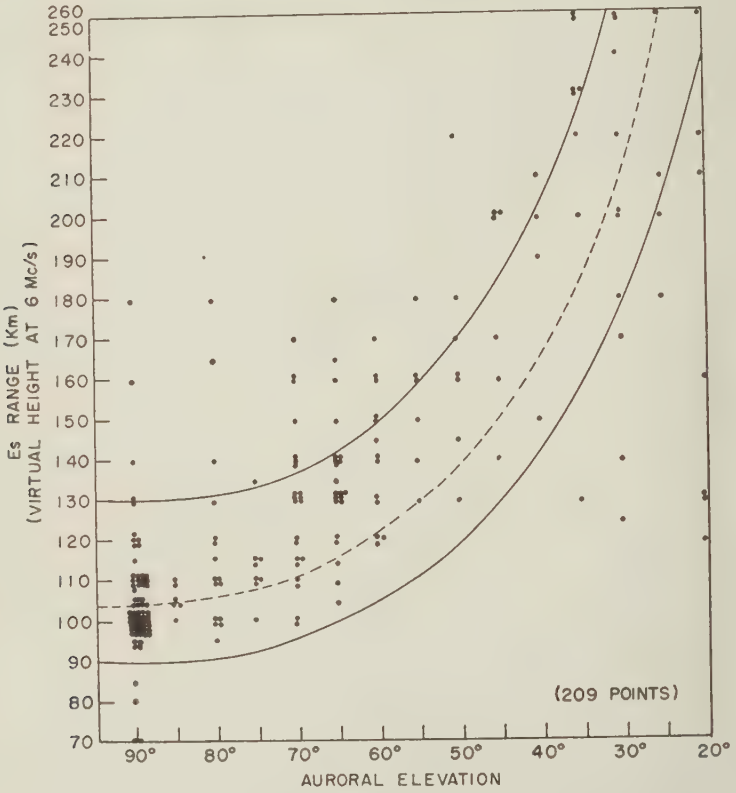

Fig. 7—Variation of *Es* range with elevation of simultaneous aurora

km, respectively, the usual range of heights of the lower border of the aurora deduced from photographic triangulation. Seventy-eight per cent of the observed points fall within these limits and only one-third of the remainder are below, with only three of these too-low values occurring at elevations $\geq 40°$. Few auroral forms have been measured photographically below 90 km.

In Figure 8, *fEs* is compared with the brightness of auroral forms. Only those forms were included that were within 30° of the zenith, for which estimates of intrinsic brightness can be expected to be somewhat more reliable. The only cases in which no *Es* echo was observed were those corresponding to great auroral activity or to rather faint (< 1) aurora. It is striking that, except for these cases and possibly the four other cases of great aurora, *fEs* bears a direct relationship to the estimates of auroral brightness, with a spread of points which is remarkably

small in view of the crudeness of the brightness estimates. There is no value of fEs less than 5.5 Mc, although the lower limit of the recorder was one megacycle. The intercept of the regression line at $\frac{1}{4}$ on the brightness scale (through points not including those labeled "no Es") is approximately 6 Mc.

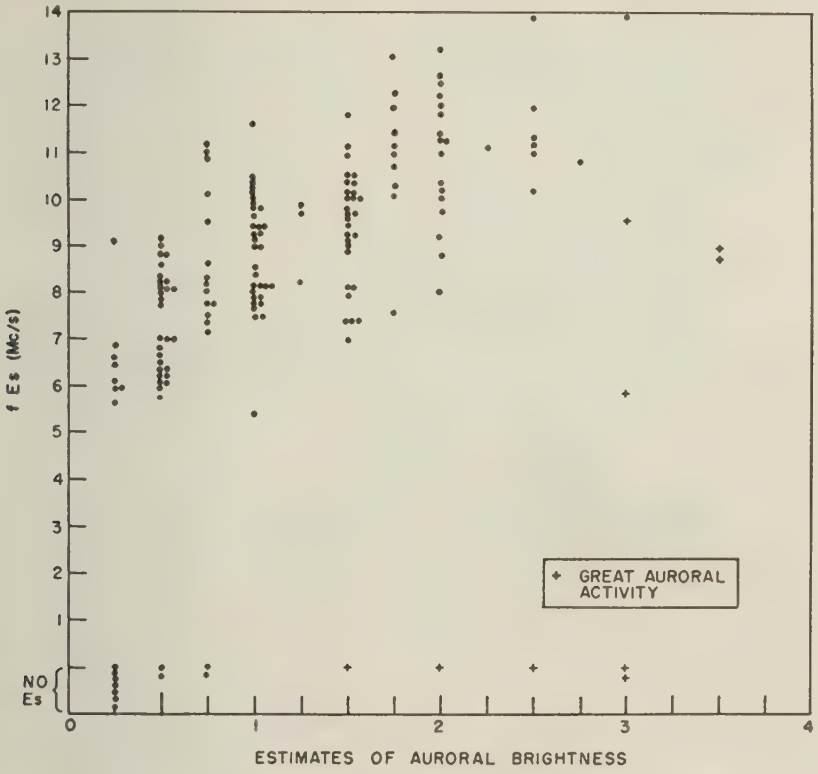

FIG. 8—fEs as a function of auroral brightness (limited to aurora within 30° of zenith)

Another effect was tested on these observations. There is a tendency, noted by Harang [4], for more intense auroral forms to be at a lower height. Since fEs appears to vary directly with crude estimates of brightness (Fig. 8), it is appropriate to compare fEs with $h'Es$. The decrease of the mean $h'Es$ from 122 to 109 km as fEs increases from 5.5 Mc to over 12 Mc compares with Harang's range from 113 km for faint forms to 101 km for very intense draperies. Contamination of Es data by oblique echoes would introduce a systematic error in the direction noted. Only Es echoes having ranges $\leq$ 150 km were used in this phase of the study.

5. DISCUSSION AND CONCLUSIONS

This investigation bears on the question of whether Es echoes recorded during systematic ionospheric soundings are returned from regions of the ionosphere which contain visual aurora. The results are consistent with the view that Es echoes with $fEs > 7$ Mc are returned from the lower region of visual aurora near

the zenith, and, furthermore, that *Es* echoes with $fEs > 5.5$ Mc may be returned from visually observable auroral forms at elevations as low as 25°. Why there should be low frequency limits for *Es* to be aurora-associated is not clear, although it appears likely that other mechanisms for producing *Es* reflections predominate for the lower frequencies.

If our sample is representative, it appears that the large majority of inactive auroral forms correspond with *Es* echoes, the correlation breaking down conspicously only when there is great activity in the aurora, with associated increased ionospheric absorption lasting somewhat beyond the period of visual activity. Also fEs appears to be closely related to the brightness of near-zenith aurora. Recalling from Figure 8 that on the average the values of fEs range from about 6 Mc for brightness $\frac{1}{4}$ to about 12 Mc for brightness $2\frac{1}{2}$, the range of electron densities in the aurora observed near the zenith may be calculated if fEs is interpreted as a critical frequency. Electron densities corresponding to critical frequencies 6 and 12 Mc are 4.5×10^5 electrons/cm^3 and 1.8×10^6 electrons/cm^3, respectively. If this interpretation is correct, the observations lend some support to the theoretical calculations of auroral electron densities by Omholt [15], based on a theory by Seaton [16], which relates electron density to the absolute intensity of the negative nitrogen bands. Omholt deduced a value of 1.6×10^6 electrons/cm^3 for faint arcs.

It is noted that no attempt has been made to classify the *Es* echoes according to apparent reflection coefficient, spreadiness, retardation, etc. Lindquist [11] and Meek [12] have been concerned with such classification for other purposes, but Lindquist did suggest that two types (his N1 and N2) were correlated with the aurora and that a type of auroral form (rayed arc) may, on occasion, be associated with ionospheric absorption. Meek, in his recent papers [13, 14] on the relations between magnetic, auroral, and ionospheric variations at Saskatoon, found that ionospheric and auroral light observations may be directly related to positive and negative magnetic bays, but found little evidence for a direct relation between auroral and ionospheric changes at this location. This may be due to the fact that aurora is only observed at the zenith at this lower geomagnetic latitude (60°) during considerable magnetic activity which is usually accompanied by complete ionospheric absorption. This means that inactive, overhead aurora (found to be a good reflector at Barrow) would be rare at this location.

Any experiment conceived in the field and carried on by improvisation in competition with other work, as this one was, suffers from limited facilities and limited planning. If repeated, one would insist, at least, on a grid to make estimates of auroral elevation more reliable and a simple photometer to take some of the guesswork out of auroral intensities. That some consistency comes out of the crude observations lends confidence to the results of the analysis.

ACKNOWLEDGMENTS

The assistance and advice of Mr. A. H. Shapley in the preparation of this paper is gratefully acknowledged. The author also wishes to thank the United States Coast and Geodetic Survey for the use of the magnetograms from their Barrow Magnetic Observatory.

References

[1] E. V. Appleton, R. Naismith, and G. Builder, Nature, **132**, 340 (1933).
[2] K. Franz and W. Stoffregen, Elek. Nachr.-Tech., **11**, 1 (1934).
[3] S. Chapman and J. Bartels, Geomagnetism, Oxford, Clarendon Press (1940).
[4] L. Harang, The aurorae, John Wiley and Sons, Inc., New York (1951).
[5] A. C. B. Lovell, J. A. Clegg, and C. D. Ellyett, Nature, **160**, 372 (1947).
[6] A. Aspinall and G. S. Hawkins, J. Brit. Astr. Assoc., **60**, 130 (1950).
[7] H. G. Booker, C. W. Gartlein, and B. Nichols, J. Geophys. Res., **60**, 1 (1955); K. L. Bowles, Ph.D. thesis, Cornell University (1955); R. B. Dyce, Ph.D. thesis, Cornell University (1955).
[8] D. W. R. McKinley and P. M. Millman, Can. J. Phys., **31**, 171 (1953).
[9] B. W. Currie, P. A. Forsyth, and F. E. Vawter, J. Geophys. Res., **58**, 179 (1953).
[10] J. P. Heppner, E. C. Byrne, and A. E. Belon, J. Geophys. Res., **57**, 121 (1952).
[11] R. Lindquist, Ark. Geofysik., **1**, No. 11, 247 (1951).
[12] J. H. Meek, International Union of Geodesy and Geophysics, Association of Terrestrial Magnetism and Electricity, Transactions of the Oslo meeting, August 19-28, 1948, Washington, D. C., Bull. No. 13, 373 (1950).
[13] J. H. Meek, J. Geophys. Res., **58**, 445 (1953).
[14] J. H. Meek, J. Geophys. Res., **59**, 87 (1954).
[15] A. Omholt, J. Atmos. Terr. Phys., **5**, 243 (1954).
[16] M. J. Seaton, J. Atmos. Terr. Phys., **4**, 285 (1954).

TEMPERATURE DISTRIBUTION OF THE IONOSPHERE UNDER CONTROL OF THERMAL CONDUCTIVITY

By Francis S. Johnson*

United States Naval Research Laboratory, Washington 25, D. C.

(Received November 12, 1955)

ABSTRACT

The effect of thermal conductivity in controlling the temperature distribution of the high atmosphere is considered. The energy absorbed in the F region is conducted downward into a denser region of the atmosphere, where it is dissipated by infrared emission. The calculations indicate that the atmosphere is isothermal above about 250 km, and that between 100 and 200 km there is a very strong positive temperature gradient. The temperature in the isothermal region is assumed to be 1100°K, in order to provide enough atmosphere near 300 km to support an $F2$ region. The low temperature at 80 km is due primarily to the lack of absorbed energy there rather than to the presence of a strongly emitting layer at that level.

INTRODUCTION

The high thermal conductivity of the upper atmosphere was first pointed out by Spitzer [see 1 of "References" at end of paper]; and, more recently, Bates [2] has considered the importance of conductivity in a number of model atmospheres. Bates concludes that there must be more energy absorbed in the high atmosphere than the amount normally considered necessary to produce the ionosphere. In this paper, Bates' ideas are extended by making more detailed assumptions and calculations. A relatively large rate of absorption of solar energy is assumed and the temperature variation with height is computed, assuming that thermal equilibrium prevails and that all the heat absorbed above 130 km is conducted downward into a denser region of the atmosphere where it is lost by infrared emission. The calculations show that above about 250 km the atmosphere is isothermal; this results from the fact that in a very tenuous gas the thermal capacity is very small compared to the thermal conductivity, because the conductivity is independent of pressure while the heat capacity depends linearly upon density. The rates at which solar energy is absorbed at different altitudes require that there must be a very steep positive temperature gradient between 100 and 200 km, in order that all the absorbed energy be conducted downward into an atmospheric region where it can be dissipated by radiation.

*Present address: Missile Systems Division, Lockheed Aircraft Corporation, Van Nuys, California.

ASSUMPTIONS

It is difficult to estimate accurately the value of the thermal conductivity at high levels. It is assumed here that atomic oxygen and nitrogen act as a rare gas, and that the thermal conductivity can be estimated by interpolating between helium and neon. For a mixture of atomic and diatomic oxygen and nitrogen, it is assumed that the conductivities can be combined according to a linear law, although for some gases this method of combining conductivities is known not to be valid. Finally, the temperature dependence of the thermal conductivity is taken to be proportional to the square root of the temperature. The expression used is

$$K = (3.5 + 6.7f)T^{1/2} \times 10^{-6} \quad \ldots\ldots\ldots\ldots\ldots\ldots (1)$$

where f is the fractional number of particles which are atomic, T is the absolute temperature, and K is the conductivity in cal cm^{-1} sec^{-1} deg^{-1}. For atmospheric composition, the values of Havens, Friedman, and Hulburt [3] are used.

Although loss of energy by radiation in the infrared plays an important role in the energy balance of the upper atmosphere in certain altitude ranges, above 130 km this is not the case, for at these altitudes there are not many mechanisms for infrared radiation; O_2 and N_2 are not good radiators, since they have no dipole moments, and most other molecules are dissociated. As pointed out by Bates, some radiation can be expected from the transition $2p^4\ ^3P_2 - 2p^4\ ^3P_1$ in atomic oxygen, the excitation being provided by collision.

In this paper, it is assumed that at altitudes above 130 km the equilibrium temperatures are determined by conductivity rather than by radiation. This is probably a satisfactory assumption, because with the rate of absorption of solar energy assumed in this study, the temperature would have to be about 2000°K in order that all the energy absorbed above 200 km be lost through radiation by atomic oxygen. Conductivity does not permit so high a temperature to be attained; most of the absorbed energy is conducted downward into a denser region of the atmosphere, from 80 to 130 km, where it is lost by radiation in the infrared by heteronuclear diatomic and polyatomic molecules. Conductivity in this manner controls the temperature distribution above about 130 km by providing a fairly rigid relationship between the temperatures at high levels and those near 80 km, where radiation is important in determining the equilibrium temperature. To take into account the radiation by atomic oxygen, it is necessary to assume only that more solar energy is absorbed than the amount considered in connection with the conductivity.

It is not possible to compute the temperature in the high isothermal region, as this would involve evaluating the radiative heat losses at all altitudes down to 80 km, and the radiation properties of this atmospheric region are not well enough known to do this. Therefore, a temperature has been arbitrarily assumed, and a value of 1100°K was selected for the following reasons: (1) A temperature as high as this is necessary to account for scale heights and ion densities measured in the $F2$ region; (2) it is necessary to assume a high temperature in order to get enough air at high levels to absorb solar radiation and produce the $F2$ layer; and (3), without the higher density which this model produces in the $F2$ region, diffusion

would dominate and rapidly spread the $F2$ region, so that it could not exist near 300 km.

The relative rates of energy absorption are taken from Havens, Friedman, and Hulburt [3] and are shown in the curves of Figure 1. The radiation is assumed to consist of two components: component 1 consists mainly of soft X-rays, which are principally absorbed near 120 km; component 2 consists of very soft X-rays

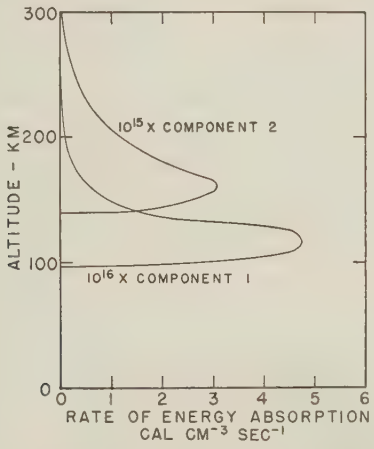

FIG. 1—The rate of absorption of solar energy in the atmosphere. Component 1 is taken directly from Havens, Friedman, and Hulburt, and consists of soft X-rays in the wavelength region from 13A to 230A. Component 2, consisting mainly of the resonance lines of He I and He II, is 15 times greater than the corresponding quantity of Havens, *et al.*

or very short ultraviolet, mainly the resonance lines of He I and He II, which are very strongly absorbed, the strongest absorption being near 160 km. However, the absolute values of component 2 are increased by a factor of 15 over the values assigned by Havens, *et al.* The reason for increasing their estimate by the factor of 15 is that this is approximately the amount of energy required to give temperatures as high as 1100°K in the isothermal region. In addition, some experimental justification for increasing their estimate is found in the solar spectrum obtained in the rocket flight of February 20, 1955 [4]. The "Balmer alpha" line of He II at 1640A was observed and estimated to contain about 0.006 erg cm^{-2} sec^{-1}. According to the calculations of Brennan [5], the Lyman series of this ion, which lies in the spectral range 230 to 305A, may be expected to contain about 50 times as much energy as the Balmer alpha line, or 0.3 erg cm^{-2} sec^{-1}. Somewhat more energy than this may be expected in the radiations from neutral helium, and if we estimate 0.45 erg cm^{-2} sec^{-1} for He I, we have 15 times more energy than the value 0.05 assumed by Havens, *et al.*, to be included in the resonance lines of neutral and ionized helium. To compensate for the radiation by atomic oxygen, the absorption of about 0.1 erg cm^{-2} sec^{-1} in other lines and continua through this spectral region would be required, with an absorption coefficient about the same as for component 2. It is necessary to assume that the ionization produced by the solar energy in

excess of the amount assumed by Havens, *et al.*, is largely "unobserved ionization," suggested by Bates [2] as being so quickly destroyed by recombination as to be unobserved in ionospheric experiments. There is some experimental evidence for such a fast decaying component in the F region, found in eclipse observations by Minnis [6].

CALCULATION OF TEMPERATURE DISTRIBUTION

The rates of energy absorption above each altitude were obtained by graphical integration of the curves of Figure 1. The temperature lapse-rates required to conduct downwards the amount of heat absorbed above any given level were than calculated for each such level, using the conductivity as determined from equation (1). Then the temperature differences between the isothermal region above 300 km and each level were found by graphical integration. Since the temperature above 300 km was assumed to be 1100°K, the temperature curve could be constructed downwards; however, below about 120 km, the temperature resulting from this calculation became unreasonably low or negative. It was necessary, therefore, to assume that below about 130 km there was a loss of energy by some process other than conduction; this would undoubtedly be through radiation by the same radiator which so effectively cools the region near 80 km. The temperatures calculated from the conductivity theory for altitudes down to 130 km are shown in Figure 2, where they are compared with the temperatures given by Havens, *et al.* [3], and with temperatures given by the Rocket Panel [7] for two different assumptions concerning molecular weight.

The rate of conduction of energy downward at 130 km is about 2×10^{-8} cal cm^{-2} sec^{-1}, and the radiation of this amount of energy between 130 and 80 km requires a rate of emission per unit mass of about 2×10^{-5} cal gm^{-1} sec^{-1}, which can be compared with 3×10^{-5} cal gm^{-1} sec^{-1} required to maintain day-to-day equilibrium near 50 km, where absorption of solar energy by ozone causes a warm layer in the atmosphere [8]. This rather close agreement indicates that the cool layer near 80 km is due to the lack of absorbed energy rather than to the presence of a strongly emitting layer there; the region below it is warmed by absorption

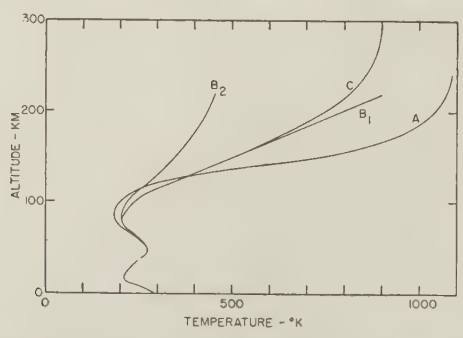

FIG. 2—The temperature distribution with altitude. Curve A results from the assumptions made in this paper, curves B_1 and B_2 are those proposed by the Rocket Panel for constant and varying molecular weight with altitude, and curve C gives the values used in the $F2$ ionospheric theory of Havens, Friedman, and Hulburt.

by ozone, and the region above it by absorption of the energy considered in this paper. Some radiation is absorbed near 80 km, namely, solar X-rays [9] and hydrogen Lyman alpha radiation [10], but the amount is about an order of magnitude smaller than the energy conducted downwards, a value of 2.4×10^{-9} cal cm^{-2} sec^{-1} being given by Byram, Chubb, and Friedman [9, 10]. The radiating gases from 50 km up to at least 130 km are probably H_20, OH CO_2 , and possibly CO.

Below 130 km, the temperature curve was arbitrarily extended with values lower than those of the Rocket Panel [7], in order to obtain a density at 120 km which was in agreement with the density determined from solar X-ray data [3, 11], which is about three times lower than the Rocket Panel density. The differences in the density values from these two sources may be real and indicative of the normal range of variation. Hence, selection of the X-ray data in this paper is arbitrary, but serves to show that densities as low as these at 120 km are consistent with relatively high densities in the $F2$ region. The arbitrarily extended curve is shown in Figure 2, along with curves from the Rocket Panel and from Havens,

TABLE 1

Altitude	Molecular weight	Temperature	Log p	Particles per cc	Scale height
km		°*K*	*dyne* cm^{-2}		*km*
50	28.8	271	2.955	2.4×10^{16}	8.6
60	28.8	245	2.400	7.4×10^{15}	7.3
70	28.8	210	1.760	2.0×10^{15}	6.3
80	28.8	185	1.020	4.1×10^{14}	5.7
90	28.8	183	0.220	6.6×10^{13}	5.6
100	28.8	200	−0.535	1.06×10^{13}	6.1
110	27.0	230	−1.199	2.0×10^{12}	7.4
120	25.3	280	−1.704	5.1×10^{11}	9.8
130	25.3	423	−2.082	2.1×10^{11}	14
140	25.0	594	−2.326	5.8×10^{10}	20
150	24.5	737	−2.507	3.0×10^{10}	26
160	23.7	846	−2.655	1.9×10^{10}	32
170	23.0	925	−2.783	1.3×10^{10}	36
180	22.3	979	−2.899	9.3×10^{9}	39
190	21.7	1017	−3.006	7.0×10^{9}	42
200	21.1	1043	−3.107	5.4×10^{9}	44
210	20.6	1061	−3.202	4.3×10^{9}	47
220	20.0	1074	−3.294	3.4×10^{9}	48
230	19.6	1082	−3.382	2.8×10^{9}	50
240	19.2	1088	−3.468	2.3×10^{9}	52
250	18.7	1092	−3.549	1.9×10^{9}	54
260	18.2	1095	−3.629	1.6×10^{9}	55
270	17.8	1097	−3.707	1.3×10^{9}	57
280	17.5	1098	−3.783	1.1×10^{9}	58
290	17.2	1099	−3.857	9.1×10^{8}	60
300	16.8	1100	−3.930	7.7×10^{8}	61
310	16.5	1100	−4.001	6.5×10^{8}	62

et al. The curve based on thermal conductivity results in a pressure at 220 km about three times as great as the Rocket Panel pressure. Tabulated values of the temperatures, pressures, particle densities, and scale heights are given in Table 1; molecular weights from the paper of Havens, *et al.*, are included for convenience.

Both solar and ionospheric observations indicate a considerable variability of the radiations responsible for the high temperatures in the $F2$ region. The temperatures arrived at in these calculations may represent typical or average conditions. Whenever unusual solar activity is present, the temperatures will be substantially higher. It may be possible in this way to account for the escape of helium from the earth's atmosphere with an average temperature lower than the 1500°K value calculated by Spitzer [1].

DIURNAL TEMPERATURE CHANGES

To calculate the diurnal temperature changes, it is necessary to make stepwise calculations, as was done by Lowan [12] for a different temperature distribution. These tedious calculations were not performed, but one can estimate the magnitude of the diurnal variations. The heat capacity of the atmosphere above any altitude becomes large compared to the heat conducted downwards at that altitude only for altitudes below 130 km. It appears, therefore, that during the night the entire atmosphere above 130 km will cool to the temperature at 130 km, or to about 400°K. The rate of energy absorption after sunrise is sufficient to cause heating at a rate of approximately 100°K per hour, hence temperature equilibrium would be re-established by about noon. The result of such a large diurnal temperature variation would be to cause a high pressure bulge over the afternoon quadrant of the earth. The data in Table 1 and curve A of Figure 2 apply to the equilibrium conditions which prevail during the afternoon.

References

[1] L. Spitzer, The terrestrial atmosphere above 300 km, in "Atmospheres of the Earth and Planets," edited by G. P. Kuiper, University of Chicago Press, Chicago, p. 213 (1949).
[2] D. R. Bates, Proc. Phys. Soc., B, **64**, 805 (1951).
[3] R. J. Havens, H. Friedman, and E. O. Hulburt, The ionospheric $F2$ region, Report of 1954 Cambridge conference on physics of the ionosphere, The Physical Society London, p. 237 (1955).
[4] F. S. Johnson, H. Malitson, J. D. Purcell, and R. Tousey, Emission lines in the solar ultraviolet, in preparation.
[5] J. G. Brennan, unpublished material quoted in "An Ultraviolet Multiplet Table," C. E. Moore, Nat. Bur. Stan. Circular 488.
[6] C. M. Minnis, J. Atmos. Terr. Phys., **6**, 91 (1955).
[7] The Rocket Panel, Phys. Rev., **88**, 1027 (1952).
[8] F. S. Johnson, Bull. Amer. Met. Soc., **34**, 106 (1953).
[9] E. T. Byram, T. A. Chubb, and H. Friedman, Solar X-rays and E-layer ionization, in "Rocket Exploration of the Upper Atmosphere," edited by R. L. F. Boyd and M. J. Seaton, Pergamon Press, Ltd., London (1954).
[10] E. T. Byram, T. A. Chubb, and H. Friedman, The study of extreme ultraviolet radiation from the sun with rocket-borne photon counters, in "Rocket Exploration of the Upper Atmosphere," edited by R. L. F. Boyd and M. J. Seaton, Pergamon Press, Ltd., London (1954).
[11] E. T. Byram, T. A. Chubb, and H. Friedman, unpublished material.
[12] A. N. Lowan, J. Geophys. Res., **60**, 421 (1955).

ARCTIC UPPER-ATMOSPHERE PRESSURE AND DENSITY MEASUREMENTS WITH ROCKETS*

By H. E. LaGow and J. Ainsworth

United States Naval Research Laboratory, Washington 25, D. C.

(Received November 19, 1955)

ABSTRACT

Data were obtained from four balloon-launched Deacon rockets during the summers of 1953 and 1954, without the aid of ground-based trajectory measurements. The atmospheric density profile in the 25- to 45-km region was found within the experimental error to be the same as the Rocket Panel, White Sands values. The measured atmospheric pressure and the computed temperature for the flights at 62° and 74° north were found to be up to 30 percent higher in the 30- to 45-km region, but approximately equal to the White Sands values at 70 km. At 74° north, a high lapse-rate is indicated within the region 44 to 60 km.

INTRODUCTION

The results of upper atmosphere pressure, density, and temperature measurements prior to 1952 have been presented by the Rocket Panel [see 1 of "References" at end of paper], a description of the various methods of measurement has been presented by Newell [2], subsequent experiments are described by Boyd, Seaton, and Massey [3], and a recent survey paper has been given by Newell [4]. The bulk of the experiments have been made at White Sands, New Mexico. Measurements at more northern latitudes (Fig. 1) were made possible in the summers of 1953 and 1954 by the availability of a new and less expensive vehicle which was introduced by Van Allen [3] in 1952.

VEHICLE

A Deacon rocket was attached to a General Mills 68′ diameter, 0.001″ polyethylene "skyhook" balloon (Fig. 2) and was released from shipboard. Ascent of the balloon was about 300 meters per second during flight, and atmospheric pressure and temperature were continuously transmitted by a radio-sonde unit attached to the balloon. As the balloon approached its ceiling altitude of 25 km, a pressure-actuated switch fired the rocket from its suspension 100′ below the raising balloon. At the time of firing, a rip-cord removed a plastic bag placed about the rocket to prevent convective cooling during the balloon ascent, and the firing gondola was at the same time released from the rocket.

*This project was supported by the Office of Naval Research, the Bureau of Aeronautics, and the U. S. Atomic Energy Commission.

The Deacon rocket produced a 6,000-pound thrust and an acceleration of 30 to 50 gravitational units during its three-second burning-period. The rocket was $6\frac{1}{2}''$ in diameter, $147\frac{1}{2}''$ long; its total weight with pay-load, and its burnout weight, were 218 and 118 pounds, respectively. For sea-level launching, the Deacon had a peak altitude of approximately 30 km. When launched from 25 km, the reduced drag on the missile allowed a maximum altitude of about 80 km.

INSTRUMENTATION

The data obtained during rocket flight were stagnation and ambient pressures, and these data coupled with the trajectory were sufficient to determine the pressure, density, and temperature profiles. Stagnation pressures at the nose probe-tip (Figs. 3 and 4) were measured by a 0-250 mmHg differential pressure bellows

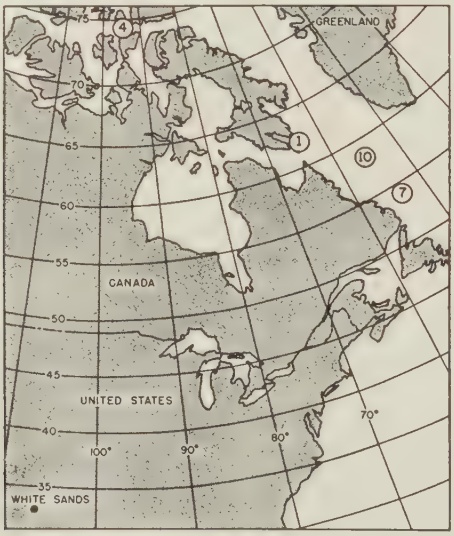

FIG. 1—Rocket launching-sites

gauge. The gauge repeatability was 1 mmHg, and its acceleration sensitivity was approximately 1 mmHg per 2g. The value of the stagnation pressure was constant [5] for rocket yaw-angles up to 30°. For ambient pressure measurement, holes located 7 calibres from the probe-tip maintained an ambient pressure chamber in the nose of the rocket. The value of the pressure in this chamber was sensitive to Mach number and yaw [6], as shown in Figure 5. The ambient-pressure bellows gauge possessed the same range and characteristics as the stagnation pressure gauge. It was necessary, therefore, to measure ambient pressure compressed by a factor, taken for convenience as about eight. Ambient pressure below 100 microns was measured by a Pirani gauge, located 7 calibres back from the rocket nose. The gauge was constructed of 0.00015″ tungsten wire, wound on insulated posts. Additional instrumentation consisted of a resistance thermometer to measure the Pirani gauge-case temperature, an accelerometer to measure rocket-propellant

burning-time, and a 25-mmHg pressure switch to start the ambient pressure compressor and a data commutator.

The data were telemetered by a two-channel FM-FM, 300-milliwatt transmitter driving the rocket after-body and the nose section as the two elements of a dipole.

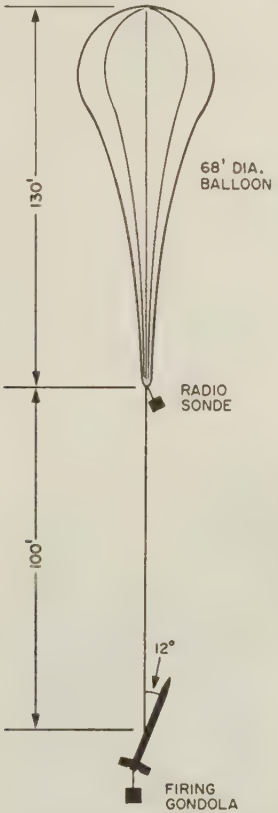

FIG. 2—Instrument suspension

Channel 1 recorded the burning time of the rocket. Data from all gauges and all calibration voltages were placed on commutator contacts, which were connected to Channel 2 by a 1.5 cycle per second motor-driven wiper-arm. The ground-station consisted of a Clarke receiver, two NRL demodulators, and a two-channel Sanborn recorder. Figure 6 is a typical portion of a flight record. A plot of stagnation pressure and ambient pressure *vs* time is shown in Figure 7 for the rocket fired at 74° north.

TRAJECTORY

The radio-sonde record provided the rocket launching-altitude. The rocket-fuel burning-time, coupled with rocket thrust and first-order drag estimates [7], yielded the burnout altitude and burnout velocity. Determination of the vertical

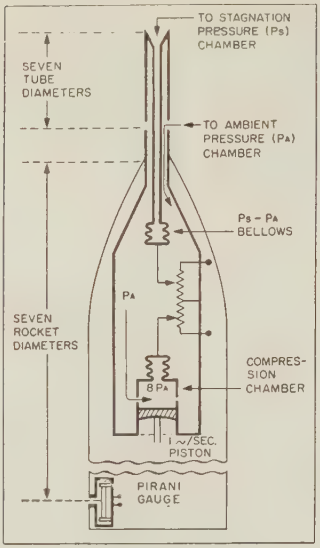

FIG. 3—Pressure instrumentation

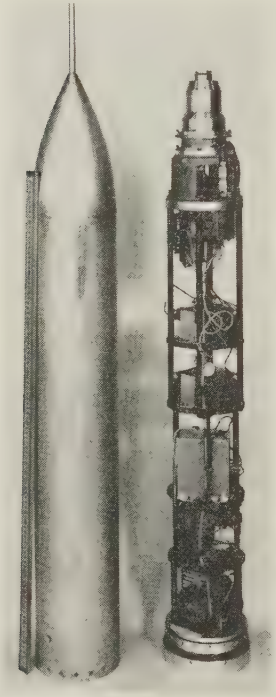

FIG. 4—Deacon rocket instrument section

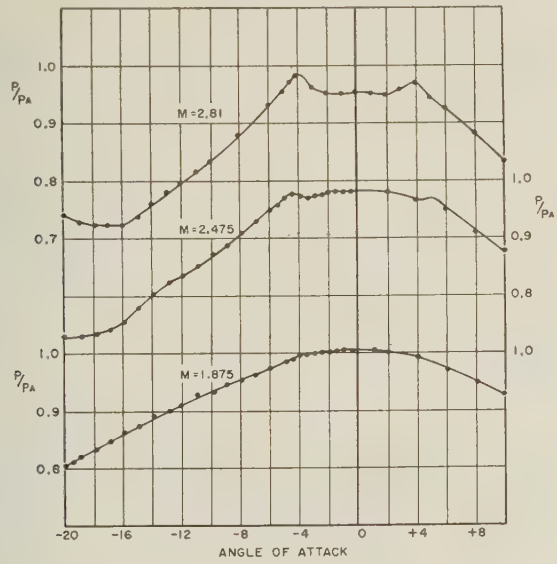

FIG. 5—Ambient pressure-probe sensitivity

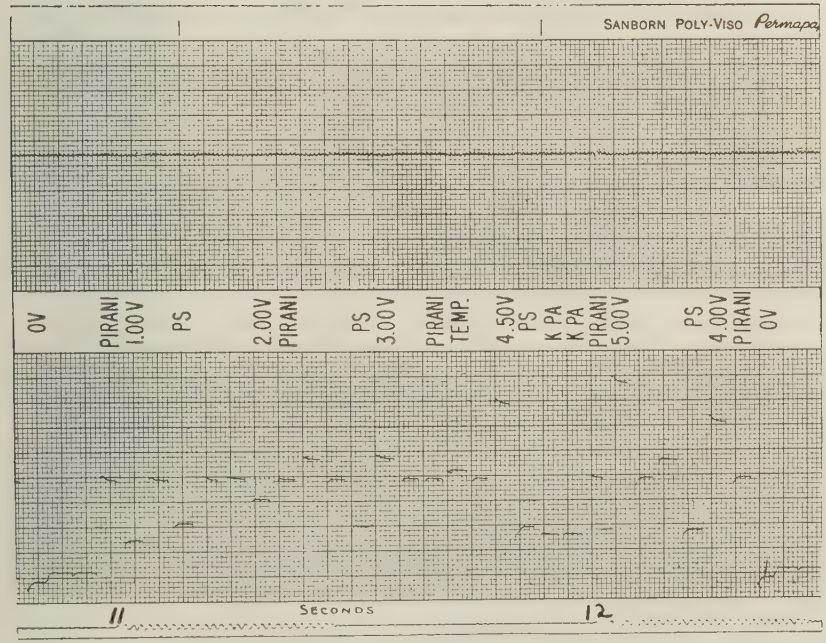

FIG. 6—Section of NRL-4 telemetering record

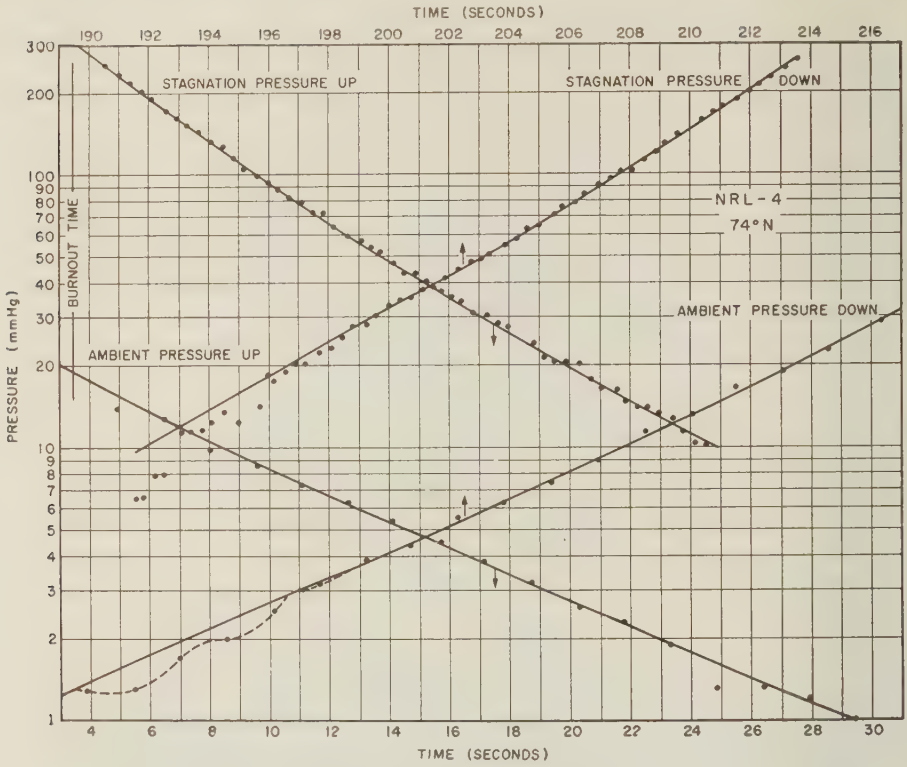

FIG. 7—Stagnation and ambient pressure *vs* time

trajectory, beginning with the burnout altitude, was a process of successive approximations to obtain a suitable vertical velocity throughout the flight. A first approximation to the vertical velocity was obtained by assuming free fall from the burnout time to the approximate peak time obtained from the times of equal stagnation (or ambient) pressure on ascent and descent. The amount of yaw indicated by the ambient pressure data formed the basis for the estimate of the first-order drag to be used for that part of the trajectory below 55 km. Above 55 km, free fall was assumed. Using the first vertical trajectory obtained, the ambient pressure was plotted *vs* altitude. The values of the ambient pressure and the slopes of the ambient pressure *vs* altitude curves must be the same on both ascent and descent of the rocket. Inspection of successive curves of ambient pressure *vs* altitude yielded a quickly converging vertical trajectory and thus a final profile of ambient pressure *vs* altitude. The methods by which horizontal velocities and first-order drag were obtained are discussed in the following paragraph.

DENSITY COMPUTATION

Stagnation pressure, ambient pressure, and total velocity were used to compute density from the relation [8]

$$\rho = \frac{0.144Ps - 0.066Pa}{V^2} \qquad \left[\frac{\text{grams}}{\text{meter}^3}\right] = \left[\frac{\text{mm Hg}}{\text{km}^2}\right] \quad \ldots\ldots\ldots (1)$$

This equation is valid for Mach numbers greater than one and for mean free-path lengths much smaller than the probe diameter. The vertical trajectory determined the vertical velocity, and to obtain the total velocity V it was necessary to complete the trajectory by assigning values of horizontal velocity throughout the flight. Burnout and final horizontal velocities were determined by the requirement that the densities measured at the burnout altitude must correspond to the extrapolated (1.5 km approx.) radio-sonde density at the time of firing. Values of the horizontal velocity above the burnout altitude are determined by the requirement that the density *vs* altitude curves for ascent and descent must be identical. The horizontal velocity obtained in this way must decrease at a rate indicated by the first-order drag assigned to the vertical trajectory. This served as a final check on the consistency of the whole process of approximation.

The large lift accelerations developed during yaw [7] effected a considerable perturbation of the vertical and horizontal components of the total velocity and introduced difficulty during the trajectory analysis. Because of the short yaw periods, however, it was possible to combine the lift and drag forces into an average total drag force as a function of time, as follows:

$$F = K\rho V^2 \quad \ldots\ldots\ldots (2)$$

Equation (1) determined ρV^2, and an average total drag coefficient $K_{(t)}$ was determined by trial. $K_{(t)}$ was about twice the zero angle of attack value.

ANALYSIS OF 1953 FLIGHTS

The flight schedule is given in Table 1. Table 2, along with Figures 8, 9, and 10, present the final data for the two successful flights.

TABLE 1—*Flight summary*

Rocket	Launching time	Location of release	Launching altitude	Peak altitude	Peak time
			km	*km*	*sec*
NRL-1	Aug. 53 052154Z	62° 04′ N 63° 55′ W	24.2	71.7	100.8
NRL-2	Aug. 53	Telemetering failed			
NRL-3	Aug. 53	Balloon failed at 9 km			
NRL-4	Aug. 53 111709Z	74° 34′ N 94° 29′ W	23.9	78.4	108.1
NRL-5	Sep. 53	Large yaw prevented satisfactory ambient pressure measurement			
NRL-6	Sep. 53	Balloon and rocket separated at 25 km; rocket did not fire			

For both flights, the radio-sonde temperatures during balloon ascent were found to be in error. It is believed that mounting the ratio-sonde unit close to the balloon did not allow the minimum required air circulation about the thermistor element. In both instances, however, temperature soundings taken at approximately the same launching times were available from nearby weather-stations. The error

TABLE 2—*Final data*

h	NRL-1			NRL-4		
	ρ	Pa	T	ρ	Pa	T
km	*grams/meter*^{3}	*mmHg*	°*K*	*grams/meter*^{3}	*mmHg*	°*K*
20	88.0	43.5	229	90.0	43.7	226
24	48.3	23.8	229	49.3	23.8	228
28	26.2	13.3	235	26.5	13.7	240
32	13.9	7.65	256	14.3	8.65	280
36	7.60	4.67	285	7.80	5.55	329
40	4.30	2.95	319	4.34	3.26	348
44	2.52	....	....	2.46	1.84	347
50	....	....	....	....	....	293
60	....	....	....	....	....	220
72	....	0.034	....	0.076	0.038	216
78	....	....	....	0.030	0.014	....

in launching altitude due to the substitution of nearby temperatures is believed to be less than 0.15 km. It should be noted that the radio-sonde pressure-altitudes for the two flights agree with the four-year averages [9] for July-August for the respective locations. For the 1954 flights, the radio-sonde unit was suspended below the rocket and correct temperatures were obtained.

The roll period of NRL-4 was two seconds; yaw was relatively small below 45 km and was a maximum of about 35° on reentry. NRL-1 had a five-second roll period, and large yaw on both ascent and descent. Where large yaw existed, the ambient pressure curve was drawn through the average positions on ascent and descent of those pressure points which indicated the least angle of attack.

Figure 11 shows the effect of roll combined with large average angle of attack upon the Pirani pressure measurements made at the peak of flight for NRL-1. Theory and measurement [7, 10, 11] of "roll" pressure for yawed cylindrical bodies in sub- and super-sonic air-streams place the free-stream pressure points at angles of approximately 30° from the point of maximum pressure. The smaller yaw and smaller average angle of attack of NRL-4 allowed the analysis of its Pirani data to be extended over a greater range than that of NRL-1. At the same time, the faster roll rate required a correction for the time-constant of the Pirani gauge. This correction was about 5 percent when applied to the ascent data, but shortly after the peak of flight the average angle of attack increased rapidly and the correction was difficult to apply. The Pirani descent data for NRL-4 were plotted (Fig. 10) without the time-constant correction.

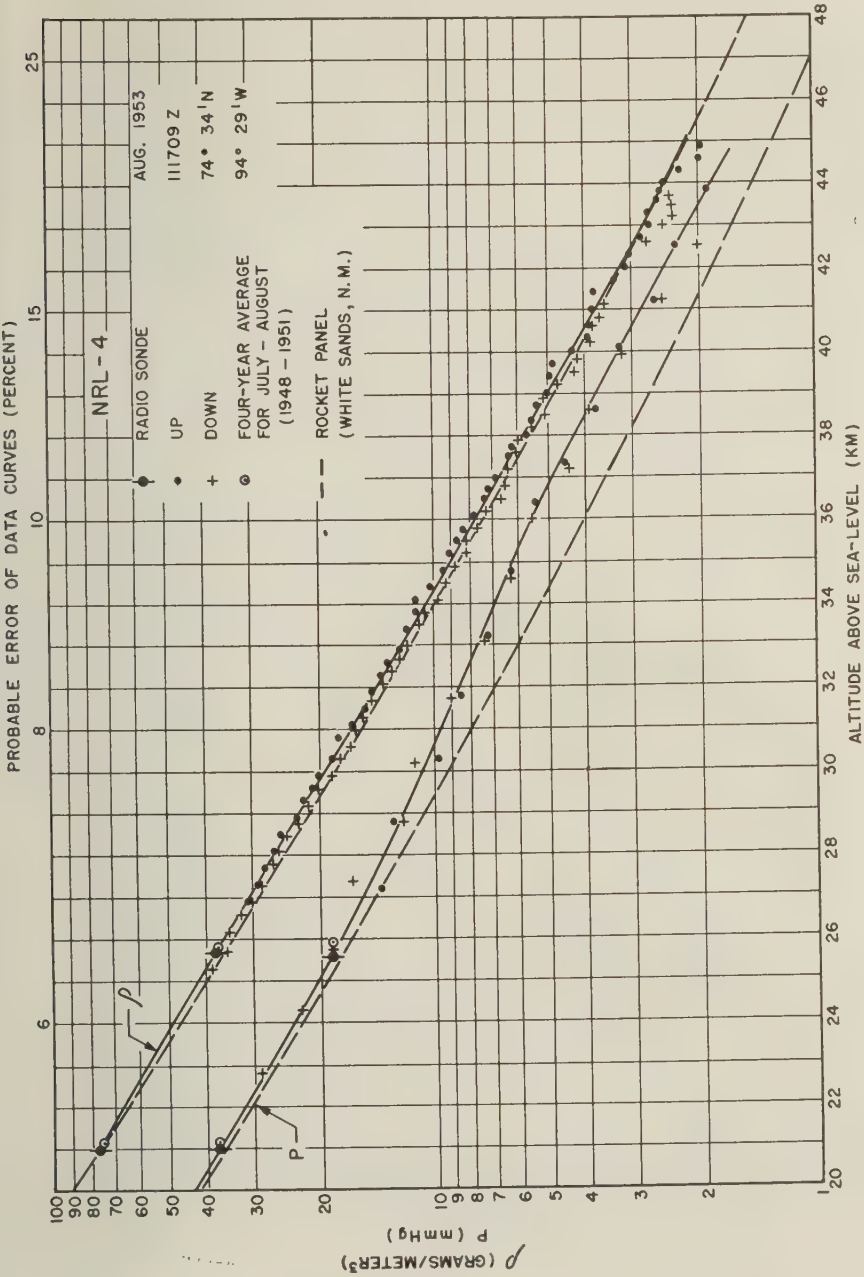

FIG. 8—Density and pressure *vs* altitude

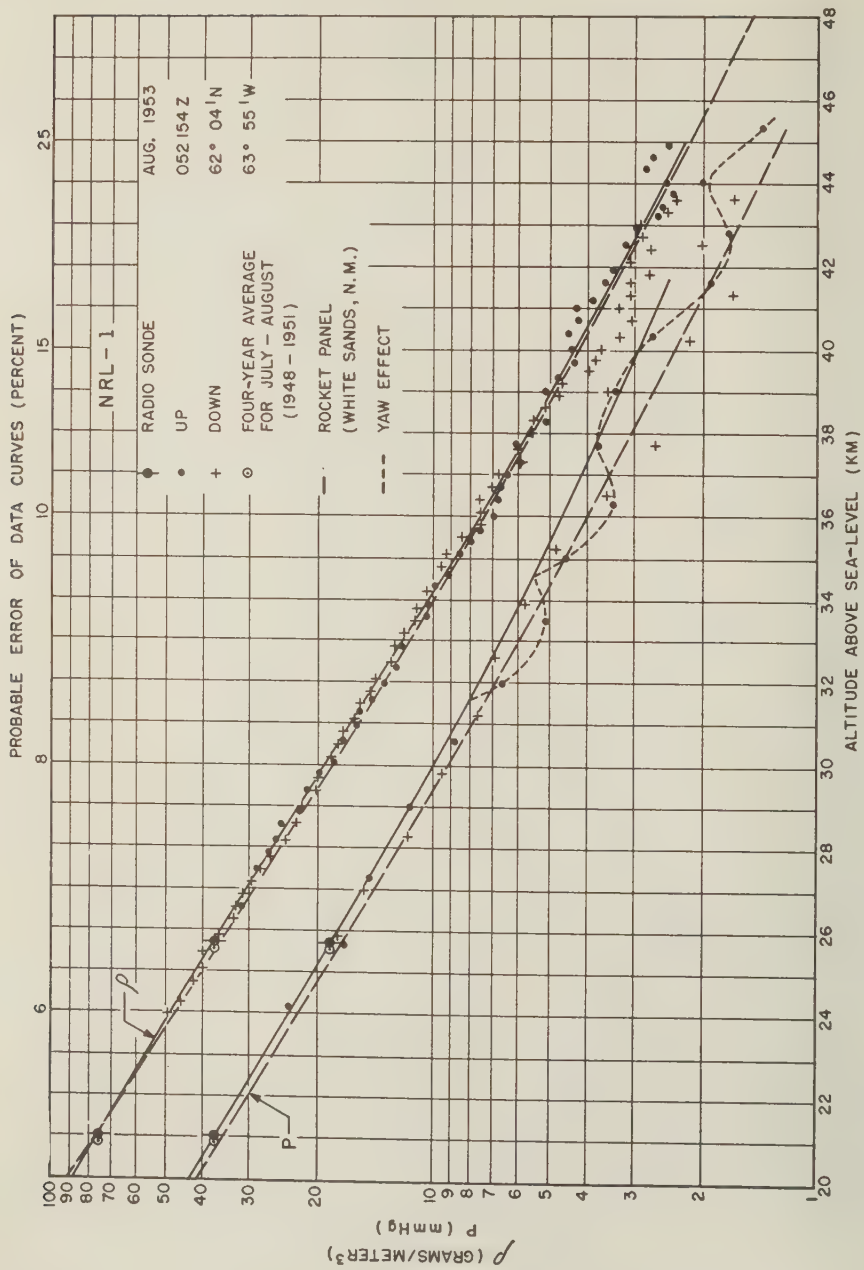

FIG. 9—Density and pressure *vs* altitude

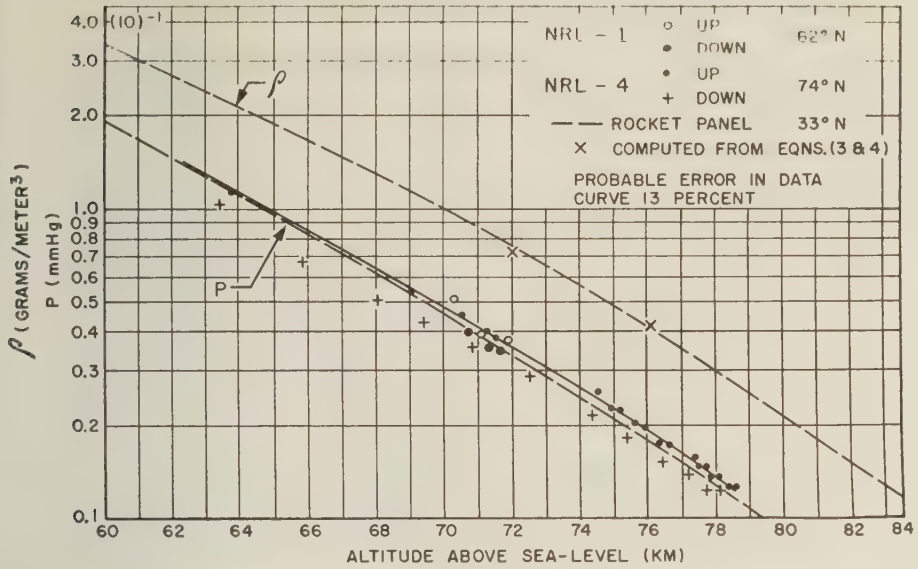

FIG. 10—Pirani gauge pressure *vs* altitude; density was computed from the slope of the NRL-4 ascent data

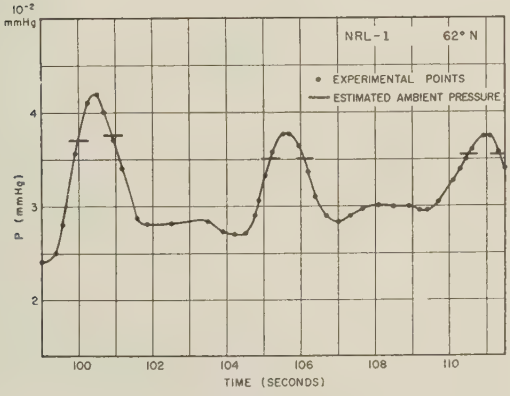

FIG. 11—Pirani gauge "roll" pressures *vs* time

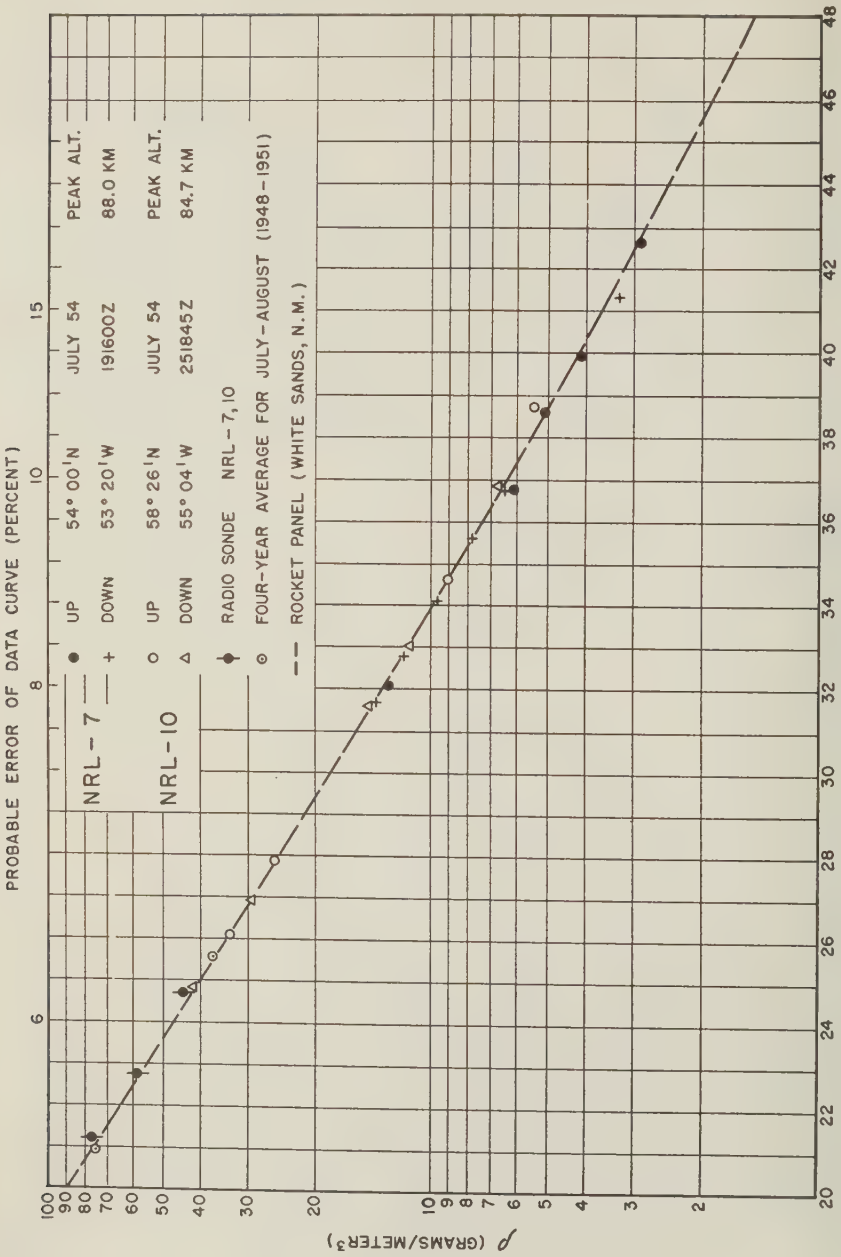

FIG. 12—The 1954 density data

1954 FLIGHTS

During the summer of 1954, stagnation pressure data were obtained from snap-action diaphragm pressure-switches, installed as supplementary equipment on Deacon rockets NRL-7 and NRL-10. Both flights compared with NRL-4 in stability, and the approximations to the vertical trajectories could be determined without the aid of ambient pressure data. Density (Fig. 12) was then computed from equation (1).

TEMPERATURE

At the lower altitudes, where both pressure and density were measured, temperature (Fig. 13) was obtained from the ideal gas law, as follows:

$$T = \frac{M}{R}\frac{P}{\rho} = 464\frac{P}{\rho} \qquad \left[\frac{\text{mmHg}}{\text{grams/meter}^3}\right] \ldots\ldots\ldots\ldots\ldots\ldots (3)$$

At 72 and 76 km, where the pressure profile was accurately obtained on ascent, temperature was determined from the relation [2]

$$T = -g\frac{M}{R}\frac{\mathrm{d}h}{\mathrm{d}(lnP)} = -33.8\frac{\mathrm{d}h}{\mathrm{d}(lnP)} \qquad [h(\text{km}), P(\text{mmHg})] \ \ldots\ldots (4)$$

The dotted curve of Figure 13 represents an average interpolated temperature obtained from equation (4), using the temperature and pressure values at 44 and 72 km. It should be noted, however, that both the method of processing the data and the large range over which interpolation occurs allow the presence of additional maxima and minima along the total temperature profile.

DISCUSSION OF RESULTS

Pressure and density measurements require accurate trajectory measurement, and the present series of flights demonstrated that this could be achieved with small, balloon-launched rockets without the aid of ground-based tracking services. The increased operational simplicity of the method allowed for an increase in the total number of flights and for launching at remote sites. In addition, launching at high altitude removed the necessity for protecting sensitive differential pressure-gauges from the high pressures obtained in sea-level launching. The principle difficulty encountered in the experiment was trajectory analysis. This analysis problem could be considerably reduced by increasing the stability of the rocket with an increase of fin area, by establishing a roll rate of about one cycle per second, by removal of any protective covering on the rocket just prior to firing, and by removing the possibility of the rocket hitting the balloon. Trajectory analysis could be further simplified by inclusion of accelerometers and aspect measuring equipment. It is believed that with these improvements, the labor in trajectory analysis would be comparable with that required to process the trajectory data furnished by ground-stations.

Comparison of the data with the Rocket Panel average values shows that the 1953 density profiles at 62° and 74° north and the 1954 density measurements are approximately the same as the values at 33° north, while the 40-km values of the pressure and temperature are considerably higher. At the present time, there

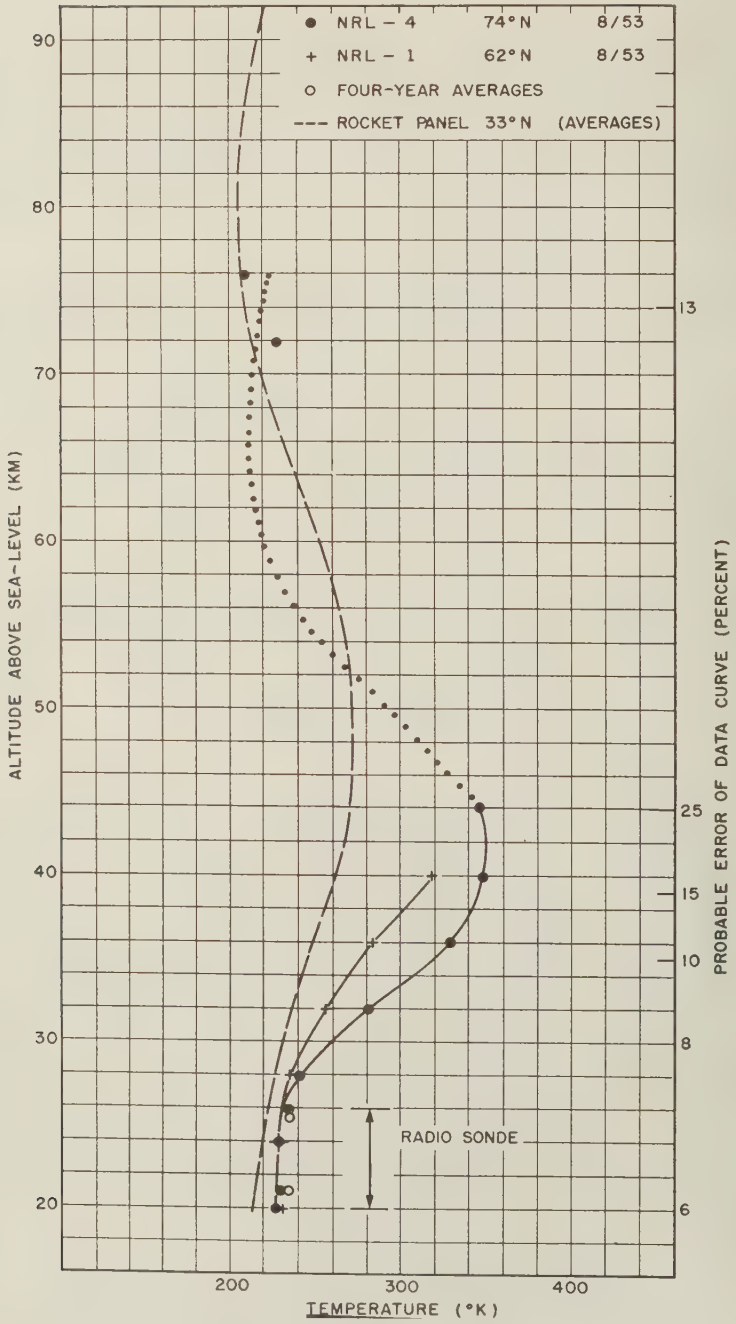

FIG. 13—Temperature *vs* altitude

are not, however, a sufficient number of measurements to indicate whether these pressures and temperatures represent unusual effects, such as those indicated at the Berlin-Tempelhof [12] radio-sonde station and at Shemys [13], or whether the long periods of summer sunlight at the higher latitudes result in high temperatures over periods of several weeks or perhaps months. The AWS survey of radio-sonde 10-mb heights and temperatures [13] and the work of Crary with anomalous sound studies of 20- to 70-km winds and temperatures [14] seem to indicate that the data might represent unusual events. At the same time, a search of radio-sonde measurements preceding and following the 1953 firings indicated normal temperatures at the 25- and 50-mb levels, rather than the high temperatures at these levels which accompanied the Berlin and Shemys events, and there was no indication of a subsequent downward shift of the high temperature region to the 150-mb level, such as that which followed shortly after each of the Berlin events.

Consideration of solar radiation [15] suggests that the high temperatures at 40 km might be of extended duration. Application of the Stefan-Boltzman law in a simplified examination of the absorption and radiation of a layer of air requires that because of the 24-hour period of sunlight, the temperature maximum of the 40-km layer at 74° north will be about 50°K higher than the maximum at White Sands, where the sunlight period is roughly 12 hours. Assumption of a constant meridional pressure-gradient [16], based on the 40-km pressure values at 74° north and 33° north, gives easterly geostrophic winds increasing in value with decreasing latitude. Wind velocities are about twice those established by the observations of Crary [14] and of Brasefield [17] and used in the recent discussion of stratosphere circulation by Kellogg and Schilling [18] and Pant [19], but the disagreement is not outside the limits of error in establishing the meridional pressure-gradient.

ACKNOWLEDGMENTS

Many people and groups assisted in this program. At NRL there were valuable discussions on planning and conducting the program with Drs. H. E. Newell, Jr., and R. J. Havens; J. Bush, S. Adler, and H. Caulk assisted in the design and manufacture of the pressure instrumentation; K. Medrow and R. Groves assisted with the telemetering problem, and R. Newell aided in the data analysis. Dr. J. Van Allen, of the State University of Iowa, furnished considerable rocket and radio equipment for the flights. Lt. M. Jones, of ONR, directed the field operations. Field assistance was rendered by Drs. M. Gottlieb, L. Meredith, and R. Ellis of S.U.I., D. Church and R. King of General Mills, and the personnel of the U.S.S. *Staten Island* and U.S.C.G.C. *Eastwind*. The supplementary data of 1954 were supplied by R. Newell and L. Davis and Dr. S. Kupperian of NRL, aided by the personnel of the U.S.S. *Atka*. Analysis of the radio-sonde records was performed by L. Hafer, and additional radio-sonde data were furnished by W. Moreland of the U.S. Weather Bureau.

References

[1] The Rocket Panel, Phys. Rev., 88, 1027 (1952).

[2] H. E. Newell, Jr., High altitude rocket research, Academic Press, Inc., New York (1953).

[3] R. L. F. Boyd and M. J. Seaton (Editors), Rocket exploration of the upper atmosphere, Pergamon Press, Ltd., London (1954).
[4] H. E. Newell, Jr., Rocket data on atmospheric pressure, temperature, density, and winds, Ann. Géophys., **11**, 115 (1955).
[5] W. Gracey, D. E. Coletti, and W. R. Russell, Wind-tunnel investigation of a number of total-pressure tubes at high angles of attack, Nation. Advisory Comm. Aeronaut., Washington, D. C., Tech. Note No. 2261 (Jan. 1951).
[6] R. Ormsby, Jr., Calibration of Deacon rocket static nose probe, David Taylor Model Basin, Washington, D. C., Aero Rep. No. 860 (1954).
[7] R. Hartley, Wind-tunnel tests of two Deacon rocket models at subsonic and supersonic airspeeds, David Taylor Model Basin, Washington, D. C., Aero Rep. No. 875 (1954).
[8] R. J. Havens, R. T. Koll, and H. E. LaGow, The pressure, density, and temperature of the earth's atmosphere to 160 kilometers, J. Geophys. Res., **57**, 67 (1952).
[9] Analysis and wind flow at the 50- and 25-mb levels, Headquarters, Air Weather Service, Washington, D. C., Pub. AWS TR 105-96 (1953).
[10] H. J. Allen and E. W. Perkins, A study of effects of viscosity on flow over slender inclined bodies of revolution, Nation. Advisory Comm. Aeronaut., Washington, D. C., Rep. No. 1048 (1951).
[11] S. Goldstein, Modern developments in fluid dynamics, Oxford, Clarendon Press, Vol. 2, p. 422 (1943).
[12] R. Scherhag, Die Explosionartigen Stratosphärener wärmungen des Spatwinters 1951/1952, Berichte des Deutschen Wetterdienstes in der US-Zone, No. 38 (1952).
[13] Temperatures at the 10-mb (101,000-foot) level, Headquarters, Air Weather Service, Washington, D. C., Pub. AWS TR 105-108 (1953).
[14] A. P. Crary, Stratosphere winds and temperatures from acoustical propagation studies, J. Met., **7**, 233 (1950).
[15] S. K. Mitra, The upper atmosphere, Asiatic Society, Calcutta, 2nd ed. (1952).
[16] W. J. Humphreys, Physics of the air, McGraw-Hill Book Co., Inc., New York, 3rd ed. (1940).
[17] C. J. Brasefield, Winds and temperatures in the lower stratosphere, J. Met., **7**, 66 (1950).
[18] W. W. Kellogg and G. F. Schilling, A proposed model of the circulation in the upper stratosphere, J. Met., **8**, 222 (1951).
[19] P. S. Pant, Circulation in the upper atmosphere, Air Force Cambridge Research Center, Cambridge, Mass., Pub. AFCRC-TN-55-651 (1955).

VARIATIONS IN STRENGTH OF WIND SYSTEM, IN THE DYNAMO MECHANISM FOR THE MAGNETIC DIURNAL VARIATION, DEDUCED FROM SOLAR-FLARE EFFECTS AT HUANCAYO, PERU

By Scott E. Forbush

Department of Terrestrial Magnetism, Carnegie Institution of Washington, Washington 15, D. C.

(Received January 15, 1956)

ABSTRACT

Hourly means of solar-flare effects, or crochets, in magnetic horizontal intensity (H) at Huancayo exhibit, during daylight, a diurnal variation like that in H. This variation is expected, since McNish showed [see 1 of "References" at end of paper] that flares produce magnetic effects indistinguishable from those which would result from an increase in strength of the current system responsible for the normal magnetic diurnal variation, S_q . On the other hand, it is found that the average crochet size in H is greater by a statistically significant amount for groups of days with greater S_q amplitude. For example, the average crochet size is 80 per cent larger for a group of 49 days with average $\delta W_2 = 25.2$ (Bartels' measure of amplitude of S_q) than for a group of 48 days with average $\delta W_2 = 1.6$. Although δW_2 increases with sunspot number, the crochet size does not. Thus, the larger average size of crochets, at Huancayo, on days when S_q is larger, indicates that the strength of the wind system is, on the average, greater on days with larger S_q . From the change in crochet size, the strength of the wind system must vary by 50 per cent at least.

INTRODUCTION

The seasonal variation of the latitude of the northern and southern foci of the current system which causes the quiet-day magnetic diurnal variation, S_q , is well known [2]. Hasegawa [2] found two cases, in each of which from one day to the next the latitude of the focus of the northern current-system shifted about 15°. In addition, there were marked changes from one day to the next in the morphology of the current system. In neither of the two cases was there much change, on the successive days, in Bartels' δW_2 measure [3] for the amplitude of S_q at Huancayo. These facts indicate changes in the morphology of the air motions or wind patterns which, according to the dynamo theory, generate the S_q current-system. Since it has not yet been possible to measure directly the total conductivity in the ionospheric layer (below the E-region) where the S_q currents flow, the strength of the wind pattern or changes in its strength cannot be determined by this procedure. Suppose, however, we have a group (I) of crochets for days with large S_q and

another group (II) for days with small S_q . Then, if the number of crochets in each group is large enough, the average increase in conductivity in the layer where the S_q currents flow should be the same for both groups. If we find that the average size of crochets is significantly greater in group I than in group II, this would indicate that the strength of the wind system for group I was greater than for group II and consequently that, in part, the larger S_q in group I is due to a stronger average wind-system. Thus far, we have assumed that the current system for crochets is at the same level (below the E-layer) as that for S_q . The fact that the magnetic effects from solar flares are indistinguishable from those which would

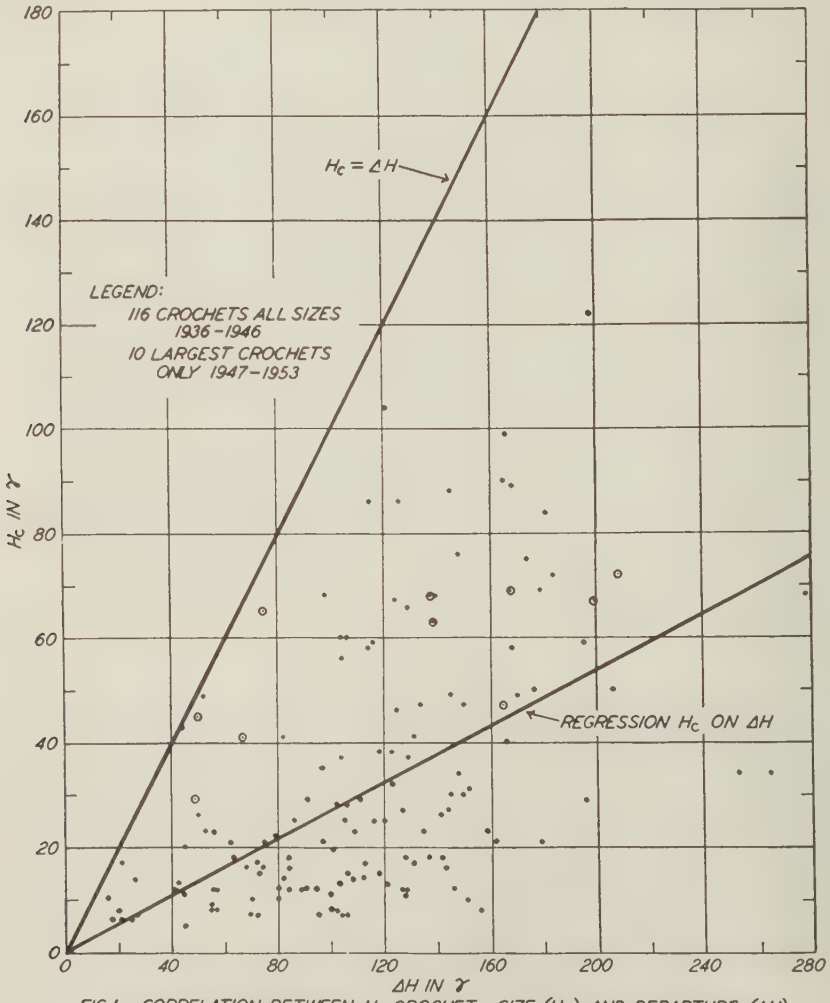

FIG. 1 — CORRELATION BETWEEN H-CROCHET SIZE (H_c) AND DEPARTURE (ΔH) IN SQ AT TIME OF CROCHET AT HUANCAYO, PERU

(*Correction:* In Legend, read 1947 for 1946 and 1948 for 1947)

esult from an increased strength of the existing S_q current-system either indicates hat both are in the same layer or in layers in which the morphology of the wind pattern is the same.

INCREASE OF *H*-CROCHET SIZE WITH AMPLITUDE OF DIURNAL VARIATION IN *H*

Figure 1 depicts, as ordinate, the size, H_c, of 126 crochets in horizontal intensity, H, at Huancayo (see Appendix A at end of paper). Each H_c is plotted against the departure, ΔH, of the value of H immediately preceding the crochet from the midnight bihourly mean value of H. The graph indicates, in spite of the large scatter, the tendency for larger crochet sizes to occur with larger values of ΔH.

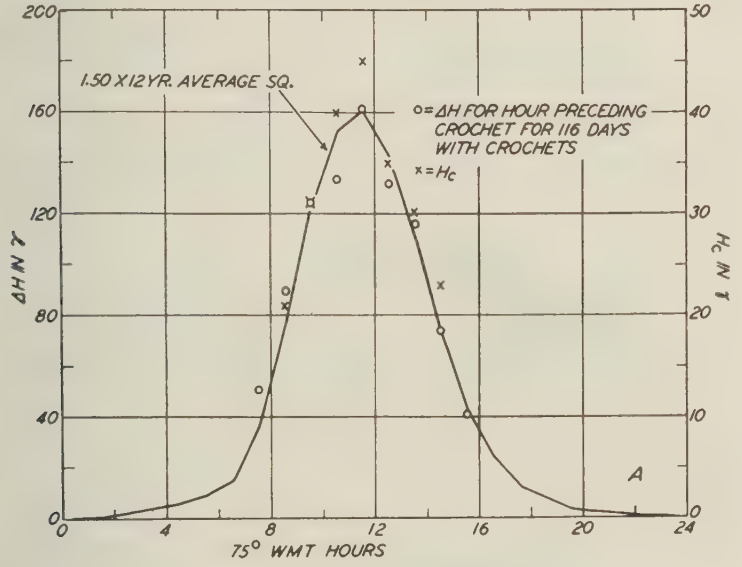

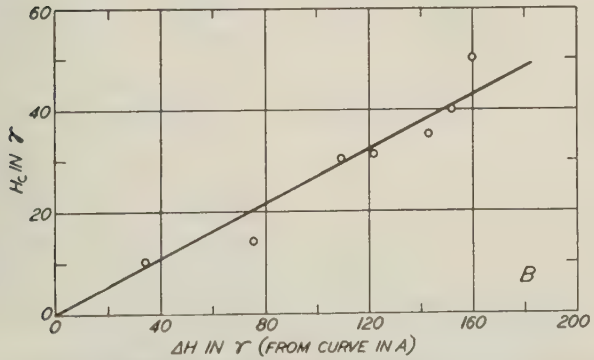

FIG. 2—(A) AVERAGE DIURNAL VARIATION OF HOURLY MEAN H-CROCHET SIZES (H_c) COMPARED WITH SQ AT HUANCAYO
(B) REGRESSION OF H_c ON DEPARTURES (ΔH) IN SQ

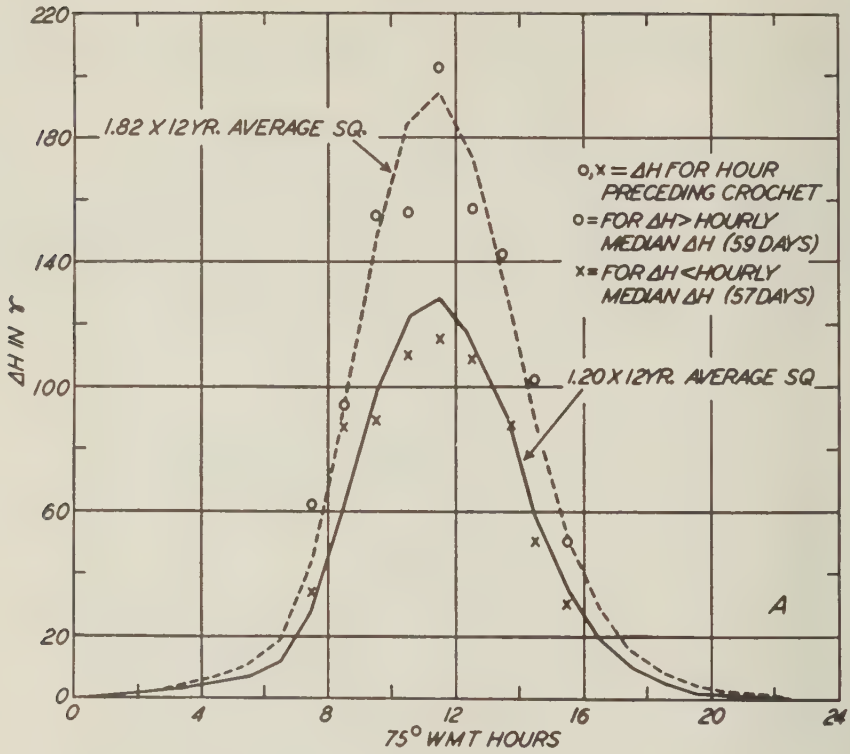

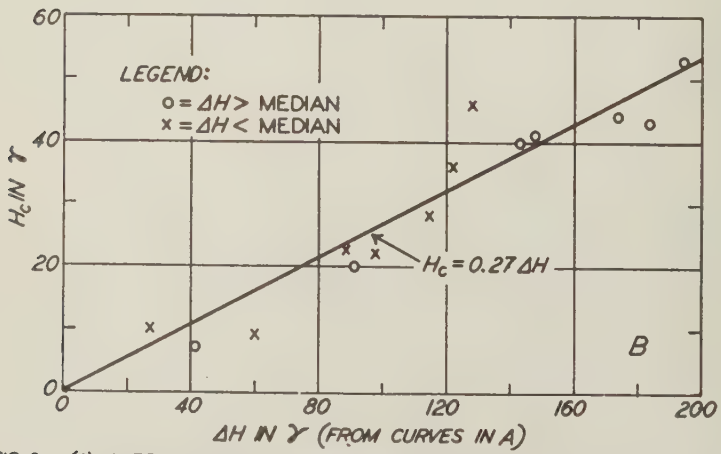

FIG. 3 — (A) AVERAGE DIURNAL VARIATION OF ΔH IN SQ AT HUANCAYO FOR CROCHET DAYS WITH LARGE AND SMALL SQ
(B) REGRESSION OF H-CROCHET SIZE (H_c) ON DEPARTURES (ΔH) IN SQ FROM MIDNIGHT VALUE

Since no point is above the line $H_c = \Delta H$, no crochet size is found to exceed ΔH. The lower line is the regression of H_c on ΔH from Figure 2. Figure 2(A) compares the hourly mean values of H_c with the average diurnal variation S_q estimated for the days on which the 116 crochets occurred. The solid curve is 1.50 times the 12-year average S_q in H. The values of ΔH (circles in Fig. 2A), to which the S_q curve is fitted, were obtained as follows: For those days on which crochets occurred in a particular hourly interval, t, the departure, δH, from the midnight bihourly mean H of the hourly mean for the interval $(t - 1)$ was computed; ΔH is the average of these departures δH for a given hour. This avoids basing the diurnal variation from days with crochets on hourly values which are augmented by the crochet. Since the open circles are well fitted by the solid curve, the mean hourly value of ΔH may be read from the curve for any particular hourly interval for which the mean H_c is shown. In Figure 2(B), the hourly mean crochet size H_c is plotted against the hourly mean ΔH for the same hour as read from the curve in Figure 2(A). Since the magnetic effect of solar flares is indistinguishable [1] from that which would result from an enhancement of the S_q current-system, the hourly averages of many H-crochets would be expected to exhibit a diurnal variation similar to that in H. The combined number of H-crochets in the two 75° WMT hourly intervals (0800–0900) and (1400–1500) was 19, which is about the average number observed in the single hourly intervals between 0900 and 1400. Since the average H-crochet size increases with ΔH, it is not surprising that fewer crochets are observed in the hours when ΔH is smaller. This occurs, not because the expected number of crochets is less, but because a larger fraction of them will be too small (less than about 7γ) to be seen in the background noise.

Figure 3(A) shows the estimated diurnal variation of ΔH, derived as described above, for two groups of days on which crochets were observed. Values of δH greater than the median δH for a given hour were averaged to give ΔH for the first group, as indicated by the circles in Figure 3(A). Values of δH less than the median for a given hour were averaged to obtain the values of ΔH for the second group, as indicated by the crosses. As before, the values of ΔH corresponding to any hour for which the average crochet size was obtained can be read from the curves in Figure 3(A). In Figure 3(B), the average for each hour of the H-crochet size, H_c, is plotted against the average ΔH for the same hour. The slope of the line in Figure 3(B) is the same as that in Figure 2(B). Figure 3(B) also indicates that H_c is proportional to ΔH and that the diurnal variation of the average H_c size is greater on days with larger S_q.

It remains to test the statistical reality of the difference between the average crochet size on days with large and small S_q in Figure 3. For each day with crochet, the value of Bartels' δW_2 measure [3] is used to determine the size of S_q in H at Huancayo. This measure is derived from the difference: average H for the 75° WMT interval, 0900 to 1400 hours, less the average H for the interval 0000 to 0500 hours. This difference is then corrected for the lunar variation in H at Huancayo, and for post-perturbation recovery. After normalizing for each month to eliminate seasonal influences, the final values, except for a scale-factor, give δW_2. For Figure 4, the crochet days with δW_2 greater than the median δW_2 (for 97 days with crochets) were placed in one group and those with δW_2 less than

the median in another. Only crochets between 0900 and 1400 hours, 75° WMT, were used, since there were no statistically significant differences between the hourly frequencies of crochets within this interval. Also the δW_2 measure is based on these same hours. Before deriving the frequency distributions of crochet sizes, each observed crochet size H_c was corrected for diurnal variation between 0900

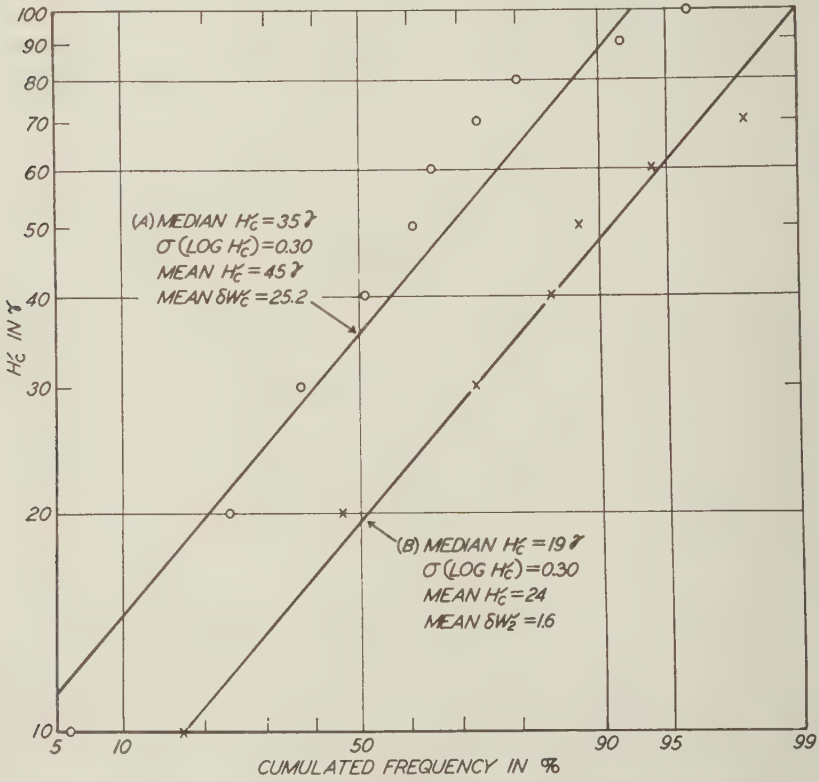

FIG. 4—FREQUENCY DISTRIBUTION OF H-CROCHETS (H_c) CORRECTED FOR DIURNAL VARIATION 0900–1400, 75° WMT
(A)-FOR δW_2 >12.5 49 CROCHETS (MEAN 49 γ)
(B)-FOR δW_2 <12.5 48 CROCHETS (MEAN 25 γ)

and 1400 hours, 75° WMT. It was assumed, from the evidence in Figure 3(*B*), that the shape of the diurnal-variation curve for H_c is that of the 12-year average diurnal variation S_q in H. From this 12-year average, the hourly average for each of the five hourly intervals between 0900 and 1400 was taken, with the mean for the five hours 0000 to 0500 deducted. The ratio of these resulting five values of ΔH to the average ΔH for the five hours 0900 to 1400 was then found. These consecutive ratios, starting with the value for the interval 0900 to 1000 hours, were as follows: 1.13, 0.90, 0.86, 0.96, and 1.25. The observed size H_c of each crochet was multiplied by one of the above factors according to the hour in which the crochet

occurred, to give the crochet size, H_c' , corrected for diurnal variation. This procedure provides a normalized crochet size, H_c' , which is independent of the time, between 0900 and 1400 hours, at which the crochet occurred but which does depend upon the amplitude of S_q in H. Finally, Figure 4 shows, on log normal probability paper, the frequency distribution of H_c' for 49 days with δW_2 greater

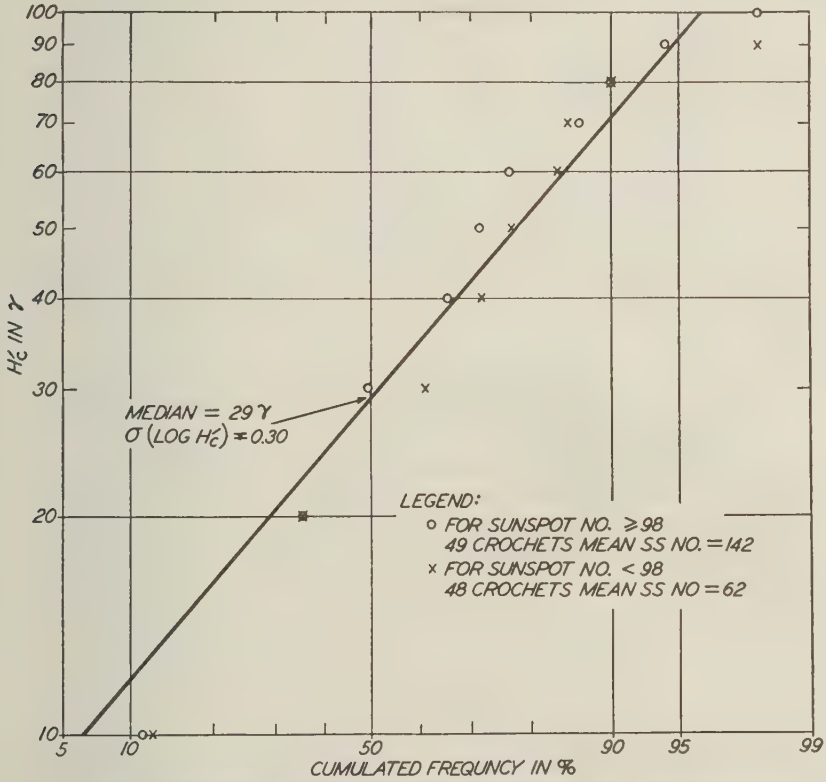

FIG. 5—FREQUENCY DISTRIBUTION OF H-CROCHETS (H_c') CORRECTED FOR DIURNAL VARIATION 0900–1400, 75°WMT

than the median δW_2 and for 48 days with δW_2 less than the median. Using the parameters indicated in Figure 4, the hypothesis that both samples came from the same population was tested. Differences as great or greater than those shown in Figure 4 between the samples should occur by chance only about once in about 10^5 such pairs of samples, thus leaving little doubt of the reality of the difference. Thus, the average crochet size is greater for the group of days with larger S_q . Although the frequency distributions in Figure 4 are approximately logarithmic normal, the means of samples of this size will, by the central limit theorem, be nearly normally distributed. The standard deviations of the means for the upper and lower distributions in Figure 4 are roughly 4γ and 2γ, respectively.

The seasonal variation in the amplitude of S_q at Huancayo is well known [3].

It is not due to a seasonal variation in solar radiation. It may arise from a seasonal variation in wind pattern or from the seasonal variation in conductivity of the S_q layer, at a given latitude, due to the seasonal variation in the sun's zenith distance. Either of the latter two causes would also result in a seasonal variation in the size of crochets. The frequency distributions of crochet sizes were plotted on log normal probability paper for the equinoxes and both solstices. The resulting estimates of mean crochet sizes, with estimated probable errors, were as follows: Equinoxes $42 \pm 4\gamma$, winter solstices $42 \pm 4\gamma$, and summer solstices $35 \pm 4\gamma$. The differences among these means are not statistically significant. From the sample of 97 days with crochets between 0900 and 1400 hours, 75° WMT, at Huancayo, the estimated mean values of ΔH for the interval 0900 to 1400 hours, 75° WMT, for the three seasons, were as follows: Equinoxes 149γ, winter solstices 129γ, and summer solstices 112γ. From Figure 2(*B*), the resulting mean crochet sizes would be 0.27 times the above values of ΔH, or as follows for the three seasons: Equinoxes 40γ, winter solstices 35γ, and summer solstices 30γ. The differences between these values and those obtained above for the mean crochet sizes are within the statistical uncertainties.

Since monthly and yearly averages of δW_2 were shown, by Bartels [3], to have a higher correlation with sunspot numbers than any other geophysical variable, it is expected that δW_2 in our sample will be correlated with sunspot number. If H_c' is also correlated with sunspot number, then the apparent correlation between H_c' and δW_2 might arise because both are influenced by causes related to sunspot numbers. Figure 5 shows the frequency distributions of H_c' for two groups with different mean sunspot number. There is no significant difference between the two distributions and thus no indication that H_c' varies with sunspot number. Thus, it seems reasonable to conclude that the reason for the larger average H-crochet on days with larger average S_q (or δW_2) is that on the average the strength of the wind system generating the S_q currents is greater on days with larger S_q .

CORRELATION ANALYSIS

The above conclusions may be verified from a study of the correlations between pairs of the three variables involved: Crochet size, δW_2 , and sunspot number. While it has been indicated that the logarithms of crochet sizes are approximately normally distributed, the distribution of actual crochet sizes was not found to deviate sufficiently from a normal distribution to render a correlation analysis useless. Figure 6 shows the regression lines for the correlation berween H_c' and δW_2 . From the slopes of the two regression lines, the correlation coefficient, r, can be obtained, as indicated on the graph. The value $P = 10^{-5}$ indicates the probability, based on Fisher's z transformation [4], of obtaining, from a sample of 97 pairs, a value of $r \geq 0.45$, if the sample came from a population with $r = 0$, and with the variates normally distributed. This result also leaves little doubt that H_c' depends on δW_2 . Similarly, the correlation between δW_2 and daily mean sunspot numbers, for the sample of 97 days on which crochets were observed between 0900 and 1400 hours, 75° WMT, is shown in Figure 7. Here $r = 0.62$ and the probability of obtaining $r \geq 0.62$ in a sample of 97 from a population with $r = 0$ is less than 10^{-5}. Finally, Figure 8 indicates the correlation between sunspot

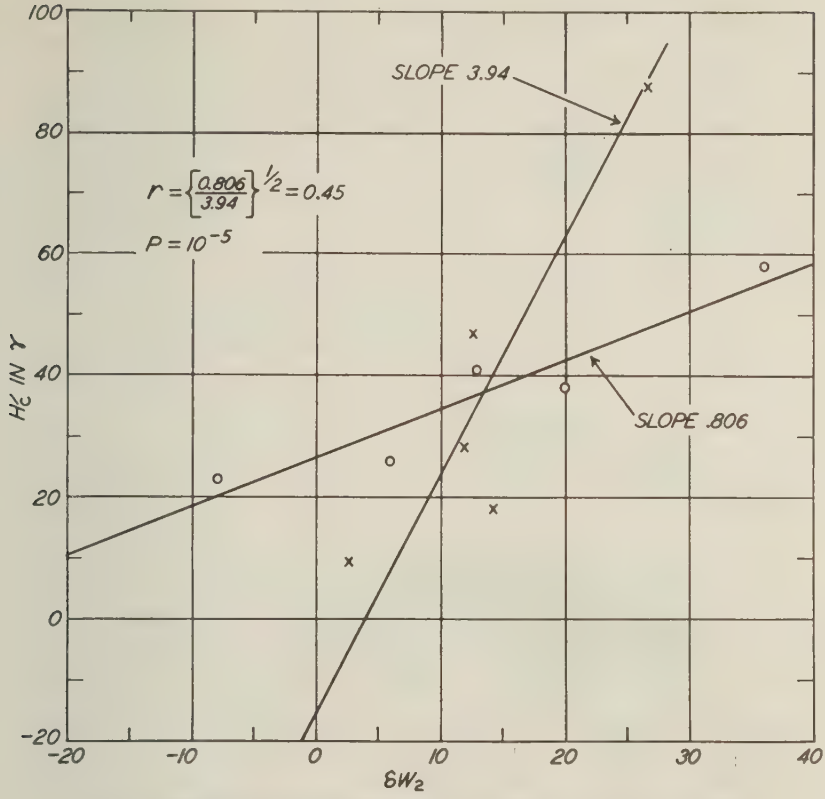

FIG. 6 — CORRELATION BETWEEN H_c' AND δW_2; REGRESSION LINES INDICATED

numbers and H_c'. Here $r = 0.12$ and the probability of reality is only 0.3, indicating that r does not differ significantly from zero. In general, if we have the three total correlation coefficients r_{12}, r_{13}, and r_{23} between three pairs of variables, then the partial correlation coefficient $r_{12.3}$, for example (to give the correlation between variables 1 and 2 that would obtain if variable 3 remained constant), is given by [4]

$$r_{12.3} = \frac{r_{12} - r_{13} \cdot r_{23}}{[(1 - r_{12}^2)(1 - r_{23}^2)]^{1/2}}$$

and similar formulas for the other two partial correlation coefficients. In the above formula, let variable 1 represent H_c', variable 2 represent δW_2, and variable 3 represent sunspot number. If we accept $r_{12} = 0.45$ (from Fig. 6) and $r_{23} = 0.62$ (from Fig. 7), it is readily found that $r_{12.3} = 0$ if $r_{13} = 0.73$; in other words, in order that the partial correlation between H_c' and δW_2 (with sunspot number constant) be zero (with $r_{12} = 0.45$ and $r_{23} = 0.62$), the total correlation between H_c' would need to be 0.73, a value which is most unlikely for the population value, since, from the sample in Figure 8, $r_{13} = 0.12$. Thus, the correlation between

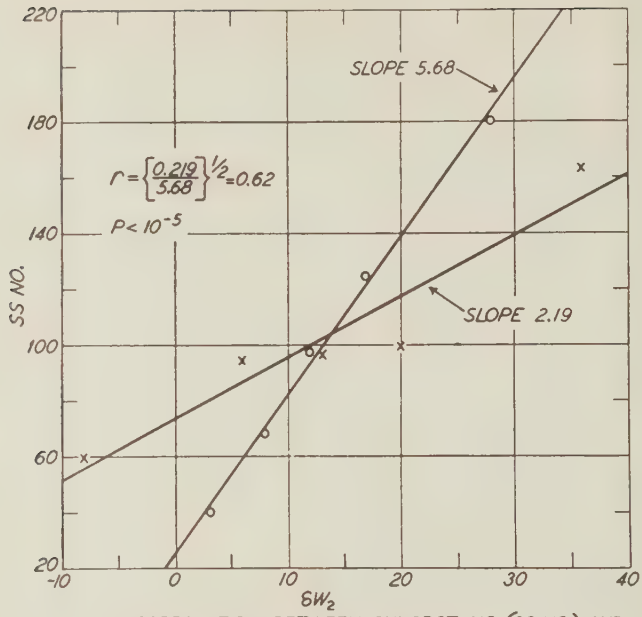

FIG. 7—CORRELATION BETWEEN SUNSPOT NO. (SS NO.) AND δW_2; REGRESSION LINES INDICATED

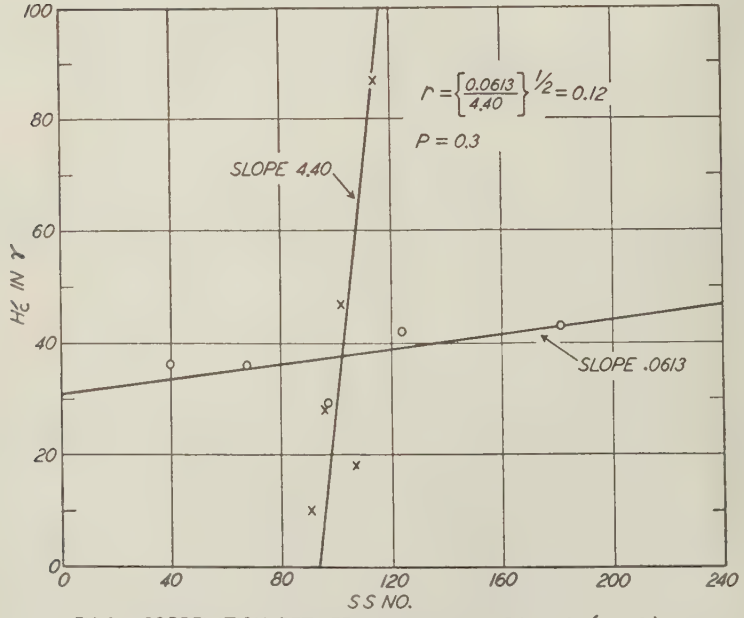

FIG 8—CORRELATION BETWEEN H_ℓ AND SUNSPOT NO. (SSNO.) AND δW_2; REGRESSION LINES INDICATED

H-crochet size and amplitude of S_q does not arise from a common effect on both due to a mechanism correlated with sunspot number.

A more direct test of this conclusion was made, as follows: As shown in Table 1,

TABLE 1—*Arrangement for dichotomizing δW_2 to eliminate main effect of sunspot number on δW_2*

Sunspot numbers	No. of crochets	Group A		Group B	
		δW_2	No.	δW_2	No.
		γ		γ	
150–258	19	≥ 30	10	<30	9
110–148	20	>15	10	≤ 15	10
89–108	17	>11	8	≤ 11	9
56– 87	21	≥ 8	11	< 8	10
0– 55	20	> 0	10	< 0	10
Totals	97		49		48

each day with crochet was placed in one of five groups according to the sunspot number for that day. There were about 20 such days in each group. Within each group, the median δW_2 was found; all days with $\delta W_2 >$ median were placed in group A and those with $\delta W_2 <$ median were placed in group B. The frequency distribution of crochet sizes H_c' in Table 2 was obtained for the 49 crochets in

TABLE 2—*Cumulative frequency distribution of crochet sizes, H_c', for groups A and B*

H_c'	Group A		Group B	
	Cumulated number	Cumulated frequency	Cumulated number	Cumulated frequency
		per cent		*per cent*
0– 10	3	6	8	17
11– 20	14	29	20	42
21– 30	22	45	31	65
31– 40	27	55	39	81
41– 50	32	65	40	83
51– 60	33	67	44	92
61– 70	36	74	47	98
71– 80	39	80	48	100
81– 90	45	92	...	...
91–100	47	96	...	...
>100	49	100	...	...

group A and for the 48 crochets in group B. The mean sunspot numbers for groups A and B were, respectively, 106 and 98, a difference of only 8. However, the mean values of δW_2 for the two groups were, respectively, 23.4 and 3.4 for groups A and

B. The frequency distributions for groups A and B were sensibly logarithmically normal, with estimated standard deviation, s.d., of log size = 0.30. The median values of H_c' for groups A and B were, respectively, 34.0γ and 21.6γ, giving a difference in the mean logarithms of log (34.0/21.6) = 0.197. The s.d. for this difference is about (0.30 $\sqrt{2}/7$) = 0.06, or the difference is about 3.3 times its estimated s.d. A difference as large or larger than this should occur from sampling with probability about 10^{-3}. Thus, the difference between the means of the two distributions is statistically significant. The mean H_c' for group A is 43γ and for group B is 27γ, with corresponding δW_2 values 23.4 and 3.4, respectively. These two points lie quite close to the line with slope 0.806 in Figure 6. This result then shows directly that the correlation between H_c' and δW_2 is not due to a common effect of sunspot number on both.

CONCLUSION

The simplest explanation for the correlation between crochet size and amplitude of S_q is that it arises because of variations in the strength of the wind pattern, which by the dynamo theory generates the diurnal variation current-system. The stronger wind patterns result on the average in a proportionate increase in crochet size and in amplitude of S_q . The results obtained in Figure 4, for example, indicate that the strength of the wind pattern averages about 50 per cent greater for days in group A than for days in group B. On the other hand, the correlation between sunspot number and δW_2 probably is due to changes in solar radiation with sunspot number, and its effect on the ionospheric conductivity at the level where the S_q currents flow. The correlation coefficient r = 0.62 between δW_2 and sunspot number, as shown for the sample in Figure 7, can be used [5] to determine the magnitude of the part of δW_2 that is linearly correlated with sunspot numbers relative to the part which is not. This ratio is given [5] by $r/(1 - r^2)^{1/2}$. With r = 0.62, the ratio is about 0.8, which means that the standard deviation of the values of δW_2 predicted from daily sunspot numbers is for this sample somewhat smaller (0.8 as large) than the standard deviation of the residuals after making a linear prediction. Thus the variability of S_q due to variability in strength of wind patterns could be slightly larger than the variability due to changing sunspot number.

References

[1] A. G. McNish, Terr. Mag., **42**, 109-122 (1937).
[2] S. Chapman and J. Bartels, Geomagnetism, Oxford, Clarendon Press (1940).
[3] J. Bartels, Terr. Mag., **51**, 181-242 (1946).
[4] R. A. Fisher, Statistical methods for research workers, G. E. Stechert and Co., New York, 8th ed. (1941).
[5] J. Bartels, Terr. Mag., **37**, 1-52 (1932).

APPENDIX A—*Date, GMT of beginning, and magnitude, H_c, of H-crochets at Huancayo, Peru, 1936–1947, with daily sunspot number, and other relevant data*

Date	GMT	H_c	ΔH	ΔH^*	δW_2	Sun-spot No.	Date	GMT	H_c	ΔH	ΔH^*	δW_2	Sun-spot No.
	h m	γ	γ	γ				*h m*	γ	γ	γ		
8 Apr. 26	12 50	+18	42	63	+23	92	1937 July 13	17 56	+12	158	127	+29	188
5 Jun. 16	13 27	+10	27	70	+12	55	1937 Oct. 5	17 05	+68	289	278	+39	175
5 July 15	13 26	+8	36	55	+10	67	1938 Jan. 15	17 08	+26	137	141	+25	118
7 Jun. 24	13 27	+43	44	44	+19	133	1938 Feb. 3	17 30	+49	230	170	+21	68
0 Feb. 8	13 45	+32	53	123	+13	64	1938 May 3	17 45	+41	164	131	+16	160
5 Feb. 1	13 34	+22	56	79	−4	94	1938 Sep. 20	17 47	+84	199	181	+28	57
5 Aug. 3	13 00	+12	40	56	+19	137	1939 Apr. 29	17 10	+75	163	174	+33	136
7 Jun. 28	13 05	+21	73	97	+20	144	1940 Jan. 28	17 23	+10	171	151	+8	43
6 Apr. 6	13 52	+25	37	86	+22	91	1940 Mar. 26	17 40	+34	256	263	+26*p*	108
7 Apr. 21	13 58	+7	125	95	+11	127	1940 May 14	17 48	+28	100	102	0	93
7 July 9	14 19	+86	80	126	+44	181	1941 Jun. 4	17 44	+60	106	106	+14	53
1 Jun. 5	14 27	+17	52	72	+11	61	1942 Jan. 23	17 20	+12	136	128	−3	31
1 Jun. 30	14 00	+20	32	45	−5	98	1942 Mar. 25	17 45	+31	152	152	+11	100
2 Jan. 29	14 23	+35	72	97	−3	11	1943 Feb. 10	17 30	+38	114	118	−4	37
3 Apr. 19	14 39	+7	53	72	−11	41	1945 Mar. 29	17 13	+10	106	80	−22	60
3 Apr. 22	14 23	+12	40	80	−17	45	1946 Feb. 11	17 30	+37	106	104	+3	115
3 Apr. 24	14 42	+25	52	105	+6	36	1947 Sep. 2	17 55	+29	227	196	+46	196
6 Feb. 10	14 32	+29	30	91	+11	121	1946 Mar. 8	17 58	+122	198	198	+13	71
6 Aug. 12	14 00	+14	98	108	+9	98	1936 Jun. 16	18 00	+12	100	90	+12	55
7 Jan. 14	14 30	+58	118	168	+29	150	1936 Aug. 25	18 26	+68	151	139	+19	90
7 Apr. 10	14 40	+30	152	150	+15	171	1937 Jun. 10	18 52	+11	97	44	+17	98
7 July 3	14 50	+11	75	128	+17	148	1937 July 7	18 46	+17	166	131	+24	143
7 Aug. 31	14 53	+88	110	145	+36*p*	213	1937 Oct. 28	18 24	+56	136	104	+16	104
6 Feb. 14	15 26	+59	112	195	+6	77	1938 July 11	18 03	+17	120	113	+5	205
6 Oct. 21	15 35	+23	140	159	+7	65	1938 July 25	18 00	+16	149	143	+38	202
7 Jun. 14	15 32	+23	90	135	+42	185	1938 Oct. 15	18 59	+15	166	118	+10	103
7 July 29	15 36	+8	70	102	+12	128	1938 Dec. 7	18 13	+12	122	89	+18	117
8 Jan. 13	15 30	+34	218	252	+28*p*	106	1939 July 15	18 30	+29	127	111	+11	87
8 May 21	15 12	+15	79	106	+11	106	1939 Aug. 29	18 55	+13	152	121	+6	69
8 Jun. 29	15 04	+12	69	94	+8	72	1939 Sep. 12	18 26	+41	111	82	+3	150
8 Oct. 14	15 38	+21	133	179	+12	122	1940 Jan. 8	18 03	+23	94	53	+16	38
9 Mar. 21	15 17	+31	86	120	−1*p*	89	1940 Feb. 17	18 34	+59	142	116	+14	51
9 Sep. 3	15 25	+69	156	179	+10*p*	124	1940 May 25	18 29	+8	108	100	−9	76
9 Sep. 13	15 36	+72	164	184	+12	127	1940 Sep. 20	18 59	+19	148	101	+11	98
0 Feb. 24	15 40	+12	116	146	−3	40	1942 Jan. 12	18 34	+66	143	129	+18	48
1 Feb. 27	15 44	+90	105	165	+16	50	1945 Apr. 27	18 23	+12	125	84	+11	56
1 Feb. 28	15 27	+49	94	145	+4	55	1946 Feb. 24	18 42	+18	145	137	+11	87
1 Apr. 3	15 43	+25	100	120	−13	21	1946 Feb. 28	18 05	+38	135	123	+18	90
6 July 21	15 10	+86	115	115	−34*p*	110	1946 Mar. 21	18 15	+13	114	103	−8	101
6 Aug. 7	15 35	+67	127	124	+15	116	1946 Sep. 13	18 20	+30	176	145	+25	92
6 Oct. 13	15 30	+6	198	249	+25	92	1947 May 22	18 47	+34	181	148	+40	258
7 Apr. 4	15 40	+50	211	206	+27	194	1947 July 31	18 48	+6	45	25	−27	113
6 Apr. 8	16 46	+89	119	168	−3	76	1937 Jun. 2	19 40	+16	114	84	+18	89
6 Apr. 25	16 53	+13	115	42	−5	72	1937 Aug. 28	19 25	+47	186	150	+32	130
6 Aug. 5	16 05	+14	63	82	−4	87	1937 Sep. 29	19 55	+18	129	84	+19	126
6 Nov. 6	16 10	+47	119	134	+14	151	1939 May 8	19 41	+18	152	128	+13*p*	105
6 Nov. 27	16 50	+7	125	106	+10	145	1940 Feb. 15	19 17	+14	126	112	+1	78
7 May 25	16 49	+99	166	166	+40*p*	171	1941 Feb. 26	19 11	+58	124	114	+9	46
7 Sep. 29	16 31	+20	175	175	+19	126	1942 Nov. 6	19 27	+12	52	41	−12	33
8 July 9	16 33	+18	134	142	+30	175	1944 Dec. 10	19 14	+21	75	75	+8	45
8 July 29	16 10	+37	105	129	+6	151	1945 Apr. 25	19 47	+15	66	73	0	52
8 Sep. 23	16 54	+50	179	177	+19	86	1945 Sep. 3	19 59	+9	102	55	+11	26
9 Apr. 21	16 56	+181	196	213	+36*p*	125	1945 Sep. 26	19 23	+11	129	100	+19	53
9 July 16	16 40	+40	139	166	+22*p*	74	1945 Oct. 29	19 37	+16	122	68	+9	68
9 Aug. 9	16 10	+8	122	156	+32	157	1936 May 8	20 19	+5	64	45	+15	46
1 Mar. 7	16 30	+60	113	104	−1	47	1936 Jun. 10	20 53	+17	50	21	+1*p*	40
2 Jan. 13	16 24	+76	129	148	+14	50	1937 May 1	20 27	+16	99	74	+19	89
2 Mar. 31	16 23	+27	144	144	−4	55	1939 Sep. 6	20 00	+68	118	98	+29	136
2 Apr. 29	16 23	+27	122	127	+2	65	1942 Mar. 6	20 40	+7	129	70	+5	20
2 Oct. 26	16 18	+25	118	116	−9	13	1943 Apr. 19	20 30	+26	59	50	−11	41
6 July 25	16 21	+104	121	121	+56*p*	117	1945 Apr. 27	20 50	+21	59	62	+11	56
6 Aug. 4	17 26	+7	110	104	+1	65	1945 Apr. 28	20 44	+6	50	18	+6	55
6 Sep. 4	17 11	+21	194	162	+25	57	1945 Aug. 17	20 20	+48	60	52	+3	34

*Used only in Figure 1.

A NEW METHOD FOR OBTAINING ELECTRON-DENSITY PROFILES FROM P'-f RECORDS

By John E. Jackson

United States Naval Research Laboratory, Washington 25, D. C.

(Received November 29, 1955)

ABSTRACT

A practical and accurate method for reducing P'-f records to electron densities *vs* true height is described and used to analyze P'-f records taken at White Sands. Direct measurements of electron densities in the ionosphere obtained with the aid of rockets are used to check the method. Results obtained by these two independent techniques are shown to be in excellent agreement. Twenty P'-f records were reduced for the period from 1948 to 1954, all of which reveal a considerable degree of regularity in the height of the daytime $E1$ and $F2$ regions. Some of the profiles obtained are shown. One of the illustrations shows a one-hour sequence, where the $F2$ virtual height varied from 650 km to 410 km, whereas the true height remained essentially unchanged.

INTRODUCTION

One of the basic problems in ionosphere research is the determination of the electron-density distribution as a function of altitude. The most readily available source of data is undoubtedly the multitude of P'-f recordings which are taken daily on a world-wide basis. Yet very few of the millions of recordings which are now available have ever been used to provide the distribution of ionization in the upper atmosphere. Since any analysis of this type must be based on an accurate knowledge of group velocities at a particular location, the first part of this paper is devoted to the computation of group velocities. The second part of the paper deals with the actual analysis of P'-f records and with results obtained by the proposed method.

An excellent treatment of group velocities in the ionosphere has been given by Whale and Stanley [see 1 of "References" at the end of paper], in terms of a "group refractive index" n', which is defined as the free-space velocity of light divided by the group velocity of the wave. Their results show in a general way how the group indices vary as a function of electron density, frequency, and earth's magnetic field, but do not provide the detailed accuracy needed for quantitative analysis at a given geographic location. The need for direct computation was indicated by Shinn and Whale [2], when they derived the group-index curves applicable to southeast England. In view of the complicated formulas and laborious calculations required, the numerical work in references [1] and [2] was carried out with an

electronic computer. One can appreciate the tediousness of the computations by noting that to evaluate a single group index approximately 45 mathematical operations are required. Consequently, a simplified procedure for obtaining the group indices was developed by the author and used to compute group-velocity curves for conditions existing at White Sands, New Mexico. The analysis was carried out in sufficient detail to enable computation of virtual heights at vertical incidence for any distribution of ionization over White Sands. The results lend themselves to verification, since direct measurements of electron densities by rocket techniques (references [3], [4], [5], [6]) provide a means for checking computed group heights *vs* P'-f records.

The treatment presented in this paper assumes that the ionosphere is horizontally stratified and that propagation follows the laws of geometrical optics up to the reflection point. Collision frequency has been neglected, since it affects very little the group velocities in the E and F regions. The computations are for vertical propagation at White Sands, using the ground value of the angle of magnetic dip (60° 31′) and a value of 0.487 oersted for the earth's magnetic field, which is the computed field intensity at 150 km obtained by extrapolation of the ground value according to the inverse cube law.

CALCULATION OF GROUP INDEX

The discussion which follows deals only with frequencies above the gyrofrequency, since these are the frequencies of interest in the analysis of P'-f records.

1. *The nn′ product*

In view of its definition, the group index can be expressed as follows:

$$n' = n + f\frac{\partial n}{\partial f} \qquad (1)$$

where n = the real part of the refractive index of the medium and f = exploring wave frequency.

The conventional graphical presentation is to plot the refractive indices as a function of the parameter $x = Ne^2/\pi m f^2$, where e, m = charge and mass of an electron, and N = electron density.

Such a presentation is not desirable in the case of the group index, since the group index becomes infinite at the values of x for which the refractive index n becomes zero. This occurs at $x = 1$ for the ordinary ray and, when f is above the gyrofrequency, at $x = 1 - y$ for the extraordinary ray, where y = gyrofrequency/exploring wave frequency.

As indicated by Whale and Stanley (reference [1]), it is preferable to calculate the quantity nn'. The results illustrate the effect of the magnetic field, since nn' is equal to unity in the absence of magnetic field. The nn' products are conveniently shown graphically, since the values remain finite for all cases of interest. (The only exceptions occur when propagation is exactly transverse or exactly longitudinal.) The limiting value of the nn' product as n approaches 0 is readily computed from the following simple formulas:

For the ordinary ray,

$$[nn']_{x=1} = \frac{1}{\sin^2 \theta} \quad \ldots\ldots(2)^*$$

For the extraordinary ray,

$$[nn']_{x=1-y} = \frac{2 - y}{(1 - y)(1 + \cos^2 \theta)}; \qquad y < 1 \quad \ldots\ldots(3)^*$$

where θ = the angle between the direction of the earth's field and the direction of propagation.

In the present case of vertical propagation, $\theta = 90° -$ (angle of magnetic dip). The formula for nn',

$$nn' = n^2 + nf \frac{\partial n}{\partial f} \quad \ldots\ldots(4)$$

indicates the need for computing n^2 and $\partial n/\partial f$. The most laborious operation is in determining $\partial n/\partial f$, since it requires differentiation of the Appleton-Hartree formula with respect to frequency. The present treatment avoids this operation.

2. *The ordinary component*

The ordinary phase index is given by an expression of the form

$$n^2 = F(x, y)$$

where x and y have the meaning previously indicated. Differentiating gives

$$2n \frac{\partial n}{\partial f} = \frac{\partial F}{\partial x} \frac{\partial x}{\partial f} + \frac{\partial F}{\partial y} \frac{\partial y}{\partial f}$$

$$= -\frac{2x}{f} \frac{\partial F}{\partial x} - \frac{y}{f} \frac{\partial F}{\partial y}$$

Thus,

$$nn' = n^2 - x \frac{\partial F}{\partial x} - \frac{y}{2} \frac{\partial F}{\partial y} \quad \ldots\ldots(5)$$

The quantity $\partial F/\partial x$ is readily obtained by numerical differentiation of the function n^2 *vs* x, and $\partial F/\partial y$ is obtained from the family $n^2 = F(x, y)$. Since n^2 must be computed in any event, the procedure simply makes use of the numerical results obtained in evaluating n^2. At medium latitudes, the slope of the n^2 *vs* x curves (see Fig. 1) varies in a sufficiently gradual fashion to use the approximation

$$\frac{\partial F}{\partial x} \cong \frac{F(x + \Delta x, y) - F(x - \Delta x, y)}{2\Delta x}$$

*These formulas are also given in reference [1]. The formula for the extraordinary ray (eq. 16 of ref. [1]) was incorrectly shown. This was obviously a typographical error, since the calculated results shown by Whale and Stanley are in agreement with the correct formula.

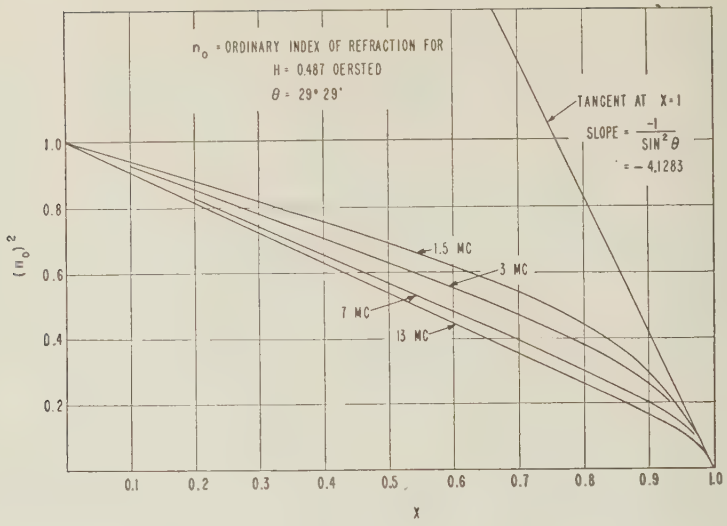

FIG. 1—Ordinary indices of refraction for White Sands, New Mexico

For the White Sands data which we use to illustrate the method, the accuracy is better than one per cent if we take the following increments:

$$\Delta x = 0.1 \quad \text{for} \quad 0 < x < 0.9$$

$$\Delta x = 0.01 \quad \text{for} \quad 0.9 < x < 0.95$$

$$\Delta x = 0.005 \quad \text{for} \quad 0.95 < x < 0.99$$

$$\Delta x = 0.002 \quad \text{for} \quad 0.99 < x < 1$$

The values of n^2 were computed with a calculating machine, using five significant figures in the computations. It should also be noted that the n^2 curves have a finite slope everywhere, with a maximum magnitude of 4.128 at $x = 1$.

The family $n^2 = F(x, y)$ was computed for White Sands, New Mexico, and

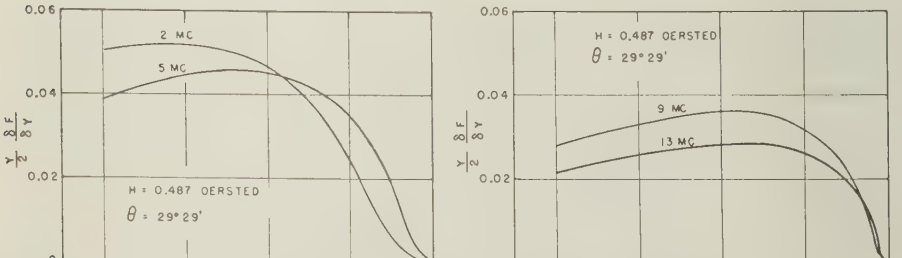

FIG. 2—Contribution of the term $(y/2)(\partial F/\partial y)$ to the nn' product

for the frequencies 1.5, 2, 3, 5, 7, 9, 11, and 13 Mc. From this family, the quantity $\partial F/\partial y$ can be computed with about five per cent accuracy. Since the term $(y/2)(\partial F/\partial y)$ contributes at most 1/20 of the final value of nn', the maximum error in n' introduced by the approximation used in computing $\partial F/\partial y$ is less than one-fourth of one per cent.

Figure 2 indicates the magnitude of the term $(y/2)(\partial F/\partial y)$ as a function of x and for selected frequencies. It is of interest to note that the term $(y/2)(\partial F/\partial y)$ approaches zero as x approaches unity.

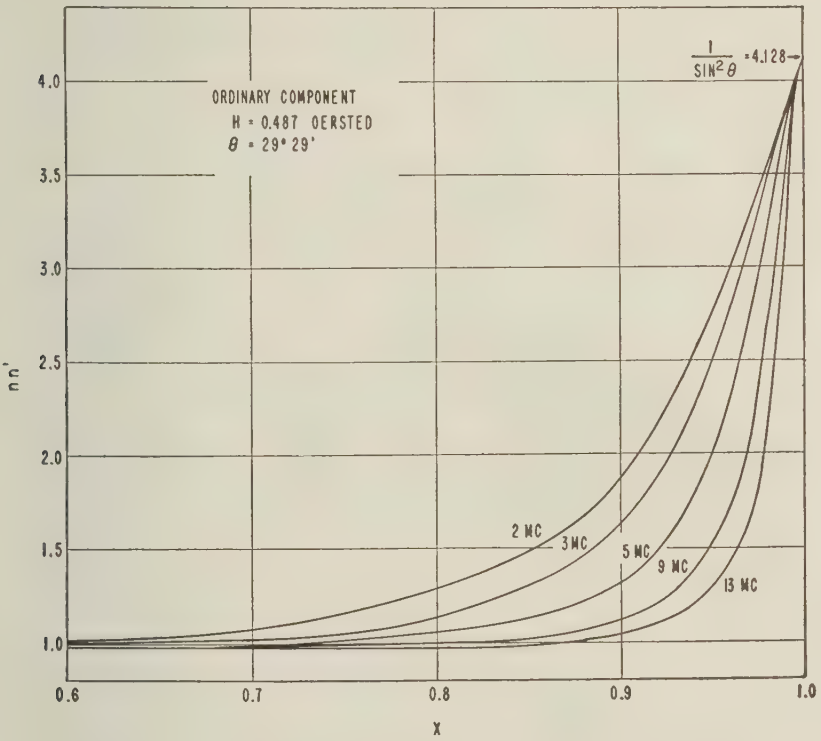

FIG. 3—nn' product for the ordinary ray, White Sands, New Mexico

Selected nn' curves for the ordinary ray at White Sands are given in Figure 3.

3. *The extraordinary component*

A slightly different procedure is used for the extraordinary ray, based on the fact that plotting n^2 *vs* $x/(1 - y)$ yields curves that are almost straight lines. Thus, we may write

$$n^2 = 1 - \frac{x}{1 - y} + G\left(\frac{x}{1 - y}, y\right) \qquad (6)$$

where the G function is a small quantity, illustrated in Figure 4. Differentiating gives

$$2n\frac{\partial n}{\partial f} = \frac{\partial}{\partial j}\left(1 - \frac{x}{1-y}\right) + \frac{\partial G}{\partial\left(\frac{x}{1-y}\right)}\frac{\partial\left(\frac{x}{1-y}\right)}{\partial f} + \frac{\partial G}{\partial y}\frac{\partial y}{\partial f}$$

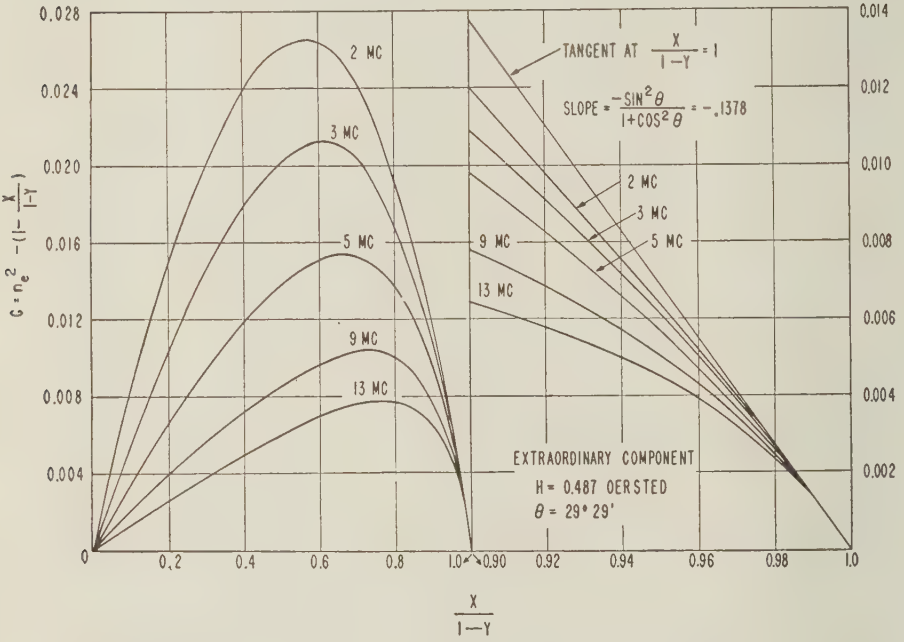

FIG. 4—Difference between $(n_e)^2$ and linear approximation, White Sands, New Mexico

which leads to

$$nn' = 1 + \frac{xy}{2(1-y)^2} - \frac{x(2-y)}{2(1-y)^2}\frac{\partial G}{\partial\left(\frac{x}{1-y}\right)} - \frac{y}{2}\frac{\partial G}{\partial y} + G \quad \ldots\ldots\ldots(7)$$

For a given value of y, the expression becomes

$$nn' = 1 + Ax + Bx\frac{\partial G}{\partial\left(\frac{x}{1-y}\right)} + C\frac{\partial G}{\partial y} + G$$

where A, B, and C are constants and where the terms

$$\frac{\partial G}{\partial\left(\frac{x}{1-y}\right)} \quad \text{and} \quad \frac{\partial G}{\partial y}$$

are determined from the numerical data used to plot the G family. It should be

noted that the G curves have everywhere a finite slope, with a maximum value of 0.1378 at $x = 1 - y$. The contribution of the term

$$B.x \frac{\partial G}{\partial\left(\frac{x}{1-y}\right)}$$

to the final answer can be as much as 15 per cent. For frequencies above 2 Mc, the term $(y/2)(\partial G/\partial y)$ contributes, at most, 0.6 per cent to the final answer, and in most cases is completely negligible. The nn' curves for the extraordinary ray at White Sands are given in Figure 5.

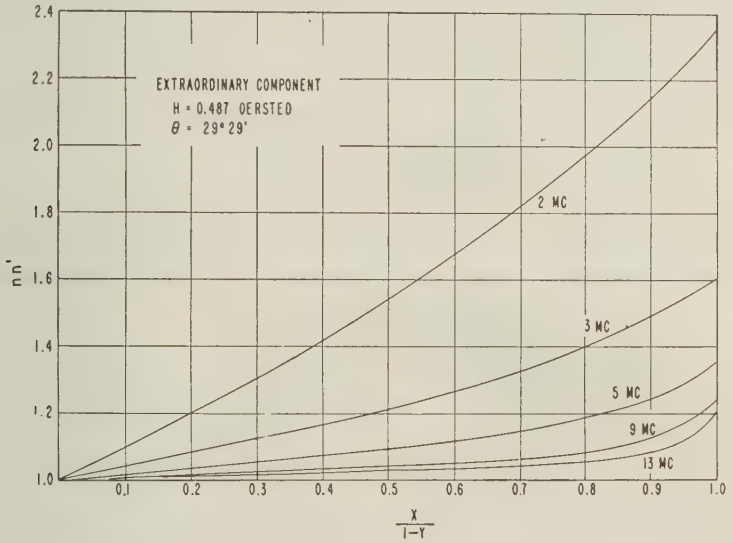

FIG. 5—nn' product for the extraordinary ray, White Sands, New Mexico

VIRTUAL-HEIGHT COMPUTATIONS

1. *General procedure*

A typical electron-density distribution as obtained from rocket measurements at the White Sands Proving Ground, New Mexico [3, 4] is shown in Figure 6. Successive points on the distribution curve are shown as P_1 , P_2 , P_3 , etc., so that heights, density, and critical frequency corresponding to a given point P_i can be represented by h_i , N_i , and f_i . The corresponding points on the virtual-height curve are indicated as P'_1 , P'_2 , P'_3 , etc. This presentation of virtual heights differs from a P'-f plot, since the virtual heights of reflection are plotted *vs* density, rather than *vs* critical frequency.

The contribution to the virtual height at a given frequency, due to an ionospheric region of thickness D, increasing linearly from a density N_0 to a density N_1 is

$$D' = \int_0^D n' \, dh = \frac{D}{x_1 - x_0} \int_{x_0}^{x_1} n' \, dx \quad \ldots\ldots\ldots\ldots\ldots\ldots (8)$$

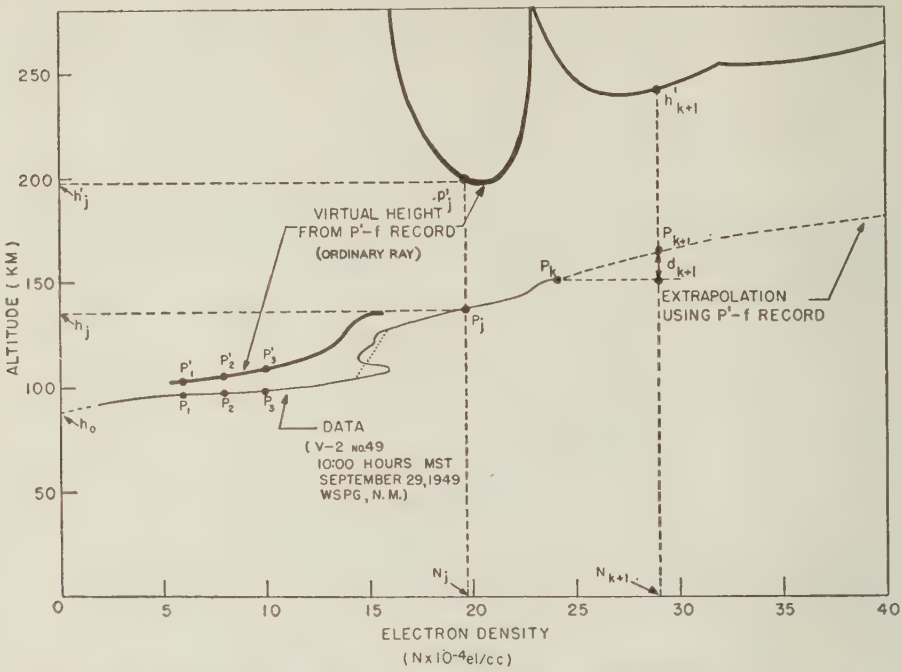

FIG. 6—Electron-density distribution obtained from rocket measurements and corresponding virtual heights

where x_0 and x_1 are the values of x corresponding to N_0 and N_1 for the particular frequency.

To evaluate $\int_{x_0}^{x_1} (n'\,dx)$, we introduce a function Q defined as

$$Q(f, x) = \int_0^x n'\,dx$$

Thus,

$$\frac{D'}{D} = \frac{1}{x_1 - x_0}\,[Q(f, x_1) - Q(f, x_0)] \qquad (9)$$

The Q function is represented as a family of curves obtained by evaluating $\int_0^x n'\,dx$ as a function of x and for various frequencies. We should note that, if a region has a constant density, formula (9) becomes indeterminate. In this case,

$$\frac{D'}{D} = n' \qquad (9a)$$

2. *The ordinary ray*

To evaluate the integral $\int_0^x n'\,dx$ at a given frequency, we must determine the area under the corresponding n' *vs* x curve. To prevent the integrand from becoming

infinite at $x = 1$, we make the following change in variable, as suggested by Shinn and Whale (reference [2]): Let

$$t = \sqrt{1 - x}$$

Then,

$$\int_0^x n'\, dx = -2 \int_{t=1}^{t=\sqrt{1-x}} n' \sqrt{1 - x}\, dt$$

The integral is then twice the area under the curve $n' \sqrt{1 - x}$ *vs* $\sqrt{1 - x}$, which can be obtained by numerical integration. Typical $n' \sqrt{1 - x}$ curves for White Sands are shown in Figure 7. These curves can be used to compute n' whenever

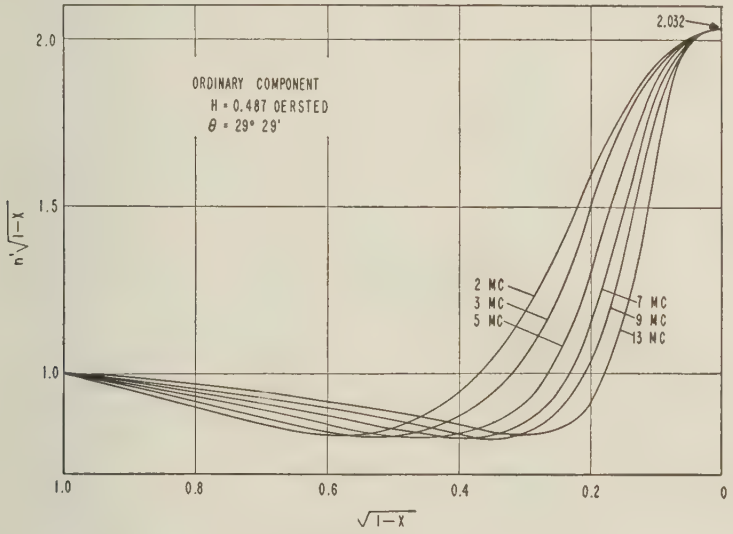

FIG. 7—$n' \sqrt{1 - x}$ for ordinary ray, White Sands, New Mexico

formula (9*a*) must be used. The Q function is shown in Figure 8 for $f = 2$ Mc and $f = 13$ Mc. The Q curve obtained when the magnetic field is ignored is also shown in Figure 8. Since the curves for the intermediate frequencies cannot be shown in Figure 8 without excessive crowding, the frequency dependence of the Q function was illustrated in Figure 9, by means of the quantity ΔQ_f, defined as $\Delta Q_f = Q_{2\text{Mc}} - Q_f$. Thus, at a given frequency f, Q_f is obtained by reading the $Q_{2\text{Mc}}$ value from Figure 8 and subtracting the ΔQ_f value from Figure 9.

The procedure for computing group height at a frequency f is then as follows. The distribution curve is approximated by a succession of linear segments P_1P_2, P_2P_3, etc., up to the critical density N_k for the frequency f_k. Let d_1, d_2, etc., be the thickness of these intervals. The virtual height is then a summation of the form

$$h' = h_0 + \sum_{i=1}^{k} \frac{d_i}{x_i - x_{i-1}} (Q_i - Q_{i-1}) \quad \ldots\ldots\ldots\ldots\ldots\ldots (10)$$

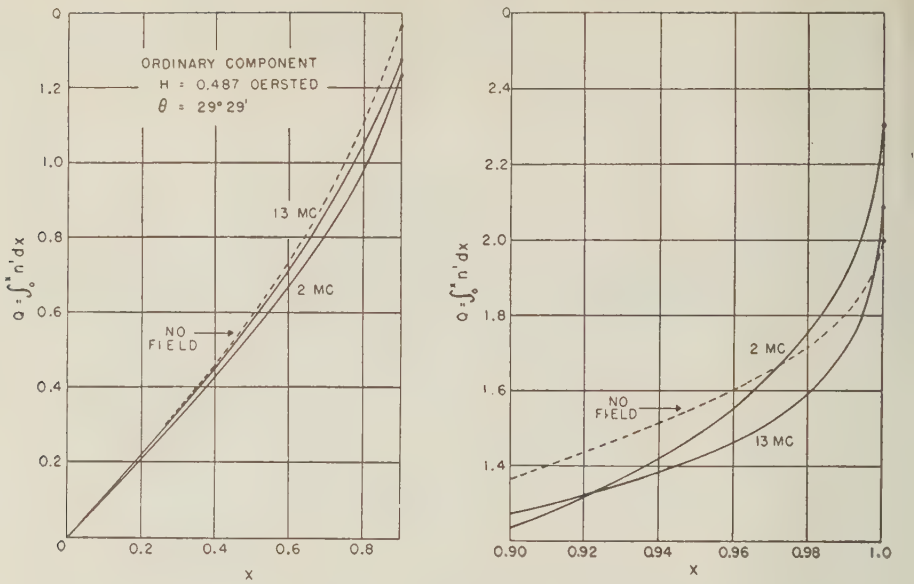

FIG. 8—Q curves for ordinary ray, White Sands, New Mexico

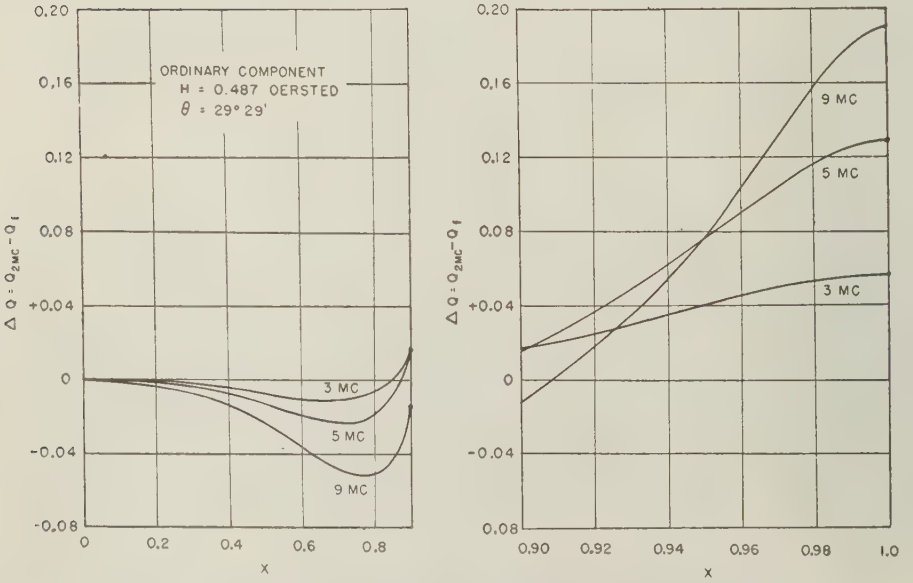

FIG. 9—Data for interpolation of Q curves, White Sands, New Mexico

where x's and Q's must, of course, be computed for the frequency used and for the densities corresponding to the end-points of each interval, that is,

$$x_i = \frac{80.6}{f_k^2} N_i = \frac{N_i}{N_k} \quad \ldots\ldots\ldots\ldots\ldots\ldots\ldots\ldots\ldots\ldots (11)$$

(if we express N_i in electrons per cc and f in kc/sec).

3. *The extraordinary ray*

Virtual heights for the extraordinary ray are computed by a similar procedure. The device used to evaluate $\int_0^{x_1} n'\,dx$ is to let

$$t = \sqrt{1 - \frac{x}{1 - y}}$$

Then,

$$\int_0^{x_1} n'\,dx = -2(1 - y) \int_1^{t_1} n' t\,dt = Q(x)$$

Typical $n'\sqrt{1 - [x/(1 - y)]}$ curves for White Sands are shown in Figure 10.

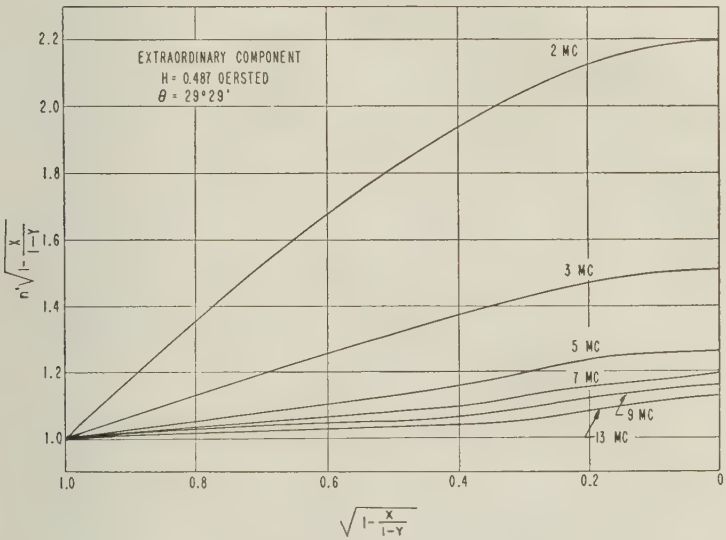

FIG. 10—$n'\sqrt{1 - [x/(1 - y)]}$ for the extraordinary ray, White Sands, New Mexico

The Q function for the extraordinary ray is shown in Figure 11, where for convenience Q is plotted as a function of $x/(1 - y)$. Thus, to use Figure 11 at a given frequency, one should divide the values of x by the corresponding value of $1 - y$. Virtual heights for the extraordinary ray are then computed by formula (10), where the values of Q are those for the extraordinary ray.

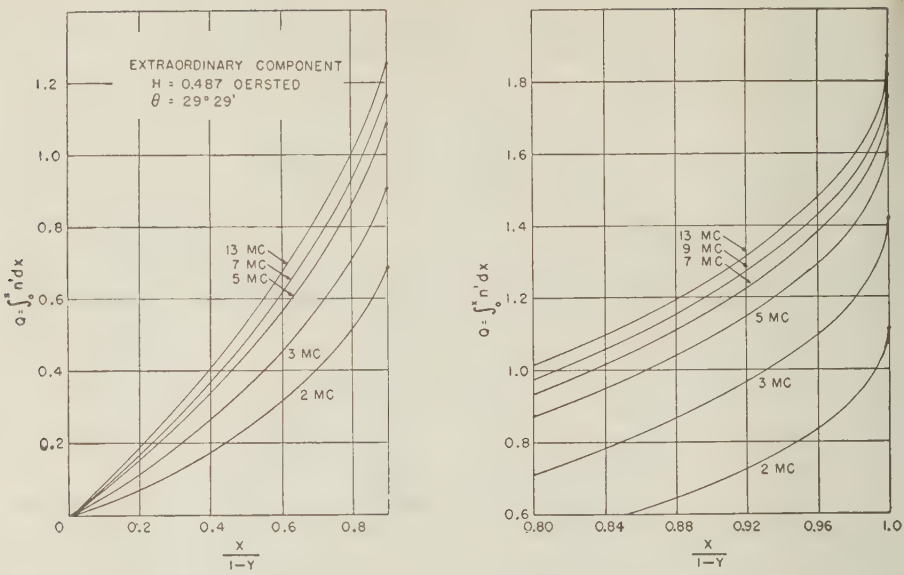

FIG. 11—Q curves for the extraordinary ray, White Sands, New Mexico

ANALYSIS OF P'-f RECORDS

The previous discussion has shown how virtual heights can be deduced from the curve of electron density *vs* altitude. The analysis of P'-f records presents a problem which is exactly opposite to the one discussed, namely, to find the electron-density distribution when the virtual heights are known.

Since the ordinary trace on the P'-f record yields, in general, more complete information than does the extraordinary trace, the procedure for deriving the electron-density distribution is based on the ordinary ray. Computations using the extraordinary ray are actually slightly more complicated. The extraordinary-ray data, however, is useful as a means of checking results. This is done by comparing the extraordinary trace computed from the distribution curve with the actual extraordinary trace on the P'-f record.

The most difficult step in the analysis of a P'-f record is the actual reading of the virtual heights, since this is the task which requires the most judgment. If one can choose the ionogram to be analyzed, it is usually possible to select a clear record, with sharp ordinary and extraordinary traces, with a minimum of discontinuities, and with freedom from sporadic echoes. If, in addition, multiple echoes can be seen on the ionograms, these can be used to check the indicated height scale and to correct the heights if necessary.

1. *Treatment of a simple case*

A simple case will be considered first, in which the lower portion of the ionization curve is known from rocket measurements and where the ordinary trace is continuous for the upper regions. These conditions were met in the 29 September 1949

data shown in Figure 6. Rocket measurements provided the electron-density distribution up to 150 km. The computed ordinary virtual heights for the lower region agreed with the P'-f record within the accuracy to which the record could be read. The problem here was simply to extend the rocket results with the aid of the P'-f record. Let P_k represent the last known point on the distribution curve. The next point P_{k+1} is obtained by selecting a small density increment and by assuming that this small increment takes place linearly in a region of thickness d_{k+1} . This assumption is justified if the points on the virtual-height curve corresponding to P_k and P_{k+1} are not too far apart. The problem is then to compute d_{k+1} for the specified density increment. Let the assumed density at P_{k+1} be N_{k+1} and the corresponding critical frequency be f_{k+1} . The virtual height h'_{k+1} corresponding to f_{k+1} , as obtained from the P'-f record, must satisfy equation (10) applied to the electron distribution of Figure 6, namely,

$$h'_{k+1} = h_0 + \sum_{j=1}^{k} \frac{d_j}{x_j - x_{j-1}} (Q_j - Q_{j-1}) + \frac{d_{k+1}}{x_{k+1} - x_k} (Q_{k+1} - Q_k) \ldots . (12)$$

where all quantities are known except d_{k+1} , and where x's and Q's are for the frequency f_{k+1} . Solving equation (12) gives d_{k+1} . The coordinates of P_{k+1} are thus $N = N_{k+1}$ and $h = h_k + d_{k+1}$. After the point P_{k+1} is located, the procedure is repeated for consecutive points until the complete distribution curve is obtained. The complete extrapolation of the 29 September 1949 data gave the electron-density distribution shown in Figure 12. For comparison purposes, the extrapolation of the results of three other rocket flights conducted by the Naval Research

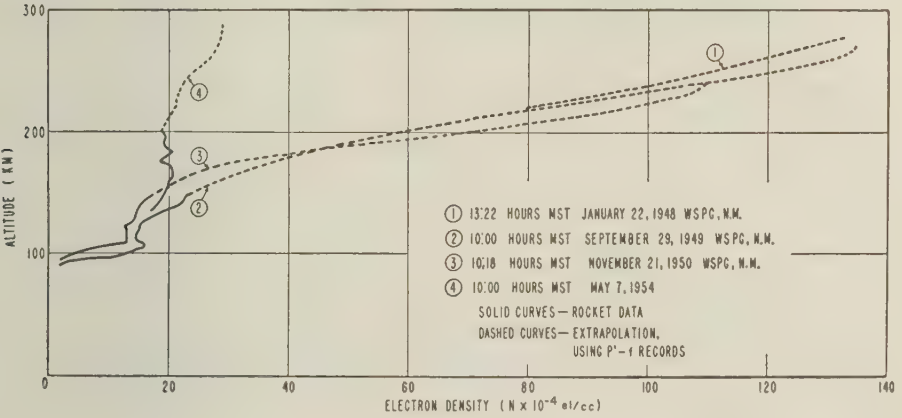

FIG. 12—Extrapolation of the data provided by four rocket flights

Laboratory (NRL) were also included in Figure 12. To avoid crowding the Figure, the curve for 22 January 1948 was not shown below 220 km, since it nearly coincides with the 29 September 1949 curve. For similar reasons, the curve for 7 May 1954 was not shown below 140 km. The P'-f records were not shown, since they appeared in previous publications [3, 4, 5, 6, 7]. Extension of the results for the flight of 21 November 1950 was done in exactly the same manner. The rocket

measurements [5] were first used to compute virtual heights, and these virtual heights were compared against the P'-f record. The results agreed for the densities measured up to 150 km. The virtual heights computed for the electron distribution between 150 and 160 km were too large and, consequently, the extrapolation was begun at 150 km. Between 150 and 160 km, the rocket-measured densities appear to be too low by about 10 per cent. This was the largest discrepancy noted in the NRL rocket results, and it occurred during the upper portion of a rocket experiment which, as previously explained [5], was performed under very unfavorable conditions. When the measurements are performed under favorable conditions, the results are in very close agreement with the P'-f record. The rocket experiment of 7 May 1954 and the corresponding ionogram provide an excellent illustration of the correlation which can be obtained between rocket measurements and ionogram analyses. However, before this can be discussed, it is necessary to introduce the more general procedure, which is outlined in the next section.

2. *General case*

The procedure just described is used also in the general case, except for a few points which require a special treatment.

In general, P'-f records exhibit one or more discontinuities, the most frequent one occurring between the E and $F1$ traces. The lack of a starting or reference point (that is, a point of known height and electron density) also introduces a difficulty in the analysis. The analysis can be performed if we assume that the ionosphere remains densely ionized between the E and F regions, and if we assume that the lower edge of the E region is linear. The ionization below the E region will be neglected, since it contributes so little to the virtual heights shown in P'-f records.

The first assumption is supported by experimental results and also by theoretical considerations. The experimental evidence is provided by the Naval Research Laboratory high-altitude rocket data (references [3], [4], [5], [6]) and by the work of Hollingsworth (reference [8]). By measuring differential retardation for the ordinary and extraordinary rays above the E critical frequency, Hollingsworth was led to the conclusion that the interlayer ionization remained uniformly distributed over the space between the E and F layers, and that the density was only a few per cent less in value than at the maximum of the E layer. Theoretical investigations leading to similar conclusions are the work of Havens, Friedman, and Hulburt (reference [9]) and the work of Kallmann (reference [10]). The second assumption is supported by rocket data and by the E-region traces exhibited by typical P'-f records.

The simplifying assumption regarding the linearity of the lower E region is used to locate the lower edge of the E region by a comparison process. The difference in recorded heights is compared with the corresponding values obtained from a reference curve. Figure 13 shows such a curve for White Sands, New Mexico. The straight line L in Figure 13 shows a region with initial density $N = 0$ at $h = h_0$ and increasing linearly in density at a rate of 10^4 el/cc per km. The contribution of such a region to the virtual height is shown in Figure 13 by the quantity $h' - h_0$, which is plotted as a function of critical frequency. The curve $h' - h_0$ *vs* f is used

n the following manner: Two frequencies f_1 and f_2 are selected well below the critical frequency for the E region, and the corresponding virtual heights h'_{f_1} and h'_{f_2} are measured on the P'-f record under study. Let $a' = h'_{f_2} - h'_{f_1}$. For the same frequencies f_1 and f_2, we measure the quantities a and b in Figure 13. The bottom of the E region for the record being analyzed is a line L defined by

$$h_0 = h'_{f_2} - (a + b)\frac{a'}{a} \quad \ldots\ldots(13)$$

$$\text{Slope} = \frac{a'}{a} \text{ km}/10^4 \text{ el/cc} \quad \ldots\ldots(14)$$

The line L is extended up to the density corresponding to f_2. This provides a reference point and the analysis can then proceed with the aid of equation (12),

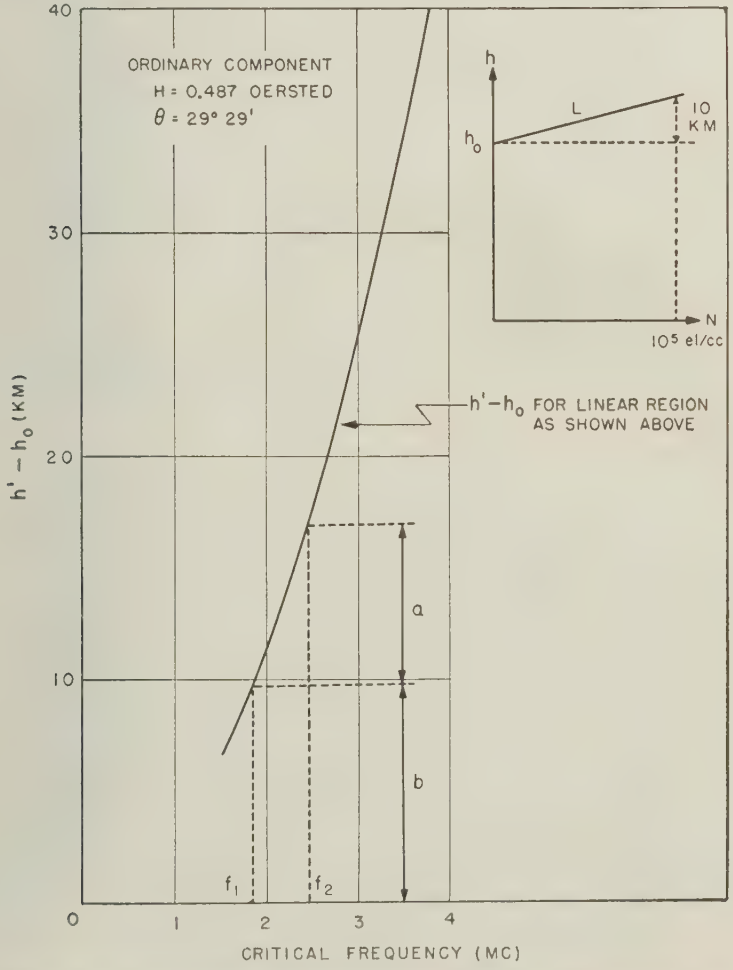

Fig. 13—Graph used for locating the lower edge of the E region, at White Sands, New Mexico

as previously indicated. The procedure is carried out up to the critical frequency for the E region, at which time the P'-f record usually shows a discontinuity. The method at this point makes use of the assumption that the ionosphere remains densely ionized between the E and F regions. If we assumed that the electron density increased linearly from the maximum of the E region until the first point where an $F1$ echo occurs, the assumed densities would probably be too large. In an attempt to avoid overestimating the "interlayer" density, the region between E and $F1$ is approximated by a straight line intersecting the lower edge of the E region at a density which is nine-tenths the critical density for the E region. The approximation, which is illustrated by the dotted line in Figure 6, gives very nearly the correct virtual heights for the $F1$-region in the case of the rocket results. This procedure was used when the ionogram was discontinuous at other places. The straight-line approximation was made to intersect the distribution curve at a density equal to nine-tenths the density at which the discontinuity occurred. Occasionally, when a discontinuity occurs on the P'-f record, double echoes can be seen, indicating that reflections at the lower level extend somewhat beyond the

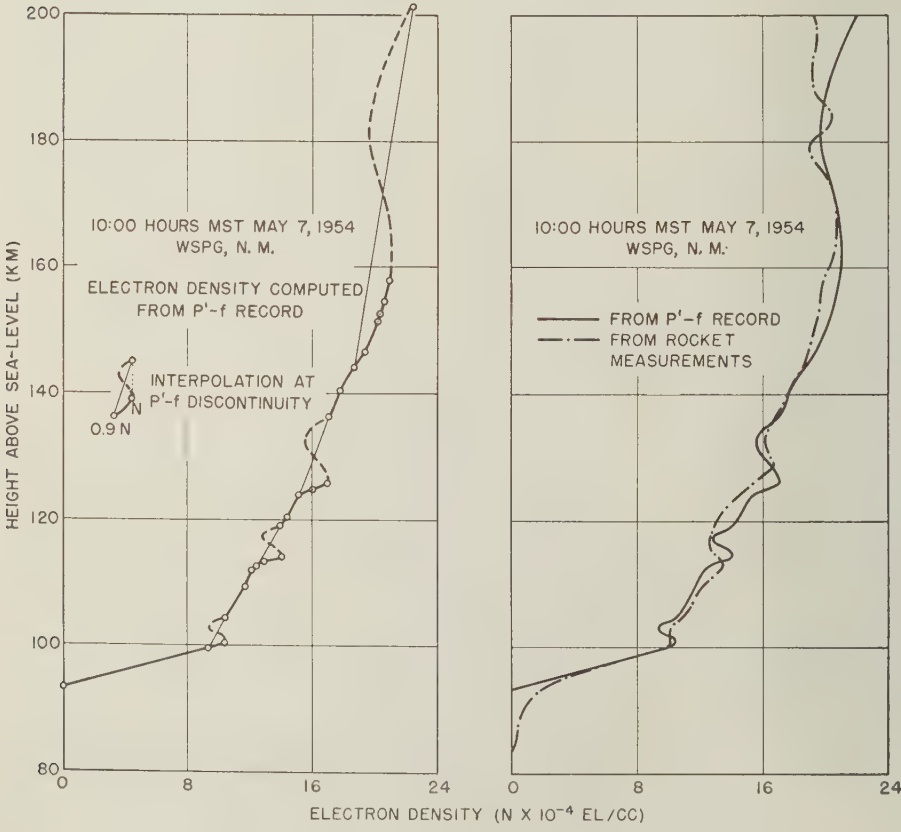

FIG. 14—Electron densities computed from P'-f record and comparison with rocket measurements

enetrating frequency [11]. In such cases, the author used the actual penetrating requency to determine the density at which the discontinuity occurred.

A complete illustration and test of the recommended procedure will now be iscussed, using the data obtained during the flight of 7 May 1954. First, the ocket measurements (Fig. 14) were verified against the *P'-f* records (Fig. 15). his was done by computing the ordinary- and extraordinary-ray virtual heights

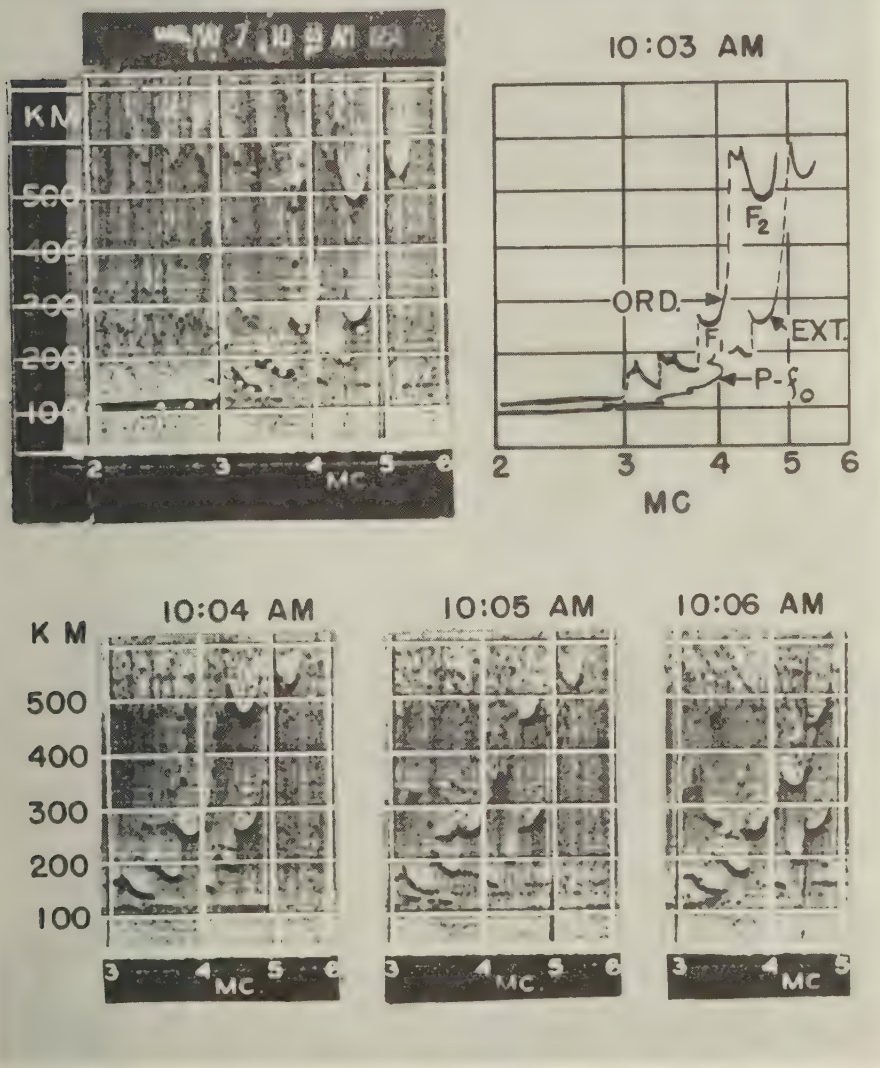

Fig. 15—Sample ionograms taken during the Viking 10 flight, 10:03–10:06 A.M., MST, May 7, 1954, WSPG, N.M.

for the electron distribution measured up to 165 km and by plotting the results on the original P'-f record (Fig. 15). The computed points, shown as white dots, are in excellent agreement with the P'-f record. (The densities measured in the 165- to 200-km region could not be used to compute virtual heights, since no reflections can theoretically occur in this region for the distribution obtained.) The rocket results were then used to verify the method proposed for the analysis of P'-f records. The electron-density distribution was computed directly from the P'-f record for 10:03 A.M. (Fig. 15), and the resulting curve was compared with the rocket results. The ionization curve (Fig. 14) obtained from the ionogram agrees with the rocket results in the 90- to 165-km region within the accuracy to which the P'-f record could be read. Interpolations performed at P'-f discontinuities were done as indicated. The absence of F-region echoes for frequencies between 4.1 and 4.3 Mc prevented an accurate density computation for the 154- to 200-km region. Interpretation of the P'-f record, nevertheless, was attempted by estimating the missing portion of the ionogram on the basis of the trend revealed in subsequent records for 10:04 A.M. and 10:05 A.M. The interpolation used between the $F1$ and $F2$ traces was as shown in the sketch included with the ionograms of Figure 15. The agreement obtained appears to be extremely good, considering that more than 5 per cent error can easily occur in reading the P'-f records,

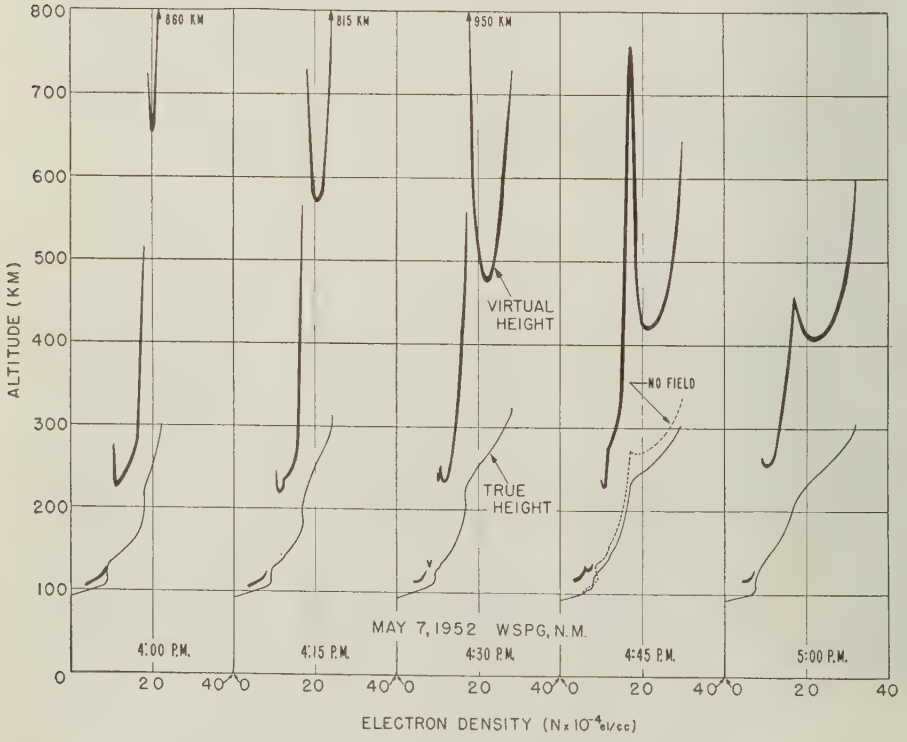

FIG. 16—Analysis of a daytime sequence of P'-f records

that the record used presented an unusual number of discontinuities, and that the rocket results can themselves be in error by as much as 5 per cent. In addition, the ionograms indicated rapid changes in the ionospheric regions. This could also account for some of the differences observed, since the measurements made by the two methods are for regions separated horizontally by a distance up to 40 km.

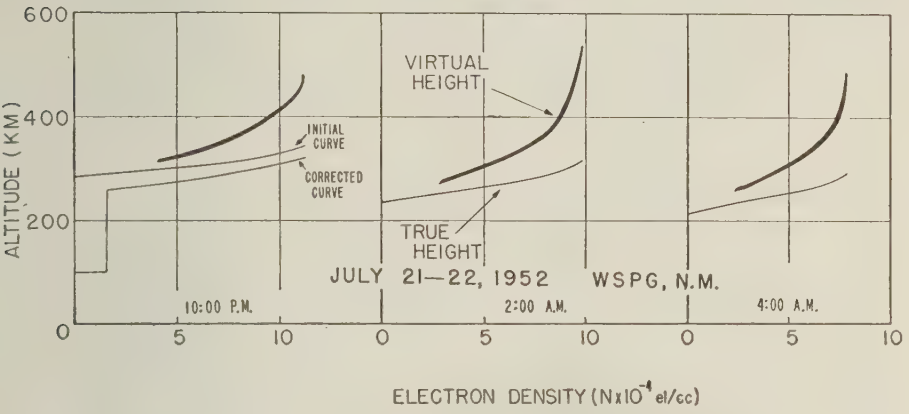

FIG. 17—Analysis of a night-time sequence of P'-f records

Additional examples of ionogram analyses are shown in Figures 16 and 17. The sequence of events shown in Figure 16 is a rather interesting illustration of the distorted picture provided by P'-f records when the densities in the $F2$ region are not much greater than the E and $F1$ densities. In lieu of showing the P'-f records, the ordinary-ray virtual heights were measured and replotted as a function of electron density. This provides a direct correlation with the actual electron-density distribution curve. It is of interest to note that the actual height of the $F2$ region remains essentially constant and that the considerable variation in virtual heights is due entirely to retardation in lower regions. To show the effect of neglecting the earth's magnetic field, the P'-f record for 4:45 P.M. was also analyzed, assuming no magnetic field. The resulting curve is about 20 km higher than the curve computed taking the magnetic field into consideration. In addition, the no-field curve is inconsistent in the neighborhood of 270 km, where two values of density are obtained at the same altitude. An inconsistency of this type never occurred in the analyses which were done taking the magnetic field into consideration. It is of interest to note that when the Q curves are available, ignoring the field does not make the analysis appreciably easier; the only simplification is in using the same Q curve for all frequencies.

The analysis of night-time ionograms is illustrated in Figure 17, with ordinary-ray virtual heights shown in the same manner as in Figure 16. Night recordings appear somewhat easier to analyze than daytime recordings, in view of the simpler shape of the ordinary and extraordinary traces. The lower edge of the F region was assumed linear and was determined with the aid of equations (13) and (14). The remainder of the distribution curve was then obtained using the methods

previously described. The extraordinary trace (computed from the distribution curve) was found to be in good agreement with the recorded extraordinary trace on the 2 A.M. and 4 A.M. recordings. However, on the 10 P.M. recording, the computed extraordinary trace was 25 km too low. This was attributed to differential retardation below the $F2$ region. A uniform density of 2×10^4 el/cc was arbitrarily assumed, beginning at an altitude of 100 km and extending up to the bottom of the $F2$ region. A new ionization curve was determined and the computed extraordinary trace was then about 15 km too high. A second attempt, using 1.5×10^4 el/cc for the rectangular region, yielded the corrected ionization curve shown in Figure 17. The extraordinary trace computed from this corrected curve was then found to agree with the recorded extraordinary trace. The ionization shown below the $F2$ region in Figure 17 (10 P.M. curve) should not be considered as representing the true distribution. It merely indicates the effective average electron density of this lower region. It is of interest to note that the discrepancy, observed when the results were checked with the aid of the extraordinary trace, revealed that a substantial amount of daytime ionization was still present below the $F2$ region at 10 P.M. In addition, the corrected calculation indicated that the height of the $F2$ region was about 25 km lower than initially computed. The initial results suggested that the height of $F2$ region had dropped by about 50 km between 10 P.M. and 4 A.M. The revised computations showed this variation in height to be no more than 25 km.

The method for analyzing ionograms was applied to a dozen additional records taken at White Sands during the period from 1948 to 1955, which includes the last sunspot-maximum and the last sunspot-minimum. The resulting electron-density distribution curves were very similar to the curves shown in this paper. The densities showed expected variations during the solar cycle, but the height of the daytime $E1$ and $F2$ regions exhibited a considerable degree of regularity.

CONCLUSIONS

It is believed that the methods described in this paper provide a simple and yet accurate procedure for studying P'-f records. The major task is in performing the initial computations to determine the Q curves. This preliminary work can be done with a calculating machine in about 100 hours. The resulting Q curves, however, are a permanent investment, since they can be used to analyze any P'-f record obtained at the given location. The actual analysis of a record using the indicated procedure can be done in two or three hours. The examples included in this paper were selected to illustrate the general procedure and to show various additional devices which can be used to improve the analysis. Future efforts will be devoted to additional correlations between rocket results and corresponding ionograms. This will permit a critical evaluation of the various rocket techniques used for ionospheric measurements, and will make possible further tests and refinements of the proposed method for analyzing P'-f records.

Reduction of large numbers of P'-f records to actual electron densities *vs* height should lead to a better understanding of the ionosphere, since a precise knowledge of ionization as a function of height is part of the basic information needed to explain the physical processes in the ionosphere. The value of the simul-

taneous observations planned on a world-wide scale during the International Geophysical Year will be greatly enhanced if an appropriate selection of ionograms is reduced to actual electron-density curves.

ACKNOWLEDGMENTS

The author is greatly indebted to Mr. Michael Balderston, a student at the Massachusetts Institute of Technology, who performed all numerical computations and most of the ionogram analyses during his summer employment at this Laboratory. The author also wishes to acknowledge the helpful comments and suggestions which he received from Mr. J. C. Seddon, of this Laboratory.

References

[1] H. A. Whale and J. P. Stanley, J. Atmos. Terr. Phys., **1**, 82 (1950).
[2] D. H. Shinn and H. A. Whale, J. Atmos. Terr. Phys., **2**, 85 (1952).
[3] J. C. Seddon, J. Geophys. Res., **58**, 323 (1953).
[4] J. C. Seddon, J. Geophys. Res., **59**, 463 (1954).
[5] J. E. Jackson, J. Geophys. Res., **59**, 377 (1954).
[6] J. C. Seddon, A. D. Pickar, and J. E. Jackson, J. Geophys. Res., **59**, 513 (1954).
[7] J. C. Seddon, Washington, D. C., Naval Research Laboratory, Rep. No. 4304, UARR Rep. No. 22 (1954).
[8] J. Hollingsworth, Proc. Phys. Soc. of London, **47**, 843 (1935).
[9] R. J. Havens, H. Friedman, and E. O. Hulburt, "The Ionospheric *F*2-region," paper presented at the Ionospheric Conference, Cambridge, England (Sept. 1954).
[10] H. K. Kallmann, Santa Monica, California, RAND Corporation, Rep. No. P-638 (1955).
[11] A. C. Deb, Indian J. Phys., **14**, 451 (1940).

GEOMAGNETIC AND SOLAR DATA

INTERNATIONAL DATA ON MAGNETIC DISTURBANCES, THIRD QUARTER, 1955

For explanations, please refer to a previous report in this JOURNAL (Vol. 60, No. 2, June, 1955, p. 219).

Preliminary Report on Sudden Commencements

S.c.'s given by five or more stations are in italics. Times given are mean values, with special weight on data from quick-run records.

Sudden commencements followed by a magnetic storm or a period of storminess (s.s.c.)

1955 July: None.

1955 August 05d 03h 59m: SM Hu.—27d 15h 14m: Ci Ka Qu.

1955 September: None.

Sudden commencements of polar or pulsational disturbances (p.s.c.)

1955 July 02d 15h 09m: Fu Qu Ap. *-02d 19h 12:* five.—02d 19h 28: SM Hr.—03d 00h 28: SM Ta.—03d 00h 40: Ma Ta.—04d 20h 24: So Gi El. -05d 02h 11: Ta MB Va.—*06d 14h 58:* six.—*06d 23h 03:* ten.—08d 16h 33: Ci SM Ta. -11d 01h 34: Eb Tl SM Va.—11d 13h 30: Ap To Am.—11d 15h 55: Qu Ta.—*12d 00h 24:* nineteen.—15d 20h 35: So Do Fu Eb. —*16d 00h 40:* nine.—16d 01h 08: SM MB Ba Va.—*16d 21h 04:* eight.—17d 21h 08: Eb Tl Gi El.—18d 04h 33: SM Va.—20d 02h 05: Wn IK Tl Ta.—*20d 20h 13:* twelve.—*21d 21h 32:* seventeen.—26d 19h 49: So Tl. -*26d 21h 15:* five.—*28d 22h 52:* twelve. -29d 20h 00: So Gi Qu.—*29d 22h 46:* sixteen.—*30d 22h 14:* nine.—31d 00h 49: Fu SM Ta.

1955 August *01d 00h 44m:* nine.—02d 00h 26: Eb Mb Bi. -02d 01h 35: Fu IK El.—02d 02h 07: CF SM. —02d 20h 54: Tr So Gi. *-03d 22h 37:* five.—*03d 23h 00:* thirteen.—04d 04h 00: SM Ta.—04d 17h 38: Wn Ma Gi Hr. -04d 21h 51: Qu Ta Bi.—*05d 20h 09:* seventeen.—05d 23h 01: Do Ta. -05d 23h 18: Ma Bi.—*06d 22h 09:* nine.—08d 23h 38: Tl Ta.—*10d 03h 06:* six.—19d 19h 55: Gi El. -19d 20h 29: Tr So Fu Gi.—*21d 00h 02:* fourteen.—21d 18h 15: Gi Bi El.—*23d 21h 37:* six.—25d 02h 17: IK Hr.—*29d 20h 15:* eleven.—29d 20h 38: Tr Le Wn CF. -*29d 20h 53:* six.

1955 September 01d 13h 36m: Ka To.—*01d 19h 26:* fifteen. -01d 19h 42: Ci MB.—02d 02h 31: CF SM Ta MB.—*02d 20h 38:* five.—03d 10h 47: SM Ap To Am. —03d 19h 29: Tr So Gi.—*04d 00h 13:* ten.—*04d 03h 37:* five.—*04d 21h 05:* seven. -*05d 00h 14:* fourteen.—*06d 03h 20:* five. -06d 18h 29: So Gi. -06d 19h 05: Gi Qu.—06d 23h 17: Fu CF Ta.—08d 22h 15: So Le Fu Gi.—*08h 22d 53:* eight.—*09d 23h 07:* six.—12d 01h 10: SM Ta.—*12d 23h 05:* six.—12d 23h 37: Gi Ta Bi. -13d 00h 40: CF SM.—13d 03h 09: Gi Va.—13d 09h 54: Ap Am.—*14d 21h 10:* ten.—14d 23h 58: CF MB.—15d 00h 41: CF IK SM.—*16d 00h 40:* eight.—*16d 21h 29:* five.—17d 08h 18: Ap Am.—*19d 00h 22:* seven.—*19d 00h 52*: seven.—*19d 23h 41:* eight. *-20d 19h 51:* nine.—*20d 21h 03:* five.—20d 21h 23: Gi Tn.—20d 21h 40: Gi Tn.—*21d 23h 28:* five.—*21d 23h 42:* nine.—22d 00h 23: CF IK Gi Tl.—24d 17h 29: Fu Qu. —

TABLE 1—*Geomagnetic planetary three-hour-range indices Kp, preliminary magnetic character-figures C, average amplitudes Ap (unit 2_γ), and final selected days, July to September, 1955*

July 1955

E	1	2	3	4	5	6	7	8	Sum
1	1+	1+	2+	1+	1o	1−	0+	1−	9o
2	1+	2o	1+	2−	3−	4+	5+	4+	23o
3	3o	4−	2+	3−	1+	2−	1+	1+	17+
4	1o	1o	2−	0+	1−	0+	1−	0+	6o
5	1o	1−	1−	0+	1−	1o	1o	1+	7−
6	1−	1o	1−	0+	1−	2o	2o	3+	11−
7	3+	3+	2+	2−	2+	2o	1+	2−	18o
8	1o	2−	2o	3+	2+	4−	3−	2−	18+
9	2−	1+	1o	2+	2o	0+	1−	2o	11+
10	1+	2−	2o	3o	4o	3o	2+	2+	20−
11	3o	2o	3+	5−	4−	3+	3−	3o	26−
12	5+	2−	3o	4−	3o	2+	3−	4o	26−
13	3+	2o	1−	1−	3−	3−	1o	1+	14+
14	1+	1+	2o	2o	2o	1+	1+	0+	12−
15	1o	1−	1−	2−	4+	5−	3o	3−	19−
16	3+	2o	1+	2o	2+	1+	2+	2+	17o
17	1+	3o	3−	1+	1−	0+	1+	2o	13−
18	1+	3+	3o	2−	2−	1−	1o	0+	13o
19	1o	1−	1−	1+	1o	1−	0o	1−	6o
20	1+	1−	0+	1o	1+	1o	2−	1−	8o
21	1+	1−	0o	1−	0+	1−	1o	2+	7o
22	1o	1o	1−	1o	1−	1o	0+	2+	8o
23	3−	1+	2−	1o	1o	1o	2o	3−	13+
24	3−	3o	2+	2+	1+	1o	1+	1+	15+
25	2o	2−	2o	1+	1+	1o	1o	1+	12−
26	2o	2o	2+	3+	4−	3−	3−	4−	22+
27	3o	1+	1+	1+	1o	1o	1+	1o	11+
28	1+	1−	1−	1−	1+	1o	0+	1o	7o
29	2−	1+	2o	1−	1−	1−	3o	2o	12o
30	0+	1o	1+	2−	2−	1+	2−	3−	12−
31	3−	1+	2+	1−	2−	2−	0+	1o	12−

August 1955

1	2	3	4	5	6	7	8	Sum
1+	1−	1−	1o	2o	1+	1o	1−	9−
2+	1+	0+	0o	0+	0+	1o	3−	8+
4o	2+	2+	2−	2−	3−	2−	3−	19o
3−	4o	3o	5+	5o	4+	4o	4o	32+
2o	2o	4o	3+	3o	3+	4+	4o	26o
3+	3+	5+	5+	4−	5−	3o	5o	34−
3o	3o	4−	4−	3+	2o	4o	3−	25+
2+	1o	2−	3o	3o	2o	2o	2−	17−
2+	1+	2o	2−	2o	1o	2o	1+	14−
1o	2+	1+	2−	2−	1+	1o	2−	12o
1+	1+	1−	1−	0+	0+	1+	2−	8−
2o	1o	2−	2−	1o	0+	1o	1−	9+
1+	2o	1+	3−	1+	1o	1o	3−	13+
3o	2−	1+	3−	1+	3−	3+	3o	19o
3+	3+	2+	2o	3−	1o	0+	1−	16−
0o	2+	3o	0+	1o	0+	1o	1+	9+
1+	0+	1−	1+	2−	2+	2o	2+	12o
1+	2+	2+	2+	2−	1+	2o	2o	15+
1+	2+	2+	1+	1+	1+	2−	2o	14−
1+	1−	1o	2o	1+	2−	1o	1−	10−
2+	2o	2o	0+	1−	0+	1o	1o	10−
0o	0+	0+	0o	0+	0+	1o	1o	3+
0+	0+	1+	0+	1−	1−	0+	1o	5o
0+	1o	1+	3−	2o	1o	1−	1o	10o
1o	0+	1o	1+	2−	1+	1+	1o	9o
1+	1+	1o	2+	2+	1+	1+	2−	13−
0+	1−	1o	1−	1−	2−	2o	3−	10−
1−	4−	6o	4−	3−	2−	2−	1+	21+
3o	2o	2+	2o	2o	1+	3o	3+	19o
2−	1+	1o	2o	1−	2−	1+	1+	11o
2−	2−	1o	2o	1+	1o	1+	2+	12+

September 1955

E	1	2	3	4	5	6	7	8	Sum
1	1+	1o	3+	3−	3−	3−	3o	2o	19−
2	4o	4o	3−	4+	3+	3−	1+	2−	24o
3	3+	3o	3+	5o	3+	1+	2o	2+	24−
4	4+	4−	3−	4+	3−	3+	2−	4−	26+
5	4+	5−	4o	4o	3+	3−	3−	2o	28−
6	2o	3+	3+	3+	1+	2+	2+	3o	21o
7	3o	1+	3+	3o	1o	1+	1o	1−	15−
8	1o	2−	2o	2+	2o	3−	1o	2+	15o
9	3o	3−	1o	1+	1+	1+	1−	2−	13o
10	1+	1+	3−	2+	1+	1+	1+	1−	12+
11	2o	1+	1+	1o	1+	1o	1o	2+	11+
12	3−	4−	5−	3o	3o	2+	2−	3+	24+
13	4+	4+	4+	4+	3o	4−	2−	1−	26+
14	0+	2−	3−	3−	2−	1+	1−	1+	12+
15	2+	2o	1o	1o	1o	1+	2o	1+	12o
16	3+	3o	3−	3−	2+	1+	1−	2o	18o
17	3−	4o	4+	3o	2o	2−	2−	2−	21o
18	2o	3−	3−	3o	2o	2+	1+	1−	17−
19	3o	3−	2o	2+	2+	1+	1−	2o	16+
20	3o	2+	3+	3o	0+	1o	1+	1+	16−
21	1+	1+	1+	2−	0+	0+	1o	2−	9o
22	4−	3−	1o	1o	1+	1−	2o	2−	14o
23	1o	2o	4−	4−	2o	2−	3o	3+	20+
24	4−	2−	1o	1+	1o	2o	2+	0+	13+
25	2−	1−	1o	0+	0+	1−	0+	1+	6+
26	1o	1−	0o	0+	1−	0+	1−	1o	5−
27	3−	3o	3o	4−	3+	4o	4+	4−	28−
28	2+	4+	4o	3+	2+	2−	4−	2o	24−
29	3+	2o	2+	3−	2o	5o	5−	4−	26−
30	4+	6+	7−	6−	5o	4o	3+	4+	40−
31									

Preliminary *C*, 1955			Average amplitude *Ap*		
July	Aug.	Sep.	July	Aug.	Sep.
0.1	0.2	0.8	4	4	11
1.0	0.3	0.9	19	4	17
0.7	0.7	1.0	10	11	17
0.0	1.4	1.1	3	30	20
0.0	1.0	1.1	4	19	22
0.4	1.4	0.6	6	34	12
0.7	1.1	0.2	10	17	8
0.8	0.6	0.4	10	9	7
0.2	0.3	0.3	5	6	7
0.7	0.2	0.2	12	6	6
0.9	0.1	0.2	18	4	5
1.2	0.1	1.0	20	4	17
0.5	0.3	1.1	8	7	22
0.3	0.8	0.3	5	11	6
0.8	0.6	0.2	14	9	6
0.6	0.2	0.4	9	5	10
0.3	0.3	0.7	7	6	14
0.3	0.3	0.4	7	7	9
0.1	0.4	0.4	3	6	8
0.1	0.2	0.5	4	5	9
0.3	0.2	0.1	4	5	4
0.2	0.0	0.6	4	2	8
0.4	0.0	0.8	7	3	13
0.6	0.3	0.4	8	5	7
0.2	0.2	0.1	5	4	3
0.9	0.2	0.0	14	6	3
0.2	0.3	1.3	6	5	20
0.0	1.0	0.9	4	20	16
0.4	0.7	1.2	6	10	20
0.2	0.1	1.5	6	5	54
0.3	0.3		6	6	

TABLE 1 (Concluded)—*Final selected days, July to September, 1955*

Month	Five quiet days	Ten quiet days	Five disturbed days
July	4 5 19 21 28	1 4 5 14 19 20 21 22 25 28	2 11 12 15 26
August	1 11 22 23 25	1 2 11 12 20 21 22 23 25 27	4 5 6 7 28
September	11 15 21 25 26	8 9 10 11 14 15 21 24 25 26	5 13 27 29 30

25d 21h 15: six.—25d 21h 28: Gi El. –26d 20h 36: Gi Bi.—26d 22h 43: Eb MB Bi. – *27d 01h 43:* eight.—27d 17h 39: Ta Bi.—*27d 18h 19:* five.—*27d 20h 37:* seven. – 29d 17h 50: SM MB. –30d 07h 35: Ap Am.—30d 23h 17: Ta El.—30d 23h 36: Ci MB Hr.

Sudden impulses found in the magnetograms (s.i.)

1955 July 06h 21h 18m: Ba Bi.—*06d 23h 14:* six.—24d 03h 43: Ta Ba.—24d 03h 55: Ta Ba.

1955 August 06d 11h 30m: Ta Bi.—06d 16h 47: Ci Ta Bi.—*07d 09h 07:* six.—14d 22h 42: Gi Ta MB.—24d 10h 31: Ta Hr. –27d 21h 43: IK Ta.—*29d 01h 13:* seven.

1955 September 24d 09h 09m: Ta Hr.

Preliminary Report on Solar-Flare Effects

Effects confirmed by ionospheric or solar observations are in italics.

1955 July *02d 10h 18m–10h 26m:* CF.—*03d 16h 04–16h 25:* CF Gi.—*04d 15h 56M(?):* CF.—06d 14h 58: Va. –14d 12h 12: Hu.—15d 11h 35–12h 03: (?) El.—15d 12h 20–12h 40: (?) El.—17d 10h 02: IK.—27d 07h 45–07h 50: SM.

1955 August *06d 20h 12m:* Hu.—07d 22h 01 (?): Ap.—*08d 20h 45:* Hu.—*09d 07h 40:* CF.—12d 08h 20–08h 28: SM.—30d 16h 18 (?): Ma.

1955 September *08d 14h 15m–14h 25m (?):* CF.—*20d 14h 45:* Hu. *–27d 16h 30:* Hu.

Ionospheric or solar disturbances without clear geomagnetic effect

None.

Minor disturbances reported by one station only are listed in the De Bilt quarterly circular, but omitted here.

TABLE 2—*Monthly mean values of Ci, Cp, and Ap*

Index	July 1955	Aug. 1955	Sep. 1955
Mean *Ci*	0.43	0.45	0.62
Mean *Cp*	0.40	0.42	0.62
Mean *Ap*	8	9	*BV*13

COMMITTEE ON RAPID VARIATIONS AND EARTH CURRENTS
A. Romañá, Chairman, Observatorio del Ebro, Tortosa, Spain

COMMITTEE ON CHARACTERIZATION OF MAGNETIC DISTURBANCES
J. BARTELS, *Chairman*
University
Göttingen, Germany

J. VELDKAMP
Kon. Nederlandsch Meteorologisch Instituut
De Bilt, Holland

PROVISIONAL SUNSPOT-NUMBERS FOR OCTOBER TO DECEMBER, 1955

(Dependent on observations at Zurich Observatory and its stations at Locarno and Arosa)

Day	Oct.	Nov.	Dec.
1	37	106	99
2	54	92	87
3	58	77	75
4	64	58	86
5	62	51	100
6	60	38	100
7	71	71	84
8	71	84	72
9	79	115	60
10	56	133	74
11	55	156	86
12	61	152	79
13	41	142	71
14	22	132	63
15	7	122	75
16	0	105	76
17	0	95	70
18	0	75	85
19	11	55	89
20	21	60	92
21	31	60	105
22	42	61	85
23	57	63	64
24	86	70	51
25	95	77	53
26	107	81	61
27	98	90	62
28	108	97	65
29	119	95	72
30	124	93	81
31	123		70
Means.....	58.7	90.2	77.2
No. days.....	31	30	31

Mean for quarter: 75.2 (92 days)
Mean for year 1955: 37.9 (365 days)

M. Waldmeier

Swiss Federal Observatory
Zurich, Switzerland

CHELTENHAM THREE-HOUR-RANGE INDICES K FOR OCTOBER TO DECEMBER, 1955

[$K9 = 500\gamma$; scale-values of variometers in γ/mm: $D = 5.4$; $H = 2.4$ (until Dec. 1) and 1.7 thereafter; $Z = 4.3$]

Gr. day	October 1955		Sum	November 1955		Sum	December 1955		Sum
	Values K			Values K			Values K		
1	4333	1132	20	2431	0132	16	3123	3334	22
2	3233	2321	19	3312	2132	17	3333	1011	15
3	4443	2210	20	1110	1111	7	0111	2223	12
4	2333	1103	16	3444	1124	23	3221	1111	12
5	2212	3244	20	3333	1002	15	1100	2123	10
6	5444	2211	23	2110	0010	5	3442	2133	22
7	1112	1104	11	2000	0110	4	3321	1001	11
8	3332	1233	20	1213	1234	17	1220	2243	16
9	1110	1203	9	4332	1111	16	3222	3211	16
10	3234	2331	21	1011	0121	7	1111	3110	9
11	1333	3210	16	2121	0212	11	0001	1101	4
12	0000	0000	0	1144	3331	20	2011	1111	8
13	0011	1012	6	1321	0111	10	0000	1121	5
14	1222	1110	10	0010	2122	8	1010	0001	3
15	0310	0012	7	2344	3333	25	0000	0112	4
16	3121	1111	11	4433	2222	22	2233	2211	16
17	2220	0022	10	2512	1011	13	0111	0201	6
18	1000	0001	2	2443	2542	26	0111	0100	4
19	0110	1122	8	3225	6665	35	0012	1111	7
20	2222	1110	11	5445	4433	32	2430	2110	13
21	0021	1012	7	3432	0000	12	1222	2111	12
22	0012	2221	10	0021	1000	4	0321	1100	8
23	2101	2121	10	0211	1012	8	1200	1000	4
24	0000	0011	2	1142	1112	13	0001	0213	7
25	4355	5444	34	3322	2211	16	3532	2232	22
26	6534	3344	32	2221	0012	10	1123	3233	18
27	2332	1122	16	2112	1112	11	4333	2111	18
28	0232	2201	12	0113	2114	13	0121	1121	9
29	1232	1313	16	2222	1121	13	0000	0111	3
30	1001	2221	9	1311	1011	9	0110	0201	5
31	3332	2244	23				1231	1221	13

Ralph R. Bodle
Observer-in-Charge

Cheltenham Magnetic Observatory
Cheltenham, Maryland, U.S.A.

PRINCIPAL MAGNETIC STORMS

(Advance knowledge of the character of the records at some observatories as regards disturbances)

bservatory Observer- n-Charge)	Green- wich date	Storm-time GMT of begin.	Storm-time GMT of ending[1]	Sudden commencement Type[2]	Amplitudes[3] D	H	Z	C-figure, degree of ac- tivity[4]	Maximal activity on K-scale 0 to 9 Gr. day	Gr. 3-hr. period	K- index	Ranges D	H	Z
(1)	(2)	(3)	(4)	(5)	(6)	(7)	(8)	(9)	(10)	(11)	(12)	(13)	(14)	(15)
	1955	*h m*	*d h*		′	γ	γ					′	γ	γ
lege J. Beers)	Oct. 25	00 ..	27 02	.....	....	....	....	ms	25	5	7	240	1430	840
									26	4	7			
	Nov. 15	06 ..	17 06	.....	....	....	....	ms	15	4,5	6	170	1100	680
									16	4	6			
	Nov. 18	04 ..	21 02	.....	....	....	....	s	19	5	8	580	2770	1590
	Dec. 1	10 ..	2 14	.....	....	....	....	ms	1	5,7	6	140	1070	440
ka L.Skillman)	Oct. 25	00 ..	27 17	.....	....	....	....	s	25	4,5	8	154	1180	530
	Nov. 15	05 ..	17 06	.....	....	....	....	ms	15	4	7	56	468	564
	Nov. 18	04 ..	19 05	.....	....	....	....	ms	18	6,7	6	60	555	394
	Nov. 19	08 52	21 02	.....	....	....	....	s	19	5,6	9	243	2021	1495
	Dec. 1	09 ..	2 12	.....	....	....	....	m	1	5	5	40	258	295
eltenham R. Bodle)	Oct. 5	19 ..	6 17	.....	....	....	....	m	6	1	5	27	90	66
	Oct. 25	00 ..	27 00	.....	....	....	....	ms	26	1	6	34	145	110
	Nov. 19	09 ..	21 08	.....	....	....	....	ms	19	5,6,7	6	36	247	95
	Dec.	None												
cson F. White)	Oct. 25	00 32	26 23	.....	....	....	....	m	25	3,4,5	5	18	102	31
									26	1,2,7	5			
	Nov. 18	01 30	21 10	.....	....	....	....	ms	19	5,6,7	6	21	139	46
	Dec.	None												
n Juan G. Ledig)	Oct. 25	00 31	26 20	.....	....	....	....	m	25	1,6	5	11	105	17
									26	2,7	5			
	Nov. 19	13 19	20 05	s.c.	+1	+23	−9	m	19	5,7,8	6	11	117	37
	Dec.	None												
nolulu L. L. Cleven)	Oct. 7	22 58	8 22	s.c.	0	+25	+13	m	8	3	5	3	80	25
	Nov. 18	18 00	21 01	.....	....	....	....	ms	19	7,8	6	9	140	60
	Dec.	None												
stituto ofísico de lancayo A.Giesecke)	Oct. 7	22 57	8 21	s.c.	+2	+40	−5	m	8	6,7	4	6	212	40
	Oct. 25	00 32	26 22	.....	....	....	....	ms	25	5	6	9	299	48
	Nov. 8	10 25	9 20	.....	....	....	....	ms	8	7	6	7	255	42
	Nov. 14	10 00	16 23	.....	....	....	....	m	16	5,6	5	8	197	40
	Nov. 18	05 21	20 23	.....	....	....	....	s	19	6	9	14	660	80
	Dec. 1	09 00	1 24	.....	....	....	....	ms	1	5,7	6	12	310	42
	Dec. 24	09 20	25 20	.....	....	....	....	m	25	5,6	5	7	175	35
ia L.Burrows)	Oct. 7	22 56	8 10	s.c.	0	+25	−9	m	7	8	5	3	113	23
	Nov. 19	13 20	20 05	s.c.	+1	+42	−15	ms	19	7,8	6	8	146	29
	Dec. 5	22 16	6 11	s.c.	+1	+23	−5	m	5	8	4	3	113	23
rmanus M.van Wijk)	Oct. 5	11 ..	6 18	.....	....	....	....	m	5	7	5	17	68	79
	Oct. 25	00 43	26 23	s.c.	....	....	....	ms	25	7	6	25	145	94
	Oct. 31	12 ..	1 07	.....	....	....	....	m	31	7	5	21	63	80
	Nov. 12	7 ..	12 19	.....	....	....	....	m	12	4,5,6	5	17	91	81
	Nov. 14	19 ..	16 22	.....	....	....	....	m	15	4	5	18	99	50
	Nov. 18	02 ..	.. ..	.....	....	....	....	ms	18	6,7	6	(25)	(164)	(136)
			(*Note:* End merged in succeeding storm)											
	Nov. 19	13 19	21 00	s.c.*	+15	+85	+85	ms	19	5	7	51	200	226
	Dec. 1	08 ..	1 23	.....	....	....	....	m	1	6,7,8	5	20	124	109
	Dec. 24	16 ..	25 21	.....	....	....	....	m	25	5	5	16	91	58

[1]Approximate time of ending of storm construed as the time of cessation of reasonably marked disturbance movements in the ces; more specifically, when the *K*-index measure diminished to 2 or less for a reasonable period.

[2]s.c. = sudden commencement; s.c.* = small initial impulse followed by main impulse (the amplitude in this case is that of the *in impulse only*, neglecting the initial brief pulse); . . . = gradual commencement.

[3]Signs of amplitudes of *D* and *Z* taken algebraically; *D* reckoned positive if towards the east and *Z* reckoned positive if verti- ly downwards.

[4]Storm described by three degrees of activity: *m* for moderate (when *K*-index as great as 5); *ms* for moderately severe (when = 6 or 7); *s* for severe (when *K* = 8 or 9).

PRINCIPAL MAGNETIC STORMS—Concluded

Observatory (Observer-in-Charge)	Greenwich date	Storm-time GMT of begin.	Storm-time GMT of ending[1]	Sudden commencement Type[2]	Amplitudes[3] D	H	Z	C-figure, degree of activity[4]	Maximal activity on K-scale 0 to 9 Gr. day	Gr. 3-hr. period	K-index	Ranges D	H	Z
(1)	(2)	(3)	(4)	(5)	(6)	(7)	(8)	(9)	(10)	(11)	(12)	(13)	(14)	(15)
	1955	h m	d h		′	γ	γ					′	γ	γ
Watheroo	Oct. 25	06 00	26 20	.....	....	....	....	ms	25	6	6	26	108	1
(A.F.Tillott)	Nov. 18	02 ..	21 01	.....	....	....	....	ms	19	5,6	7	29	257	1
	Dec.	None												
Amberley	Sep. 29	15 ..	1 13	.....	....	....	....	m	30	2,3,4,5	5	20	124	
(A.L.Cullington)	Oct. 25	00 ..	27 23	.....	....	....	....	m	25	3,4,5	5	22	137	
									26	1	5			
	Oct. 31	01 ..	1 13	.....	....	....	....	m	31	7,8	5	13	132	
									1	2	5			
	Nov. 12	07 ..	13 08	.....	....	....	....	m	12	3	5	18	86	
	Nov. 18	01 ..	.. ..	.....	....	....	....	m	18	6,7	5	26	131	
		(*Note:* Continued until following storm)												
	Nov. 19	13 20	21 10	s.c.*	+5	+98	−22	ms	19	5	6	30	190	1
	Dec. 1	08 ..	2 14	.....	....	....	....	m	1	7	5	11	164	
	Dec. 5	22 16	7 08	s.c.	−1	+8	+6	m	6	3	5	12	118	
	(*Note:* On Dec. 5, type s.c. in case of *D* and *Z*: s.c.* in case of *H*)													
				Reports added in galley-proof:										
Witteveen	Oct. 5	11 18	6 18	s.c.	−4	+19	0	ms	5	7	7	39	221	
(D.van Sabben)	Oct. 25	00 00	26 24	.....	....	....	....	ms	25	6,7	7			
									26	7	6	44	185	1
	Nov. 15	08 00	17 06	.....	....	....	....	m	15	7	5	27	106	
									16	1,8	5			
	Nov. 18	16 48	18 23	.....	....	....	....	ms	18	6,7	6	34	173	
	Nov. 19	13 19	21 05	s.c.*	−11	+81	−6	ms	19	5	7	66	274	2
	Dec. 1	12 00	2 06	.....	....	....	....	ms	1	7	6	30	127	
	Dec. 26	20 00	27 06	.....	....	....	....	ms	26	8	6	31	180	
Vassouras	July 2	15 04	3 09	.....	....	....	....	m	2	7	5	5	181	
(Lelio I. Gama)	Aug.	None												
	Sep.	None												
	Oct. 7	22 56	8 22	s.c.	+2	36	+9	m	7	8	3	10	86	
	Nov. 19	13 19	20 05	s.c.*	+9	80	+24	m	19	5	5	16	245	
	Dec.	None												
Elisabethville	Oct. 25	01 00	26 24	.....	....	....	....	ms	25	4,5,6	...	8	166	
(A. Alexandre)	Nov. 18	16 00	20 24	.....	....	....	....	s	19	5,6,7,8	...	14	260	
	Dec.	Néant												
Binza	Oct. 7	22 50	8 24	s.c.	−1	+33	−2	m	8	2	...	3	21	
(Ch. Staes)	Nov. 18	09 00	20 05	s.c.	−2	−24	+5	ms	19	6,7	...	7	282	
	Dec.	None												
Toolangi (I.B.	Oct. 7	22 57	..	s.i.	−5	−12	...	...	....	...	...	....	....	....
Everingham)	Oct. 22	13 16	.. ..	s.c.	....	....	....	...	....	...	...	....	....	....
	Oct. 25	01 ..	27 18	.....	....	....	....	ms	25	5	6	23	157	
	Nov. 18	02 ..	20 23	.....	....	....	....	ms	19	5,6	6	32	250	1
	Dec.	None												

REVIEWS AND ABSTRACTS

ROYAL GREENWICH OBSERVATORY: *Sunspot and geomagnetic-storm data derived from Greenwich observations, 1874-1954* (compiled under the direction of Sir Harold Spencer Jones, Sc.D., F.R.S., Astronomer Royal). London, H. M. Stationery Office, special publication additional to the annual Greenwich Observations Series, viii + 106 pp. + 2 app. + 2 diagrams (1955). 30 cm.

The book is noteworthy because of its extended series of sunspots and quantities related to the geomagnetic field. For instance, it contains tables of mean daily areas of sunspots and faculae, including geomagnetic data of ranges in magnetic declination for Greenwich. It also lists umbrae, whole spots, and faculae. Lists are also given of spotless days during the interval from 1874 to 1954.

Another section deals with the mean heliographic latitudes of sunspots (both north and south of the equator) and their corresponding areas, for each year from 1874 to 1954. There are listed also mean latitudes of sunspots for each solar synodic rotation, and a latitude-time curve is given. An attractive illustration presents a butterfly diagram for the heliographic latitudes of sunspots, 1874-1954, together with spot areas and geomagnetic indices.

There is also a catalog of larger sunspots, for which the mean area is in excess of 500 units, and great magnetic storms and small magnetic storms are referred to for this period. Descriptions of these larger sunspots are included.

The next section includes a catalog of great and small geomagnetic storms, 1874–1954, an appendix of great geomagnetic storms recorded at the Royal Observatory, Greenwich, 1840-1874, and an appendix of comparative sunspot and geomagnetic (S_q range) curves, 1841-1950. An interesting Figure illustrates the comparative sunspot and geomagnetic S_q range for the entire period 1841-1950.

Some of the illustrations which the book contains should find their way into future text-books on solar and terrestrial relationships. The entire work represents a document which will be highly valued and warmly welcomed by students of geophysics the world over.

A notable virtue of this publication is that it includes solar and geophysical time-series covering a period of over 100 years.

W. E. SCOTT

LETTERS TO EDITOR

AIRBORNE IONOSPHERIC MEASUREMENTS IN THE NORTH POLE AREA

Abstract

The preliminary results of the subsequent arctic flights by members of the Geophysics Research Directorate and of the 6520th Test Group are presented.

The installation of ionospheric equipment in a high-speed aircraft has proved to be a valuable tool in studying the dynamic behavior of the ionosphere in equatorial and moderate latitudes. For the arctic, however, the measuring technique and equipment are still in the development stage.

The airborne equipment, which has been operated over the North Pole on several occasions in 1954 and 1955, was installed in a four-engine Boeing C-97 strato-cruiser.

(1) *Drift measurements*—With the airplane constantly circling in four-minute turns, the speed of fading of an ionospheric reflection behaves as shown in Figure 1. Under simplifying assumptions, the direction of the drift is marked by the minimum of the curve. The speed V_{drift} follows then from

$$\frac{V_{airplane} + V_{drift}}{V_{airplane} - V_{drift}} = r$$

where $V_{airplane}$ is the ground speed of the aircraft; $r = a/b$ follows from Figure 1. In the derivation of this formula, the normalized average speed of fading, as shown in Figure 1, has been considered to vary linearly with speed difference between airplane and ionospheric pattern; it has been obtained by taking

$$\frac{\sum | \partial(\text{amplitude}) |}{\partial(\text{time})}$$

over a period of 10 seconds, and then normalizing by dividing through the average amplitude. The analysis of Figure 1 then results in a drift of 41 m/sec toward 290°. Another drift measurement at the North Pole on June 2, 1954, 0000 hour UT, with a frequency of 1.4 Mc/sec (*Es*-reflections from 105 km), resulted in 33 m/sec toward 270°.

The actual drift speeds are definitely higher, since this analysis disregards turbulence in the ionosphere and also that the shape of the inhomogeneities may not be circular and may change with time. But the results show that even at the North Pole the inhomogeneities are constant enough during several minutes in order to apply this method. Future measurements will be made with two different speeds of the airplane. It is planned to apply auto-correlation methods for the evaluation.

(2) *Ion density*—The airborne *h'f* records show no principal difference from

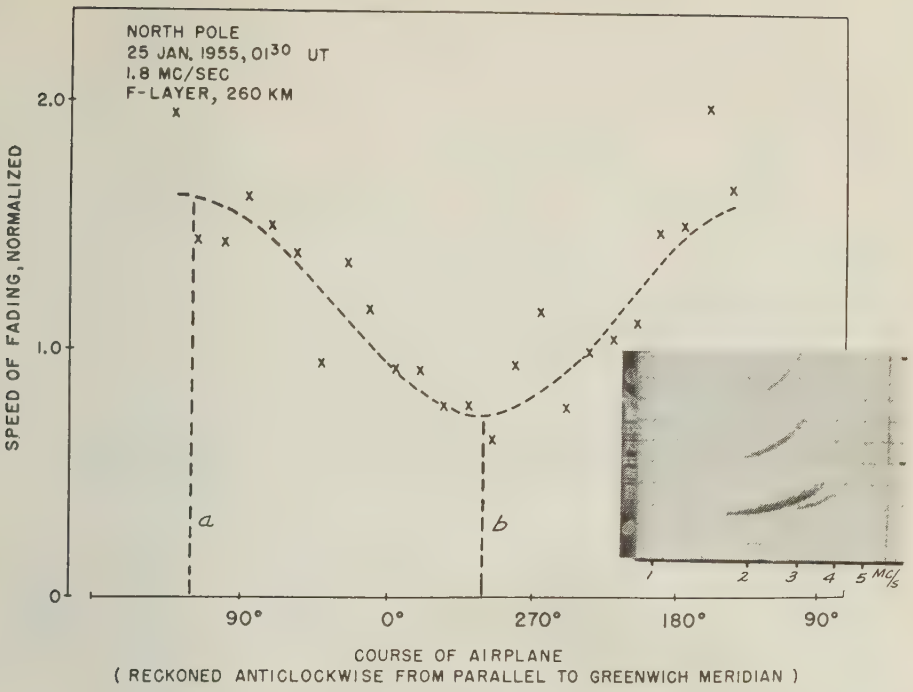

FIG. 1

those of Resolute Bay, Baker Lake, or Point Barrow. The same close correspondence to magnetic activity has been found. Even in January, during a period of low sunspot-number, the ionization at the North Pole has been found at the same level as at Resolute Bay, in the twilight zone 1,000 miles away. In the example given in Figure 2, the position of the aircraft at different times is indicated on the dark areas representing the North Pole area within the Arctic Circle. The critical frequencies of *o*- and *z*-modes (if any) are drawn in, as is the spread,* the frequencies appearing as a scattered tail of the trace.

(3) *Vertical reflections*—The analysis of a large number of *h'f* records reveals that often no traces of vertical reflections from the *F*-layer were present, but that spread of frequencies higher than f_oF or f_zF was (in Fig. 2, all lines are shown without *o* or *z*). This was proved not to be an effect of the airplane antennas. During a magnetic storm, this phenomenon occurred more than 50 per cent of the time. Ray-path geometry suggests a scattering or diffracting layer in the *E*- or *F*1-region with a structure similar to a curtain of half-closed Venetian blinds. Reflecting properties, non-symmetrical with respect to the vertical, already have been deduced by other workers interpreting "down-coming" traces as coming from the front side of traveling inhomogeneities.

(4) The *z-component* has been seen several times (see Fig. 2, 0200 hours). No

*According to a proposal of J. H. Meek, Defence Research Board of Canada.

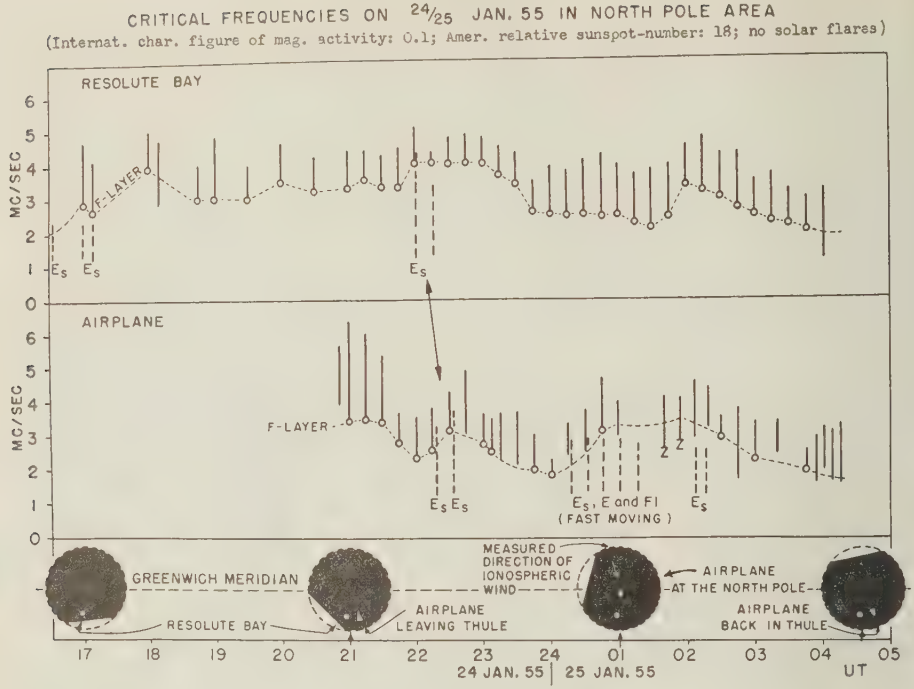

Fig. 2

distinct appearance in the vicinity of the Magnetic Pole could be established. This is expected for a smooth ionosphere.

(5) *Reflections from large virtual heights* of 400 to 800 km and of frequencies up to 20 Mc/sec have been observed on almost all flights, the traces lasting for minutes and traveling. All of them could be interpreted in terms of ray geometry within the already known layers.

(6) *Plans* —The speed of the airplane, faster than most of the irregularities, will be used in order to improve the method under (2), and to prove the interpretations employed under (3) and (5), and to investigate the correlation with aurora phenomena and with the dip of the geomagnetic field. This will contribute to a better knowledge of the strange ray-path geometry and the dynamic behavior of the arctic ionosphere. Furthermore, the construction of an additional logarithmic receiver is initiated, which will make possible continuous records of the ionospheric reflection coefficient by using the reflection from the ground as reference signal.

George J. Gassmann

Air Force Cambridge Research Center,
Bedford, Massachusetts, November 28, 1955
(Received December 7, 1955)

THE "NOSE" WHISTLER—A NEW HIGH-LATITUDE PHENOMENON*†

Whistlers of a new type have been recorded by the Geophysical Institute, at College, Alaska (geomagnetic latitude 65°). Spectrographic analysis of tape recordings of these whistlers has revealed a remarkable property, not readily detectable by ear. Two spectrograms‡ of one such whistler, recorded near local midnight on July 10, 1955, are shown in Figure 1. Each is a plot of amplitude, measured by the

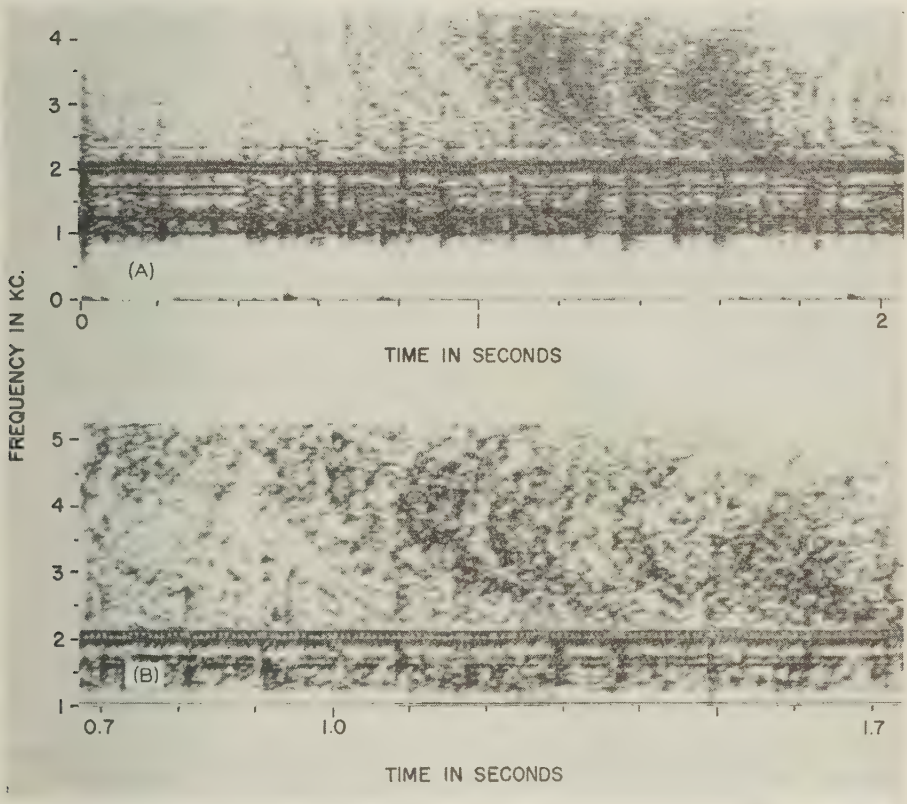

FIG. 1—Spectrograms of a typical nose whistler recorded at College, Alaska, just after local midnight on July 10, 1955: (*A*) Normal tape speed, standard Vibralyzer frequency range; (*B*) one-half normal tape speed, modified frequency range

relative darkness of the display, *vs* frequency and time. Figure 1(*B*) is the same as Figure 1(A), except that the frequency and time ranges have been changed so as to show more of the higher frequencies. To the ear, the sound of this whistler gives

*This research was sponsored by the Electronics Research Directorate of the Air Force Cambridge Research Center.

†Presented at the Fall meeting of URSI, Gainesville, Florida, December 15, 16, 17, 1955.

‡Made with a Vibralyzer, manufactured by the Kay Electric Company, Pine Brook, New Jersey.

the impression of a wide band of noise whose frequency of maximum intensity gradually falls with time, somewhat similar to an ordinary whistler of the "swish" type. The spectrograms clearly show numerous separate traces, each roughly parabolic in shape. They exhibit both rising and falling parts, lasting perhaps 0.1 to 0.2 second, and extending roughly 1500 cps on either side of the starting frequency. Because of the shape, we have chosen to call each trace a "nose" whistler and its starting frequency the "nose" frequency. During a train of such nose whistlers, the nose frequency gradually descends, and in the example shown, starts at about 4500 cps and ends at 3000 cps about 1.5 seconds later.*

A small number of the whistlers observed at College on July 10, 1955, were apparently of the conventional type in that only a descending trace was observed. These were probably produced at lower latitudes. In the records so far available, there is no clear-cut evidence of an impulsive atmospheric which can be definitely associated with any of the trains. This could mean that the source was an impulse located near the conjugate point in the southern hemisphere, or that the source is of some other type as yet unknown.

A possible explanation of the nose whistler has been found with the aid of a new and more general form of Eckersley dispersion law[1] and derived** from the magneto-ionic theory. If the collisional frequency is placed equal to zero and the wave frequency is less than the gyrofrequency, it can readily be shown that the group velocity in the longitudinal extraordinary mode is given by

$$v_g = 2c \frac{(f_L - f)^{3/2}[f^2(f_L - f) + ff_0^2]^{1/2}}{2f^3 - 4f^2 f_L + 2ff_L^2 + f_L f_0^2} \quad \ldots\ldots\ldots\ldots\ldots\ldots (1)$$

where c = velocity of light, f = wave frequency, f_L = gyrofrequency, and f_0 = plasma frequency.

When f_0 is large compared with f and not small compared with f_L, equation (1) can be approximated by

$$v_g = 2c \frac{f^{1/2}(f_L - f)^{3/2}}{f_L f_0} \quad \ldots\ldots\ldots\ldots\ldots\ldots\ldots\ldots (2)$$

It is clear from equation (2) that as f increases the group velocity will first increase, reach a maximum for some value of f between zero and f_L, and then decrease. By differentiating equation (2) with respect to f, it is easily found that v_g is

*At the time of the presentation of this paper, Harold E. Dinger, of the Naval Research Laboratory, reported observing on one occasion at Washington, D. C., a number of unusual whistlers, each showing the properties of a nose whistler. The nose frequencies were about 6 kc.

[1]T. L. Eckersley, Musical atmospherics, Nature, **135**, 104 (1935).

**Work on the exact form of the dispersion law was started at Stanford in August, 1955. The initial purpose was to try to explain certain small but significant departures of the experimental dispersions from the Eckersley law which can be detected in Storey's published data[2] and in certain Stanford data. By a fortunate coincidence, the theoretical result and the first experimental nose whistler spectrograms were obtained at essentially the same time. R. M. Gallet, of the Boulder Laboratories of the National Bureau of Standards, pointed out at about this same time in private discussions that the behavior of the refractive index at frequencies near the gyrofrequency was such that rising tones could be produced by an impulse.

a maximum* when $f = f_L/4$. Now consider the propagation of an electromagnetic impulse through a homogeneous medium under the conditions of equation (2). As the impulse propagates along the magnetic field lines, it becomes dispersed, the energy at $f = f_L/4$ traveling at maximum velocity, while the energy at higher and lower frequencies travels more slowly. Thus, at any point along the path, there would be observed two gliding tones, one rising in frequency and the other falling, and both originating at the nose frequency $f = f_L/4$.

The predicted form of a dispersed impulse is thus similar to the observed nose whistlers, such as the one described above. It is proposed, therefore, that nose whistlers are the result of the dispersion of an impulse, such as that produced by a lightning discharge, which has traveled through ionized regions along lines of the earth's magnetic field. The existence of the nose at these relatively low frequencies implies that a substantial contribution to the total dispersion must occur in the regions of relatively low gyrofrequency near the top of the path.

It is more difficult to explain the occurrence of a train of nose whistlers in which the nose frequency gradually descends. One possibility is that a single impulse excites all of the nose whistlers in a train, each following a different line of the earth's magnetic field. The existence of such discrete paths probably results either from factors in the excitation process or from irregularities in the distribution of ionization. As the length of the field line increases, the time delay becomes greater. The nose frequency drops with increasing time delay because the average gyrofrequency over a line of the earth's field decreases with increasing path length.

Calculations show that for the dipole approximation to the earth's magnetic field and uniform ionization over the path, the nose frequency is about 0.34 times the gyrofrequency at the top of the field line originating at College. If this relation is applied to the example described, the gyrofrequency at the top of the path would have to vary between 13,000 and 8,800 cps. The corresponding geomagnetic latitudes are 60° and 62°. If substantially all the dispersion takes place along the outermost parts of the path, the nose frequency would be about one-fourth of the gyrofrequency at the top of the path. In this case, the corresponding gyrofrequencies would be 18,000 and 12,000 cps. The corresponding geomagnetic latitudes are 58° and 60°. The maximum distance from College would be about 800 km, well within the effective area of a whistler.[2,3]

According to our hypothesis, the usual whistlers observed at middle latitudes are the descending portions of nose whistlers. The nose frequency at Stanford (geomagnetic latitude 44°) is estimated to be somewhere in the range of 30 to 50 kc. Whistlers recorded at Stanford, extending up to 25 kc, show clearly a departure from the Eckersley approximation in the direction predicted by the new theory.†

The nose whistler and the general form of the dispersion law appear to be of

*If f_L is large compared with f, equation (2) reduces to $v_g = 2c\sqrt{ff_L}/f_0$, the form developed by Eckersley and used by Storey, and the maximum in v_g does not appear.

[2]L. R. O. Storey, Phil. Trans. R. Soc., A, **246**, 113 (1953).

[3]J. H. Crary, R. A. Helliwell, and R. F. Chase, Stanford-Seattle whistler observations, J. Geophys. Res., **61**, 35 (1956).

†Additional evidence of such a departure has been obtained by R. M. Gallet from whistlers recorded at Boulder, Colorado.

basic importance in this area of ionospheric research. Since the nose frequency depends primarily on the gyrofrequency, it should be possible to separate the effects of gyrofrequency and plasma frequency on the dispersion and thus obtain more reliable estimates of the ionization density in the outer ionosphere. Investigation of the strength of the earth's magnetic field at great distances from the surface of the earth is now conceivable using this tool. Since the assumed paths of nose whistlers extend from five to six earth radii into space, it may be possible to verify the existence of the "ring current" which is postulated to account for magnetic storms and the aurorae.[4] A fresh approach to the unsolved problems of the dawn chorus and the various combinations of rising and falling whistlers described by Storey[2] and others† is offered by the new dispersion equation.

Acknowledgment—Valuable assistance was rendered by T. F. Bell, who performed the numerical calculations which led to the development of the new dispersion law.

R. A. Helliwell
J. H. Crary
J. H. Pope
R. L. Smith

Radio Propagation Laboratory, Stanford University (R.A.H., J.H.C., and R.L.S.),
Stanford, California, January 23, 1956
Geophysical Institute, University of Alaska (J.H.P.),
College, Alaska

(Received January 27, 1956)

[4]D. F. Martyn, The theory of magnetic storms and auroras, Nature, **167**, 92 (1951).
†Additional references are given by Storey in reference 2.

NOTES

(1) *Automatic ionosphere recorder* –Model C-4 ionosphere recorder is being developed and produced in quantity by Barker and Williamson, Inc., Upper Darby, Pennsylvania, under contract with the U.S. National Bureau of Standards. The C-4 will be used on a world-wide basis to make precise ionospheric measurements as part of the International Geophysical Year (IGY) cooperative program of observations beginning in July 1957 and extending through 1958. The C-4 is a transceiver-type radar set, consisting of a pulse transmitter, pulse receiver, master-clock programming, and display and recording system. These are tracked together as the C-4 sweeps from 1 to 25 megacycles with 50-microsecond pulses at 10 kilowatts peak power. The unit is automatic, requiring attention only for film replacement and servicing. With slight modifications, the C-4 can be used in an oblique-incidence, back-scatter application as a frequency-prediction device in long distance communications. The unit costs $32,500, and includes a generous complement of spare parts to permit prolonged, continuing operations. Deliveries on new orders from other nations will be scheduled to permit IGY participation.

(2) *Research positions in the US-IGY Antarctic program* –Opportunities for physical scientists, engineers, and technicians exist in the Antarctic program planned by the U. S. National Committee for the International Geophysical Year, 1957-58. The U. S. Antarctic program emphasizes the following fields: Aurora and airglow, cosmic rays, geomagnetism, glaciology, gravity, ionospheric physics, meteorology, and seismology. Major geophysical research stations will be established at Little America, Marie Byrd Land, the South Geographic Pole, on the Knox coast, and along the Weddell Sea. Initiation of this program began last year with the site-reconnaissance voyage of the U.S.S. *Atka*. Operation Deepfreeze, currently under way, will establish the Little America station, cache supplies for the interior stations to be set up in the fall of 1956, and explore site possibilities for stations on the Knox coast and the Weddell Sea.

The scientific program will cover slightly over two years from January 1956 to April 1959. Scientists and technicians will leave the United States about November 1, 1956. Positions are open for either the full period of investigations or for the two periods November 1956-April 1958 and November 1957-April 1959. Prior to departure, approximately two months of advance training will be provided in problems of research, instrumentation, and operations in the polar regions. Opportunities are available to candidates at the bachelors, masters, and doctorate levels of training and experience. Scientists, engineers, and technicians, with training in physics, geophysics, electronics, or closely allied areas and interests in the fields of study enumerated above, are invited to address inquiries to the National Academy of Sciences, United States National Committee for the International Geophysical Year, 2101 Constitution Avenue, N.W., Washington 25, D. C.

(3) *Three scientists named to geophysical posts, IGY* –Appointment of three well-known scientists who will direct the United States' participation in the pro-

gram of the International Geophysical Year (IGY) was announced in Washington, D. C., December 21, 1955. Dr. Edward O. Hulburt, retiring director of research at the Naval Research Laboratory in Washington, was named senior scientist of the U.S. National Committee for IGY. The Weather Bureau's director of meteorological research, Dr. Harry Wexler, was appointed chief scientist for the Antarctic program. Albert P. Crary will serve as Dr. Wexler's assistant, and also as chief scientist for glaciology studies in the Antarctic area.

(4) *Satellite panel members named*—Membership of the Technical Panel on the Earth Satellite Program was announced by Dr. Joseph Kaplan, Chairman of the U. S. National Committee for the International Geophysical Year (USNC-IGY). The Panel will have fundamental responsibilities for the development, coordination, and direction of the over-all scientific satellite effort, which is one part of the U. S. International Geophysical Year program. The members and their professional affiliations are as follows: R. W. Porter, Chairman (Consultant, Communication and Control Equipment, Engineering Services Division, General Electric Company); Hugh Odishaw, Secretary (Executive Secretary, U. S. National Committee-IGY, National Academy of Sciences); Joseph Kaplan (Professor of Physics, University of California at Los Angeles; Chairman, U. S. National Committee-IGY, National Academy of Sciences); H. E. Newell, Jr. (Acting Superintendent, Atmosphere and Astrophysics Division, Naval Research Laboratory); W. H. Pickering (Director, Jet Propulsion Laboratory, California Institute of Technology); A. F. Spilhaus (Dean, Institute of Technology, University of Minnesota); Lyman Spitzer, Jr. (Professor of Astronomy, Princeton University); J. A. Van Allen (Professor of Physics and Head of Department of Physics, State University of Iowa); and F. L. Whipple (Director, Smithsonian Astrophysical Observatory; Professor of Astronomy and Chairman of the Department of Astronomy, Harvard University).

(5) *New cosmic-ray neutron monitor*—The National Science Foundation has granted New York University $11,500 to build a cosmic-ray neutron monitor for the International Geophysical Year (IGY). The monitor will be constructed on the NYU campus, and will be installed in the summer of 1956 at Fairbanks, Alaska, in the University of Alaska geophysical observatory. NYU will maintain it throughout the IGY, a period of concerted international study of the earth from July 1957 to December 1958.

(6) *Special issue celebrating the 250th anniversary of Benjamin Franklin*—The January 1956 number of the *Journal of the Franklin Institute* is entitled "Panorama of progress" and honors the 250th anniversary of the birth of Benjamin Franklin, for whom the Franklin Institute was named. Written by distinguished men, the 20 papers presented give a broad picture of the advances made in the physical sciences (both pure and applied), in the social sciences and in economics, since the time when Franklin was born.

(7) *Return of radiosondes requested by USAF Air Weather Service*—The USAF Air Weather Service has appealed to the public for the return of lost weather equipment. Hundreds of times each day, weather stations release radiosonde balloons at points all over the United States. Fastened beneath these balloons are radiosondes, small-sized radio transmitters which signal back to the ground data on temperature, humidity, and pressure at various levels, used to prepare weather forecasts. When the balloon breaks, sometimes at heights above 100,000 feet in the

air, the radiosonde descends to the earth by parachute, at times miles away from the launching site. It is these sets which the weather services would like to recover. Properly repaired, they can be used again, saving the cost of a new instrument. If taken to the nearest post office, the set will be shipped to a repair center without cost to the finder. Cost of a new set is around $35, while the expense of rehabilitating a set is between $6 and $7, including postage.

(8) *Joint fellowship program for research in theoretical and experimental geology*—The Department of Geology and Geophysics at the Massachusetts Institute of Technology and the Geophysical Laboratory of the Carnegie Institution of Washington announced plans for a joint fellowship program for research in theoretical and experimental geology. Its purpose will be to learn more about conditions in the interior of the earth. The research will be fundamental in character. But its new knowledge may in the end, for instance, lead to a better understanding of the causes of earthquakes, conditions in the earth's interior, and possibly the location of deep and now-unknown mineral and oil deposits. This innovation in scientific work and education will be carried on by the award of pre-doctoral fellowships to be known as the Vannevar Bush Fellowships in Earth Sciences, named in honor of Dr. Bush, former Dean and Vice-President of M.I.T. and, more recently, President of the Carnegie Institution of Washington, who retired in December 1955. Under the new program of fellowships, M.I.T. will provide training and guidance in theoretical interpretation, while the Carnegie Institution of Washington will make available its unique experience and facilities in experimental geology, and a generous part of the financial support for the project.

(9) *Geomagnetic activities of the U. S. Coast and Geodetic Survey*—A standard magnetograph was put into routine operation at Fredericksburg Magnetic Observatory in December 1955. Cheltenham Magnetic Observatory is expected to continue recording throughout 1956, giving a full year of simultaneous record at the two sites.

Captain Vera Suvannooss of Thailand has been studying the methods and procedures of the Coast and Geodetic Survey in office and field work in geomagnetism.

Captain Elliott B. Roberts, Chief of the Geophysics Division, attended the third meeting of CSAGI (Special Committee for the International Geophysical Year) in Brussels, Belgium, as a member of the U. S. National Committee, IGY.

(10) *Magnetic observations on Fletcher's Ice Island in the Arctic Ocean*—Observations of magnetic declination and horizontal intensity were made during 1955 on Fletcher's Ice Island T-3 in the Arctic Ocean by scientists from the Geophysical Research Directorate, U. S. Air Force.

(11) *Spring meeting of URSI*—The spring meeting of the International Scientific Radio Union (URSI) is scheduled to be held at the National Bureau of Standards, Washington, D.C., on April 30, May 1, 2, and 3, 1956. The co-sponsors this year will include the IRE Professional Groups on Antennas and Propagation, and on Microwave Theory and Techniques. A combined technical session of interest to all participants is scheduled for the morning of May 1, to be followed by one or more sessions in each of the following fields: Commission 1, on radio measurements and standards; Commission 2, on radio and troposphere; Commission 3, ionospheric radio; Commission 4, on radio noise of terrestrial origin; Commission 5,

on radio astronomy; Commission 6, on radio waves and circuits; and Commission 7, on radio electronics.

(12) *Personalia*—Following the death on November 7, 1955, of Mrs. Fleming, in Nashville, Tennessee, Dr. *John A. Fleming*, Honorary Editor of this Journal and retired Director of the Department of Terrestrial Magnetism, Carnegie Institution of Washington, returned to Washington, D. C., the latter part of December 1955. He is now residing at the Cosmos Club, 2121 Massachusetts Avenue, N.W., Washington 8, D. C. Dr. Fleming, well-known both nationally and internationally for his scientific work, is also honorary president of the American Geophysical Union.

Recognizing the increasing need for water resources, the Society of Exploration Geophysicists appointed *Victor Vacquier*, authority on terrestrial magnetism and professor of geophysics at the New Mexico Institute of Mining and Technology, to the post of distinguished lecturer. Storage underground of water is largely confined to certain receptive geological formations. "Geophysical prospecting by induced electrical polarization," a technique developed specifically for location of ground water, was the subject of Prof. Vacquier's tour in January 1956 throughout the western United States and Canada.

Dr. *George Gamow*, well-known theoretical physicist of George Washington University, Washington, D. C., has been granted university leave for the spring term to work with Convair (division of the General Dynamics Corporation) in San Diego, California.

The Optical Society of America, at its Pittsburgh meeting in October 1955, awarded the Frederic Ives Medal for distinguished work in optics to Dr. *Edward O. Hulburt*, former director of research, Naval Research Laboratory, and now senior scientist of the U. S. National Committee for IGY.

Ronald N. Bracewell has been appointed associate professor of electrical engineering at Stanford University, California. He was a research officer for a number of years with the Commonwealth Scientific and Industrial Research Organization at Sydney, Australia; last year he served as a visiting faculty member at the University of California.

Through arrangements with the Exchange of Persons Service of UNESCO and the Institute of International Education, Sr. *Augusto Eduardo Llano Eck* arrived in the United States in December 1955, for studies during 1956 in geomagnetism at the Department of Terrestrial Magnetism, Carnegie Institution of Washington, the U. S. Coast and Geodetic Survey, and possibly at some Washington university. On completion of his studies, Sr. Llano will be responsible for the work in geomagnetism to be undertaken by Chile during the International Geophysical Year 1957-58 and also for the training of personnel in the field.

We regret to record the death on February 15, 1956, of Rev. *James B. Macelwane*, S. J., at the age of 73. A seismologist of world fame, he established at St. Louis University the first Department of Geophysics in the Western Hemisphere. He also organized an American network of seismograph stations for the study of earthquakes throughout the world. His death came at a time when he was serving as President of the American Geophysical Union and while engaged in United States activities in connection with the International Geophysical Year, 1957-58.

LIST OF RECENT PUBLICATIONS

By W. E. Scott

Department of Terrestrial Magnetism,
Carnegie Institution of Washington,
Washington 15, D. C.

(Received January 5, 1956)

A—*Terrestrial Magnetism*

Amberley Observatory. Magnetic results for 1953. Wellington, R. E. Owen, Govt. Printer, 58 pp. (1955). 25 cm. [Issued under the authority of the Hon. R. M. Algie, Minister of Scientific and Industrial Research.]

Bartels, J., and J. Veldkamp. Geomagnetic indices *K* and *C*, 1954. Internat. Union Geod. Geophys., Assoc. Terr. Mag. and Aeronomy, Bull, No. 12i, 116 pp. (1955). 24 cm.

Bartels, J., A. Romañá, and J. Veldkamp. International data on magnetic disturbances, second quarter, 1955. J. Geophys. Res., **60**, No. 4, 525-527 (1955).

Bullard, E. The stability of a homopolar dynamo. Proc. Cambridge Phil. Soc., **51**, Pt. 4, 744-760 (1955).

Burkhart, K., et E. Selzer. Analyse de la variation de forme sinusoidale zur la déclinaison magnétique du 11 avril 1954. Ann. Géophys., **11**, No. 3, 353-368 (1955).

Burmeister, F. Erdmagnetische Messungen am Bodensee. München, D. Geodätische Forschungsinst., Reihe B (Angew. Geodäsie), 8, Heft 8, 9 pp. + isogonic, isoclinic, and iso-dynamic charts, epoch 1955.0 (1955). 30 cm.

Ferraro, V. C. A. The origin of magnetic storms and aurorae. Ann. Géophys., **11**, No. 3, 284-304 (1955).

Gerard, V. B., and J. A. Lawrie. Aeromagnetic surveys in New Zealand, 1949–1952. Wellington, R. E. Owen, Govt. Printer, Geophys. Mem. No. 3, 20 pp. + maps and profile sheets (1955). 28 cm. [Issued under the authority of the Hon. R. M. Algie, Minister of Scientific and Industrial Research.]

Greenwich, Royal Observatory. Sunspot and geomagnetic-storm data derived from Greenwich observations. London, H. M. Stationery Office, viii + 106 pp. + 2 app. + 2 diagrams (1955). 30 cm. [Reviewed in this issue.]

Greenwich Royal Observatory. Results of the magnetic and meteorological observations made at the Abinger Magnetic Station, Surrey, and the Royal Observatory, Greenwich, respectively, in the year 1942. London, H. M. Stationery Office, xx + 87 (1955). 30 cm.

Greenwich Royal Observatory. Results of the magnetic and meteorological observations made at the Abinger Magnetic Station. Surrey, and the Royal Observatory, Greenwich, respectively, in the year 1943. London, H. M. Stationery Office, xx + 87 (1955). 30 cm.

Greenwich Royal Observatory. Results of the magnetic and meteorological observations made at the Abinger Magnetic Station, Surrey, and the Royal Observatory, Greenwich, respectively, in the year 1944. London, H. M. Stationery Office, xxi + 85 (1955). 30 cm.

Greenwich Royal Observatory. Results of the magnetic and meteorological observations made at the Abinger Magnetic Station, Surrey, and the Royal Observatory, Greenwich, respectively, in the year 1946. London, H. M. Stationery Office, xx + 95 (1955). 30 cm.

Kakioka Magnetic Observatory. Report of the Kakioka Magnetic Observatory, Geomagnetism, 1944, 1945. Kakioka, No. 20, 109 pp. (1955). 30 cm. [Contains hourly values of magnetic elements at Kakioka for 1944 and 1945.]

Kawabata, K. The motion of the ionized cloud in the magnetic field and its application to the escape of the corpuscular stream from the sun. Pub. Astr. Soc. Japan, **7**, No. 1, 40-47 (1955). [Reprint No. 120, Tokyo Astronomical Observatory.]

Knopoff, L. The interaction between elastic wave motions and a magnetic field in electrical conductors. J. Geophys. Res., **60**, No. 4, 441-456 (1955).

Leighton, H. I., and D. E. Billings. Solar H_α filaments and geomagnetic disturbances. J. Atmos. Terr. Phys., **7**, No. 6, 349-350 (1955). [Research note.]

Mauritius, Colony of. Annual report of the Observatory Department for the year 1954. Port Louis, J. E. Félix, Govt. Printer, No. 17, 14 pp. (May 1955). 25 cm. [Contains mean values of the magnetic elements for 1954 derived from eye observations.]

McDonald, K. L. Geomagnetic secular variation at the core-mantle boundary. J. Geophys. Res., **60**, No. 4, 377-388 (1955).

Meek, J. H., and F. S. Hector. A recording magnetic variometer. Can. J. Phys., **33**, No. 7 364-368 (1955).

Murphy, T. A vertical force magnetic survey of the Counties Roscommon, Longford, Westmeath and Meath with parts of the adjacent Counties of Galway, Cavan, Louth, and Dublin. Dublin Institute for Advanced Studies, Geophys. Bull. No. 11, 14 pp. (Jan. 1955). 28 cm.

Nagata, T., and S. Abe. Notes on the distribution of SC* in high latitudes. Rep. Ionosphere Res. Japan, **9**, No. 1 , 39-44 (1955).

Néel, L. Some theoretical aspects of rock-magnetism. Adv. Phys., **4**, No. 14, 191-243 (1955).

Nicholls, G. D. The mineralogy of rock magnetism. Adv. Phys., **4**, No. 14, 113-190 (1955).

Nicholson, S. B., and O. R. Wulf. The diurnal variation of irregular geomagnetic fluctuations. J. Geophys. Res., **60**, No. 4, 389-394 (1955).

Palmer, T. M. A battery-operated magnetometer. Commonwealth of Australia, Commonwealth Scientific and Industrial Research Organization, reprint from "Proceedings of Symposium on Precision Electrical Measurements," **1**, No. 9, 11 pp. (Nov. 1954).

Runcorn, S. K. Rock magnetism—geophysical aspects. Adv. Phys., **4**, No. 14, 244-291 (1955).

Tromsö, Auroral Observatory. Observations 1953. Bergen, Norske Inst. Kosmisk Fysikk, No. 37, 31 pp. (1955). 31 cm. [Contains results of magnetic and ionospheric observations for the year 1953, at Tromsö.]

Uyeda, S. Magnetic interaction between ferromagnetic materials contained in rocks. Kyoto, J. Geomag. Geoelectr., **7**, Nos. 1-2, 9-36 (1955).

Waters, G. S. A measurement of the earth's magnetic field by nuclear induction. Nature, **176**, 691 (Oct. 8, 1955). [Letter to Editor.]

B—*Terrestrial Electricity*

Fedele, D., e O. Vittori. Sonda dinamica per la misura del campo ellettrico terrestre. Rev. Met. Aer., Roma, **15**, No. 1, 21-24 (1955). [In Italian, with English, French, and German abstracts.]

Gandolfo, S. Sul regime di variazione diurna del potenziale del campo elettrico atmosferico normal, a Messina. Ann. Geof., Roma, **8**, No. 3, 315-324 (1955).

Swann, W. F. G. The present status of atmospheric electricity. J. Frank. Inst., **260**, No. 4, 283-294 (1955). [An address given at the Conference on Atmospheric Electricity held at Wentworth-by-the-Sea, Portsmouth, New Hampshire, May 19-21, 1954.]

Uchikawa, K., and G. Kondo. Measurements of the atmospheric electricity with captive balloon. J. Met. Soc. Japan, **33**, No. 3, 124-132 (1955). [In English.]

C—*Cosmic Rays*

Barker, P. R. Cosmic-ray electrons near sea level and at mountain altitudes. Phys. Rev., **100**, No. 3, 860-869 (1955).

Carmichael, H., and J. F. Steljes. Cosmic-ray ionization bursts in an unshielded 8-inch pressurized sphere at sea level. Phys. Rev., **99**, No. 5, 1542-1550 (1955).

Harris, F. B., and I. Escobar V. East-west asymmetry of positive and negative mesons at the geomagnetic equator. Phys. Rev., **100**, No. 1, 255-268 (1955).

Meyer, P., and J. A. Simpson. Changes in the low-energy particle cutoff and primary spectrum of cosmic radiation. Phys. Rev., **99**, No. 5, 1517-1523 (1955).

Miyazaki, Y., and M. Wada. Eleven year variation of cosmic-ray disturbance and its relation to solar and geomagnetic activities. Kyoto, J. Geomag. Geoelectr., 7, Nos. 1-2, 1-8 (1955).

Nagashima, K. The diurnal variation of cosmic rays. Kyoto, J. Geomag. Geoelectr., 7, Nos. 1-2, 51-68 (1955).

Sarabhai, V., U. D. Desai, and D. Venkatesan. Solar influence on the anisotropy of primary cosmic radiation. I. Studies at low latitudes. Phys. Rev., 99, No. 5, 1490-1502 (1955).

Simpson, J. A. The cosmic radiation and solar-terrestrial relationships. Ann. Géophys., 11, No. 3, 305-329 (1955).

Soberman, R. K., A. Beiser, and S. A. Korff. Variation of the position of the cosmic-ray neutron intensity maximum with geomagnetic latitude. Phys. Rev., 100, No. 3, 859-860 (1955).

Trumpy, B. On the correlation between the intensity of different components of cosmic rays, the meteorological conditions and magnetic storms. Universitetet i Bergen, Arbok 1954. Naturv. rekke No. 2, 19 pp. (Sept. 1955). 25 cm.

Van Heerden, I. J., and T. Thambyahpillai. The 27-day recurrence tendency of cosmic ray intensity. Phil. Mag., 46, No. 382, 1238-1251 (1955).

Venkatesan, D., and T. S. G. Shastry. Effect of lunar atmospheric tide on the meson intensity at Kodaikanal. Proc. Indian Acad. Sci., 42, No. 4, Sec. A, 204-214 (1955).

D—*Upper Air Research*

Abel, W. G., J. T. deBettencourt, J. H. Chisholm, and J. F. Roche. Investigations of scattering and multipath properties of ionospheric propagation at radio frequencies exceeding the MUF. Proc. Inst. Radio Eng., 43, No. 10, 1255-1268 (1955). [Special issue—Scatter Propagation.]

Aiya, S. V., and K. R. Phadke. Atmospheric noise interference to broadcasting in the 3-Mc/s band at Poona. J. Atmos. Terr. Phys., 7, Nos. 4/5, 254-277 (1955).

Akasofu, S. Geomagnetic control to the diurnal variation of the $F2$ layer on the temperate latitude. Sci. Rep. Tôhoku Univ., Ser. 5, Geophysics, 7, No. 2, 45-50 (1955).

Appleton, E. V., A. J. Lyon, and A. G. Pritchard. The detection of S_q current system in ionospheric radio sounding. J. Atmos. Terr. Phys., 7, Nos. 4/5, 292-295 (1955). [Research note.]

Appleton, E., A. J. Lyon, and A. G. Turnbull. Distortion of the E layer of the ionosphere by electrical currents flowing in it. Nature, 176, 897-899 (Nov. 12, 1955).

Bailey, D. K., R. Bateman, and R. C. Kirby. Radio transmission at VHF by scattering and other processes in the lower ionosphere. Proc. Inst. Radio Eng., 43, No. 10, 1181–1230 (1955). [Special issue—Scatter Propagation.]

Banerji, R. B. Heights of irregularities giving rise to the fading of 150-kc waves. J. Geophys. Res., 60, No. 4, 431-439 (1955).

Barber, D. R. Changes in brightness, polarization, and colour of the zenith day sky accompanying geomagnetic activity. J. Atmos. Terr. Phys., 7, No. 3, 170-172 (1955). [Research note.]

Bates, D. R. Theory of the auroral spectrum. Ann. Géophys., 11, No. 3, 253-278 (1955).

Bennington, T. W. Observations of the effects of ionospheric storms over a North Atlantic circuit. J. Atmos. Terr. Phys., 7, Nos. 4/5, 235-243 (1955).

Beynon, W. J. G. Solar eclipses and the ionosphere. Nature, 176, 947-948 (Nov. 19, 1955).

Booker, H. G. On the level at which fading is imposed on waves reflected vertically from the ionosphere. J. Atmos. Terr. Phys., 7, No. 6, 343-344 (1955). [Research note.]

Branscomb, L. M., and S. J. Smith. Negative oxygen ions in the upper atmosphere. The affinity and radiative attachment coefficient of atomic oxygen. Trans. Amer. Geophys. Union, 36, No. 5, 755-758 (1955).

Bullington, K. Characteristics of beyond-the-horizon radio transmission. Proc. Inst. Radio Eng., 43, No. 10, 1175-1180 (1955). [Special issue—Scatter Propagation.]

Chamberlain, J. W. Auroral rays as electric-discharge phenomena. Astroph. J., 122, No. 2, 349-350 (1955). [Note.]

Court, G. W. G. Ionospheric wind determination from spaced radio receiver fading records. J. Atmos. Terr. Phys., 7, No. 6, 333-340 (1955).

Davids, N., and R. W. Parkinson. Wave solutions for critical and near-critical coupling conditions in the ionosphere. J. Atmos. Terr. Phys., 7, Nos. 4/5, 173-202 (1955).

Dungey, J. W., and A. J. Willson. Viscosity in the *F* region. J. Geophys. Res., **60**, No. 4, 521-523 (1955).

Fan, C. Y. Is helium a component of auroral particles? Astroph. J., **122**, No. 2, 350-351 (1955). [Note.]

Fejer, J. A. The interaction of pulsed radio waves in the ionosphere. J. Atmos. Terr. Phys., **7**, No. 6, 322-332 (1955).

Gallet, R. M. Aerodynamical mechanisms producing electronic density fluctuations in turbulent ionized layers. Proc. Inst. Radio Eng., **43**, No. 10, 1240-1252 (1955). [Special issue—Scatter Propagation.]

Groves, G. V. Geometrical theory of sound propagation in the atmosphere. J. Atmos. Terr. Phys., **7**, No. 3, 113-127 (1955).

Gush, H. P., and A. Vallance Jones. Infrared spectrum of the night sky from 1.0μ to 2.0μ. J. Atmos. Terr. Phys., **7**, Nos. 4/5, 285-291 (1955).

Hirono, M. Part IV. Effect of gravity and ionization pressure gradient on the vertical drift in the *F*2 region. Rep. Ionosphere Res. Japan, **9**, No. 2, 95-104 (1955).

Hirono, M., and H. Maeda. Part III. Characteristics of the *F*2 layer on the magnetic equator. Rep. Ionosphere Res. Japan, **9**, No. 2, 86-94 (1955).

Hoffman, W. C. A theoretical model for high-frequency backscatter from the sea surface via the ionosphere. J. Atmos. Terr. Phys., **7**, Nos. 4/5, 278-284 (1955).

Hulbert, E. O. Advances in the physics of the upper air since 1950. Washington, D. C., Naval Research Laboratory, NRL Rep. No. 4600, ii + 33 pp. (Oct. 25, 1955). 27 cm.

Hunaerts, J., and M. Nicolet. Interpretation of ionospheric results during eclipses. J. Geophys. Res., **60**, No. 4, 537-538 (1955). [Letter to Editor.]

Hunten, D. M. Some photometric observations of auroral spectra. J. Atmos. Terr. Phys., **7**, No. 3, 141-151 (1955).

International Scientific Radio Union, Commission III on Ionospheric Radio. Proceedings of the XIth General Assembly held in The Hague from August 23rd to September 2nd, 1954. Secretary General of U. R. S. I., Brussels, Vol. X, Pt. 3, 194 pp. (1954). 25 cm. [This publication is available from the General Secretariat of the U. R. S. I., 42 Rue des Minimes, Brussels, Belgium, at the following price: 200 Belgian francs, or £1.90, or $4.00 U.S., postage included.]

Johnson, C. Y., and J. P. Heppner. Night-time measurement of positive and negative ion composition to 120 km by rocket-borne spectrometer. J. Geophys. Res., **60**, No. 4, 533 (1955). [Letter to Editor.]

Jursa, A. S., F. J. LeBlanc, and Y. Tanaka. Results of a recent attempt to record the solar spectrum in the region of 900-3000A. J. Optical Soc. Amer., **45**, No. 12, 1085-1086 (1955). [Letter to Editor.]

Kaiser, T. R. (Ed.). Meteors. London, Pergamon Press, Ltd., Special supplement (Vol. II) to the J. Atmos. Terr. Phys., 204 pp. (1955). 25 cm. [Papers in this volume were presented at a symposium on meteor physics, held at Jodrell Bank Experimental Station, in July 1954.]

Kaiser, T. R., and K. Bullough. Radio echoes from aurorae. Ann. Géophys., **11**, No. 3, 279-283 (1955).

Kaplan, J., and H. Odishaw. Satellite program. Science, **122**, 1003-1005 (Nov. 25, 1955).

Lepechinsky, D. L'influence sur les enregistrements de sondages ionosphériques de la couche *E*, du niveau de séparation des régions de propagation quasi longitudinale (*Q.L.*) et quasi transversale (*Q.T.*). Paris, C.-R. Acad. sci., **241**, No. 14, 897-900 (1955).

Lowan, A. N. On the cooling of the upper atmosphere after sunset. J. Geophys. Res., **60**, No. 4, 421-429 (1955).

Maeda, H. Daily variations of the electrical conductivity of the upper atmosphere as deduced from the daily variations of geomagnetism. Part I. Equatorial zone. Rep. Ionosphere Res. Japan, **9**, No. 3, 148-165 (1955).

Maeda, K. Part II. Theoretical study on the geomagnetic distortion in the *F*2 layer. Rep. Ionosphere Res. Japan, **9**, No. 2, 71-85 (1955).

Mange, P. W. Neutral constituent molecular diffusion in the high atmosphere: The calcium distribution. Pennsylvania State University, Ionosphere Res. Lab., Sci. Rep. No. 77, 49 pp., mim. (Aug. 15, 1955). 28 cm.

Minnis, C. M. Brightening of the solar limb in the far ultra-violet. Nature, **176**, 652-653 (Oct. 1, 1955).

Minnis, C. M. A new index of solar activity based on ionospheric measurements. J. Atmos. Terr. Phys., **7**, No. 6, 310-321 (1955).

Mitra, S. N., and R. B. L. Srivastava. Analysis of sky-wave field intensity—Parts I and II. Indian J. Phys., **29**, and Proc. Indian Assoc. Cultivation of Science, **38**, No. 4, 167-178, and No. 5, 227-242 (1955).

Miya, K., and S. Kanaya. Radio propagation prediction considering scattering wave on the earth's surface. Rep. Ionosphere Res. Japan, **9**, No. 1, 1-15 (1955).

Newell, H. E., Jr. The satellite project. Sci. Amer., **193**, No. 6, 29-33 (1955).

Nicolet, M. The aeronomic problem of nitrogen oxides. J. Atmos. Terr. Phys., **7**, No. 3, 152-169 (1955).

Nicolet. M. Nitrogen oxides and the airglow. J. Atmos. Terr. Phys., **7**, No. 6, 297-309 (1955).

Obayashi, T. Movements of irregularities in the *E*-region. Rep. Ionosphere Res. Japan, **9**, No. 2, 105-113 (1955).

Omholt, A., and L. Harang. Measurements of the mean lifetime of the metastable ^1S-state of the oxygen atom in the upper atmosphere during auroral displays. J. Atmos, Terr. Phys., **7**, Nos. 4/5, 247-253 (1955).

Omholt, A. The recombination coefficient in the *E*-layer during aurorae. J. Atmos. Terr. Phys., **7**, No. 6, 345-346 (1955). [Research note.]

Paetzold, H. K. New experimental and theoretical investigations on the atmospheric ozone layer. J. Atmos. Terr. Phys., **7**, No. 3, 128-140 (1955).

Parkinson, R. W. The night-time lower ionosphere as deduced from a theoretical and experimental investigation of coupling phenomena at 150 kc/sec. J. Atmos. Terr. Phys., **7**, Nos. 4/5, 203-234 (1955).

Peterson, A. M., O. G. Villard, Jr., R. L. Leadabrand, and P. B. Gallagher. Regularly-observable aspect-sensitive radio reflections from ionization aligned with the earth's magnetic field and located within the ionospheric layers at middle latitudes. J. Geophys. Res., **60**, No. 4, 497-512 (1955).

Piddington, J. H. The four possible waves in a magneto-ionic medium. Phil. Mag., **46**, No. 381, 1037-1050 (1955).

Piggott, W. R. On the variation of ionospheric absorption at different stations. J. Atmos. Terr. Phys., **7**, Nos. 4/5, 244-246 (1955).

Piggott, W. R. The measurement of normal *E*-layer critical frequencies at night. J. Atmos. Terr. Phys., **7**, No. 6, 341-342 (1955).

Rawer, K. Some remarks concerning ionospheric absorption-work. J. Geophys. Res., **60**, No. 4, 534-535 (1955). [Letter to Editor.]

Regener, V. H. Recordings of the zodiacal light. Astroph. J., **122**, No. 3, 520-529 (1955).

Roach, F. E., and A. B. Meinel. The height of the nightglow by the van Rhijn method. Astroph. J., **122**, No. 3, 530-553 (1955).

Roach, F. E., and A. B. Meinel.Nightglow heights: A reinterpretation of old data. Astroph. J., **122**, No. 3, 554-558 (1955).

Ross, L. W. Accuracy of solar-flare observations. J. Atmos. Terr. Phys., **7**, No. 6, 344-345 (1955). [Research note.]

Roy, R., and J. K. D. Verma. Polarization of electromagnetic waves for vertical propagation in the ionosphere. J. Geophys. Res., **60**, No. 4, 457-482 (1955).

Sen, H. K., and M. L. White. Thermal and gravitational excitation of atmospheric oscillations. J. Geophys. Res., **60**, No. 4, 483-495 (1955).

Shain, C. A. Changes in the absorption of cosmic noise observed during two ionospheric disturbances. J. Atmos. Terr. Phys., **7**, No. 6, 347-348 (1955). [Research note.]

Staras, H. Forward scattering of radio waves by anisotropic turbulence. Proc. Inst. Radio Eng., **43**, No. 10, 1374-1380 (1955). [Special issue—Scatter Propagation.]

Stoffregen, W. Variation of *fEs* during solar eclipses. Nature, **176**, 610 (Sept. 24, 1955). [Letter to Editor.]

Sulzer, P. G. Sweep-frequency pulse-transmission measurements over a 2400-km path. J. Geophys. Res., **60**, No. 4, 411-420 (1955).

Thomas, J. A., and R. W. E. McNicol. Automatic recording of the direction of arrival of radio waves reflected from the ionosphere. Proc. Inst. Elec. Eng., B, **102**, No. 6, 793-799 (1955).

Trolese, L. G. Characteristics of tropospheric scattered fields. Proc. Inst. Radio Eng., **43**, No. 10, 1300-1305 (1955). [Special issue—Scatter Propagation.]

Villard, O. G., Jr., V. R. Eshleman, L. A. Manning, and A. M. Peterson. The role of meteors in extended-range VHF propagation. Proc. Inst. Radio Eng., **43**, No. 10, 1473-1481 (1955). [Special issue—Scatter Propagation.]

Villars, F., and V. F. Weisskopf. On the scattering of radio waves by turbulent fluctuations of the atmosphere. Proc. Inst. Radio Eng., **43**, No. 10, 1232-1239 (1955). [Special issue—Scatter Propagation.]

Watanabe, K., F. F. Marmo, and J. Pressman. Formation of the lower ionosphere. J. Geophys. Res., **60**, No. 4, 513-519 (1955).

White, M. L. Extension of the Sen-White paper on atmospheric oscillations. J. Geophys. Res., **60**, No. 4, 531-532 (1955). [Letter to Editor.]

Wieder, B. Some results of a sweep-frequency propagation experiment over an 1150-km east-west path. J. Geophys. Res., **60**, No. 4, 395-409 (1955).

Yonezawa, T. A consideration of the mechanism of electron removal in the $F2$ layer of the ionosphere. II. Rep. Ionosphere Res. Japan, **9**, No. 1, 17-37 (1955).

E—*Radio Astronomy*

Bracewell, R. N. A proposal for a microwave spectroheliograph. Stanford University, Radio Propagation Lab., 19 pp., mim. (Sept. 15, 1955). 28 cm.

Bracewell, R. N. Chord construction for correcting aerial smoothing. Aust. J. Phys., **8**, No. 2, 200-205 (1955).

Budějický, J. Observations of the partial eclipse of the sun on June 30th, 1954, by means of a radio telescope. Prague, Bull. Astron. Inst. Czechosl., **6**, No. 5, 97-100 (1955).

Covington, A. E., W. J. Medd, G. A. Harvey, and N. W. Broten. Radio brightness distribution of the sun at a wave-length of 10.7 centimeters, June 30, 1954. J. R. Astr. Soc. Can., **49**, No. 6, 235-247 (1955).

Gordy, W., S. J. Ditto, J. H. Wyman and R. S. Anderson. Three-millimeter wave radiation from the sun. Phys. Rev., **99**, No. 6, 1905 (1955). [Letter to Editor.]

Hagen, J. P., A. E. Lilley, and E. F. McClain. Absorption of 21-cm radiation by interstellar hydrogen. Astroph. J., **122**, No. 3, 361-375 (1955).

Hartz, T. R. Radio star scintillations and the ionosphere. Can. J. Phys., **33**, No. 8, 476-482 (1955).

Hatanaka, T. The Faraday effect in the earth's ionosphere with special reference to polarization measurements of solar radio emission. Cornell University, School of Electrical Engineering, Sci. Rep. No. 5, 18 pp. (Aug. 30, 1955). 28 cm.

Kraus, J. D. A preliminary study of the magnitude distribution of celestial radio sources. Astr. J., **60**, No. 10, 398-400 (1955).

McClain, E. F. An approximate distance determination for radio source Sagittarius A. Astroph. J., **122**, No. 3, 376-389 (1955).

Mills, B. Y. The observation and interpretation of radio emission from some bright galaxies. Aust. J. Phys., **8**, No. 3, 368-389 (1955).

Pawsey, J. L., and R. N. Bracewell. Radio astronomy. Oxford, Clarendon Press, x + 361 + 23 pls. (1955). 24 cm. [International monographs on radio.]

Ryle, M. Radio stars and their cosmological significance. Observatory, **75**, No. 887, 137-147 (1955).

Shain, C. A. Location on Jupiter of a source of radio noise. Nature, **176**, 836-837 (Oct. 29, 1955). [Letter to Editor.]

F—*Earth's Crust and Interior*

Ahrens, L. H. Implications of the Rhodesia age pattern. Geochim. et Cosmochim. Acta, **8**, Nos. 1/2, 1-15 (1955).

Buddington, A. F., J. Fahey, and A. Vlisidis. Thermometric and petrogenetic significance of titaniferous magnetite. Amer. J. Sci., **253**, No. 9, 497-532 (1955).

Bullard, E. C. Discussion of "The earth's core" by S. K. Runcorn. Trans. Amer. Geophys. Union, **36**, No. 3, 491 (1955).

Manley, H., and D. J. Burdon. The thermo-magnetic properties and history of some Plutonic rocks from the Leinster Granite, Ireland. Kyoto, J. Geomag. Geoelectr., **7**, Nos. 1-2, 37-50 (1955).

Shillibeer, H. A., and R. D. Russell. The argon-40 content of the atmosphere and the age of the earth. Geochim. et Cosmochim. Acta, **8**, Nos. 1/2, 16-21 (1955).

Verhoogen, J. Thermal expansion of solids and the temperature at the boundary of the earth's core. Trans. Amer. Geophys. Union. **36**, No. 5, 866-874 (1955).

G—*Miscellaneous*

Arriaga, N. Relations between solar activity and the center of gravity of the planetary system. J. Geophys. Res., **60**, No. 4, 535-536 (1955). [Letter to Editor.]

Dauvillier, A. Cosmologie et chimie (L'origine des éléments chimiques et l'évolution de l'Univers). Paris, Presses Universitaires de France, 215 pp. + 9 pls. (1955). 19 cm.

Jager, C. de. The ultra-violet and X-ray spectrum of the sun. Ann. Géophys., **11**, No. 3, 330-352 (1955).

Landsberg, H. E. (Ed.). Advances in geophysics. Academic Press, Inc., New York, Vol. 2, x + 286 pp. (1955). [Second volume in a series.]

LARGE INCREASE OF COSMIC-RAY INTENSITY FOLLOWING SOLAR FLARE ON FEBRUARY 23, 1956

The fifth and largest increase in cosmic-ray intensity yet recorded[1,2] at Cheltenham began at $03^h\ 48^m$ GMT, February 23, 1956. Mr. Roger Moore, of the North Atlantic Radio Warning Service, at Fort Belvoir, Virginia, has informed us that a large solar flare was reported first seen in Tokyo at $03^h\ 34^m$ GMT, February 23, 1956; and that at Kodaikanal, India, this solar flare was observed between 03^h

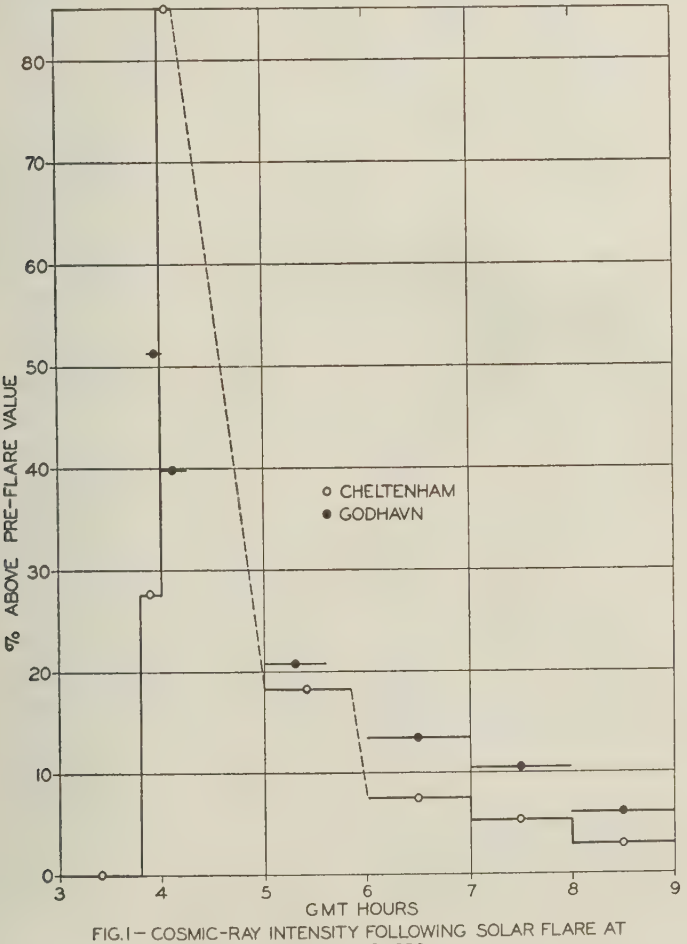

FIG. 1 — COSMIC-RAY INTENSITY FOLLOWING SOLAR FLARE AT 0330 GMT FEBRUARY 23, 1956

[1]S. E. Forbush, Phys. Rev., **70**, 771-772 (1946).
[2]S. E. Forbush, T. B. Stinchcomb, and M. Schein, Phys. Rev., **79**, 501-504 (1950).

30^m and 05^h 10^m GMT. Thus the increase in cosmic-ray intensity at Cheltenham began within about 18 minutes of the reported beginning of the flare. The Geophysical Observatory at Godhavn, Greenland, informed us that the increase there began at 03^h 53^m GMT.

The ionization in per cent above the pre-flare level is shown in Figure 1 for Cheltenham and for Godhavn, both derived from Compton-Bennett meters shielded by 11 cm Pb, for the period 03^h 00^m to 09^h 00^m GMT, February 23, 1956. The length of the horizontal bars attached to the points in the Figure indicates the duration of the interval in each hour for which a record was available. The maximum intensities recorded at Cheltenham and Godhavn were, respectively, about 85 and 50 per cent above the pre-flare values. At Cheltenham and at Godhavn, the record was off scale for the major part of the interval 04^h 00^m to 05^h 00^m. However, excellent averages were obtained for every six-minute interval from a large shielded ionization chamber at Derwood, Maryland (near Washington). These results, which will be reported later by others, indicate that the maximum intensity occurred between 04^h 00^m and 04^h 12^m GMT.

Dr. J. C. Barton, of the Physics Department of the University College of the West Indies, in Jamaica, B.W.I., wrote that a large increase was detected there at 500 feet elevation, by Dr. J. H. Stockhausen, with a wide-angle telescope shielded by 10 cm Pb. He indicated that the average counting rate for the interval 03^h 30^m to 04^h 00^m GMT, February 23, was about 33 per cent above the pre-flare value and that the rate for the next half-hour was about 27 per cent above normal; thereafter, the counting rate was about normal.

The results of Dr. Barton and Dr. Stockhausen at geomagnetic latitude 29° north show the largest increase yet reported for so low a geomagnetic latitude, thus indicating that the influx of particles on February 23, 1956, coming probably from the sun, contained a greater number of charged particles, above the cut-off momentum for this latitude, than has been observed in the four previously recorded large cosmic-ray increases.[1,2]

Note added in proof: Starting at 03^h 45^m GMT, February 23, 1956, the increase in cosmic-ray ionization from shielded Compton-Bennett meters averaged for the next 15 minutes was 18 per cent at Huancayo (geomagnetic latitude $\Phi = 0.6°S$) and about 36 per cent at Ciudad Universitaria, México, D.F. ($\Phi = 29.7°N$). Starting with either of these values, the increase averaged for subsequent 15-minute intervals decreased exponentially with half life 15 minutes. For the excellent records from Huancayo and from México, we are indebted to Mr. Alberto A. Giesecke, Jr., of the Instituto Geofísico de Huancayo, and to Dr. José y Coronado of the Universidad Nacional de México.

Scott E. Forbush

Department of Terrestrial Magnetism,
Carnegie Institution of Washington,
Washington 15, D. C., February 28, 1956
(Received February 28, 1956)

NOTICE

When available, single unbound volumes can be supplied at $6 each and single numbers at $2 each, postpaid.

Charges for reprints and covers

Reprints can be supplied, but prices have increased considerably and costs depend on the number of articles per issue for which reprints are requested. It is no longer possible to publish a schedule of reprint charges, but if reprints are requested approximate estimates will be given when galley proofs are sent to authors. Reprints without covers are least expensive; standard covers (with title and author) can be supplied at an additional charge. Special printing on covers can also be supplied at further additional charge.

Fifty reprints, without covers, will be given to institutions paying the publication charge of $8 per page.

Alterations

Major alterations made by authors in proof will be charged at cost. Authors are requested, therefore, to make final revisions on their typewritten manuscripts.

Orders for back issues and reprints should be sent to Editorial Office, 5241 Broad Branch Road, N.W., Washington 15, D.C., U.S.A.

Subscriptions are handled by The Editorial Office, 5241 Broad Branch Road, N.W., Washington 15, D.C., U.S.A.

CONTENTS—Concluded

TEMPERATURE DISTRIBUTION OF THE IONOSPHERE UNDER CONTROL OF THERMAL CONDUCTIVITY, - *Francis S. Johnson* 71

ARCTIC UPPER-ATMOSPHERE PRESSURE AND DENSITY MEASUREMENTS WITH ROCKETS, *H. E. LaGow and J. Ainsworth* 77

VARIATIONS IN STRENGTH OF WIND SYSTEM, IN THE DYNAMO MECHANISM FOR THE MAGNETIC DIURNAL VARIATION, DEDUCED FROM SOLAR-FLARE EFFECTS AT HUANCAYO, PERU, *Scott E. Forbush* 93

A NEW METHOD FOR OBTAINING ELECTRON-DENSITY PROFILES FROM *P'-f* RECORDS, *John E. Jackson* 107

GEOMAGNETIC AND SOLAR DATA: International Data on Magnetic Disturbances, Third Quarter, 1955, *J. Bartels, A. Romañá, and J. Veldkamp;* Provisional Sunspot-Numbers for October to December, 1955, *M. Waldmeier;* Cheltenham Three-Hour-Range Indices *K* for October to December, 1955, *Ralph R. Bodle;* Principal Magnetic Storms, - - - - - - - 129

REVIEWS AND ABSTRACTS: *Royal Greenwich Observatory,* Sunspot and geomagnetic-storm data derived from Greenwich observations, 1874-1954, W. E. Scott, - - - - - - - - - - - - 135

LETTERS TO EDITOR: Airborne Ionospheric Measurements in the North Pole Area, *George J. Gassmann;* The "Nose" Whistler—A New High-Latitude Phenomenon, *R. A. Helliwell, J. H. Crary, J. H. Pope, and R. L. Smith,* - 136

NOTES: Automatic ionosphere recorder; Research positions in the US-IGY Antarctic program; Three scientists named to geophysical posts, IGY; Satellite panel members named; New cosmic-ray neutron monitor; Special issue celebrating the 250th anniversary of Benjamin Franklin; Return of radiosondes requested by USAF Air Weather Service; Joint fellowship program for research in theoretical and experimental geology; Geomagnetic activities of the U.S. Coast and Geodetic Survey; Magnetic observations on Fletcher's Ice Island in the Arctic Ocean; Spring meeting of URSI; Personalia, - - - - - - - - - - - 143

LIST OF RECENT PUBLICATIONS, - *W. E. Scott* 147

LETTER TO EDITOR: Large Increase of Cosmic-Ray Intensity Following Solar Flare on February 23, 1956, *Scott E. Forbush,* - 155

JOURNAL OF GEOPHYSICAL RESEARCH